MAPPING CELLULAR AND SYNAPTIC DISTRIBUTIONS IN THE MOUSE RETINA

ADAM ANTHONY BLECKERT

A dissertation submitted in partial fulfillment of the requirements for the degree of

Doctor of Philosophy

University of Washington
2014

Reading Committee:
Rachel OL Wong (Chair)
Fred Rieke
Andres Barria

Program authorized to offer degree:
Neurobiology & Behavior

University of Washington

ABSTRACT

MAPPING CELLULAR AND SYNAPTIC DISTRIBUTIONS IN THE MOUSE RETINA

Adam Anthony Bleckert

Chair of the Supervisory Committee:
Professor Rachel OL Wong
Department of Biological Structure

The first step in perception occurs within the circuits of an organism's sensory systems. Throughout many sensory modalities, diverse arrays of neurons are often spatially organized to sample salient features and/or regions within the external environment. Furthermore, within a neuronal circuit, each individual neuron must form correct patterns of connectivity with its synaptic partners to perform the computations necessary to extract and encode these particular features or regions. This thesis attempts to demonstrate how mapping the distributions of the principle output neurons of the retina, the retinal ganglion cells, and their patterns of synaptic connectivity can provide insight to how information within the external environment is sampled and encoded from a synaptic to cellular circuit level within the first stage of the visual system. In Chapter 1, I provide an overview of the importance of understanding cellular and synaptic distributions across neuronal circuits, and how they are established during development. In Chapter 2, I demonstrate that mapping the topographies of functionally and morphologically distinct types of retinal ganglion cells may reveal how visual space is sampled by the mouse retina. In Chapter 3, I utilize a combination of light and electron microscopy to demonstrate that the distributions of inhibitory and excitatory synaptic sites across individual retinal ganglion cells show spatial constraints that may reflect stereotyped patterns of local circuit connectivity. In chapter 4, I assess how inhibitory and excitatory patterns of synaptic connectivity onto individual retinal ganglion cells are established during development by selectively disrupting inhibitory neurotransmission in the

retina. In Chapter 5, I summarize the results from each preceding chapter and provide some future directions for questions raised from this work.

LIST OF FIGURES

LIST OF TABLES

LIST OF MOVIES

DEDICATION

This work is dedicated to my paidakia: the best n = 2 results I have ever obtained.

CHAPTER I

INTRODUCTION*

1.1 CELLULAR AND SYNAPTIC MAPS FOR SENSORY PROCESSING

An organism's ability to perceive and engage the external environment begins at its sensory systems. Across many sensory modalities, information is encoded by a diverse array of sensory neurons and the processing of sensory input relies partly upon the distribution patterns of sensory neurons across the sensory surface, and the connectivity patterns onto each of the individual neurons within the circuits. By understanding the distinct topographies of sensory neurons, we can gain insight into the salient features and regions within the environment to which an organism is attuned. Likewise, by understanding the patterns of connections onto individual neurons, such as the balance of inhibitory and excitatory inputs, we can gain insight into the computations performed by individual neurons and potentially the stimulus features they encode.

1.1.1 TOPOGRAPHIC MAPS IN SENSORY SYSTEMS

A common feature observed across all sensory modalities is the topographic mapping of information from sensory neurons to higher cortical regions. Thus, the topology of sensory neurons can in and of itself provide information about the external environment. However, the way in which maps are used varies across sensory systems.

Maps can organize similar sensory information into discrete representations (Luo and Flanagan 2007). For example, in the olfactory system, different odorants trigger responses in unique clusters of

---

* Portions of this chapter were published in Bioessays, which maintains copyrights for this material, and has been reprinted with permission. The full citation for this publication is: Bleckert A, Wong RO. Identifying roles for neurotransmission in circuit assembly: insights gained from multiple model systems and experimental approaches. *Bioessays* 33: 61-72, 2011.

neighboring sensory neurons arrayed across the olfactory epithelium. This is accomplished by the expression of the same type of olfactory receptor by each neuron within the cluster. These subpopulations of sensory neurons make connections with distinct clusters of neurons in higher cortical regions, thus creating a spatial map of discrete olfactory stimuli (Mombaerts 2006) (Figure 1.1A). A similar pattern is present in the gustatory system, whereby taste receptors encode and represent the canonical categories of taste (Liman et al. 2014).

Other sensory modalities utilize the spatial arrangement of arrays of sensory neurons as a continuous representation of information within the environment (Luo and Flanagan 2007). In this way information is transferred by a point-to-point mapping of neighboring sensory neurons to neighboring populations of neurons in higher cortical centers (Figure 1.1B). In the auditory system, a continuous map of frequency space (tonotopy) resides in the cochlea, and is preserved within auditory cortical regions (Schreiner and Winer 2007). Not all of the cochleotopic maps encoded by the auditory system, however, are a direct reflection of spatial information in the environment. In the somatosensory system a continuous spatial representation of the body surface is mapped onto primary somatosensory cortex (Kaas 1983). Direct mapping of spatial information is most evident in the visual system, whereby images captured by the retina are recast through the visual pathway to higher visual cortical areas (Hubel and Wiesel 1962; Woolsey 1982). The discrete or continuous mapping of sensory input to primary cortical regions appears to be an efficient means of processing and organizing sensory information (Chklovskii and Koulakov 2004) within the limitations of developmental (Luo and Flanagan 2007) and evolutionary (Kaas 1997) constraints. However, more complex mapping patterns - varying between continuous and discrete - extend beyond primary afferent connections throughout higher cortical areas, and have led a search for the functions of maps in information processing.

Within both the auditory and visual systems, additional maps of specific features within the environment are overlaid on top of the continuous primary sensory maps. For instance, in auditory

cortex, in addition to the continuous frequency map, there are maps of amplitude, frequency modulation, sharpness of tuning, and even sound location (Schreiner and Winer 2007). These more complex features can form maps, often organized into more discrete clusters within additional auditory cortical areas (Schreiner 1995). Furthermore, the initial sensory topography may not be detectable in some higher auditory cortical regions (Schreiner and Winer 2007), even though these regions receive afferents input, which preserves the mapped organization present at primary and intermediate cortical regions (Lee and Winer 2005). Similar patterns are also present in the visual system. The retinotopic mapping of visual space in primary visual cortex, is accompanied by the presence of ocular dominance maps corresponding to the inputs from the two eyes. Furthermore there are more discrete maps of physiological features such as selectivity for spatial temporal frequencies, orientation, and direction (Felleman and Van Essen 1991; Van Essen et al. 1992; Swindale 1998). Similar to auditory cortex, there is not a complete preservation of retinotopic mapping in all higher visual areas; some cortical regions can have either an incomplete representation of the visual field or an enhanced representation of particular regions (Swindale 2000). It may be that this apparent lack of maps in higher visual and auditory cortical areas is a result of the relatively simple stimuli utilized to probe the features encoded in primary sensory cortex (Lee and Winer 2005; Schreiner and Winer 2007). Much work has attempted to characterize and determine the roles for maps in cortical processing (Knudsen et al. 1987; Kaas 1997; Swindale 2000; Chklovskii and Koulakov 2004). Although the spatial organization of cortical processing conferred by continuous or discrete maps appears to be a ubiquitous feature not only across sensory cortex but also other neocortical regions (Kaas 1997; Knudsen et al. 1987; Chklovskii and Koulakov 2004; Douglas and Martin 2007; Nummenmaa et al. 2014), the function of maps in cortical sensory processing is still unclear (Kaas 1997; Horton and Adams 2005). To begin to gain a better understanding for how spatial organization of sensory information can have direct implications for the processing of input from the environment, we can look to the topographic mapping within the retina of the visual system.

1.1.2 NONUNIFORM DISTRIBUTIONS OF NEURONS ACROSS THE RETINA

A common feature across the retina of almost every species that has been examined is a variation in the densities of retinal neurons with respect to the topographical coordinates of the eyes (Collin 2008). The magnitude of cell density change, and the patterns of cell topographies vary across species. For most species, the result is an increase in cell density towards regions of the retina corresponding to areas of enhanced visual acuity. Although many retinal cell types (Figure 1.2) show variations in their density distribution across the retina (Wässle and Boycott 1991; Kolb 1994; Masland, 2011), the topographic distributions of RGCs, the output neurons of the retina, have been best documented (Hughes 1977; Collin 2008).

In mammals, the retinas of simians show the greatest magnitudes of change in RGC densities from central to peripheral regions. RGC density is highest at a circular region in temporal retina, the fovea centralis. A steep density gradient spreads out radially from this area of central vision (Curcio and Allen 1990; Kolb and Dekorver 1991; Harman et al. 2000; Provis et al. 2013). Similar central areas of specialization (area centralis) are found in species with forward facing eyes such as dogs (Peichlcu 1992) and cats (Hughes 1975). However, in cats the increased region of RGC density extends horizontally into nasal retina (Stone 1965; Hughes 1975). This horizontal elongation of the region of peak density (visual streak) is most extreme in species with more lateralized eyes, such as the rabbit, ground squirrel and cow (Hughes 1977; Provis 1979). Lastly, some species have a more uniform distribution of RGCs across their retinas; small nocturnal mammals such as the rat, mouse, and guinea pig, have comparatively lower densities of RGCs, with relatively little central to peripheral gradient (Hughes 1977; Perry 1979; Dräger and Olsen 1981; Do-Nascimento et al. 1990; Nadal-Nicolás et al. 2012), whereas small diurnal mammals such as the squirrel have little variation in RGC density, but overall a comparatively higher total RGC density (Long and Fisher 1983). See Figure 1.3 for a comparison of differential distributions

across species. For most species with forward facing eyes, it appears that regions of enhanced RGC density are specialized to capture, track and encode high spatial frequencies (visual acuity), as well as set up the focal point for binocular vision (Hughes 1977; Kowler 2011; Provis et al. 2013). The importance of the regional specialization of the fovea and parafovea in animals with frontal vision is further reflected in the disproportionate amount of higher cortical regions devoted to these retinal areas, for example 50% of primary visual cortex is devoted to the central 20% (cat) or 8% (primate) of the visual field (Tusa et al. 1978; Perry and Cowey 1985; Wässle et al. 1989; Wässle et al. 1990).

When looking at the diverse topographies of retinal specializations across species, most RGC distributions are a reflection of the topography of the animal's local environment and the methods by which they obtain food, avoid becoming food, and navigate (Hughes 1977; Archer et al. 1999; Warrant 2004; Coimbra et al. 2013). This is particularly evident in Aves, wherein possibly the greatest diversity and specializations of RGC topographies have been documented (Crescitelli and Meyer 1977; Archer et al. 1999). In addition to the topographies described above, the retinas of birds such as eagles and pigeons can be multi-foveated (Güntürkün and Whittow 2000). Furthermore, some species of birds are able to alter their behavior and position of their eyes, with respect to the environment, to differentially utilize their distinct retinal specializations (Fernández-Juricic et al. 2011; Tyrrell et al. 2013; Lisney et al. 2013; Baumhardt et al. 2014). In all species with pronounced retinal specializations, it appears that they utilize their high acuity regions to maximally attend to and sample salient regions within the environment. This draws into question how species with little variation in RGC topography may utilize their vision. One possible explanation comes from rats, in which eye movements are controlled to maximally sample binocular overhead visual space. However, these eye movements are non-conjugate, and no region in visual space is fixated onto the modest area centralis in this species. Instead, they appear to be maximizing the efficiency of detecting movement in overhead space (Wallace et al. 2013).

This is not to say that rodents such as the rat or mouse are not able to perform more complex visual tasks. Rats can utilize vision for depth perception or object recognition (Legg and Lambert 1990; Prusky et al. 2000; Zoccolan et al. 2009; Huberman and Niell 2011), and can perform conjugate eye movements under some conditions (Chelazzi et al. 1989). Furthermore, both rats and mice have multiple cortical representations of retinotopic space, and greater cortical representation within the binocular region of visual space (Montero et al. 1973; Adams and Forrester 1968; Wagor et al. 1980; Andermann et al. 2011). Nor is this to say that species with very pronounced visual specializations do not utilize their peripheral retinas. Indeed, the peripheral retina in primates has been shown to have: increased contrast sensitivity, speed of processing, and enhanced detection of motion compared with central regions (McKee and Nakayama 1984; Wandell 1995; Carrasco et al. 2003; Palmer and Rosa 2006).

Ultimately the ability to detect each of these visual features comes about from the combination of the topographical patterns of RGCs and other neurons within the retina (Wandell 1995; Masland, 2011), but also in part by the specialization of distinct types of RGCs in the retina. One specialization that is shared across all RGC types is a direct reflection of the changes in their densities across the retina. The increase in cell density is accompanied by a decrease in dendritic arbor territory size and the corresponding size of the visual space that each RGC samples (Boycott and Wässle 1974a; Kier et al. 1995; Dacey and Petersen 1992; Wandell 1995). To date there are approximately 20 distinct RGC types that have been described across multiple species, and for some of them we are beginning to discover the stimulus features within the visual scene that they best encode, and the potential implications they have on animal behavior (Berson et al. 2008; Masland, 2011; Dhande and Huberman 2014). These few RGC types provide us with a glimpse of what information the retina can potentially encode. In total the distinct populations of RGCs reveal the retina to be a parallel processing array of sensory receptors (Azeredo da Silveira and Roska 2011).

1.1.3 RETINAL GANGLION CELL SPECIALIZATION AND PARALLEL PROCESSING

Even though the physiological responses of RGCs are often thought of as having either simple or complex receptive fields corresponding the classically defined X and Y cell types discovered in cat (Enroth-Cugell and Robson 1966), there is growing evidence that the morphologically diverse array of RGCs in multiple species may be selective for more complex visual stimuli (Lettvin et al. 1959; DACEY 2004; Field and Chichilnisky 2007; Berson et al. 2008; Azeredo da Silveira and Roska 2011; Dhande and Huberman 2014). Indeed, to encode the vast amount of information present within the visual environment, the retina parses and distributes the representation of the environment across diverse RGC types, which can be selective and specialized for detection of unique visual features. Across mammalian species, there appear to be approximately 20 different RGC types, which have primarily been described by their unique dendritic morphologies and areas of central projection, as well as their physiological responses (Boycott and Wässle 1974b; Cleland and Levick 1974b; Rockhill et al. 2002; DACEY 2004; Völgyi et al. 2009; Hong et al. 2011), some of which appear to be conserved across multiple mammalian species (Peichl 1991; Berson et al. 2008). However, of the approximately 20 different RGC types, which have been identified, only few have been examined in enough detail to understand their preferred stimulus selectivity, and potential functions. These are species specific RGC types such a as the primate midget and the cat beta (β) cells (Boycott and Wässle 1974a; Stanford 1987), the parasol and blue/yellow cells of the primate (Watanabe and Rodieck 1989; Dacey and Lee 1994; Calkins et al. 1998; Field et al. 2010), and more ubiquitous RGC types such as the local edge detector (Levick 1967; van Wyk et al. 2006; Zhang et al. 2012), direction selective RGCs (Barlow and Levick 1965; Wei and Feller 2011), intrinsically photosensitive RGCs (Berson et al. 2002; Hattar et al. 2002; Schmidt et al. 2011a; Schmidt et al. 2011b), and lastly, alpha (α) RGCs, a population that has been observed in almost every mammalian species (Peichl et al. 1987; Peichl 1991).

Like many RGCs types, midget RGCs are divided into two populations; ON midgets, which respond to increments in light, and OFF midgets, which respond to decrements in light (See Figure 1.2). The midget RGCs are best understood as the cells responsible for high acuity vision in primates (Watanabe and Rodieck 1989; Dacey and Petersen 1992). In order to attain high acuity within the fovea, midget RGCs are connected in a one-to-one relationship with individual photoreceptors, the cells responsible for detection of light in the retina. Photoreceptors confer the smallest spatial receptive resolution limit (Wässle and Boycott 1991), and within the fovea, individual photoreceptor cells make sole connections with individual midget bipolar cells, the interneurons of the retina, which in turn provide input to individual midget RGCs (Kolb and Dekorver 1991). At further eccentricities, midget bipolar cells increase their dendritic arbors, and in turn receive in increased photoreceptor convergence (Telkes et al. 2008). It is possible, that at these greater eccentricities, midget RGCs may also be capable of encoding chromatic information (Field et al. 2010; Schiller 2010). In the cat, the smallest RGC type are an ON and OFF population of β-cells. Whereas β-cells do not share the same one-to-one connectivity as midgets (McGuire et al. 1986; Cohen and Sterling 1990; Cohen and Sterling 1991; Kolb and Nelson 1993), they have been suggested to be the RGCs responsible for high acuity vision in cats (Wässle et al. 1981; Pasternak et al. 1983), and are analogous to the physiologically defined X-cells (Enroth-Cugell and Robson 1966; Cleland and Levick 1974a; Fukuda et al. 1984; Fukuda et al. 1985).

Parasol cells of the primate are larger than midgets and also come in ON and OFF variants. Unlike the midget RGCs, parasol cells have larger receptive fields, and convey achromatic information concerning luminance, low spatial acuity, flicker, and movement (Merigan 1989; Field and Chichilnisky 2007; Nassi and Callaway 2009; Schiller 2010). The blue/yellow RGCs of the primate retina respond to both increments and decrements in light due to their bistratified dendritic arbors (See Figure 1.2). Their chromatic information comes from color opponency set up by their selective connectivity with distinct photoreceptor populations that encode different wavelengths of light (Dacey and Lee 1994; Calkins et

al. 1998). Whereas the circuitry underlying the blue/yellow RGCs was the first to be characterized, they appear to be one of a number of primate RGCs capable of detecting chromatic information in the environment (Dacey and Packer 2003).

The local edge detector cell, first described in rabbit (Levick 1967), is able to selectively detect contrast borders, but is insensitive to full field changes in luminance (Levick 1967; van Wyk et al. 2006). The local edge detector is the smallest and most numerous RGC in the rabbit (Amthor et al. 1989; Devries and Baylor 1997) and rodents (Heine and Passaglia 2011; Zhang et al. 2012). Its density is high enough to confer the spatial resolving abilities in rabbits, but its spatio-temporal response to light stimuli suggests that it is not involved in acuity (van Wyk et al. 2006), and may be more concerned with object motion detection (Zhang et al. 2012). Furthermore, a functionally similar local edge detector has also been observed in cat and primate (Cleland and Levick 1974b; Rodieck and Watanabe 1993; Berson et al. 1998), suggesting it is not analogous to the β, midget, and X-cell, and that possibly species such as rabbits and mice may not have a dedicated cell type for high acuity vision.

In rabbits, cats, and mice, a functionally distinct population of RGCs have been identified that respond selectively to specific directions of motion (Barlow and Hill 1963; Famiglietti 1987; Weng et al. 2005). There are believed to be four populations of direction selective RGCs, each encoding one of the four cardinal directions. These direction selective RGCs are bistratified and respond to both increments and decrements in light. Extensive research has uncovered the mechanism by which direction selectivity is conferred to these populations of RGCs. Their preferred direction comes about from a unique patterning of connection with an inhibitory retinal interneuron called the starburst amacrine cell, which itself displays motion selectivity (Euler et al. 2002; Fried et al. 2002; Wei and Feller 2011; Taylor and Smith 2012; Vaney et al. 2012a). Direction selective RGCs in mice have been revealed to have a direct pathway to higher cortical areas, and may influence direction and orientation selectivity within primary visual cortex (Cruz-Martín et al. 2014). A secondary population of direction selective RGCs, which do not

likely contribute to vision processing, are important for compensating for eye movements to stabilize visual images on the retina and improve visual performance. These correspond to three populations of ON direction selective cells found in mouse and rabbit that encode directions mirroring the vestibular system (He and Masland 1998; Sun et al. 2006; Yonehara et al. 2009; Borst and Euler 2011; Dhande et al. 2013).

Intrinsically photosensitive RGCs are a functionally distinct ganglion population, in that they express their own light sensitive photopigment (melanopsin), which grants them their ability to detect light in the absence of input from the retinal photoreceptors (Berson et al. 2002; Hattar et al. 2002; Schmidt et al. 2011a; Schmidt et al. 2011b). These RGCs were initially discovered because of their unique projection to a specific cortical area, the suprachiasmatic nucleus that regulates circadian rhythms (Berson et al. 2002). There are believed to be four types of melanopsin expressing RGCs, which have been segregated by their morphology and physiological responses (Tu et al. 2005; Ecker et al. 2010); a morphologically similar pair of ON and OFF – the M1 and M2 cells, a bistratified M3 cell (Berson et al. 2010), and a second morphologically and physiologically distinct ON cell (Estevez et al. 2012). Their function has directly been linked to the control and regulation of the circadian clock in multiple species (Schmidt et al. 2011b; Schmidt et al. 2011a).

Studies of almost every mammalian retina have revealed the presence of a population of α RGCs (Peichl et al. 1987; Peichl 1991), a notable exception being primates. The α RGCs consist of an ON and OFF population, and were discovered to be the morphological correlate of the physiological defined Y-cells (Enroth-Cugell and Robson 1966; Peichl and Wässle 1981; Fukuda et al. 1984; Fukuda et al. 1985). α RGCs have a complex non-linear receptive field (Freed et al. 1992; Brown et al. 2000; Schwartz et al. 2012), and they are among the most sensitive RGCs in the retina to dim light and motion (Demb et al. 1999). Surprisingly, there is still little understanding of their potential functional role, even though they have been observed and studied in almost every mammalian species (Peichl et al. 1987; Peichl 1991).

The diversity of spatial and temporal features that each RGC type is optimally tuned to detect has led to the postulate that information within the visual scene is transmitted to higher cortical areas along separate discrete channels (Figure 1.4). It is believed that the different RGC types share similar topographies across the retina, at least for cats, rabbits and primates, suggesting the visual scene is processed in parallel (Wässle and Boycott 1991; Kolb 1994; Masland, 2011). However, it is not known if these patterns are consistent across all species and for all RGC types. We have started to gain some understanding of the unique types of visual features extracted from the environment, and the RGCs that attend to them best. However, there are many RGC types for which we still have limited knowledge. There have been attempts to model how much, and what possible types of visual features could be encoded under the limitations set up by the total number of RGCs within the retina for particular species (Meister 1996; Warland et al. 1997; Van Rullen and Thorpe 2001; Schnitzer and Meister 2003; Koch et al. 2004). Intriguingly, in these modeling studies, the features within natural scenes commonly extracted are very similar to the salient features triggering responses in many of the cell types currently identified (Del Viva et al. 2013; Gütig et al. 2013). These modeling studies, however, do not include the changes in densities and topographies of the unique types of RGCs across the retina, which may permit differential processing by distinct RGC types at different retinal regions (Field et al. 2010; Schiller 2010), and may increase the diversity of information that can be encoded by the retina.

Within the visual system, it is apparent that the topography of RGCs and their specificity for detection of features within the visual scene provides the foundation for further visual processing. The characterization of distinct morphological and physiological RGCs and their functions have been greatly aided by the development of genetic markers and methods for identification and manipulation of individual cell types in the mouse (Dhande and Huberman 2014). Furthermore, the use of the mouse visual system to understand visual processing and behavior has expanded greatly in recent years (Huberman and Niell 2011). However, as described above, the mouse retina is organized in a manner

distinct to that of human or other animals with forward facing eyes (Figure 1.3). How similar is the mouse visual system to that of other mammals, in particular to primates?

1.1.4 GOALS AND SIGNIFICANCE OF THE CURRENT WORK

In chapter 2, we attempt to provide answers to these questions by characterizing the distributions of α RGCs in mouse retina. Unlike most mammals, mice have 3 distinct types of α RGCs, 2 OFF and 1 ON type (Pang et al. 2003; Murphy and Rieke 2006; van Wyk et al. 2009). We find that a pair of ON and OFF α RGCs shows unique distributions across the retina, with a nasal-to-temporal gradient in size and density. By mapping the receptive fields and spatial coverage of α RGCs, we further show that the peak density found in temporal retina is biased to enhance sampling of the mouse frontal visual scene. The gradient in the α RGC distributions is in stark contrast to the total RGC distribution in mouse, and the distributions of other known identified mouse RGCs. Together, these nonmatching distributions suggest that visual space in mouse is not sampled by parallel circuits, like in cat or primate, but instead distinct populations of RGCs in mice may be organized to sample specific regions or features of the visual scene. In particular, the topography of α RGCs is particularly suited to encode frontal binocular space in the mouse. Recently α RGCs have been shown capable of encoding high spatial frequency and chromatic information, and possibly even have intrinsic photosensitivity (Estevez et al. 2012; Chang et al. 2013; Schwartz et al. 2012), however, it is still unknown if these features are behaviorally relevant stimuli for which the mouse utilizes α RGCs. Our work suggests that in addition to these distinct features, α RGCs in the mouse are best positioned for encoding binocular visual information.

There has been much effort to understand how α RGCs process visual information, and what circuit mechanisms confer their abilities to encode the features described above. Through combined methods to reconstruct α RGCs and their presynaptic partners using light and electron microscopy, we have an understanding of the bipolar cell types that make connections, and provide excitatory input to α

RGCs (Freed and Sterling 1988; Kolb and Nelson 1993; Kerschensteiner et al. 2009; Schwartz et al. 2012; Okawa et al. 2014). Furthermore, direct physiological measurements from α RGCs and modeling of their receptive field properties suggest that much of their spatial and chromatic sampling capabilities come from their patterns of connections and input from bipolar cells (Freed et al. 1992; Demb et al. 1999; Brown et al. 2000; Morgan et al. 2008; Schwartz et al. 2012; Chang et al. 2013). However, like other cells in the nervous system, the output of RGCs is shaped by the combination of excitation and inhibition onto their dendrites. Thus, we next developed and applied imaging methods to map and compare the distributions of inhibitory and excitatory synapses on the dendritic arbors of individual RGCs, focusing on 3 major morphological and functionally distinct types including the α RGCs (chapter 3).

1.2 Distributions and development of inhibitory and excitatory connections onto individual neurons

The patterns of inhibitory and excitatory connections onto individual cells must be regulated such that the correct numbers of inputs are formed by excitatory and inhibitory connections onto an individual cell. In addition, these inputs often must also target distinct spatial localizations on the postsynaptic cell such as the dendrite, soma, or axon. The ratios and correct patterning of inputs onto these cellular compartments are crucial for the complex functioning of neuronal networks. Disruptions to inhibition or excitation during development can also result in mature circuit dysfunction and disease (Gibson et al. 2008; Yizhar et al. 2011). However, our understanding of how the normal patterns of excitatory and inhibitory inputs are set up during development is far from complete.

For many circuits in the CNS, the possibility of mapping even the mature ratio of inhibitory and excitatory inputs for entire cells has been restricted by the diversity and complexity of the inputs to a given cell (Huang et al. 2007; Klausberger and Somogyi 2008). Whereas in vitro culture systems have provided us with valuable information on synaptic development, it is important to understand how the

endogenous network develops in vivo. The retina, because of its compact patterns of connectivity and the more stereotyped structure of its architecture, and cell morphologies, has provided an ideal circuit for studying in vivo development of connectivity (Sernagor et al. 2001; Sanes and Zipursky 2010). Thus, comparisons between patterns of connectivity across cortical neurons, and the retina will be made in the following sections.

1.2.1 SYNAPTIC DISTRIBUTIONS ONTO INDIVIDUAL NEURONS

To date there are extremely few examples of the total distributions of inhibitory and excitatory inputs onto individual cells even in most well studied CNS circuits, such as the hippocampus. Two studies stand out, where serial section transmission electron microscopy (ssTEM) reconstructions were utilized to map the distributions and ratios of inhibitory and excitatory inputs onto an individual pyramidal neuron (Megias et al. 2001) and three types of interneurons (Gulyás et al. 1999) in the hippocampus. These studies reveal that even within a single cell the ratios of inhibitory and excitatory connections can be vastly different on individual compartments of a neuron. For instance, the distal apical dendrites of a pyramidal neuron can have an inhibitory to excitatory (I/E) ratio of ~0.2 while the perisomatic and proximal dendrites can have as high of an I/E as 0.98, and the cell body almost complete void of excitatory synapses (Megias et al. 2001). In addition, for different types of interneurons the total number of excitatory and inhibitory inputs as well as the ratio of I/E onto each type of neuron can vary several fold (Gulyás et al. 1999). This suggests that in order to understand the full dynamics of an individual type of neuron, its inputs must be reconstructed in their entirety, and this also suggests that the distributions of inhibitory and excitatory inputs onto individual types of neurons may provide them with unique processing capabilities indicative of their function. A partial reason for the scant amount of characterizations of I/E inputs distributions is the difficulty in reconstructing single neurons using ssTEM. In addition, many cortical networks in the CNS have extremely complex connectivity patterns where the

types and connectivity of cells in these networks is still emerging (Markram et al. 2004; Klausberger and Somogyi 2008). However, recent advances in scanning electron microscopy (SEM) whereby entire blocks of tissue can be serially scanned followed by semi-automated reconstruction of individual neurons are starting to allow for the mapping of synaptic connections between multiple neurons even in these complex circuits (DeFelipe 2010; Kleinfeld et al. 2011).

But why is it important to obtain the ratios and distributions of the inhibitory and excitatory inputs onto individual neurons with such specificity? Computational modeling of neuronal integration has predicted that the integrative and functional units of neuron are individual dendrites (Branco and Häusser 2010). Functional studies which directly examined the spread of integration between synaptic inputs suggest that the actual subunits of integration and computational processing may even be local sections of dendrites spanning ~10µm (Tao et al. 2001; Harvey and Svoboda 2007; Polsky et al. 2004). However, much of this work has only looked at the interaction of excitatory inputs onto dendrites. While some modeling studies suggest that inhibitory inputs onto dendrites could further the computational abilities of individual dendrites (Koch et al. 1982; Koch et al. 1983; Sjöström et al. 2008; Spolidoro et al. 2009), there is little direct evidence examining the interaction of inhibitory and excitatory inputs during dendritic integration. We do know from work in neuronal cell culture that the capacity for inhibitory inputs onto dendrites to affect excitatory inputs has both spatial and temporal limitations similar to those seen for excitatory inputs described above (Liu 2004). Together this suggests that much of the integration and computation taking place within a neuron is distributed onto partially independent local sections of dendrites, and that the ratio of I/E within these regions has the potential to alter the total processing capability of an individual neuron.

However, it is not sufficient to only map the local distributions of inputs onto a neuron in order to predict its output. It is known that for some cortical circuits the inputs onto a single neuron are clustered depending upon the regions from where they project. For instance in the visual system of the

Xenopus tadpole, inputs projecting from neighboring regions in the retina correspond to neighboring regions on the dendrites of tectal neurons (Bollmann and Engert 2009). Similarly, the subcellular organization of excitatory inputs onto pyramidal neurons in mouse somatosensory cortex are reflective of their regions of presynaptic projection, whereby local interconnections are clustered more basally and distal connections are found on more apical dendrites with a gradient in between (Petreanu et al. 2009). Again, these studies only examined the distributions of excitatory inputs to an individual neuron. However, it is possible that inhibitory inputs may display a similar pattern. We know from the visual system of Xenopus tadpoles the areas in the retina that provide excitatory and inhibitory inputs onto tectal neurons become more matched during development (Tao and Poo 2005). And recently, it has been shown in the mouse visual cortex that excitatory and inhibitory inputs most likely to be co-regulated during development are those showing equal dynamics and that possibly specific regions of dendritic segments, such as the distal apical dendritic tufts, can be independently regulated (Chen et al. 2012; van Versendaal et al. 2012). It may be that this independent regulation is also reflective of the differential input onto these dendrites (Petreanu et al. 2009; Kubota et al. 2007). However, this may not be true for all neuronal types. Jia et al (Jia et al. 2010) and Chen et al (Chen et al. 2011) have shown that in visual and auditory cortex of mouse, the sensory input onto the dendrites of individual neurons is not clustered, and that similar sensory inputs are actually heterogeneously distributed across the arbors of each neuron.

1.2.2 Spatial distributions of inhibitory and excitatory input onto retinal ganglion cells

To date much of the information about the densities and distribution patterns of inhibitory and excitatory inputs onto RGCs has been obtained from ssTEM reconstructions of mature RGCs. In the inner retina full and partial reconstructions of multiple types of RGCs from various species including cat, ferret, rabbit, and primates have shown that there can be considerable variation in the ratio of

inhibitory to excitatory connections onto different types of RGCs and even the same type of RGC across species (Dacheux et al. 2003; Famiglietti 2005; Freed and Sterling 1988; Ghosh and Grünert 1999; Kolb and Nelson 1993). The ratio of I/E can range between 1 and ~2.7 depending upon the species and the cell type examined. However, it appears that the ratio is consistent for a given cell type within a species (Cohen and Sterling 1992).

More recently the use of immunohistochemical and transgenic markers for proteins associated with excitatory and inhibitory synapses has allowed the mapping of inhibitory and excitatory distributions onto individual RGCs in adult retinas. In the primate, immunostaining for gephyrin and postsynaptic glutamate receptors has shown that for three different cell types, the large sparse, broad thorny, and small bistratified, the total densities of inhibitory and excitatory connections are evenly matched within each cell type (Percival et al. 2009; Percival et al. 2010). This suggests that some cell types may have a more consistent pattern of connectivity than was initially presumed with EM reconstructions. Furthermore, in rabbit the use of a transgenic marker for excitatory synapses, PSD95 (Koulen et al. 1998), has shown that the relative density and spatial distribution between different types of RGCs is consistent within and across cell types (Jakobs et al. 2008; Koizumi et al. 2011). Similar transgenic techniques have been used in the mouse retina to label and map excitatory postsynaptic sites on individual RGCs with PSD95 (Morgan et al. 2008) and inhibitory synapses with Neuroligin2 (Soto et al. 2011), a transsynaptic adhesion molecule known to be localized exclusively to both GABAergic and glycinergic synapses (Varoqueaux et al. 2004). These studies showed that distributions of both inhibitory and excitatory connections show a slight central to peripheral gradient in their densities, but that over all, synaptic connections are evenly distributed across the arbors. This gradient has been suggested to be related to the function of these RGCs, whereby the domed shape of each RGCs visual receptive field is partially constructed by the distribution of its inputs (Freed et al. 1992; Brown et al. 2000; Morgan et al. 2008; Schwartz et al. 2012). However, for other RGC types in the retina, the distributions of their

inputs do not predict the functional output of the cell. This is the case for bistratified direction selective cells in the rabbit and mouse. An initial hypothesis for their direction selectivity was an imbalance in the input distributions of excitatory and/or inhibitory inputs (Poggio and Reichardt 1973; Reichardt 1987). However, immunostaining for inhibitory and excitatory postsynaptic sites onto bistratified direction selective RGCs revealed that no asymmetries existed (Jeon et al. 2002). Furthermore, recently in the mouse retina, it has been shown that it is the selective input from the presynaptic inhibitory amacrine cells to bistratified direction selective cells that confers to them their selectivity (Briggman et al. 2011). This suggests that for some circuits, even knowing the location and density distributions of excitatory and inhibitory inputs is not sufficient to predict the function of these connections.

1.2.3 COORDINATED DEVELOPMENT OF INHIBITION AND EXCITATION IN THE CNS

All central nervous system (CNS) circuits studied to date have revealed that during development inhibitory GABAergic and glycinergic synaptogenesis begins prior to the formation of glutamatergic synapses (Tyzio et al. 1999; Hennou et al. 2002). It is this sequential development of inhibitory and excitatory synapses that has drawn out the question of how mature balanced inputs are formed during development. One possibility is that inhibitory synaptogenesis outpaces excitatory synaptogenesis, and that the mature ratio of inhibition to excitation is attained late in development. However, it is also possible that inhibitory and excitatory synaptogenesis is regulated early in development as soon as excitatory inputs begin to form, in order to maintain balanced input. This form of homeostatic plasticity is found in mature circuits when either excitatory or inhibitory inputs are disrupted (Turrigiano and Nelson 2004). For instance, in hippocampal culture systems, blockade of inhibitory transmission results in an initial period of hyper-excitability, however, normal levels of activity resume resulting from a down-regulation of excitatory transmission (Turrigiano et al. 1998).

Indeed, results from hippocampal cultures examining synaptogenesis suggest that a balance of excitation and inhibition is set up early in development. When the rates of inhibitory and excitatory synaptogenesis were compared from developing mixed hippocampal cultures of inhibitory and excitatory neurons, it was found that over three weeks in culture the density of inhibitory and excitatory synapses increased, however, the initial ratio of synapse density persisted (Benson and Cohen 1996; Zhao et al. 2005). It is likely that this balance of inputs may even be regulated locally within the individual dendrites of neurons. Liu (Liu 2004) found that inhibitory and excitatory inputs are only able to interact if they are present on the same dendritic branch, and that disruption to inhibitory transmission resulted in compensatory alterations in excitatory transmission such that the local balance of inputs on an individual branch was maintained.

Recently, it has become possible to examine the distribution patterns of inhibitory and excitatory inputs onto individual neurons in vivo during development by mapping the locations of dendritic spines, correlates for excitatory synapses (Okabe et al. 2001), and inhibitory postsynaptic proteins, such as gephyrin a scaffolding protein found at GABAergic and glycinergic synapses (Fritschy et al. 2008). Two studies have shown that alterations in excitatory activity during development result in decreases in inhibitory synapse number. Furthermore, they revealed that the inhibitory synapses that are most likely to be lost were a specific subset closely localized to excitatory inputs on dendritic spines (Chen et al. 2012; van Versendaal et al. 2012). This suggests that co-regulation of inhibitory and excitatory synaptogenesis may be modulated even at the level of dendritic spines.

However, this regulation of input balance may not be characteristic of all developmental synaptic connectivity patterns onto an individual neuron. For instance at the cell body, the ratio of inhibitory to excitatory connections increases with development (Benson and Cohen 1996; Liu 2004). In vitro results suggest that this development of the mature ratio of inhibitory to excitatory connections may result from an increased rate of inhibitory synaptogenesis in combination with a loss of excitatory

synapses (Benson and Cohen 1996). It is also possible that early in development, postsynaptic proteins are not always sorted to their correct matching presynaptic partners, and thus inhibitory proteins may appear apposed to excitatory presynaptic terminals and vice versa (Rao et al. 2000; Anderson et al. 2004), thus resulting in ambiguity over a synapses true identity. This is in direct contrast to mature synaptic patterns where synaptic proteins correctly sort to matching presynaptic terminals (Craig et al. 1994). How inhibitory synapses are preferentially distributed onto the cell body of many CNS neurons is still now known. Some clues come from the cerebellum, where one type of inhibitory input is directly targeted to the cell body and axon initial segment of a neuron by gradients of cell adhesion molecules (Ango et al. 2004). It is possible that the patterns of excitatory and inhibitory inputs onto the dendrites of neurons are also regulated by gradients of signaling molecules, which instruct the location and position of inputs within stratified circuits (Sanes and Yamagata 2009). For instance, in the retina recent evidence suggests that the distributions and expression patterns of transmembrane signaling molecules can instruct the patterning and development of both axonal and dendritic processes (Matsuoka et al. 2011a; Matsuoka et al. 2011b; Kay et al. 2012), but how these signaling molecules affect synaptic distributions is still unknown.

1.2.4 COORDINATED DEVELOPMENT OF INHIBITORY AND EXCITATORY INPUTS IN THE RETINA

Like in other cortical circuits, inhibitory synaptogenesis precedes excitatory synaptogenesis in the retina (Johnson et al. 2003). Early anatomical analysis from electron microscopy studies of the circuitry of the inner retina showed that conventional synapses from GABAergic and glycinergic amacrine cells are present shortly after birth in mouse, around postnatal day 3 (P3) and increase at a constant rate until P21. However, ribbon synapses characteristic of glutamatergic bipolar cells are not present until P11, after which they also increase at an equivalent rate (Fisher 1979). Physiological recording from RGCs, the postsynaptic partners of amacrine and bipolar cells, have also shown that spontaneous inhibitory inputs

are present prior to excitatory inputs (Unsoeld et al. 2008). Measures of spontaneous inputs increase during development to reach a peak in activity level at P22, after which they both show a decrease in activity, which stabilizes by P60 (Tian and Copenhagen 2001). The developmental rates of spontaneous inhibitory and excitatory inputs to RGCs appear similar at each age examined, and suggest that there is a regulated balance of excitation and inhibition onto individual cells in the retina during development.

The development of synaptic densities of excitatory and inhibitory inputs onto RGCs in mouse has also been obtained by mapping the distributions of fluorescent markers of excitatory and inhibitory inputs onto individual RGCs. Intriguingly, excitatory synapses onto RGCs were already present at P5 (Morgan et al. 2008), prior to the earliest age (P7) when excitatory inputs onto RGCs have been thought to be functional (Johnson et al. 2003). Furthermore, excitatory synaptic density increased during development to peak at ~P21 and remained stable thereafter (Morgan et al. 2008). The distributions of inhibitory synapses onto RGCs were mapped in separate cells, and their densities matched those obtained for excitatory synapses at each developmental age examined (Soto et al. 2011). These results revealed that the anatomical distributions of inhibitory and excitatory synapses parallels that of the spontaneous inhibitory and excitatory activity of inputs onto individual RGCs, and further suggests that there is likely a coordination of inhibitory and excitatory synaptogenesis during development in the retina such that a balance of inhibition and excitation is maintained shortly after excitatory synaptogenesis begins. While this may seem in contrast to the rates of inhibitory and excitatory synaptogenesis suggested by previous EM studies, it is known that GABAergic and glycinergic amacrine cells also make connections with each other and with the axons of bipolar cells (Wässle and Boycott 1991). It is therefore possible that the greater density and rate of development of inhibitory synapses seen in the inner retina is partially reflective of local reciprocal connections within the inner retinal circuit itself.

A key tenant in the field of neuroscience is the belief that with the mapping of the patterns of connectivity within circuits and between individual neurons, the function of these circuits will become evident (Crick and Jones 1993; Douglas and Martin 2007; DeFelipe 2010; da Costa and Martin 2013). There is a recent resurgence and expansion of attaining these patterns of connectivity in part as a result of new techniques in mapping large-scale volumes of tissue (Helmstaedter et al. 2008; Lichtman and Denk 2011). However there are still very limited maps of connectivity patterns of the multitude of neural circuits, and even far fewer maps of connectivity onto individual cells. The importance of attaining maps of the patterns of connectivity onto individual cells has been highlighted in modeling studies, which reveal how distributions of synaptic inputs onto an individual cell can have the potential to regulate the computational capabilities of the neurons output (Koch et al. 1982; Tao et al. 2001; Harvey and Svoboda 2007; Polsky et al. 2004; Sjöström et al. 2008; Spolidoro et al. 2009). However, the connectivity between cells and the patterns of connections onto individual cells are not necessarily hard-wired; they emerge during development and can be modulated by experience (Sanes and Zipursky 2010; Petersen 2007).

1.2.5 GOALS AND SIGNIFICANCE OF THE CURRENT WORK

In chapter 3 we aimed to further our understanding of how the patterns of excitatory and inhibitory connections onto individual neurons are set up during development. We mapped the distributions of inhibitory and excitatory synapses onto three functionally distinct RGC types during development and at maturity. We present evidence that the mature patterns of inhibitory and excitatory connections onto individual RGCs can differ across cell types, and are set up at different rates during development; some RGCs attain their mature balance of inhibitory and excitatory synaptic numbers early in development, with other RGCs reach their mature connectivity pattern at a later stage. For all RGCs inhibitory and excitatory distributions appear evenly distributed across their entire dendritic arbors. However, we reveal through a combination of fluorescence imaging and electron microscopy that there appears to be

spatial constraints on the inter-synaptic distances between excitatory and inhibitory synapses that reflect local patterns of circuit connectivity. We found that inhibitory inputs are more closely apposed to excitatory inputs that would be predicted by random chance, which were consistent with feed forward inhibitory circuits observed in EM reconstructions of inputs onto the RGC's dendrites. Together our results suggest that a principle output neuronal population within a circuit, such as the RGCs, can have diverse patterns of connectivity, and that these patterns may be sculpted over different developmental time periods. These observations led us to ask what mechanisms regulate the development and establishment of the appropriate balance of inhibitory and excitatory inputs onto individual cells (chapter 4). Specifically, we investigated the affects of altering inhibitory neurotransmission because much less is known about its roles compared to the vast knowledge we have already gained from studies elucidating the importance of excitatory transmission on synapse development.

1.3 Role of neurotransmission in patterning neuronal connectivity

The role of neuronal activity in circuit development has been of much interest since the 1960s. This is illustrated by classic studies in the visual system (Hubel et al. 1977; LeVay et al. 1980) and in the neuromuscular junction (NMJ) (Sanes and Lichtman 1999). Subsequent studies in diverse model systems have, however, provided disparate viewpoints about the importance of neuronal activity in patterning circuits. While neuronal activity often describes a broad range of cellular activities, the role of chemical neurotransmission between pre- and postsynaptic cells has become a focal point for understanding how the communication between neuron regulates the development of neuronal circuits. In particular the role of excitatory glutamatergic neurotransmission has been extensively studied. Because neurotransmission can have effects at multiple developmental time periods we must first ask which stages of circuit assembly are regulated by neurotransmission?

1.3.1 SYNAPSE FORMATION AND DIFFERENTIATION

Synaptogenesis commences upon contact between pre- and postsynaptic neurons (Figure 1.5). Thereafter, pre- and postsynaptic proteins accumulate at the site of contact, leading to differentiation of the synapse; however, even prior to physical contact, axonal growth cones can release neurotransmitters (Hume et al. 1983; Taylor et al. 1990) and dendrites are lined with transmitter receptors. Thus, it is conceivable that prior to axonal-dendritic contact, transmitter release influences synaptogenesis. One way it may do so is to regulate the probability of contact between cells; for example, the dendrites of hippocampal neurons in culture are covered with highly motile filopodia that can facilitate contact between axons and dendrites (Ziv and Smith 1996). Furthermore, focal application of glutamate, an excitatory neurotransmitter, can locally induce filopodial formation in these neurons (Smith and Jahr 1991). In RGCs (RGCs), dendritic filopodia motility is reduced upon blocking neurotransmitter receptors (Wong and Wong 2001). The decrease in filopodia motility theoretically reduces the potential contact volume presented by the postsynaptic cell. Thus, transmission may promote synapse formation by regulating filopodial formation and motility. In contrast, the loss of cholinergic neurotransmission at the rodent skeletal NMJ from embryonic stages increases the prevalence of myopodia, thin protrusions from muscle fibers (Misgeld et al. 2002). The increase in myopodia is matched by an increase in the number of receptor-bearing junctions on the myotube. Transmission at early stages of NMJ development is therefore needed to suppress hyperinnervation of muscle fibers.

Although transmitter release could play a role in facilitating the rate and regulating the extent of initial contact between cells, neurotransmission is not required for synaptogenesis per se (Rao and Craig 1997). Synapses still form in mouse mutants where transmitter release is perturbed from the very beginning (Varoqueaux et al. 2002; Verhage et al. 2000). It is clear, however, that once formed, transmission is involved in the maturation of nascent synapses (Wu et al. 1996; Okabe et al. 1999).

1.3.2 Refining connectivity: inappropriate connections are removed with maturation

Although, from the very beginning, some circuits are generated with near precision, others undergo varying degrees of reorganization before attaining their mature connectivity patterns. Circuit development thus involves not only the formation and maintenance of synaptic connections but, in many instances, necessitates the elimination of erroneous contacts (Figures 1.6 and 1.7). There is much evidence to support a role for neurotransmission in circuit refinement across diverse model systems. The skeletal NMJ is, however, arguably the most well-defined system where transmission-mediated circuit refinement occurs (Figure 1.6A). Somewhat unique to the NMJ is that innervation of each muscle fiber is confined to a single pretzel- shaped postsynaptic area bearing acetylcholine receptors. At birth, muscle fibers are initially multi-innervated, and sub- sequent refinement requires the withdrawal of all but one motor axon (Redfern 1970; Sanes and Lichtman 1999). The remaining axon terminal expands and takes over the synaptic area previously occupied by the other axons (Walsh and Lichtman 2003). This synaptic takeover behavior at the NMJ implicates motor neurons engaging in a competition for con- tact with the muscle fiber. The competition, producing winners and losers, is fueled by neurotransmission, without which, refinement does not occur.

Refinement of the initial patterns of connectivity in the mammalian visual system (Figure 1.6B) is also thought to involve a process of activity-dependent competition (Huberman et al. 2008a; Katz and Shatz 1996; Leamey et al. 2009). At maturity, RGCs from the left and right eyes form synaptic connections with different postsynaptic cells in their subcortical target, the dorsal lateral geniculate nucleus (dLGN). Likewise, in the cortex, dLGN axons representing the left and right eyes remain segregated and are distributed into ocular dominance columns. Eye-specific layers and ocular dominance columns emerge during development from initially diffuse patterns of innervation, and perturbing transmission along the visual pathway disrupts these refinements in connectivity. Depriving

one eye of vision (monocular deprivation) leads to a loss of axonal territory in the cortex representing the deprived eye and an expansion of territory subserving the seeing eye (Hubel et al. 1977; LeVay et al. 1980; Huberman et al. 2008a). Thus, as in the NMJ, some dLGN axons gain whereas others lose territory during development via a process that is mediated by neurotransmission.

Implicit in the observation that postnatal refinement always results in singly-innervated NMJs is that neurotransmission shapes the convergence of inputs within a circuit. Transmission-mediated refinement resulting in stereotypic convergence can be found in the visual system. Mouse dLGN neurons can receive inputs from as many as 20 RGCs at birth but only maintain connections with one to three cells in the adult (Chen and Regehr 2000). This refinement takes place even after eye specific layers are formed, and although it does not depend on visual experience, it does require spontaneous retinal activity (Hooks and Chen 2006). Similarly, adult Purkinje cells in the cerebellum are contacted by a single climbing fiber, but earlier in development are innervated by as many as five climbing fibers (Mariani and Changeux 1981) (Figure 1.6C).

Disrupting postsynaptic neurotransmission at Purkinje cells using a variety of methods (Hashimoto et al. 2001a; Miyazaki et al. 2004) results in persistent innervation from multiple climbing fibers. Thus, across several systems, neurotransmission regulates the stage of circuit refinement that determines the number of afferents converging onto an individual postsynaptic cell. It is important to note that circuits must also regulate the number of divergent connections each presynaptic cell makes. In the mature cerebellum, each inferior olivary cell contacts approximately seven Purkinje cells (Sugihara et al. 2001), compared to each climbing fiber axon initially contacting upwards of 100 Purkinje cells (Sugihara 2006). Much less is known about the developmental patterns of divergence in the visual system and at the NMJ; however, because transmission regulates afferent convergence in these model systems, it is possible that transmission also plays a pivotal role in customizing the number of cells each individual axon contacts within its respective network.

The notion that transmission evokes mechanisms that can bring about circuit refinement begs the question, what factors determine who wins? Multiple observations across the systems we discuss here suggest that the more active input wins. At the NMJ, axons unable to synthesize neurotransmitter lose to those that transmit (Buffelli et al. 2003). Likewise, the non-deprived eye clearly gains more territory in the visual cortex. Also, the efficacy of neurotransmission of the climbing fiber that will eventually solely innervate the Purkinje cell is greater than that of other co-innervating fibers (Bosman et al. 2008). However, it is also apparent that the ability to transmit better than one's neighbors is not the sole factor underlying the outcome of competition. In these systems, it is crucial that the postsynaptic cell is able to respond to its inputs in order to promote the appropriate refinement process. For example, inhibiting cortical neurons during monocular deprivation favors the deprived, rather than the non-deprived, eye. Thus, imbalances of transmission underlie transmission-dependent refinement in connectivity, but such imbalances need to be suitably detected by the postsynaptic cell (Hata and Stryker 1994).

Whereas multiple manipulations can nicely unmask a role for neurotransmission in circuit refinement, it is not yet clear how imbalances in transmission are normally created between competing axons. One thought is that within each cell there are limited resources of the molecular machinery underlying transmitter release. Intriguingly, at a specific NMJ, the larger axon that contacts more muscle fibers ends up losing, possibly because larger axons can provide relatively little resource to each of its terminals, compared to smaller axons (Kasthuri and Lichtman 2003). In circuits in which more than one axon remains connected to a common target cell, it may be that there is not much difference in the efficacy of transmission between individual axons but rather, winning axons fire axon potentials synchronously, together leading to a more effective depolarization of the postsynaptic cell (Bi and Poo 2001). Despite the fact that the molecular, physiologic, and cellular factors causing imbalances in transmission from competing axons are still elusive, it is evident that physiologic changes often appear

prior to structural alterations. For example, Layer IV neurons lose responses to the deprived eye prior to structural changes in dLGN axons (Silver and Stryker 1999), and functional differences between climbing fiber inputs onto Purkinje cells appear prior to the elimination of connections (Hashimoto and Kano 2003; Hashimoto et al. 2009).

1.3.3 MAINTAINING CONNECTIVITY PATTERNS AND STRENGTHENING CONNECTIONS REQUIRES TRANSMISSION

The stability of the initial contact between an axon and a dendritic filopodium does not require excitatory neurotransmission (Lohmann and Bonhoeffer 2008); but, transmission is eventually needed to initiate pathways (such as calcium/calmodulin dependent protein kinase II, CAMKII; small guanosine triphosphate hydrolyzing enzymes, GTPases) that stabilize the cytoskeletal network necessary for the overall maintenance of axons and dendrites (Threadgill et al. 1997; Zou and Cline 1999). Maintenance of axonal and dendritic structure involves the release of trophic factors, such as brain-derived neurotrophic factor (Cohen-Cory 1999). In mouse mutants lacking transmitter release, synapses are precipitously lost shortly after formation (Verhage et al. 2000). This decline may result from destabilization of connections in the absence of neurotransmission, or a consequence of cell death. Indeed, distinguishing between transmission-dependent trophic support and selective synapse maintenance under conditions of activity blockade is not trivial.

However, there is evidence to suggest that transmission influences the maintenance of connectivity patterns that are newly established. In the mouse retinogeniculate pathway, visual deprivation commencing past the period of initial circuit refinement results in a weakening of synaptic strength of inputs onto a single dLGN neuron (Hooks and Chen 2008). Thus, even remaining winning connections within this circuit need to be maintained by visually evoked transmission, at least within a critical period when they still appear malleable. Strengthening can occur via a variety of mechanisms,

including increasing the number of synapses between the winning axon and the postsynaptic cell (Chen and Regehr 2000) and increasing efficacy of transmission pre- and/or postsynaptically.

Formulating defined roles for neurotransmission in circuit patterning thus requires assessing potential effects at all stages of circuit development. It is important to emphasize that synapse formation and elimination occur concurrently within a network, and that activity-dependent mechanisms may function in tandem with activity-independent mechanisms (Huberman et al. 2008a; Leamey et al. 2009).

1.3.4 LIMITATIONS AND CONSTRAINTS ON NEUROTRANSMISSION ROLES IN CIRCUIT DEVELOPMENT

Much work has shown that an interplay of genetic and activity mediated regulation are needed for the correct formation of neuronal circuits and wiring of individual cell connectivity. For many circuits, patterns of connectivity are initially set up by genetic and intercellular guidance cues. These nascent networks can then be further sculpted by activity when neurons begin to transmit (Sanes and Yamagata 2009).

This raises the possibility that molecular cues dictating the formation of synaptic laminae (Sanes and Zipursky 2010; Yoshida 2012) may preclude axons from competing by keeping their inputs far apart. It has recently been shown in the vertebrate retina that loss of neurotransmission from one population of presynaptic bipolar cells does not affect the connectivity of a neighboring different bipolar cell type, even though they converge upon the same postsynaptic RGC (Kerschensteiner et al. 2009). Perhaps the direct targeting of these bipolar cell inputs onto separate ON and OFF dendritic arbors of the postsynaptic bistratified RGC early in development (Mumm et al. 2006; Kim et al. 2010) does not encourage competition between the ON and OFF bipolar cell axons (Kerschensteiner et al. 2009) because punishment signals, as hypothesized for the NMJ (Jennings 1994), cannot spread far enough to destabilize the synapses of the lesser competitor (Figure 1.7). This possibility is supported by the

observation that transmission is not necessary for localizing inputs representing the left and right ears onto separate dorsal and ventral arbors of nucleus laminaris (NL) neurons of the auditory system (Figure 1.7C). Indeed, differential expression of molecular guidance cues is found in the dorsal and ventral layers in the NL (Cramer et al. 2002; Cramer et al. 2004). In contrast, transmission-dependent emergence of eye-specific layers in the dLGN may occur because left and right inputs are initially intermingled on the dendrites of an individual dLGN neuron prior to segregation. Indeed, potentiation upon stimulation of an input during development of Xenopus retinotectal circuits can spread to inputs that are close-by on the dendritic arbor (Tao et al. 2001).

In the vertebrate retina, there is an additional constraint on the patterning of inputs even from neighboring afferents of the same presynaptic cell types. For example, the axonal arbors of each morphologically defined subtype of retinal bipolar cell tile, i.e. their arbors do not overlap (Figure 1.7E). This tiling is thought to arise from homotypic interactions between cells of the same subtype (Wässle et al. 2009; Reese 2010). We hypothesize that axonal tiling could restrict the developmental effects of transmission by limiting the potential overlap of converging inputs. If the axonal territories of bipolar cells are released from tiling, it is conceivable that the terminal branches of neighboring cells extend, and their synapses interdigitate, on the postsynaptic dendrite. The freedom to overlap may allow every bipolar cell to increase their connectivity, implicating a role for homotypic interactions in constraining the number of connections each bipolar cell can make. Further evidence for this restrictive role of tiling has recently been observed after creating an imbalance in the activity of neighboring bipolar cells of the same type. Under these conditions, the non-transmitting bipolar cell has fewer synapses, but its neighbors do not gain. Only when bipolar cells are removed early in development, are their neighbors (both of the same type and different types) able to expand and increase their numbers of connections with postsynaptic targets (Okawa et al. 2014). Indeed, the interplay between neurotransmission

dependent and independent mechanisms has been shown to sculpt the cell-autonomous and competitive patterns of connectivity across circuits (Figure 1.7).

1.3.5 Role of inhibitory neurotransmission in circuit development

Whereas the role of excitatory neurotransmission in circuit construction has been extensively studied, our understanding of how inhibitory transmission can instruct the patterning of the same circuits during development is much more nascent. This is in part because of the extreme diversity of inhibitory interneurons in cortical and other circuits (Markram et al. 2004) and the difficulty in selectively affecting their communication with other neurons. However, advances in genetic techniques are beginning to reveal an equally important role for inhibitory transmission in circuit development (Huang 2009).

In addition to an early modulatory role of GABA in network development (Owens and Kriegstein 2002), GABAergic transmission has increasingly been shown to regulate the development of synapses. These effects can manifest as alterations in the number or function of synapses. One source for modulation of synaptic function is the GABA receptors themselves. While there are three functional classes of GABA receptors, (Bormann 2000) the role of the ionotropic $GABA_A$ receptors have been most extensively studied. $GABA_A$ receptors are pentameric proteins composed of an array of 19 receptor subunits (Sieghart et al. 1999). The majority of functional $GABA_A$ receptors found in the CNS are constructed from the α, β and γ subunits with stoichiometry 2:2:1 respectively. The individual composition of receptors has been linked to their synaptic or extrasynaptic localization within neurons (Lüscher and Keller 2004), and individual subunits govern the variable functional kinetics of the receptors (Farrant and Nusser 2005). Selective knockout of distinct subunits has revealed that the γ2 subunit is essential for clustering and localization of receptors to postsynaptic sites (Essrich et al. 1998), and knockout of other subunits can alter the mature functions of networks (Homanics et al. 1997a; Homanics et al. 1997b; Ortinski et al. 2006) and their patterns of connectivity. For instance, GABAergic

transmission has been shown to affect both receptor localization and function. Whereas a loss of GABAergic synaptic transmission does not prevent the clustering of $GABA_A$ receptors (Brünig et al. 2002; Christie et al. 2002; Studler et al. 2002), it may affect the localization of $GABA_A$ receptors. Loss of GABAergic innervation can result in the mislocalization of $GABA_A$ receptors to excitatory synapses (Rao et al. 2000), or an alteration in the subunit composition of synaptic and extrasynaptic receptor clusters (Christie et al. 2002), which may ultimately result in changes to circuit function (Ortinski et al. 2006). Knock out of the α1 subunit of the $GABA_A$ receptor has been shown to reduce the number of dendritic synapses made onto Purkinje cells in the cerebellum (Fritschy et al. 2006). However, pharmacological blockade of GABA receptors has been shown to increase the number of GABAergic synapses onto hippocampal neurons (Meier et al. 2003; Meier 2003). Together these results suggest that different mechanisms of blocking GABAergic transmission may have differential effects on circuit development.

Recently, selective genetic methods for reducing GABAergic synthesis or blocking GABAergic neurotransmission have produced somewhat disparate results (Figure 1.8). Conditional knockdown of GAD67, the primary synthesizing enzyme for GABA (Asada et al. 1996; Asada et al. 1997) in individual inhibitory basket interneurons in the visual cortex results in their reduced axonal morphology and subsequent decreased synaptic innervation of the somata of their target pyramidal cells. Similar results were also seen in the germ-line knockdown of GAD67 but not in GAD65 (Chattopadhyaya et al. 2007a). These results were also consistent with the loss of visual sensory input (Chattopadhyaya et al. 2004), suggesting that the effects of sensory deprivation may alter GAD expression (Liang and Jones 1996; Patz et al. 2003), and that regulation of GABA synthesis by activity may be a mechanism for altering network development. However, when GABAergic transmission was blocked by genetic knock out of the vesicular inhibitory amino acid transporter (VIAAT), the sole transporter that loads inhibitory neurotransmitters into synaptic vesicles (McIntire et al. 1997; Wojcik et al. 2006), the opposite result was found; the number of synaptic sites onto the somata of pyramidal neurons in visual cortex was increased, and the

axonal arbors of the inhibitory basket interneurons were greatly expanded (Wu et al. 2012). The authors propose that what little remaining GABAergic transmission is present in the GAD knockouts was able to promote correct synapse formation but not maturation of the connections, whereas complete blockade of GABAergic transmission in the VIAAT knockout results in overabundant incorrect and immature synaptic connections (Wu et al. 2012). A similar deficit in synapse maturation was proposed in the retina after conditional knockout of GAD67 (Schubert et al. 2013). These initial insights suggest that the complexity of inhibitory transmission's roles in circuit development will likely be equal in depth to that of excitatory transmission and that there is still much to be determined. One outstanding question that has received even less attention is how these two forms of neurotransmission may affect the balance of inhibitory and excitatory inputs onto individual cells.

1.3.6 Interactions between inhibition and excitation during development

Whereas it seems pivotal for circuits to attain the correct ratio of inhibition and excitation during development, so much so that they appear to do so shortly after synaptogenesis begins, how circuits regulate this process is still not well understood. Although the role of inhibitory transmission in circuit development has recently begun to be investigated in more detail (Huang 2009), very few studies have looked at how excitatory or inhibitory neurotransmission regulates the balance of excitatory and inhibitory inputs onto individual neurons.

One hypothesis as to how GABAergic transmission may influence the development of glutamatergic synaptogenesis and regulate the mature balance of inhibitory and excitatory synaptic connectivity is via the mutual interaction with NMDA receptors (Ben-Ari et al. 1997). GABAergic transmission in mature circuits is inhibitory, but early in development GABA is depolarizing until around the time excitatory synaptogenesis begins (Ben-Ari 2002). It is this early depolarizing action of GABA that can facilitate activation of NMDA receptors and has been suggested to regulate the development of

glutamatergic connectivity (Ben-Ari et al. 1997). We know from cell culture assays that excitation, especially that mediated by NMDA receptors, is necessary for the correct sorting of inhibitory and excitatory postsynaptic proteins to their matching presynaptic partners (Anderson et al. 2004; Rao et al. 2000). In addition, in the Xenopus visual system early GABAergic transmission onto tectal neurons can facilitate NMDA signaling, and alterations to GABAergic early depolarization result in imbalances to the mature I/E ratio in these cells (Akerman and Cline 2006). Furthermore, the level of GABAergic activity has been shown to be correlated with excitatory activity onto individual neurons in the Xenopus tectum. The result being that the mature strength of GABAergic transmission can be regulated by the relative ratio of I/E during early development, with the important excitation coming from activation of NMDA receptors (Liu et al. 2007). Furthermore, if the early excitatory activity of GABAergic transmission onto individual neurons is switched to inhibitory, glutamatergic inputs do not develop at their normal rate onto these same cells. However, if exogenous activation of NMDA receptors on these cells is combined withe the early switch in GABAergic transmission, glutamatergic synaptogenesis is rescued and inputs develop normally (Wang and Kriegstein 2008). It may be that the local interaction of inhibitory and excitatory onto individual dendritic branches is what allows for this early coordination of inputs (Liu 2004). These studies provide precedence for early inhibitory neurotransmitters in setting up the mature balance of inhibitory and excitatory synaptic connectivity. It remains to be determined how coupled are the alterations in inhibitory and excitatory transmission during development. It is possible that disruptions to either transmitter system result in more homeostatic regulation of the total balance of inhibition and excitation onto individual cells, or that this balance plays out at a more confined local scale within individual cellular compartments, such as soma and dendrites (Turrigiano 2008).

In the retina, excitatory and inhibitory activity has been shown to be necessary for the correct development of the inner retina. In particular, blockade of glutamatergic (Bodnarenko and Chalupa 1993) and GABAergic (Sernagor et al. 2010) activity has been implicated in the correct development of

RGC morphology. However, less is known about the role of neurotransmission in the development of synaptic patterns of connectivity. Recently, two studies have started to implicate glutamatergic activity in setting up the correct patterns of excitatory connections onto RGCs. Blockade of transmitter release from bipolar cells, the excitatory inputs to RGCs during development resulted in a decrease in the excitatory synaptic density onto the postsynaptic RGCs (Kerschensteiner et al. 2009). Furthermore, an increase in bipolar cell spontaneous activity during development can cause an increase in excitatory postsynaptic density onto RGCs (Soto et al. 2012). This suggests that perturbations to the total level of excitatory output from bipolar cells onto RGCs can reveal bidirectional regulation of the synaptic density onto the postsynaptic partners. Furthermore, these changes in density were confined to local regions of the dendritic arbors of the RGCs where transmission was disrupted, suggesting regulation can be relegated to distinct cellular compartments. However, in neither of these studies was the density of inhibitory connections examined as a result of these disruptions to glutamatergic signaling. As in other CNS circuits, there has been less study on the role of inhibitory neurotransmission on the development of synaptic connectivity within the retina. The questions remain if inhibitory neurotransmission can also regulate the development of inhibitory input onto individual RGCs, and if alterations in inhibitory transmission spread to affect excitatory synaptogenesis, and also to whether this regulation is regulated independently across the different compartments of an individual RGC.

1.3.7 Goals and significance of the current work

In chapter 4, we begin to address these questions by selectively disrupting inhibitory transmission within the retina during development, and assessing its affect on the distributions of inhibitory and excitatory connections onto individual RGCs. We find that similar to the disruption of excitatory transmission, disruption to inhibitory neurotransmission selectivity regulates inhibitory synaptogenesis onto different compartments of the RGC. In contrast to loss of excitatory transmission, however, we find that a loss of

inhibitory neurotransmission causes an increase in the size and density of synaptic connections onto the somata, whereas little change to the density and size of connections onto the dendrites of individual RGCs is observed. Furthermore, the loss of inhibitory neurotransmission does not alter the density of excitatory synapses onto each RGC. Together our results further confirm a local regulatory role for neurotransmission during synaptic development. Thus within an individual cell inhibitory neurotransmission can locally regulated synaptogenesis onto individual cellular compartments (soma vs. dendrite), and that this differential change is not couple to an alteration in excitatory patterns of connectivity.

1.4 FIGURES

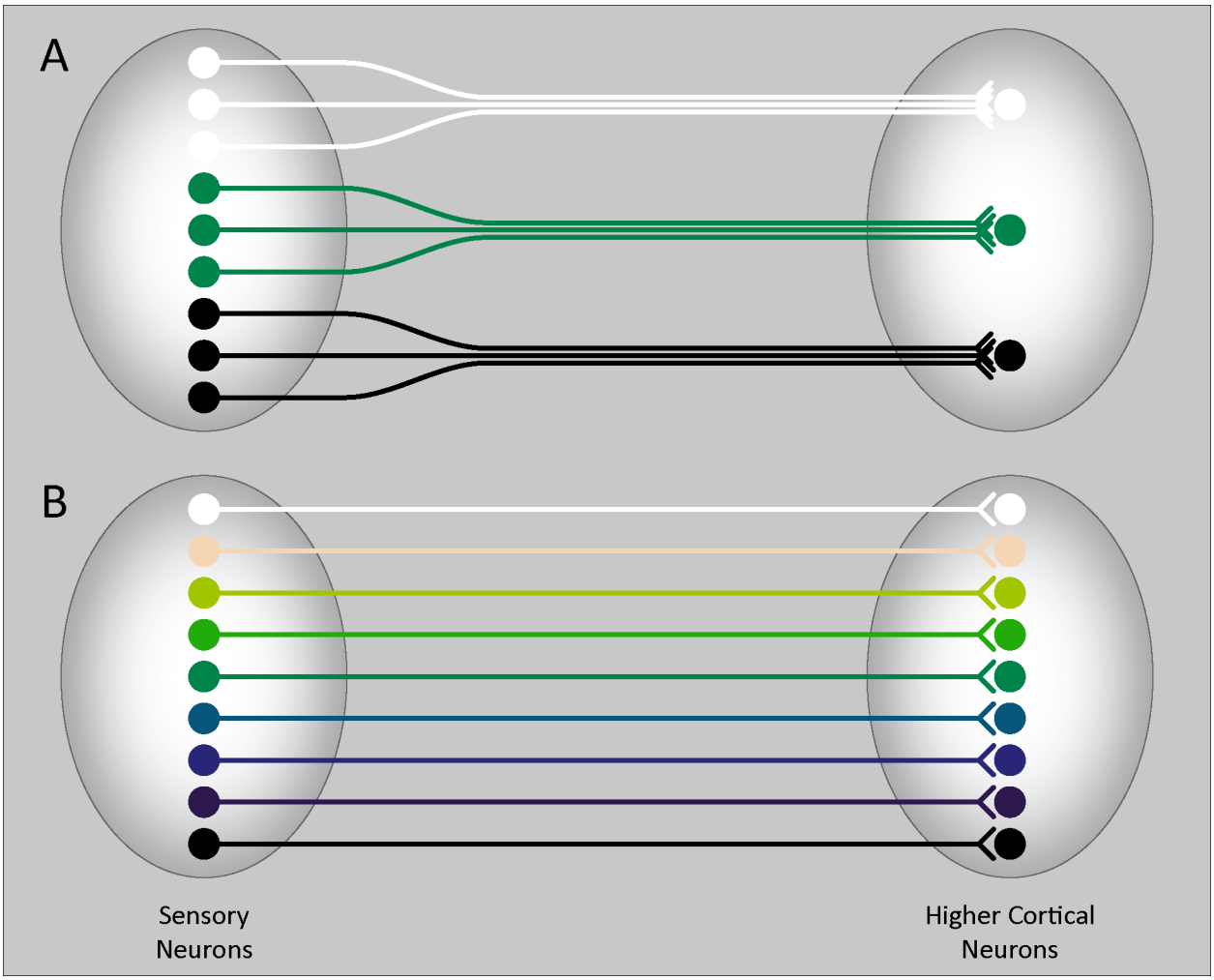

Figure 1.1 Schematic representations of topographic distributions of neurons in sensory systems. **(A)** Discrete topographic maps, such as that found in the olfactory system display the clustering of similar input types onto distinct clusters of neurons in higher cortical areas. **(B)** Continuous topographic maps such as those found in the visual system display a point-to-point mapping of neighboring sensory neurons onto neighboring populations of neurons in higher cortical areas (Luo and Flanagan 2007).

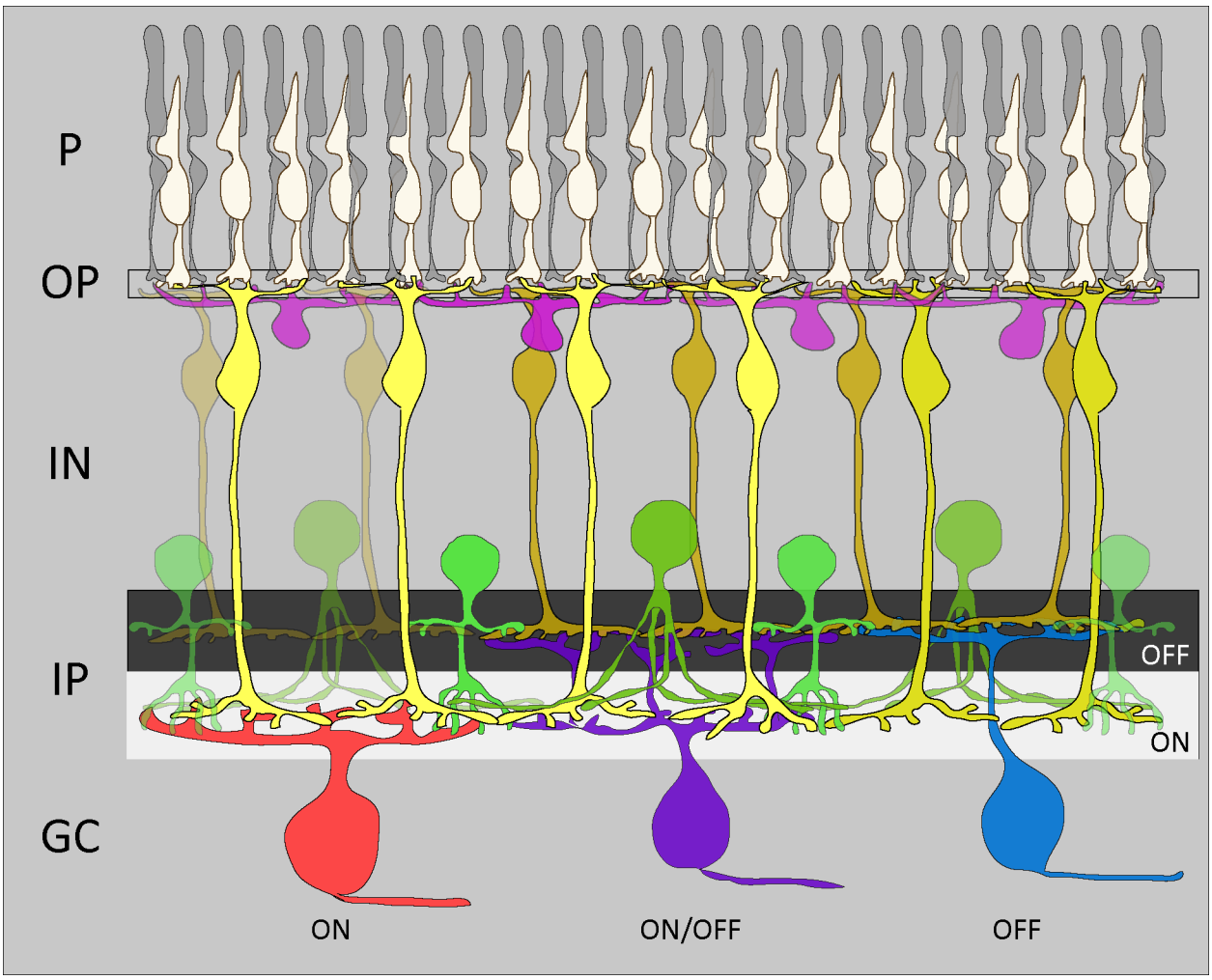

Figure 1.2 Schematic of the retina and its different cell types.
Responses to light begin at the photoreceptor layer (P) in rods (gray) and cones (tan), which transmit to bipolar cells (yellow) in the inner nuclear layer (IN). Horizontal cells (magenta) provide inhibitory regulation to bipolar cell dendrites, and photoreceptor axon terminals in the outer plexiform layer (OP). Bipolar cells project their axons to either the ON or OFF sublaminae of the inner plexiform layer (IP), where they provide excitatory glutamatergic inputs onto the dendrites of retinal ganglion cells (RGCs, red, purple, blue) whose somata lie in the ganglion cell layer (GC) and the dendrites of inhibitory amacrine cells (green). Amacrine cells in turn provide GABAergic and glycinergic inhibitory input to RGCs and bipolar cell. Dendrites of different types of RGCs stratify in distinct (ON and OFF) sublaminae of the IPL, which correspond to their physiological response to light increments, depolarization (ON) and hyperpolarization (ON/OFF) or hyperpolarization (OFF).

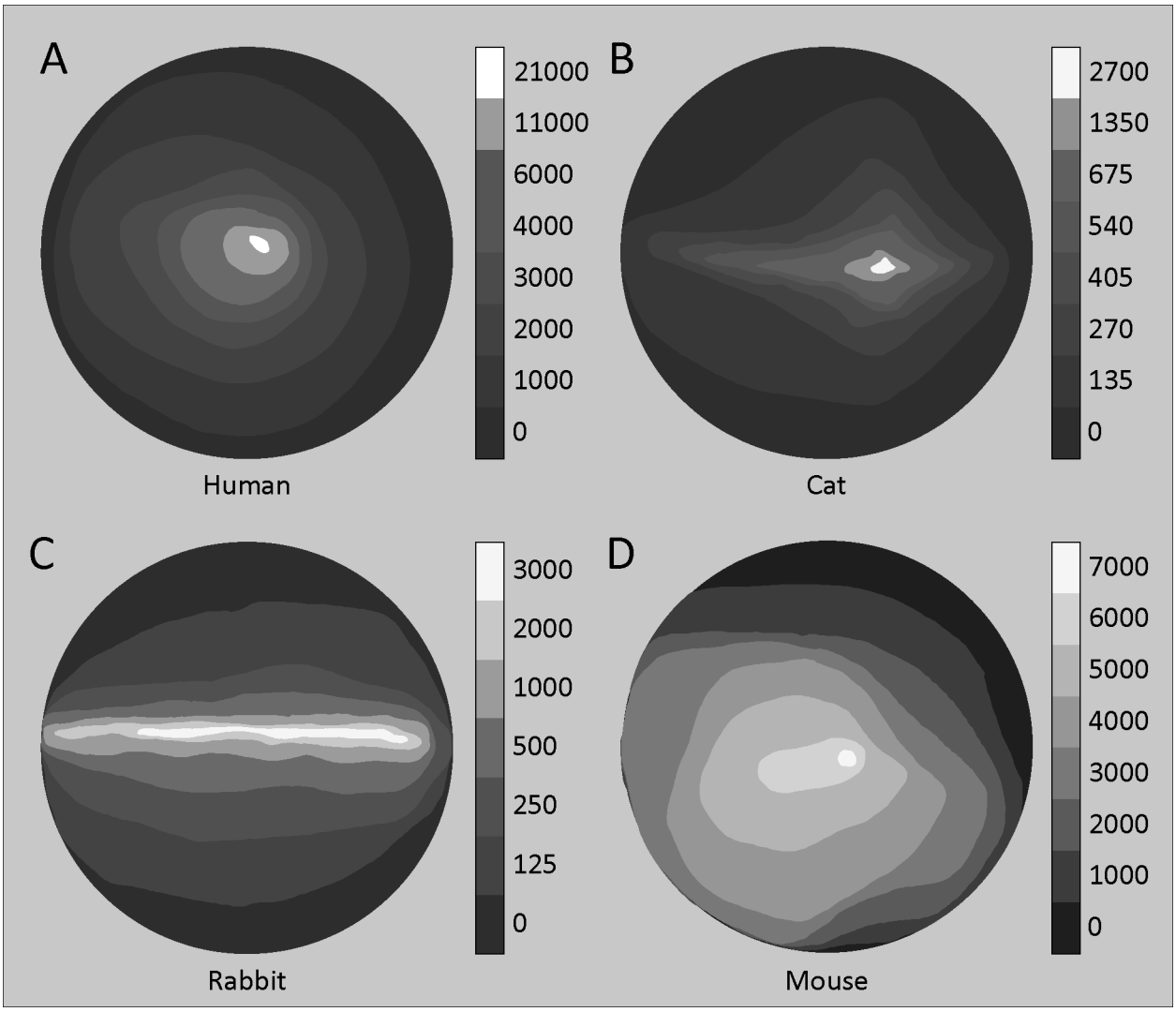

Figure 1.3 Examples of different retinal ganglion cell (RGC) topographies found across species. **(A)** Ganglion cell topographies within primates such as humans show a high-density fovea centralis (white), with a steep gradient of RGC density radiating in concentric rings (Curcio and Allen 1990; Harman et al. 2000). **(B)** In species such as cat, the area of high RGC density (area centralis, white) is found in temporal retina, and the gradient of RGC density displays an elongation into nasal retina (Hughes 1975; Stone 1978; Chalupa et al. 1984). **(C)** In rabbit the peak RGC density is distributed across the horizon of the retina in a visual streak (white) with a gradient that falls off dorsal and ventral (Hughes 1971; Provis 1979). **(D)** The topography of RGCs in the mouse is more uniform across the retina, with increased density in ventral and nasal retina (Dräger and Olsen 1981; Salinas-Navarro et al. 2009). In all schematics dorsal is up and temporal is right. Numbers represent cell/mm^2.

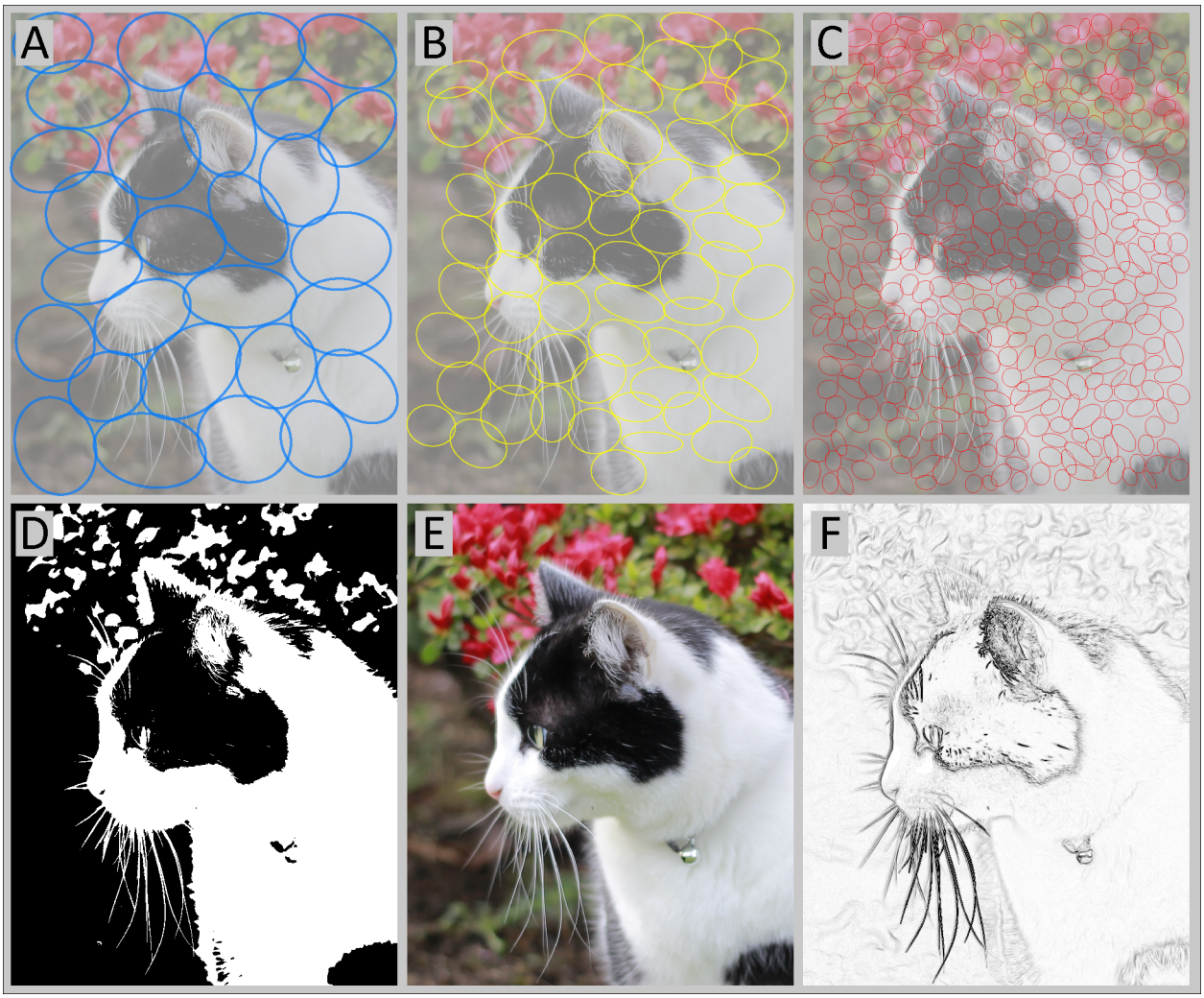

Figure 1.4 Depiction of parallel processing of the visual scene by feature specific multiple retinal ganglion cell (RGC) types.

(A-C) Each type of RGC uniformly samples the visual scene by mosaic tiling of its receptive fields across the retina. Ganglion cells with different sized dendritic arbors can have different size receptive fields, allowing them to detect and encode a range of spatial frequencies within the visual scene. **(D)** Some RGCs are responsive to specific spatiotemporal information such as, increments and/or decrements in light, chromatic information **(E)**, or local contrast edges **(F)**. Together, the total population of retina RGCs represents a distributed array of feature detecting sensory receptors (Lettvin et al. 1959; DACEY 2004; Field and Chichilnisky 2007; Berson et al. 2008; Azeredo da Silveira and Roska 2011; Dhande and Huberman 2014).

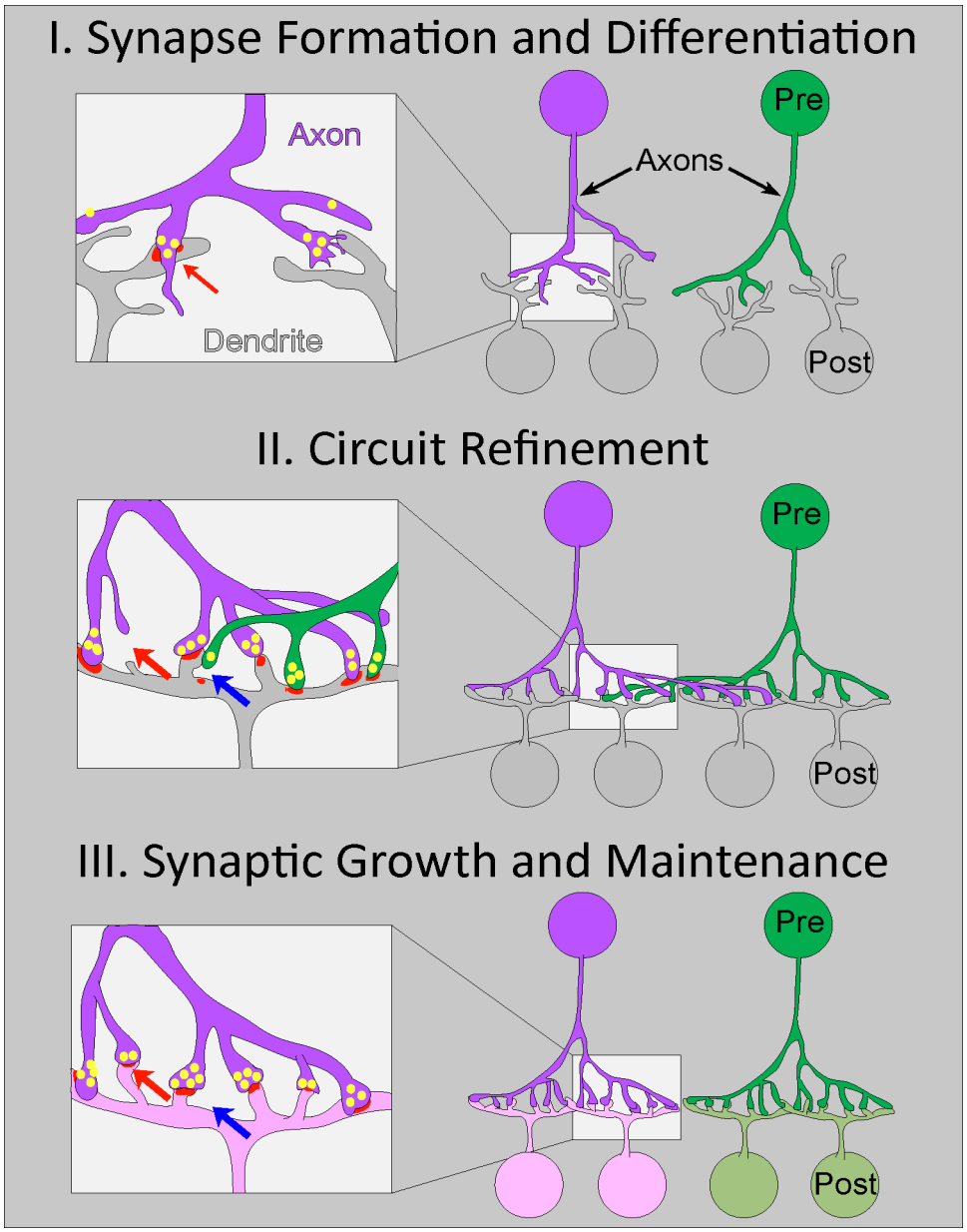

Figure 1.5 Stages of circuit development: simplified view of the major developmental events underlying the assembly of neuronal circuits.

I: Both axons and dendrites show marked motility during early stages of neuronal growth. Some sites of contact differentiate into synapses (e.g. red arrow) upon the recruitment of pre- (yellow) and postsynaptic (red) proteins. II: Many circuits undergo a period of refinement in their initial pattern of connectivity by the removal of erroneous contacts (compare with III). Individual presynaptic cells may contact more postsynaptic cells than at maturity (greater divergence), and single postsynaptic cells may receive inputs from inappropriate presynaptic cells (greater convergence). Note that synapse elimination (blue arrow) and synapse formation (red arrow) can take place concurrently. III: Mature patterns of circuits are established not only by synapse elimination but also by the subsequent growth and maintenance of appropriate connections.

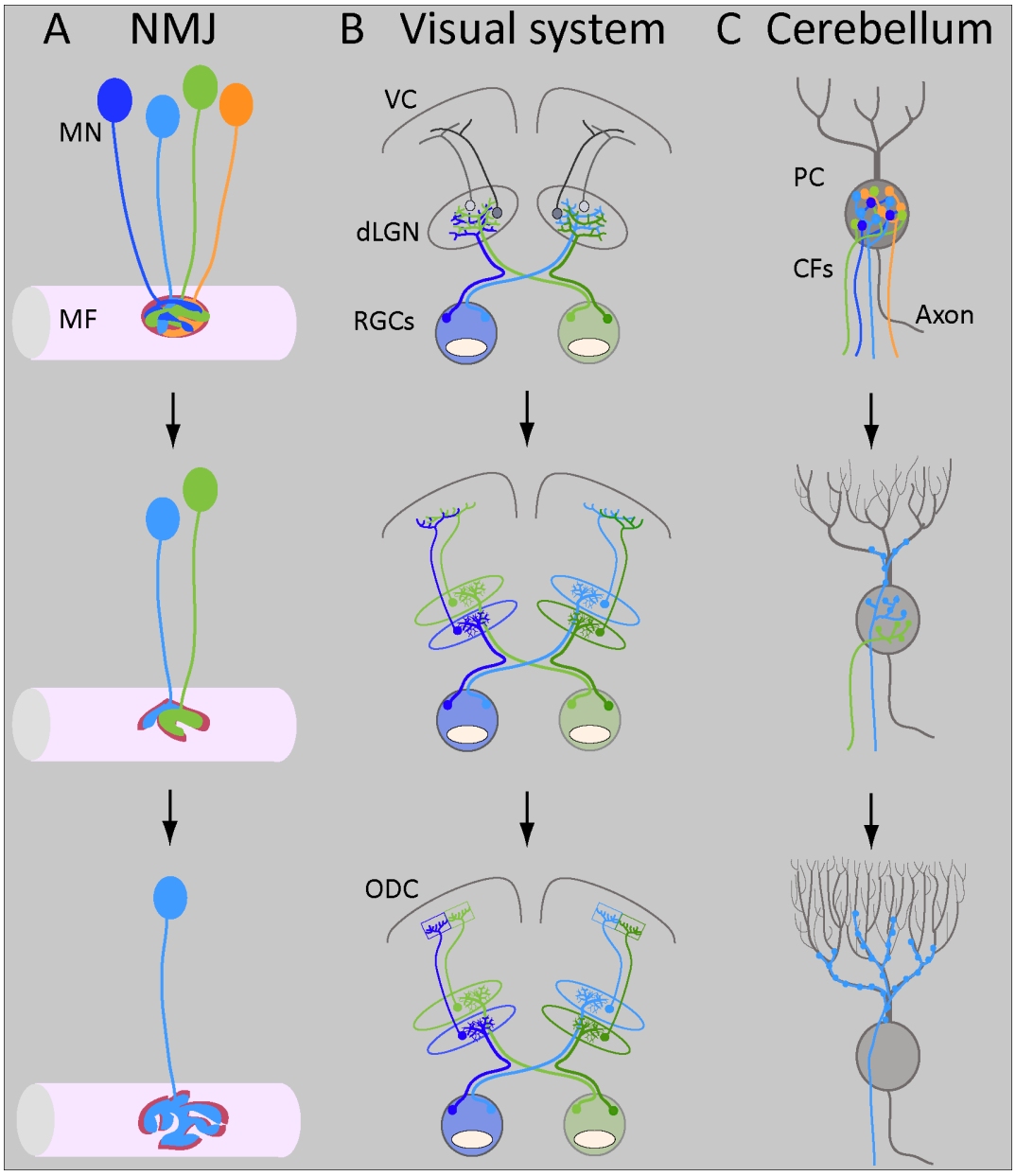

Figure 1.6 Circuits that refine their connectivity based on neurotransmission.
In many systems, postsynaptic cells receive erroneous connections that are eliminated by maturity. **(A)** At the mammalian neuromuscular junction (NMJ), multiple motor neurons (MN) contact a muscle fiber (MF) at a single junction in early development but only one axon remains at maturity. **(B)** In some vertebrate visual systems, connections from retinal ganglion cells (RGCs) representing the left and right eyes are segregated into eye-specific layers in the dorsal lateral geniculate nucleus (dLGN) and ocular dominance columns (ODCs) in the visual cortex (VC). Eye-specific layers form prior to eye opening and before ODCs appear. **(C)** In the rodent cerebellum, multiple cells from the inferior olivary nucleus make climbing fiber (CF) connections onto the cell body of each Purkinje cell (PC). All but one input is subsequently removed, and the remaining climbing fiber expands its territory to innervate the proximal dendrites of the Purkinje cell.

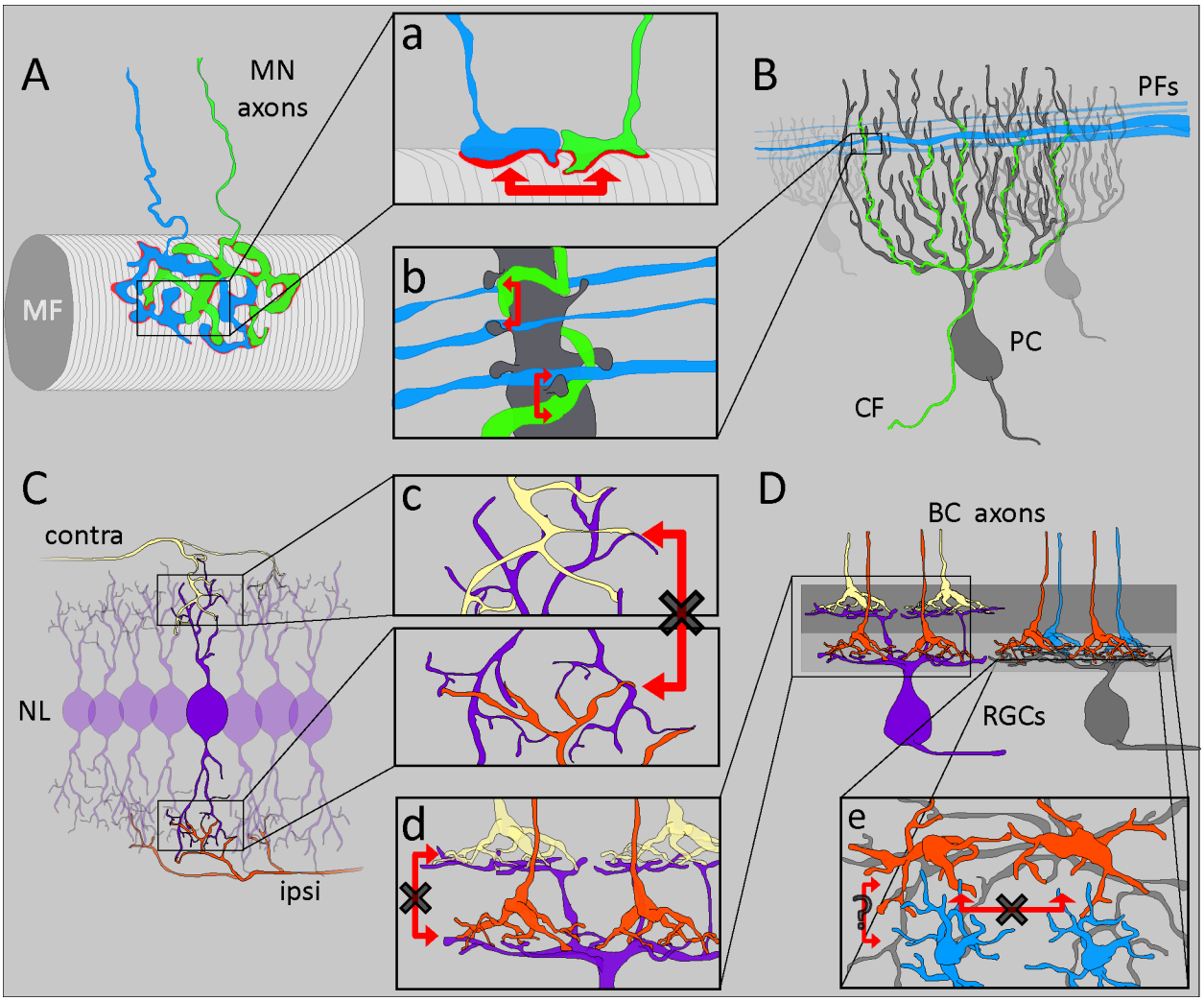

Figure 1.7 Limitation to neurotransmission-mediated circuit refinement.
(A) Neurotransmission dependent elimination of motor neuron (MN) axonal inputs that initially overlap at the neuromuscular junction is thought to employ local ‘‘punishment’’ signals (red arrows, **a**; (Jennings 1994)). MF, muscle fiber. **(B)** Parallel fibers (PFs) make connections primarily onto the distal dendrites and a single climbing fiber (CF) innervates the proximal dendrites of cerebellar Purkinje cells (PC). While climbing fibers are the first to innervate Purkinje cells, their territory becomes intermingled with the inputs of parallel fibers later in development. Disruptions to neurotransmission from either PFs or CFs result in a local take over of territory by the more active input (red arrows, **b**; (Hashimoto et al. 2009)). **(C and D)** Not all circuits with converging afferents display neurotransmission-mediated competition. **(C)** Inputs representing the ipsilateral (ipsi) and contralateral (contra) ears contact separate dendritic arbors of nucleus laminaris (NL) neurons of the auditory brainstem. These inputs do not intermingle even during development. If transmission is disrupted in one set of inputs, synaptic takeover does not occur (Deitch and Rubel 1984). **(D)** Similarly, in the mammalian retina, the axons of OFF bipolar cells (BCs) do not innervate the retinal ganglion cell (RGC) dendrites contacted by ON BC axons with suppressed transmitter release (Kerschensteiner et al. 2009). The apparent absence of activity-dependent

mechanisms (crossed arrows in **c**, **d**) in shaping the selectivity of inputs in the NL and retina may be because distinct types of afferents in their circuits show little to no spatial overlap. This limitation is also present at neighboring BCs or the same type whose, axonal arbor tile at maturity, likely restricting their ability to utilize neurotransmission to determine their relative amount of contact with retinal ganglion cells (RGCs) (**e**, en face view of the retina) (Okawa et al. 2014). It remains to be determined if different BC types, with overlapping axonal arbors can utilize neurotransmission to regulate their connectivity.

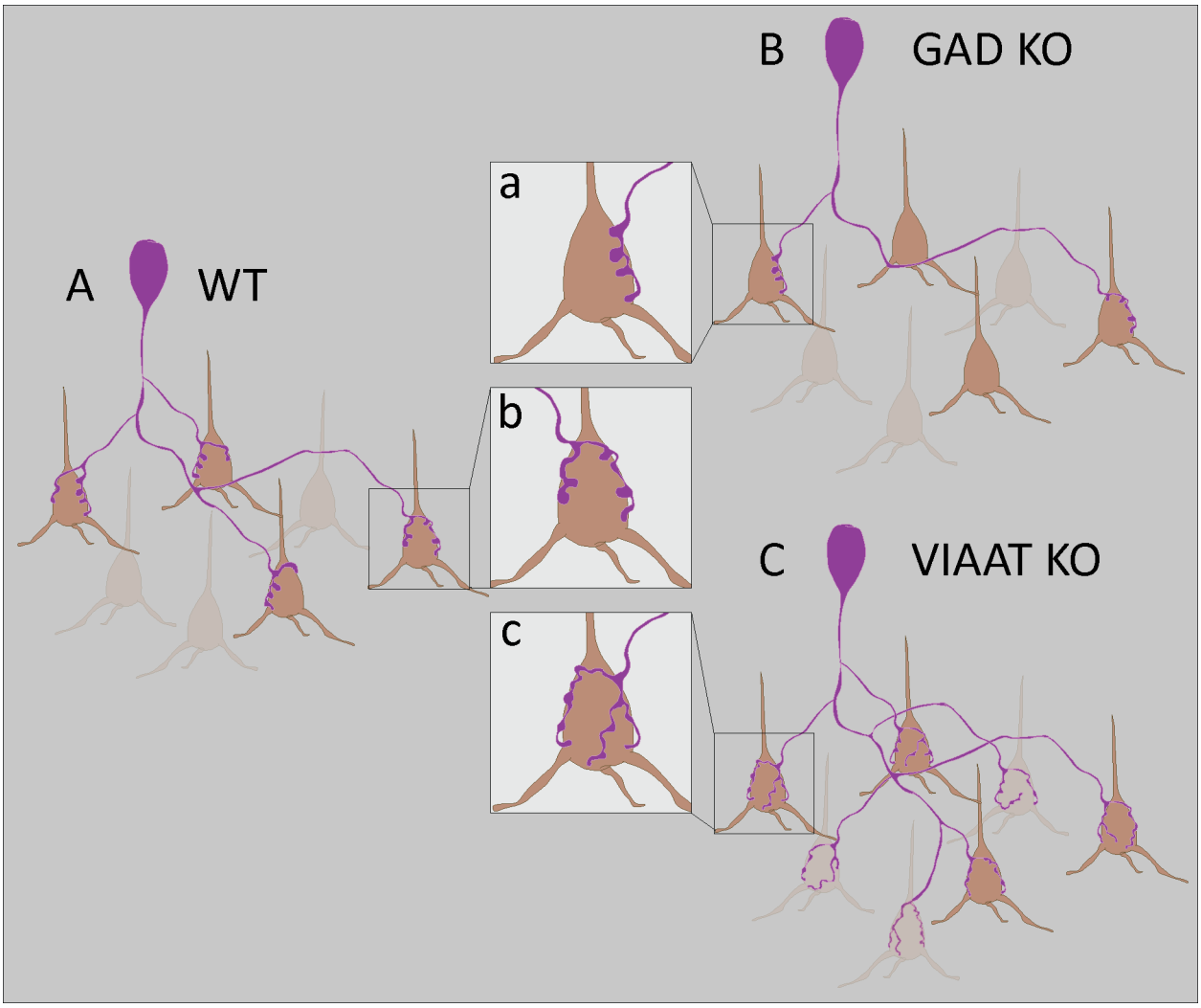

Figure 1.8 Differential effects of altering inhibitory neurotransmission on circuit connectivity in visual cortex.

(A) Inhibitory basket interneurons (purple) in wildtype (WT) visual cortex make multiple somatic connections with neighboring pyramidal cells. During maturation they refine their connections to maintain connections with appropriate targets (brown) and remove connections with inappropriate targets (tan), and form basket like varicosities surrounding the somata **(b)**. **(B)** In the GAD KO basket neurons have sparser axonal arbors and make fewer connections with pyramidal neurons, and onto individual pyramidal somata **(a)** (Chattopadhyaya et al. 2007a). **(C)** In the VIAAT KO the axonal arbors of basket interneurons are greatly expanded, and they make more contacts with pyramidal neurons, and their somata, however, these connections are smaller than in WT **(c)** (Wu et al. 2012).

CHAPTER II

VISUAL SPACE IS REPRESENTED BY NON-MATCHING TOPOGRAPHIES OF DISTINCT MOUSE RETINAL GANGLION CELL TYPES*

2.1 SUMMARY

The distributions of neurons in sensory circuits display ordered spatial patterns arranged to enhance or encode specific regions or features of the external environment. Indeed, visual space is not sampled uniformly across the vertebrate retina. Retinal ganglion cell (RGC) density increases and dendritic arbor size decreases towards retinal locations with higher sampling frequency, such as the fovea in primates and area centralis in carnivores (Wässle and Boycott 1991). In these locations, higher acuity at the level of individual cells is obtained because the receptive field center of a RGC corresponds approximately to the spatial extent of its dendritic arbor (Peichl and Wässle 1983; Yang and Masland 1994). For most species, structurally and functionally distinct RGC types appear to have similar topographies; collectively scaling their cell densities and arbor sizes towards the same retinal location (Collin 2008). Thus, visual space is represented across the retina in parallel by multiple distinct circuits (Field and Chichilnisky 2007). In contrast, we find a population of mouse RGCs, known as alpha or alpha-like (Peichl 1991), that displays a nasal-to-temporal gradient in cell density, size and receptive fields, which facilitates enhanced visual sampling in frontal visual fields. The distribution of alpha-like RGCs contrasts with other known mouse RGC types, and suggests that unlike most mammals, RGC topographies in mice are arranged to sample space differentially.

---

* This chapter was published in Current Biology, which maintains copyrights for this material, and has been reprinted with permission. The full citation for this publication is: Bleckert A, Schwartz GW, Turner MH, Rieke F, Wong RO. Visual Space Is Represented by Nonmatching Topographies of Distinct Mouse Retinal Ganglion Cell Types. *Curr Biol* , 2014.

2.2 METHODS

Mice

All procedures were conducted with the approval of the University of Washington Institutional Animal Care and Use Committee. Mice were euthanized by isoflurane overdose followed by decapitation, or by cervical dislocation. *Thy1-YFPH* mice (Feng et al. 2000) or *Grm6-tdTomato* mice (Kerschensteiner et al. 2009) of postnatal day (P)24 were used for anatomical experiments. C57BL/6 mice of age 4-10 weeks were used for physiological experiments.

Fixed Tissue Preparation

Mice were euthanized, enucleated and the eyes were immersed in oxygenated mouse artificial cerebral spinal fluid (mACSF) containing the following in (mM): 119 NaCl, 2.5 KCl, 2.5 $CaCl_2$, 1.3 $MgCl_2$, 1 NaH_2PO_4, 11 glucose, and 20 HEPES, brought to pH 7.42 with NaOH. Retinas were mounted flat, ganglion cell side up, onto filter paper (Millipore), and the tissue was subsequently fixed in 4% PFA for 20 min at room temperature. Retinal orientation was preserved using a anatomical landmarks previously described (Wei et al. 2010).

Immunohistochemistry

Retinas were washed in PBS and blocked overnight at 4°C in normal donkey serum. Retinas were then incubated in primary antibodies for 4 nights at 4°C. Primary antibodies used were: anti-nonphosphoneurofilament H (~mouse [1:1000], SMI-32, Sternberger Monoclonals Incorporated), anti-ChAT (~goat [1:100], AB144P, Chemicon), anti-synaptotagmin2 (~ms [1:200], ZNP-1, ZIRC), and anit-Lucifer Yellow (~rabbit [1:1000], A5750, Invitrogen). Retinas were then washed and incubated with secondary antibodies, Alexa (Invitrogen, 1:1000), or DyLight (Jackson Laboratory, 1:1000) conjugated fluorophores overnight at 4°C.

Image Acquisition

Image stacks were acquired using an Olympus FV-1000 laser scanning confocal microscope with an oil-immersion 20x objective (Olympus, UPLSAPO 0.85 NA). Voxel dimensions were (x-y-z in µm) 0.397-0.397-1.5 for reconstructions of entire whole-mounted mouse retinas, and 0.3-0.3-0.3 for individual RGCs acquired for quantification of dendritic morphology and stratification. Image stacks of bipolar cells were obtained using an oil-immersion 60x objective (Olympus, UPLSAPO 1.35 NA) with voxel dimensions (x-y-z in µm) 0.09-0.09-0.3. Images were median filtered to remove noise, corrected for xy drift (Thévenaz et al. 1998), and compressed to 8-bits after normalization of the entire stack histogram using Fiji (Schindelin et al. 2012). Mosaic stacks were auto-stitched together (Preibisch et al. 2009) and reconstructed in TrakEM2 (Cardona et al. 2012).

Mapping of SMI-32 labeled RGCs

$A_{ON\text{-}S}$ and $A_{OFF\text{-}T}$ RGCs were identified based on the intense labeling of their somata and dendritic arbors by SMI-32. Whereas other cell bodies in the ganglion cell layer are dimly labeled by SMI-32, only the dendritic arbors of $A_{ON\text{-}S}$, and of $A_{OFF\text{-}T}$ RGCs are labeled. This dendritic labeling allows for $A_{ON\text{-}S}$ and $A_{OFF\text{-}T}$ RGCs to be readily distinguished based upon their stratification relative to labeled cholinergic ChAT plexuses (Movie 2.1). Cell body positions of $A_{ON\text{-}S}$ and $A_{OFF\text{-}T}$ RGCs were recorded using the ROI manager of Fiji, and total retinal area was defined by marking the outline of the wholmounted retina stained by SMI-32. These parameters were imported to custom MATLAB (MathWorks) scripts for subsequent analysis.

RGC density maps and quantification

The density of cells at a given point on the retina was defined as the number of cells within a circle of diameter 1000 μm centered at that point, divided by the area of the circle. This calculation was iterated across every point on the retina at a resolution of 2 μm. To correct for edge effects, only the area of the circle within the total retinal area was utilized. For quantification of cell densities across retinas, the number cells per 1 mm^2 (1000x1000 μm) regions of nasal or temporal retina was counted.

Density recovery profile

The density recover profile (DRP) for $A_{ON\text{-}S}$ RGCs was calculated as described (Rodieck 1991). Briefly, the density of cells in 20 μm radial bins from each reference cell up to 200 μm was calculated for 1 mm^2 (1000x1000 μm) regions of nasal and temporal retina. The DRP was calculated for cells only within the inner 60% of the region to avoid edge effects.

Nearest neighbor analysis

Neighbor distances for cells identified in 1 mm^2 (1000x1000 μm) regions of nasal or temporal retina were calculated from the Delaunay triangulation of their positions. To remove edge effects of the sampled region, only neighbor distances were calculated between cells whose triangulation points lie within the region sampled.

Quantification of individual RGCs

The dendrites of RGC were skeletonized and their volume rendered using the filament function of Imaris (Bitplane). Total dendritic length, number of dendritic segments, mean segment length, 2D convex hull territory area, and number of Sholl crossings / 5 μm were calculated from the skeletonized filament. The circle diameter of each RGC was defined as the diameter of a circle whose equivalent area matched that of the 2D polygonal area. RGC soma area was calculated from a surface function of Imaris (Bitplane),

fitted to the maximum intensity projection of the soma. Soma diameter was defined as the diameter of a circle whose equivalent area matched that of the surface object area.

Position on retina

The eccentricity of a cell was mapped as its distance to the optic nerve head. To obtain a cell's position along the nasal-temporal axis, maximum intensity projections of whole-mount retinas were oriented so that the dorsal-ventral axis was set to vertical, and the nasal-temporal axis was set to horizontal. The nasal and temporal poles were defined by marking the most nasal and most temporal extents of the labeled retina. Each cells position was defined as its ratio of distance from the nasal pole to temporal pole projected onto the horizontal (nasal = 0 and temporal =1) of the retina.

Dendritic stratification

To quantify the level of stratification of a cell's dendritic arbor within the inner plexiform layer (IPL) of the retina, we mapped the location of skeletonized dendrites of individual cells as their percent distance from the inner nuclear layer (0%) to the ganglion cell layer (100%). The inner nuclear layer and ganglion cell layer were defined by the somata positions of OFF and ON starburst amacrine cells (SAC) labeled by the ChAT antibody, and identified using the spots function of Imaris. To correct for curvature, and irregularities in the flatness of the IPL in image stacks, the stratification of each node of the skeletonized filament was determined locally by its percent distance between the mean stratification levels of its nearest 3 ON and OFF SACs.

Quantification of bipolar cell axonal arbors

Individual type 6 bipolar cells were imaged from nasal and temporal retina regions. Their axons were identified by either immunoreactivity for synaptotagmin2 alone, or by synaptotagmin2 labeling and

tdTomato expression in *Grm6-tdTomato* mice (Kerschensteiner et al. 2009). Each axon's volume was segmented using the surface function of Imaris. Their axonal territory area was defined as the area of the convex hull of the Z projection of the segmented axonal arbor.

Visual field projections from reconstructed retinas

Right and left whole-mount retinas, in which all $A_{ON\text{-}S}$ RGCs were identified, were reconstructed into a standard spherical retina space using the Retistruct package (Sterratt et al. 2013). For mapping RGC distributions into visual space, the optical axis of the mouse eye was set at 64° azimuth and 22° elevation. The rim colatitude was set at 115.57 as determined for P22 mice (Sterratt et al. 2013). The sinusoidal projection of visual space is presented as though the mouse is facing the reader.

Physiological recordings

Cell recordings were performed as described previously (Murphy and Rieke 2006). Briefly, wedges of dark-adapted retina were removed from the sclera and retinal pigment epithelium and mounted, photoreceptor-side down, on a D-polylysine coated coverslip. $A_{ON\text{-}S}$ RGCs were targeted for whole-cell recording according to their soma size, morphology and the presence of a sustained spike response to light stimuli during loose-patch recording. Loose patch-recording pipettes contained Ames' solution and whole-cell voltage clamp recordings were made using a cesium-based internal solution containing the following in (mM): 105 $CsCH_3SO_3$, 10 TEA-Cl, 20 HEPES, 10 EGTA, 5 Mg-ATP, 0.5 Tris-GTP, 2 QX- 314 and 0.2 Alexa Fluor 488 or HiLyte Fluor 750, or 0.1 Lucifer Yellow (pH ~7.3 with CsOH, ~280 mOsm). For subsequent imaging and immunohistochemistry, retinas were transferred onto filter paper (Millipore), ganglion cell side up, and the tissue was subsequently fixed in 4% PFA for 20 min at room temperature.

Visual stimulation

Visual stimuli from an OLED monitor (eMagin, Bellevue, WA) were focused onto the photoreceptor outer segments from below. All experiments were carried out at a mean light level producing approximately 500 Rhodopsin isomerizations/rod/s. $A_{ON\text{-}S}$ RGCs were adapted to this background luminance level for at least 10 minutes. RGCs were judged suitable for recording if they showed robust, reliable responses to 10% positive contrast spots over the receptive field center.

Mapping of receptive and dendritic fields

Receptive field center size measurements were made by isolating excitatory synaptic currents in voltage-clamp and presenting 300% contrast bars (36 µm width) for 500 ms in sequence across the receptive field along the vertical and horizontal axes of the monitor. The integrated inward charge transfer (average over 5-10 trials) during bar presentation was taken as the response amplitude for each bar location. Gaussian curves were fit ($r^2 > 0.80$ for all cells) to the response profile in each dimension. Receptive field area was defined as the area of an ellipse with its major and minor axes equal to the 2-standard deviation widths of these two Gaussian fits. After recording, an image of each cell was taken using a confocal microscope or an infrared epifluorescence imaging camera (Andor, South Windsor, CT). Dendritic field area was measured by fitting a convex hull around the dendrites in Fiji. The circle diameter of each RGC is defined as the diameter of a circle whose area matched that of the 2D polygonal area of the dendritic field or the area of the ellipse of the receptive field. To determine if temporal and nasal dendritic and receptive fields were significantly different, the recorded RGCs were separated into temporal and nasal samples by the mean of the population of dendritic field sizes (~250 µm). Temporal dendritic field size was found to be significantly different from receptive field size ($p = 0.3$), whereas nasal dendritic and receptive field sizes were not ($p = 0.4$) (two sample t-test, unequal variance).

Dendritic and Receptive Field Coverage Factor

The coverage factor of dendritic fields was calculated by averaging the overlap of circles with equivalent dendritic diameters mapped onto each of the identified cells in 1 mm^2 (1000x1000 μm) regions of nasal or temporal retina. The diameter for each identified cell was defined by the linear relationship between each cell's 5 nearest neighbors (Delaunay neighbors, Figure 2.4A) and dendritic diameter (Figure 2.5B). The receptive field diameter for each identified cell was then defined by the linear relationship between cell diameter and receptive field diameter (Figure 2.5E). Both the dendritic and receptive field coverage factors were calculated from only the inner 60% of each region to avoid edge effects. Colormaps were generated using the perceptually improved colormaps function (pmkmp.m, Matlab MATHWORKS).

RGC Density Color Maps: Schematized topographic distributions

For each density colormap, a 2D representation of the retina is schematized such that maximum and minimum cell densities are plotted at locations relative to the optic nerve head and the retinal poles (Dorsal-Ventral, Nasal-Temporal) according to previous reports, or from density maps generated in the current study. The 2D density gradients are plotted as a linear change from maximum to minimum densities, and represented by a linear colormap generated using the perceptually improved colormaps function (pmkmp.m, Matlab MATHWORKS).

Statistical Analysis

All data are shown as mean ± SEM. Statistical analysis was performed using the two-sided Wilcoxon ranksum test, or two-sample t-test with unequal variance as stated.

2.3 Results and Discussion

Mouse ON alpha-like RGCs display a nasal to temporal gradient in cell density and dendritic arbor size

Alpha-like mouse retinal ganglion cells (RGCs) segregate into three populations: ON-sustained ($A_{ON\text{-}S}$), OFF-transient ($A_{OFF\text{-}T}$), and OFF-sustained ($A_{OFF\text{-}S}$) (Pang et al. 2003; Schubert et al. 2005; Völgyi et al. 2005; van Wyk et al. 2009). Alpha RGCs are readily identified by labeling neurofilaments (Peichl et al. 1987), and in mouse, the antibody SMI-32 directed against nonphosphorylated neurofilament heavy chain readily labels $A_{ON\text{-}S}$ and $A_{OFF\text{-}T}$ alpha-like RGCs, but not $A_{OFF\text{-}S}$ (Figure 2.1A,B and Movie 2.1) (Coombs et al. 2006; Huberman et al. 2008b). When we systematically mapped the distributions of $A_{ON\text{-}S}$ RGCs labeled by SMI-32, we found a pronounced gradient in their density (>3 fold difference) increasing from nasal to temporal retina, peaking at a temporal-dorsal location (Figure 2.1A,B and 2.2). We then reconstructed the individual arbors of SMI-32 labeled $A_{ON\text{-}S}$ RGCs using the *Thy1-YFPH* transgenic line (Feng et al. 2000), in which RGCs are sparsely labeled, and found that the increase in $A_{ON\text{-}S}$ RGC density is paralleled by a reduction in dendritic arbor size (Figure 2.1C and 2.3). Quantification of the dendritic arbors revealed that the size of each $A_{ON\text{-}S}$ RGC, represented by the diameter of a circle with an area equivalent to its arbor area (see Methods), scaled linearly across the nasal-temporal axis of the retina (Figure 2.1D), whereas no relationship existed between arbor size and retinal eccentricity from the optic nerve head (Figure 2.1E). Previously mouse RGC types have been believed to be relatively uniformly distributed across the retina, and have largely been classified according to soma and dendritic arbor size, branching patterns and stratification level (Sun et al. 2002; Badea and Nathans 2004; Kong et al. 2005; Völgyi et al. 2005; Coombs et al. 2006; Völgyi et al. 2009; Hong et al. 2011), unless a molecular-marker was available (Kim et al. 2008; Huberman et al. 2008b; Kay et al. 2011; Zhang et al. 2012; Hughes et al. 2013; Dhande et al. 2013). Based on these criteria, the alpha-like RGCs in different retinal regions were likely classified as distinct cell types in previous studies (see Table 2.1).

Further quantification of $A_{ON\text{-}S}$ RGCs indicated that their arbor size is proportional to total dendritic length, whereas soma size is uniform across cells (Figure 2.1F,G). $A_{ON\text{-}S}$ arbor size also correlated with mean dendritic segment length, but not with the total number of dendritic segments

(Figure 2.1H,I). To compare the branching patterns of $A_{ON\text{-}S}$ RGCs across the retina, we quantified dendritic branch number as a function of distance from the soma by calculating the number of Sholl intersections (Figure 2.1J). We found that the Sholl curves of $A_{ON\text{-}S}$ RGCs across retinal locations overlapped when normalized by their dendritic diameter size (Figure 2.1K; see Methods). This suggests that $A_{ON\text{-}S}$ RGCs simply scale up or down their dendritic arbors to increase or decrease their dendritic territory depending upon their position in the retina. These differences in size may be dictated by the local density of $A_{ON\text{-}S}$ RGCs, because homotypic interactions are known to regulate the dendritic territories of other mouse retinal neurons (Reese et al. 2005; Poché et al. 2008; Huckfeldt et al. 2009; Lee et al. 2011; Kay et al. 2012). Furthermore, manipulations to increase the total RGC density in cat retinas cause a decrease in alpha RGC size (Kirby and Chalupa 1986). However, homotypic regulation may not be consistent across all retinal neurons in mice (Lin et al. 2004).

$A_{ON\text{-}S}$ RGCs across the retina are arranged in mosaic distributions and have similar ON-sustained responses to light.

To further confirm that the SMI-32 labeled $A_{ON\text{-}S}$ RGCs represent variations of a single type of RGC, we performed two additional sets of experiments. First, we determined whether these cells exhibit a mosaic distribution, a feature delineating separate cell types in the retina. We mapped the distribution of $A_{ON\text{-}S}$ RGCs in 1 mm^2 regions of nasal and temporal retina and calculated their density recovery profile (Figure 2.4 and 2.2; see Methods). Populations in both regions displayed a zone of exclusion indicated by a decreased cell density near a reference cell; such an exclusion zone is a hallmark of cells distributed in a mosaic pattern (Rodieck 1991). The effective radius of this exclusion and the nearest neighbor distances in nasal retina were greater than those in temporal retina (Figure 2.4B). Second, we measured the light responses of $A_{ON\text{-}S}$ RGCs by recording whole-cell currents in response to brief steps of light from darkness (see Methods). Cells in both temporal and nasal regions showed sustained excitatory and

inhibitory currents in response to light onset, physiological hallmarks of $A_{ON\text{-}S}$ RGCs (Pang et al. 2003; Murphy and Rieke 2006; van Wyk et al. 2009). The retinas were fixed after electrophysiology and the recorded cells were subsequently confirmed to be SMI-32 positive (n = 11 out of 11 cells, 5 T and 6 N). Furthermore, nearest neighbor distributions confirmed that recorded small-arbor cells were in temporal retina, whereas large-arbor cells were located in nasal retina (examples; Figure 2.4C,D). Our structural and functional analyses therefore together uncovered a single population of RGC in the mouse retina resembling the ON-alpha RGC populations in other species (Peichl 1991).

Visual space in temporal retina has an enhanced sampling by $A_{ON\text{-}S}$ RGCs, but not by their dominant presynaptic partners

Why might $A_{ON\text{-}S}$ RGCs have an increased density in temporal retina? To gain insight, we first asked whether the dominant excitatory presynaptic partner of $A_{ON\text{-}S}$ RGCs (Schwartz et al. 2012), the type 6 cone bipolar cell (T6 BC) also scales its axonal field proportionally to the $A_{ON\text{-}S}$ RGCs dendritic arbor. Surprisingly, we found no change in the distribution of T6 BC axon sizes in nasal compared to temporal retina (Figure 2.5A). Thus, in this circuit, the presynaptic T6 BCs maintain a uniform sampling of visual space across the retina, whereas the postsynaptic $A_{ON\text{-}S}$ RGCs bias their sampling towards temporal retina. This is in contrast to species with specialized areas of central vision, where bipolar and ganglion cells both scale towards areas of peak density (Wässle and Boycott 1991; Chan et al. 2001).

To quantify how the change in size and density of $A_{ON\text{-}S}$ RGCs could affect sampling of the visual field, we first calculated their dendritic coverage factor (Figure 2.5B,C; see Methods). In temporal retina, dendritic coverage of $A_{ON\text{-}S}$ RGCs is 1.3x greater than in nasal retina (Figure 2.5D), i.e. any point in the retina is sampled, on average, by more $A_{ON\text{-}S}$ RGCs in temporal versus nasal retina. We next compared this dendritic coverage to the functional coverage of $A_{ON\text{-}S}$ RGCs by mapping the receptive field sizes for targeted $A_{ON\text{-}S}$ RGCs across the retina. The receptive field size of $A_{ON\text{-}S}$ RGCs does not parallel dendritic

field size; temporal $A_{ON\text{-}S}$ RGCs have greater receptive field size than their dendritic field size, whereas nasal $A_{ON\text{-}S}$ RGC dendritic and receptive field sizes appear more similar (Figure 2.5E; see Methods). This increase in receptive field size results in a further enhancement (2.2x) in coverage of the visual field by $A_{ON\text{-}S}$ RGCs in temporal compared to nasal retina (Figure 2.5F). Thus, each $A_{ON\text{-}S}$ RGC in temporal retina, not only encodes a smaller unit of visual space than in nasal retina, but also every point in space is sampled by a greater number of $A_{ON\text{-}S}$ RGCs.

What function might a population of RGCs with enhanced visual sampling in temporal retina serve? In rodents, ipsilateral projecting RGCs that underlie binocular vision are located in temporal retina (Dräger and Olsen 1980; Reese and Cowey 1986), and alpha-like RGCs, are overrepresented, ~10% of RGCs in the ipsilateral projecting population, whereas they constitute only ~1% of the total RGC population (Dräger and Olsen 1980; Dreher et al. 1985). Furthermore, the location of peak density of $A_{ON\text{-}S}$ RGCs is near the center of the rodent frontal visual fields (Dräger and Olsen 1980; Reese and Cowey 1986; Sefton et al. 1995; Sterratt et al. 2013) (Figure 2.6A,B). The mouse retina has commonly been believed to have a relatively uniform distribution of cell types across the retina (Jeon et al. 1998; Sun et al. 2002), and a cell type with a temporal - nasal gradient similar to those found in animals with clear binocular vision (Wassle et al. 1981; Peichl et al. 1987), is unexpected for mice. In addition to previous work showing alpha-like RGCs are adept at detecting fine-scale spatial patterns (Schwartz et al. 2012), processing chromatic information (Chang et al. 2013), and possibly displaying intrinsic photosensitivity (Ecker et al. 2010; Estevez et al. 2012), our work places $A_{ON\text{-}S}$ RGCs in this unique location specialized for encoding frontal vision.

The distributions of ON and OFF alpha-like RGCs differ from those of other known mouse RGCs and suggest an independent sampling of visual space by distinct RGC types

We next asked if the two known OFF alpha-like RGCs found in mouse also display similar distributions to ON alpha-like RGCs (Pang et al. 2003; van Wyk et al. 2009). We observed one OFF population of RGCs that varied in dendritic arbor size between nasal and temporal retina, in a manner paralleling $A_{ON\text{-}S}$ RGCs. The dendritic stratification and morphology of these cells are characteristic of $A_{OFF\text{-}S}$ RGCs (Pang et al. 2003; van Wyk et al. 2009) (Figure 2.3). This suggests that $A_{OFF\text{-}S}$ RGCs are also organized for enhanced sampling of visual space in temporal retina. Conversely, we found that the distribution of SMI-32 labeled $A_{OFF\text{-}T}$ RGCs varied much less across the retina (Figure 2.2) in contrast to most mammals (Peichl 1991), although similar to other rodents (Peichl 1989), which may be accompanied by some change in dendritic field size (Huberman et al. 2008b; Farrow et al. 2013). Taken together, our current mapping of the topographic distributions of cell densities and dendritic arbor sizes of alpha-like RGCs, strongly contrasts with that of known mouse RGCs (Figure 2.6C-D). Previous studies demonstrated a peak in W3 RGCs (presumed local edge detector) in ventral retina (Zhang et al. 2012), an increased density of M1 and M2 RGCs (intrinsically photosensitive) in dorsal retina (Hughes et al. 2013), and relatively flatter distributions for direction-selective RGC types, such as JAM-B (Kim et al. 2008; Hong et al. 2011), DRD4 (Huberman et al. 2009; Kay et al. 2011), BD RGCs (Kay et al. 2011; Hong et al. 2011) and Hoxd10 (Dhande et al. 2013). This raises a striking difference between the mouse retina and that of other mammals, whereby diverse RGC types in the mouse appear to exhibit distinct topographies and have adopted a strategy to customize the distributions of each RGC type to sample the visual environment.

2.4 CONCLUSIONS

In summary, our findings suggest that sampling of the visual scene by $A_{ON\text{-}S}$ RGCs is modulated across the retina by a non-uniform topographic distribution of their densities and receptive field sizes, distinct from the topographic patterns of other known mouse RGC types. The diversity of RGC distributions in the mouse retina suggests that visual space is not sampled uniformly by parallel processing circuits across

the retina in mice, but instead distinct populations of RGCs may be organized in separate topographies to encode specific visual features or regions (Kim et al. 2008; Huberman et al. 2009; Münch et al. 2009; Zhang et al. 2012; Hughes et al. 2013).

2.5 FIGURES & TABLES

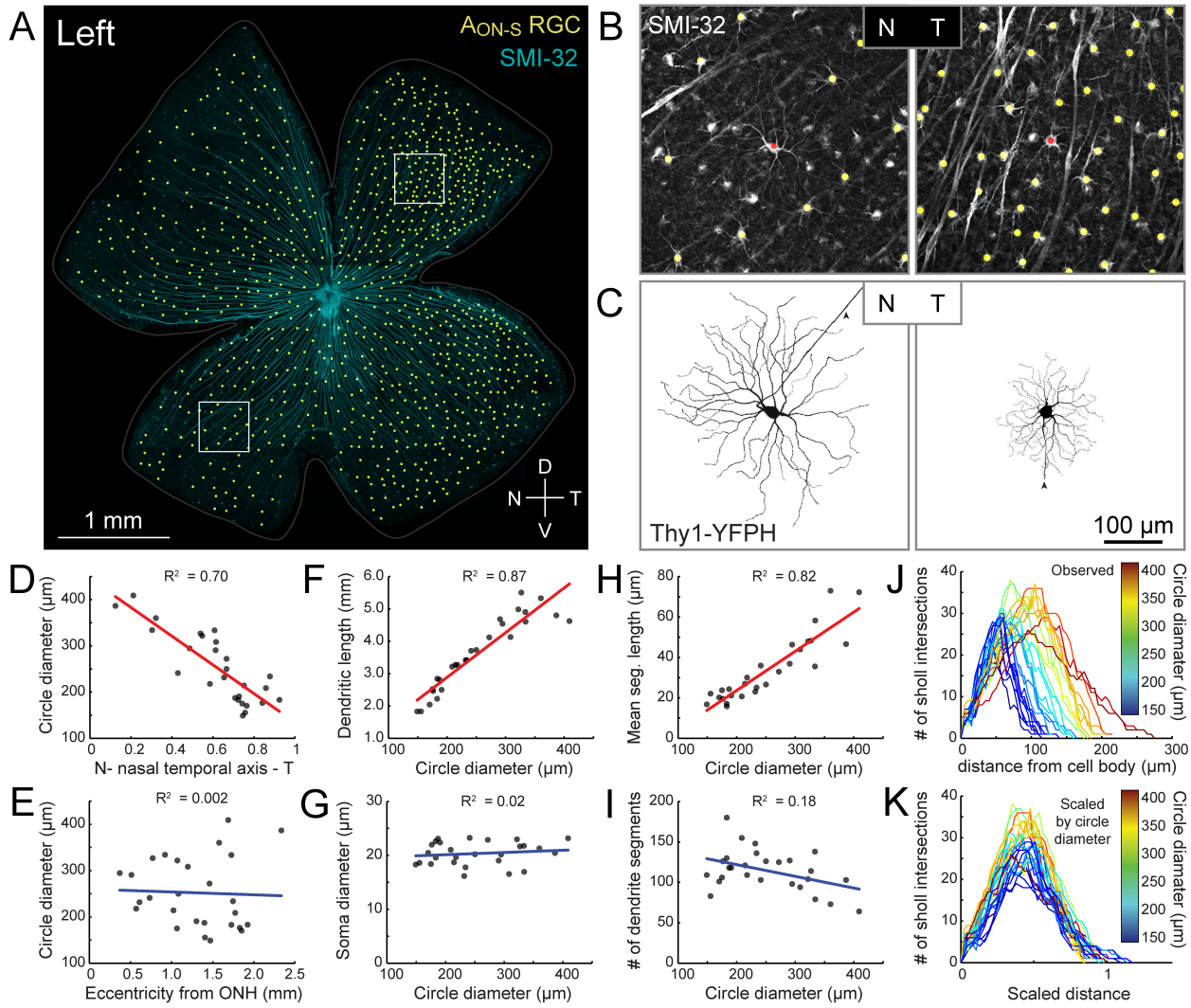

Figure 2.1 Cell density and size of AON-S retinal ganglion cells form inverse gradients across the mouse retina.

(A) Locations of $A_{ON\text{-}S}$ RGCs (yellow dots) labeled by SMI-32 immunostaining (cyan) in a whole mount retina (left eye) from a P24 mouse (V, ventral, D, dorsal, N, nasal, T, temporal). **(B)** Maximum intensity projections of image stacks encompassing SMI-32 labeled RGC somata and primary dendrites (grey) within the boxed regions in (A). $A_{ON\text{-}S}$ RGCs are identified by their relatively brighter cell bodies and dendrite labeling (yellow dots). **(C)** Sparse labeling of $A_{ON\text{-}S}$ RGCs in *Thy1-YFPH* transgenic mice enables visualization of the complete dendritic arbors of individual SMI-32 RGCs (red dots in B). Arrowhead demarcates RGC axon. **(D)** Dendritic arbor sizes of $A_{ON\text{-}S}$ RGCs represented by diameters of circles with areas equivalent to the arbor area (see Methods) are plotted across nasal-temporal retina. Relationships between $A_{ON\text{-}S}$ RGC size (circle diameter) and retinal eccentricity from the optic nerve head (ONH) **(E)**, total dendritic length **(F)**, soma size (**G),** mean segment length **(H)** and number of dendritic segments **(I)**. **(J)** Number of Sholl intersections as a function of the distance from the soma for each cell, and **(K)** Sholl intersections after normalizing the curves according to dendritic arbor size. (n = 2 retinas, 27 RGCs).

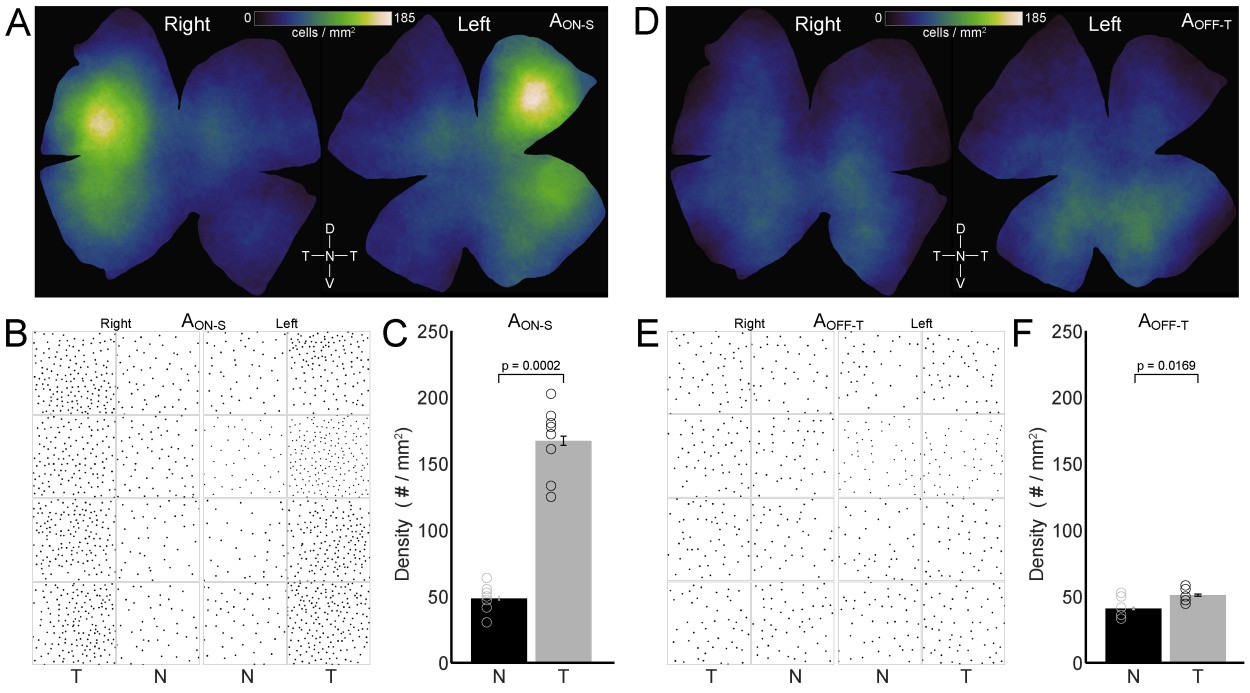

Figure 2.2 The densities of SMI-32 labeled alpha-like RGCs across the retina.

(A) Density maps of $A_{ON\text{-}S}$ RGCs across the retina. Shown are examples from the left retina displayed in Figure 1 and the corresponding right retina from the same mouse; note the peak density in temporal (T) - dorsal (D) retina. **(B)** Example mosaic distributions of $A_{ON\text{-}S}$ RGC bodies identified from 1 mm^2 nasal and temporal regions imaged from right and left retinas. **(C)** Quantification of average $A_{ON\text{-}S}$ cell densities from the regions in (B), (N = 48.60, T = 167.34 cells / mm^2; n = 8 retinas). **(D)** Density maps of $A_{OFF\text{-}T}$ RGCs from the same retinas as in (A). $A_{OFF\text{-}T}$ RGC density is more uniform across the retina. **(E)** Example mosaic distributions of $A_{OFF\text{-}T}$ RGCs from the same regions in (B). **(F)** While there does not appear to be a peak density of $A_{OFF\text{-}T}$ RGCs in temporal - dorsal retina, the density of $A_{OFF\text{-}T}$ RGCs in temporal retina is slightly but significantly greater than that of cells in the nasal retina (N = 40.97, T = 51.03 cells / mm^2; n = 8 retinas). Data are shown as mean ± SEM.

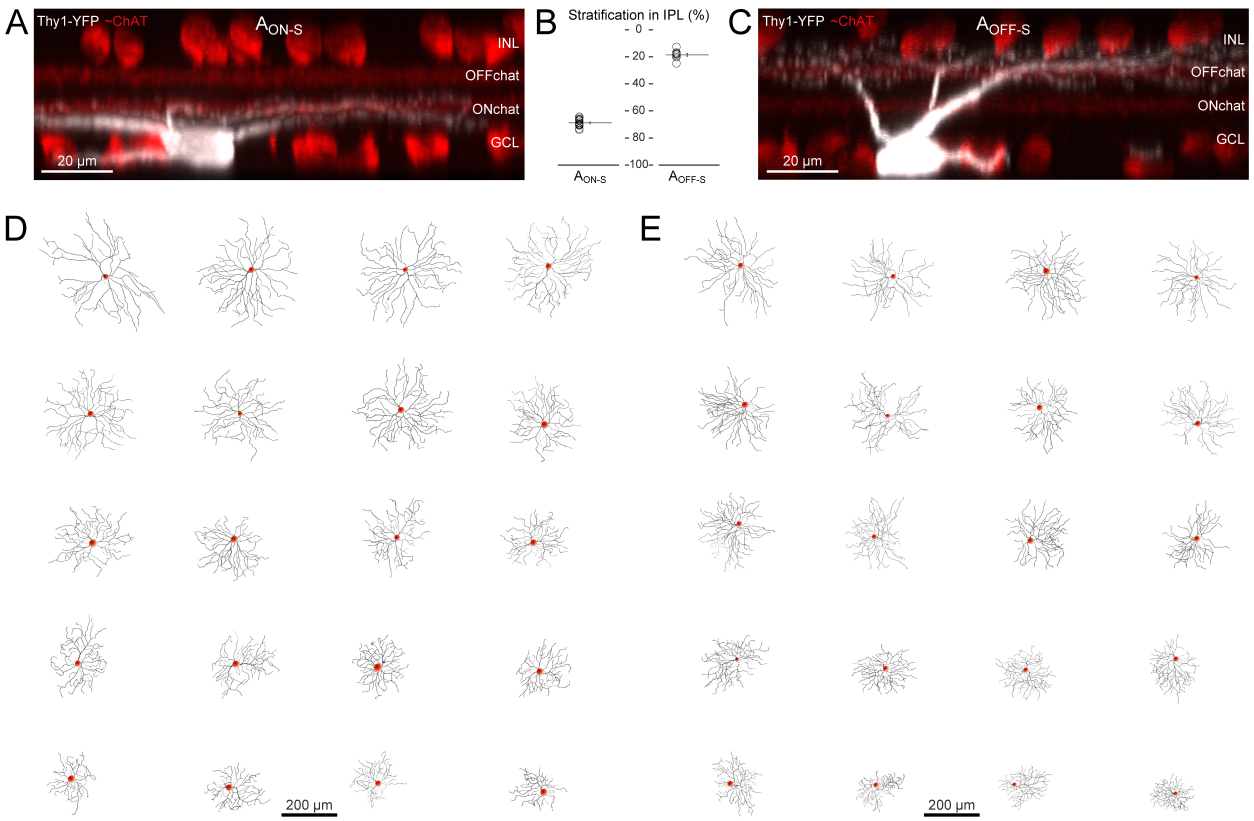

Figure 2.3 AON-S and AOFF-S RGCs show similar scaling in their dendritic arbors sizes.
(A) Sideview of the maximum intensity projection of an A_{ON-S} RGC labeled in the *Thy1-YFPH* line showing its stratification within the IPL. The majority of the dendritic arbors of the A_{ON-S} RGC stratify between the ON ChAT band and the ganglion cell layer (GCL). **(B)** Quantification of the stratification of A_{ON-S} and A_{OFF-S} RGCs. (n = 7 retinas, 36 RGCs) **(C)** Sideview of the maximum intensity projection of an A_{OFF-S} RGC labeled in the *Thy1-YFPH* line showing its stratification within the IPL. The majority of the dendritic arbors of the A_{OFF-S} RGCs stratify between the OFF ChAT band and the inner nuclear layer (INL). **(D)** Skeletonized dendritic arbors of A_{ON-S} RGCs reconstructed from nasal to temporal retina show a gradient in size. **(E)** Skeletonized dendritic arbors of A_{OFF-S} RGCs also show a gradient in size from nasal to temporal retina. Data are shown as mean ± SEM.

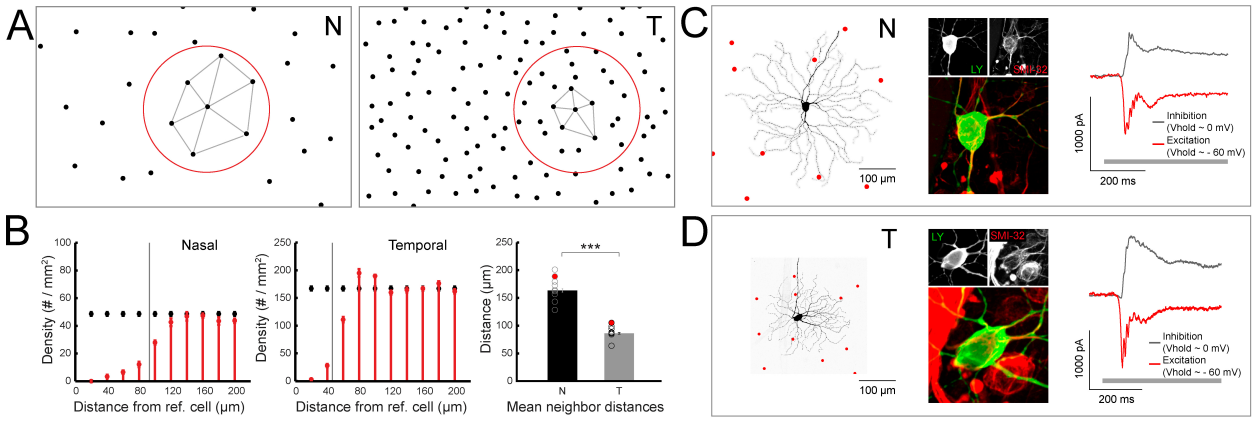

Figure 2.4 $A_{ON\text{-}S}$ RGCs have mosaic distributions and characteristic ON sustained responses to light stimuli.

(A) Example spatial distributions of $A_{ON\text{-}S}$ RGCs (black dots), sampled from nasal (N) and temporal (T) retina. The density recovery profile (DRP) was calculated using a 200 µm radius (red circles). Nearest neighbor distances (grey lines) were calculated for every RGC within a region. **(B)** DRP plots of $A_{ON\text{-}S}$ RGCs as a function of distance from the reference cell (red) compared to the DRP of cells with a random distribution (black). The effective radius of exclusion for nasal regions is greater than for temporal (grey vertical lines, N = 93.2, T = 46.5 µm, $p < 0.0002$), but the packing factor was not (T = 0.31, N = 0.36, $p = 0.10$). The average nearest neighbor distance is greater in nasal compared to temporal retina (N = 168.0, T = 88.4 µm, $p < 0.0002$). n = 8 retinas for all measures. **(C)** Left: An example $A_{ON\text{-}S}$ RGC targeted for electrophysiological recording in nasal retina. Dendritic arbors were visualized upon cell-filling with Lucifer yellow (LY), and neighboring $A_{ON\text{-}S}$ RGCs (red dots) were identified subsequently by SMI-32 labeling. Mean neighbor distances for the recorded cell are displayed as red in (B,right). Middle: Targeted $A_{ON\text{-}S}$ RGCs showing co-labeling of LY and SMI-32. Right: Excitatory (red traces) and inhibitory (grey traces) currents show characteristic sustained responses to light stimuli (grey bar, 500 ms). **(D)** An example $A_{ON\text{-}S}$ RGCs targeted in temporal retina show the same characteristic responses as in nasal retina. Data are shown as mean ± SEM.

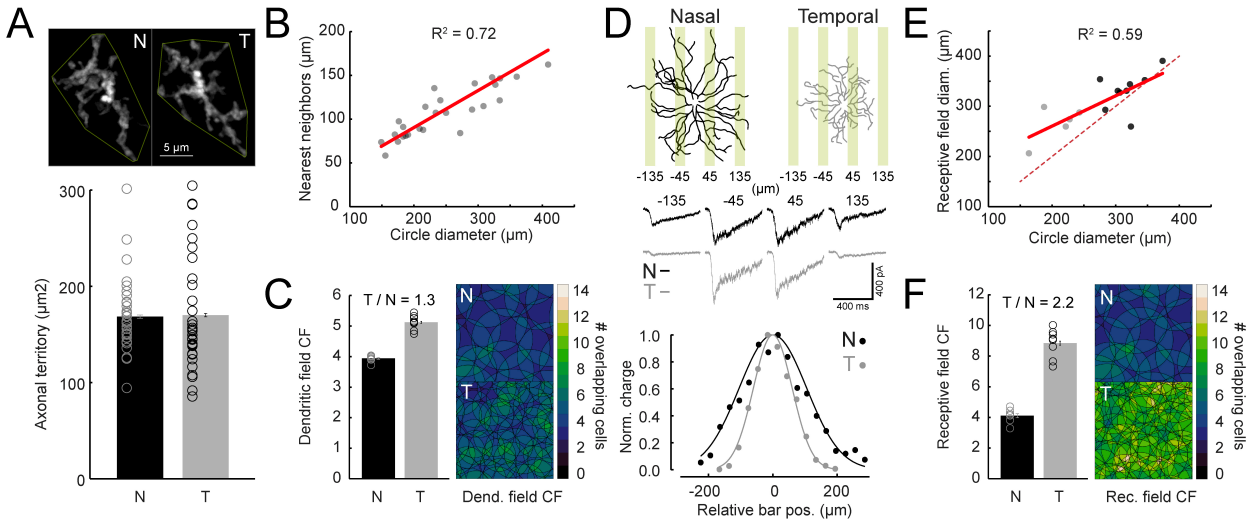

Figure 2.5 Increased density of AON-S RGCs in temporal retina results in an enhanced sampling of the visual field, which is not paralleled by their dominant presynaptic partner.

(A) Axonal terminals of nasal (N) and temporal (T) located type 6 bipolar cells visualized by expression of tdTomato in the *Grm6-tdTomato* mouse (see Methods). Their axonal territory sizes (area of the polygon) are plotted here for cells in nasal and temporal retina. (n = 4 retinas, 37 N and 34 T cells). **(B)** Plot of the diameter of $A_{ON\text{-}S}$ RGC dendritic arbors against mean nearest neighbor distances. **(C)** Dendritic field coverage factor (CF) of $A_{ON\text{-}S}$ RGCs in nasal and temporal retina (CFn = 3.9, CFt = 5.1). Coverage factor (colored) maps were calculated from maps of $A_{ON\text{-}S}$ RGCs dendritic field overlap predicted from their neighbor distances (B, see Methods). **(D)** Top: Example dendritic fields from $A_{ON\text{-}S}$ RGCs targeted across the retina, whose receptive field diameters were mapped using sequential bars of light (see Methods). Middle: Average excitatory current traces from example nasal (black) and temporal (grey) cells recorded in response to light stimuli at the indicated bar positions. Bottom: Response profiles were fit to the normalized charge transfers (dots) with Gaussian functions (smooth curves). **(E)** Dendritic diameters of $A_{ON\text{-}S}$ RGCs were reconstructed from the recorded cells and plotted against their respective receptive field diameters (see Methods) (n = 14 cells). Receptive fields of temporal cells (grey dots) are larger than their dendritic fields (p = 0.03), (dashed red line shows unity), but the two measures appear similar for nasal cells (black dots (p = 0.4) (See Methods). **(F)** Receptive field CF of $A_{ON\text{-}S}$ RGCs in nasal and temporal retina (CFn = 4.1, CFt = 8.8). Coverage factor maps were calculated for the same nasal and temporal regions in (C). Data are shown as mean ± SEM.

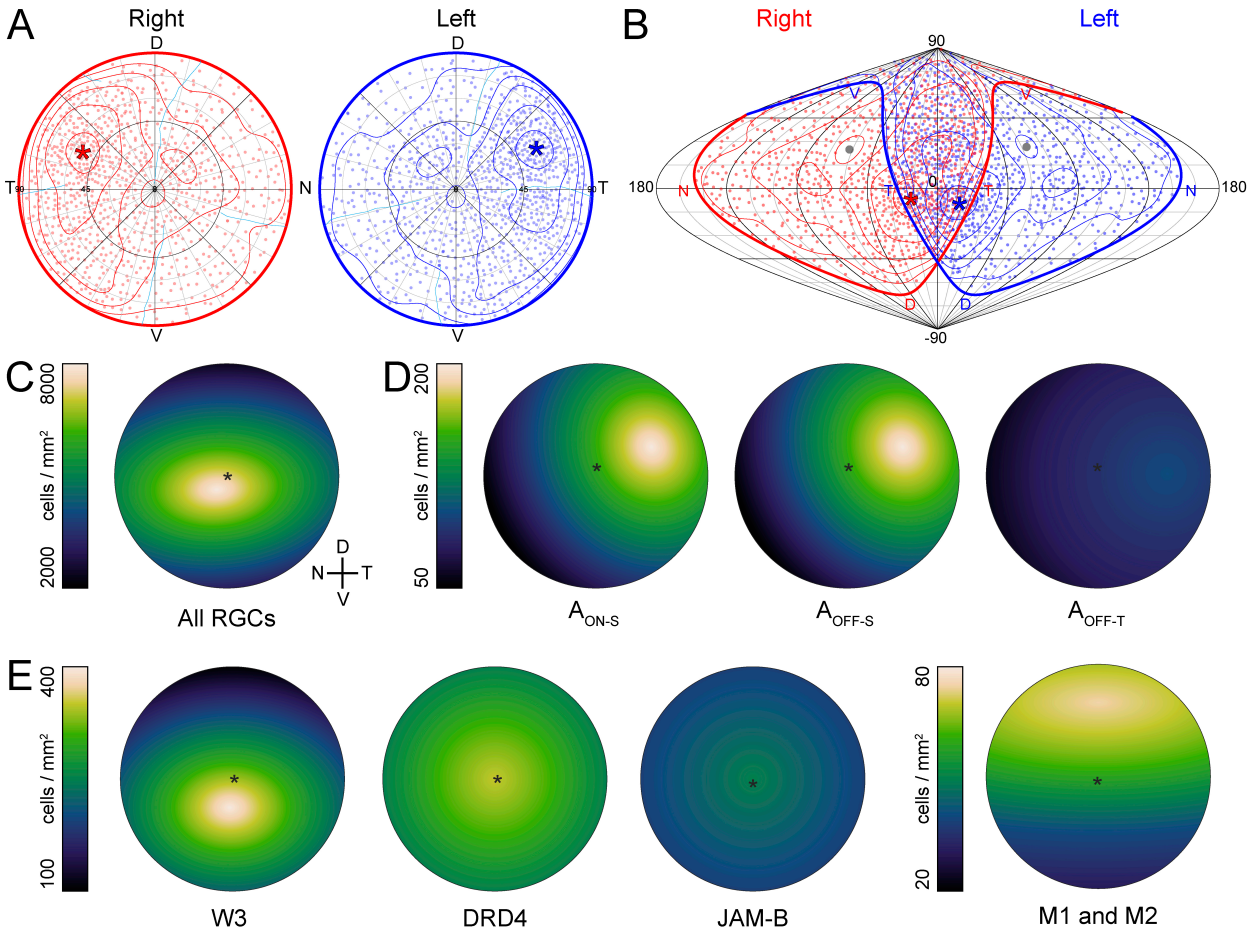

Figure 2.6 Sampling of frontal visual space is enhanced in $A_{ON\text{-}S}$ RGC distributions, which contrast with the distributions of known RGC types.

(A) Azimuthal equilateral projections of retina space for $A_{ON\text{-}S}$ RGC distributions from right (red) and left (blue) eyes shown in Figure 2.1 and 2.2, reconstructed and plotted using the retistruct package (Sterratt et al. 2013). Isodensity lines demarcate 5, 25, 50, 75, and 95% contours of the peak density located at the asterisk (~180 cells / mm^2). Cyan lines delineate computed sutures of the original relief cuts made for flat mount preparation. **(B)** Sinusoidal projection of mouse visual space for $A_{ON\text{-}S}$ RGC distributions from retinas in (A) (see Methods). Red outline represents the edge of the right retina; blue outline represents the edge of the left retina. N - nasal, D - dorsal, V - ventral, T - temporal, indicate the projection of the corresponding pole of the retina. Grey circle represents the position of the optic nerve head. Note the peak densities for right and left retinas (red and blue asterisks) and increased density (75% and 50% isodensity lines) are biased towards the vertical midline (0) corresponding to rostral frontal visual fields of mice. **(C)** The density of the total RGC population peaks at a location just nasal and ventral of the optic nerve head (black asterisk) (schematized from (Dräger and Olsen 1981) see also (Jeon et al. 1998; Salinas-Navarro et al. 2009)). **(D)** In contrast, we show here that $A_{ON\text{-}S}$ and likely $A_{OFF\text{-}S}$ RGCs have peak densities in the temporal-dorsal retina, whereas $A_{OFF\text{-}T}$ RGCs are relatively more uniformly distributed across the retina. **(E)** Furthermore, the distributions of previously characterized RGCs show varied or flat distributions. The density colormaps in (C and E) are schematics based on

previously reported RGC densities, and changes in dendritic arbor sizes (see Methods). Density colormaps in (D) are schematics based on the distributions of $A_{ON\text{-}S}$ and $A_{OFF\text{-}T}$ RGCs shown in Figure 2.2, and predicted from $A_{OFF\text{-}S}$ dendritic arbor sizes illustrated in Figure 2.3.

A_{ON-S} retinal location	(Sun et al. 2002)	(Badea and Nathans 2004)	(Kong et al. 2005)	(Coombs et al. 2006)	(Völgyi et al. 2009)	(Hong et al. 2011)	(Ecker et al. 2010)	(Farrow et al. 2013)
Temporal	Unclassified ON Fig.7	*	Cluster 4 Cluster 5	M3-on	G6	*	M5	*
Medial	A2 inner	Cluster 9	Cluster 8	M7-on M8-on	G2	X7a	M4	PV1
Nasal	A1 C2 inner	Cluster 9	Cluster 11	M9-on M10	G1 G10	X7b	M4	PV1
A_{OFF-S} retinal location								
Temporal	*	Cluster 3	Cluster 3	M3-off	G18	*	*	*
Medial	A2 outer	Cluster 7	Cluster 6	M7-off	G11	X3	*	PV6
Nasal	C2 outer	Cluster 7	Cluster 10	M9-off	G11	X3	*	PV6

Table 2.1 Potential relationship between alpha-like RGCs across the retina and previous categorizations of mouse RGCs.

Many previous classifications of mouse RGCs have identified cells with similar anatomical properties to that of alpha-like RGCs. However, the gradients of A_{ON-S} and A_{OFF-S} alpha-like RGC sizes with respect to retinal topography were not documented, and may have caused segregation of alpha-like RGCs into multiple RGC types (Sun et al. 2002; Badea and Nathans 2004; Kong et al. 2005; Völgyi et al. 2005; Coombs et al. 2006; Völgyi et al. 2009; Hong et al. 2011; Ecker et al. 2010; Farrow et al. 2013). Asterisk denotes RGCs likely not included in the study.

Movie 2.1 is available at the following location: http://dx.doi.org/10.1016/j.cub.2013.12.020

Movie 2.1 Identification of ON and OFF stratifying alpha-like RGCs by SMI-32 immunostaining and dendritic stratification.

Upper panel is a schematic representation of the dendritic stratification levels of alpha-like RGCs within the inner plexiform layer of the mouse retina. Bottom images are sequential 1 µm steps though a confocal image stack encompassing 250 μm^2 of the temporal region of a mouse inner retina labeled with SMI-32 (grey), and choline acetyltransferase (ChAT, green). ChAT labels ON and OFF populations of cholinergic amacrine cells, whose cell bodies lie in the ganglion cell layer (GCL) or the inner nuclear layer (INL), and whose processes form ON and OFF plexuses, respectively. The ChAT plexuses define specific depths within the IPL. Brightly labeled SMI-32 positive cell bodies are observed in the ganglion cell layer. Two distinct populations of SMI-32 labeled RGCs stratify their dendritic arbors either between the ganglion cell layer and the ON ChAT plexus ($A_{ON\text{-}S}$ RGCs, cyan circles), or between the ON and OFF ChAT plexuses ($A_{OFF\text{-}T}$ RGCs, white circles). $A_{OFF\text{-}S}$ RGCs, which stratify their dendrites between the OFF ChAT plexus and the INL are not labeled by SMI-32. The relative depth of each image plane in the movies is represented by the location of the red line in the schematic.

CHAPTER III

SPATIAL RELATIONSHIPS BETWEEN GABAERGIC AND GLUTAMATERGIC SYNAPSES ON THE DENDRITES OF DISTINCT TYPES OF MOUSE RETINAL GANGLION CELLS ACROSS DEVELOPMENT*

3.1 ABSTRACT

Neuronal output requires a concerted balance between excitatory and inhibitory (I/E) input. Like other circuits, inhibitory synaptogenesis in the retina precedes excitatory synaptogenesis. How then do neurons attain their mature balance of I/E ratios despite temporal offset in synaptogenesis? To directly compare the development of glutamatergic and GABAergic synapses onto the same cell, we biolistically transfected retinal ganglion cells (RGCs) with PSD95CFP, a marker of glutamatergic postsynaptic sites, in transgenic *Thy1-YFPγ2* mice in which $GABA_A$ receptors are fluorescently tagged. We mapped YFPγ2 and PSD95CFP puncta distributions on three RGC types at postnatal day P12, shortly before eye opening, and at P21 when robust light responses in RGCs are present. The mature I_{GABA}/E ratios varied among ON-Sustained (S) A-type, OFF-S A-type, and bistratified direction selective (DS) RGCs. These ratios were attained at different rates, before eye-opening for ON-S and OFF-S A-type, and after eye-opening for DS RGCs. At both ages examined, the I_{GABA}/E ratio was uniform across the arbors of the three RGC types. Furthermore, measurements of the distances between neighboring PSD95CFP and YFPγ2 puncta on RGC dendrites indicate that their local relationship is established early in development, and cannot be predicted by random organization. These close spatial associations between glutamatergic and GABAergic postsynaptic sites appear to represent local synaptic arrangements revealed by correlative

* This chapter was published in PLoS One, which maintains copyrights for this material, and has been reprinted with permission. The full citation for this publication is: Bleckert A, Parker ED, Kang Y, Pancaroglu R, Soto F, Lewis R, Craig AM, Wong ROL. Spatial Relationships between GABAergic and Glutamatergic Synapses on the Dendrites of Distinct Types of Mouse Retinal Ganglion Cells across Development. *PLoS One* 8: e69612, 2013.

light and EM reconstructions of a single RGC's dendrites. Thus, although RGC types have different I_{GABA}/E ratios and establish these ratios at separate rates, the local relationship between excitatory and inhibitory inputs appear similarly constrained across the RGC types studied.

3.2 INTRODUCTION

Proper circuit function depends on the balance of excitation and inhibition on individual neurons as well as across their network. This balance likely needs to be regulated not only across the cell, but also locally, at the level of dendritic branches and spines. This is because the spatial distributions of synaptic inputs on some neurons (Jia et al. 2010; Chen et al. 2011) appear highly organized. For example, functionally distinct synapses contact either the apical or basal dendritic segments of pyramidal neurons in somatosensory cortex (Petreanu et al. 2009). Also, *Xenopus* retinal axons map topographically onto the dendrites of tectal neurons (Bollmann and Engert 2009). Such specific patterns of excitatory inputs also suggest that different dendritic segments may have distinct ratios of inhibitory to excitatory synapse densities (I/E ratio). Indeed, the I/E ratio varies across hippocampal neuronal arbors (Megias et al. 2001). I/E ratios may be regulated at an even more local level. For instance, inhibitory and excitatory inputs in close proximity are more likely to be co-regulated by alterations in activity (Chen et al. 2012; van Versendaal et al. 2012). Moreover, I/E ratios can show considerable variation for different cell types in the adult (Gulyás et al. 1999).

How I/E ratios are established during development, across the dendritic arbor of a cell, and along local dendritic segments remains unresolved. To gain insight, it is necessary to map both synapse types throughout the dendritic arbor of the same cell. The compact circuitry of the retina (Masland 2001)makes this tissue particularly useful for mapping the connectivity of individual cells during development and at maturity (Sernagor et al. 2001; Sanes and Zipursky 2010). The extensive classification of mouse RGCs (Sun et al. 2002; Coombs et al. 2007; Völgyi et al. 2009)further enables

comparison of the I/E distributions and ratios for morphologically and functionally distinct RGC types (Masland 2001).

To map inhibitory postsynaptic sites, we previously generated a transgenic line (Soto et al. 2011) in which Neuroligin2 (NL2), a transynaptic adhesion molecule at inhibitory synapses (Varoqueaux et al. 2004), is fused to YFP. However, NL2 is present at both retinal GABAergic and glycinergic synapses (Hoon et al. 2009; Soto et al. 2011). Here, we directly compared the distributions of a defined set of inhibitory (GABAergic) synapses with that of glutamatergic synapses on the same RGC, by generating a new transgenic line in which expression of the γ2 subunit of $GABA_A$ receptor, fluorescently tagged with YFP (*Thy1-YFPγ2*), is driven by the *Thy1* promoter. We biolistically transfected RGCs in retinas from these mice with fluorescently tagged PSD95, marking excitatory postsynaptic sites, in order to simultaneously visualize GABAergic and glutamatergic synapses throughout the dendrites. We compared the arrangements of both synapse types across three RGC types at two key developmental ages: Postnatal day (P)12, shortly after the onset of excitatory synaptogenesis (Fisher 1979) but before eye opening, and at P21, when synaptic densities within the inner retina reach their mature levels (Fisher 1979), and RGCs have robust light responses (He et al. 2011; Koehler et al. 2011). We measured the distances between nearest neighbor synaptic sites and asked whether local distributions of GABAergic and glutamatergic synapses on the RGC dendrites exhibit any spatial constraints. Finally, we correlated fluorescently-labeled postsynaptic sites with amacrine and bipolar cell synapses by performing sequential light and EM reconstructions on the same cell. We were able to determine that while individual RGCs can have unique ratios of their total GABAergic and glutamatergic synapses at maturity, they establish these ratios at different times during development. However, the local spatial relationships between GABAergic and glutamatergic synapses on the dendrites of each type of RGC examined appeared similarly constrained from early in development.

3.3 METHODS

Ethics statement

This study was conducted with the approval of the University of Washington Institutional Animal Care and Use Committee (Protocol 4122-01) and the University of British Columbia Animal Care Committee (Protocol A09-0278). Mice were euthanized by isoflurane overdose followed by decapitation (Protocol 4122-01), or they were euthanized by CO_2 overdose (Protocol A09-0278).

Mice

Thy1-YFPγ2 mice were generated from cDNA for rat $GABA_A$ receptor γ2 subunit ($GABA_AR$ γ2), short form, containing hexahistidine and EYFP near the mature N-terminus (Dobie and Craig 2011) and cloned into the Thy1 vector (Feng et al. 2000). Mice of both sexes were used.

Tissue Preparation

Mice were euthanized and enucleated and the eyes immersed in oxygenated mouse artificial cerebral spinal fluid (mACSF) containing the following in (mM): 119 NaCl, 2.5 KCl, 2.5 $CaCl_2$, 1.3 $MgCl_2$, 1 NaH_2PO_4, 11 glucose, and 20 HEPES, and brought to pH 7.42 with NaOH. To prepare retinal slices, the lens and vitreous were removed and the eye cups then lightly fixed in 4% paraformaldehyde in mACSF for 5 min. The sclera was then pealed away to isolate the retina, and the tissue was subsequently post-fixed for 15-20 min at room temperature. The retinas were rinsed in PBS pH 7.42 and mounted in 4% Type VII-A Agarose (Sigma), and sliced into 60 µm sections using a vibratome. To obtain retinal whole mounts, retinas were isolated in mACSF and mounted flat, ganglion cell side up, onto filter paper (Millipore).

Biolistic transfection

Plasmids for which a cytomegalovirus promoter drives expression of tandem dimer Tomato (tdTomato) or postsynaptic density protein 95 fused to cyan fluorescent protein (PSD95CFP) were coprecipitated onto gold particles (Bio-Rad) (Morgan and Kerschensteiner 2012). Gold particles were propelled into whole mount retinas using a Helios Gene Gun (Bio-Rad), and the tissue then incubated at ~34°C in oxygenated mACSF in a humidified chamber for 24 hr. Afterwards, retinas were fixed in 4% paraformaldehyde in mACSF for 20-30 min, rinsed in PBS, and flat mounted in vectashield (Vector Laboratories) for confocal imaging.

Immunohistochemistry

Retina slices or flat mounts were incubated with primary antibodies in PBS for 4 days at 4°C. We used antibodies against gephyrin (mAb7a, SYSY, 1:500 ~mouse IgG Cat#147 011), PSD95 (ab2723, Abcam, 1:1000 ~mouse IgG2a, Cat#6G6-1C9), $GABA_AR$ α1 (gift of JM Fritschy 1:5000 ~rabbit, 1:5000 ~guinea pig), $GABA_AR$ α2 (gift of JM Fritschy 1:2000 ~guinea pig), $GABA_AR$ α3 (gift of JM Fritschy 1:3000 ~guinea pig), and $GABA_AR$ γ2 (gift of JM Fritschy 1:4000 ~guinea pig). Retinas were then washed and incubated with secondary antibodies, Alexa-568 or 633 (Invitrogen, 1:1000), or DyLight-594 or 649 (Jackson Laboratory, 1:1000) overnight at 4°C. Staining of cell nuclei was accomplished by incubating the retinas in To-Pro-3 (Invitrogen, 1:4000) for 15 min at 24°C.

Western blot

Brain tissue was collected from adult mice and homogenized in buffer (50 mM NaH_2PO_4, 300 mM NaCl, pH 8.0) with protease inhibitor cocktail (Roche), and centrifuged at 1500 x g for 10 min at 4^oC. The supernatant was collected and the protein concentration determined with the Bio-Rad Protein Assay kit. Western blot was performed directly with equal amounts of homogenate or after solubilization with 0.5% n-Dodecyl β-D-maltoside or 0.75% NP40 with equivalent results. Samples were run on SDS-

polyacrylamide gels (10%), transferred to membranes, and blocked with 5% skim milk in Tris-buffered saline/0.05% Tween-20. Membranes were incubated with primary (anti-$GABA_AR$ γ2, Novus Biologicals NB300-190 or anti-GFP, Rockland 600-401-215) and secondary (HRP conjugated, Millipore) antibodies, and signal was detected using the SuperSignal Chemiluminescent kit (Thermo Scientific).

Image Acquisition

Image stacks were acquired on an Olympus FV-1000 laser scanning confocal microscope with an oil-immersion 60x objective (Olympus, 1.35 NA). Voxel dimensions were (x-y-z in µm) 0.103-0.103-0.3 for images of single RGCs in whole mount retinas, 0.082-0.082-0.3 for images of retina slices, and 0.101-0.101-0.4 for correlative fluorescence and electron microscopy. Images were median filtered to remove noise and corrected for xy drift if necessary, and then compressed to 8-bits for analysis after normalization of the entire stack histogram using Fiji (Schindelin et al. 2012).

Image Analysis

Cross-Correlation Analysis:

To characterize the fluorescence expression within the inner plexiform layer (IPL) of retinas from *Thy1-YFPγ2* mice, we wrote custom MATLAB (Mathworks) scripts to calculate the cross-correlation coefficient between two channels of fluorescence ('red' and 'green') as described previously (Soto et al. 2011). Briefly, for two image stacks, the correlation coefficient between every 'red' voxel and every corresponding 'green' voxel was calculated using the corrcoef function of MATLAB. We could determine if this observed correlation has a spatial constraint by shifting one channel incrementally up to 4 µm (within the xy plane of the retina) with respect to the other channel. A peak at the origin in the resulting 2D correlogram suggests that there is a shared spatial pattern between the two channels. We could further assess if the observed correlation is non-random by rotating one channel by 180° with respect to

the other before shifting. A lack of peak correlation under this condition suggests that the observed correlation is not due to random distributions of fluorescence.

These measures examined the correlation within the entire IPL neuropil, however the retina IPL consists of several sublaminae which have unique distributions of cell types and synaptic profiles (Haverkamp and Wässle 2000). Thus, we divided the entire depth of the IPL into 100 percentiles and calculated the correlation coefficient between the two channels within each percentile. We also calculated the normalized fluorescence intensity for each channel (sum of intensities within each percentile / maximum sum of intensities within a percentile). When imaging two separate fluorescence channels, it is possible there will be differences in the intensities as well as signal to noise between the two channels. To determine how robust cross-correlation analysis is to these potential variations in fluorescence, we examined the cross correlation throughout the depth of a small volume of immunostained retina IPL with its duplicated volume (Figure 3.3). To test how differences in intensities affect correlation, the correlation coefficient was calculated after the histogram of the duplicated volume was linearly scaled (by 0.99, 0.95, 0.90, 0.75, 0.50, 0.25, 0.10, 0.05, 0.01). To test how signal to noise affects the correlation, the correlation coefficient was calculated after varying percentages (1, 5, 10, 25, 50, 75, 90, 95, 99) of voxels in the duplicated volume were randomly chosen and their intensities were randomly reassigned.

Quantification of RGC dendrites:

The branching patterns of RGC dendrites were skeletonized and volume rendered using the filament function of Imaris (Bitplane). Total dendritic length was calculated from the skeletonized filament. The dendritic territory was calculated by expanding a z projection of the dendritic skeleton with a 10 µm diameter disk (Morgan et al. 2008). ON-S and OFF-S A-type RGCs were identified based upon their characteristic arbor morphologies (Diao et al. 2004; Coombs et al. 2007; Völgyi et al. 2009; van Wyk et

al. 2009)and stratification within the IPL (Figure 3.6). Bistratified RGCs were assumed to be direction selective (DS) based upon their dendritic morphology and by their stratification within the densely labeled sublaminae of *Thy1-YFPγ2* expression that strongly correlated with VAChT (Figure 3.6) and $GABA_AR$ α2 labeling (Brandstätter et al. 1995; Auferkorte et al. 2012). Although previous studies of mouse RGC maturation did not find significant differences in RGC development with retinal eccentricity (Diao et al. 2004), we avoided RGCs from the inner and outer 10% of the retina.

Identification and quantification of postsynaptic puncta:

The dendritic volume was expanded (xy 1.0 µm, z 0.5 µm) and used as a mask to segment Thy1-YFPγ2 fluorescence within and juxtaposed to the dendrites. Potential PSD95CFP and YFPγ2 puncta within this masked volume were identified using custom MATLAB scripts previously described (Morgan et al. 2008). Briefly, fluorescence signals within each channel were iteratively thresholded, filtered by size and contrast, and their ratio of fluorescence to cytosolic fluorescence intensity. In addition, puncta contacting the edge of the expanded mask were removed, and a final user-guided error minimization step was conducted by manual identification of the found puncta in 3D using the spots function of Imaris (Bitplane). Colocalization of puncta was classified by the sharing of at least one voxel between each identified puncta in one channel with those identified in the second channel.

I/E density maps and Sholl analysis:

Density heat maps of puncta were calculated by dividing the total number of found puncta by the total dendritic length of the skeletonized dendrite within a 20 µm diameter sliding window along the dendrites (Morgan et al. 2008). Sholl analysis (SHOLL 1953) of the I/E ratio was calculated by dividing the total number of YFPγ2 by the total number of PSD95CFP puncta within a sliding 10 µm window from the cell body. To exclude the cell body the initial 10 µm were omitted.

Nearest neighbor analysis:

The nearest neighbor 3D distances were calculated for every found puncta on each RGC for three different groupings: Each PSD95CFP and the nearest PSD95CFP, each YFPγ2 and the nearest YFPγ2, and each PSD95CFP and the nearest YFPγ2. The median nearest neighbor distances were calculated for each group, as well as the cumulative distributions for each RGC. To determine if the median distances obtained between found puncta were non-random, we simulated a sample population of P12 and P21 RGCs with random distributions of PSD95CFP and YFPγ2 puncta on their dendrites. We utilized the dendritic volumes of one P12 and one P21 RGC of each type (ON-S A-type, OFF-S A-type, and bistratified DS) as our model RGCs. To create a sample of cells that matched our observed RGC distributions we utilized the total linear densities of PSD95CFP and YFPγ2 puncta obtained from P12 and P21 RGC to calculate the total numbers of puncta to be distributed across the dendritic volume. The total number of puncta for each simulated RGC was calculated by multiplying the linear densities by the total dendritic length of the model RGCs. These total numbers of puncta were then randomly distributed within the volume of the model RGCs with the constraints that no PSD95CFP puncta could occupy the same voxel coordinate of another PSD95 puncta, and that no YFPγ2 puncta could occupy the same voxel coordinate of another YFPγ2 puncta. Using these parameters, the median nearest neighbor distances between puncta groups and cumulative distributions were calculated for model ON-S A-type P12 (n = 9) and P21 (n = 9), OFF-S A-type P12 (n = 5) and P21 (n = 5), and bistratified DS P12 (n = 7) and P21 (n = 5) RGCs.

Correlative Fluorescence and Electron Microscopy:

For one ON-S A-type RGC at P21 we reconstructed the synaptic connectivity of bipolar cells and amacrine cells to the RGC after mapping the distributions of PSD95CFP and YFPγ2 puncta onto its dendritic arbor. A *Thy1-YFPγ2* mouse retina was biolistically transfected as described above. After

incubation for 24 hrs, the retina was fixed in 1.5% glutaraldehyde / 2.5% paraformaldehyde for 40 min. The tissue was washed and mounted under coverglass in 0.1M sodium cacodylate buffer for confocal and multiphoton imaging. An image stack of the labeled RGC was obtained for one quadrant of the dendritic arbor including the cell body. The retina was unmounted and fixed in 4% glutaraldehyde overnight. The retina was again washed and remounted in 0.1M sodium cacodylate buffer. Using a custom-built two-photon microscope with a Ti:sapphire laser (Spectra-Physics) tdTomato fluorescence of the RGC was visualized and fiduciary marks were burned into the tissue using the near-infrared branding (NIRB) method (Bishop et al. 2011). A window was branded around the cell body and dendrites at the level of the soma, and a mark was branded through the depth of the IPL onto one side of the window. These marks were clearly evident as autofluorescence under multiphoton imaging and by the absence of tissue under electron microscopy.

An image stack of the RGC and autofluorescence of the burn marks was taken, and the retina was unmounted and a small section of retina encompassing the RGC was sectioned (~1 mm^2). This tissue block was then washed in 0.1M sodium cacodylate buffer and post-fixed for 45 min in cacodylate buffered 1% osmium tetroxide. The tissue was washed in dH_2O, en bloc-stained in 1% aqueous uranyl acetate, and washed again in dH_2O before being dehydrated through a series of ethanol and propylene oxide and embedded in Epon Araldite resin. Semi-thin resin sections were cut until the burn marks could be identified in Richardsons stain (Methyl Blue Azure II) tissue sections. Serial thin sections (80 nm) were cut, placed on Formvar-coated slot grids and stained with Reynolds lead citrate. Micrographs were taken at 2200x (scanned at 2500dpi, ~8.5 nm / pixel) for image registration, and 8900x (scanned at 2500dpi, ~1.1 nm / pixel) for identification of synaptic contacts.

The EM micrographs were manually aligned and serially registered using TrakEM2 (Cardona et al. 2012). Bipolar and amacrine cell synaptic connections onto the RGC dendrites were identified using established criteria (Dowling and Boycott 1966). Briefly, bipolar cell terminals and sites of contact were

identified by the presence of a presynaptic ribbon apposed to a postsynaptic density (PSD). Amacrine cell contacts were identified by the presence of a PSD and presynaptic vesicles. Often, amacrine contacts also contained dense core vesicles. The presynaptic terminals of bipolar and amacrine cells and the RGC dendrite were traced through successive serial sections to examine local circuit connectivity. Feedforward connections were identified when a bipolar cell contacted a RGC and an amacrine cell at a dyad synapse, and the amacrine cell subsequently contacted the RGC dendrite (Calkins and Sterling 1996). To correlate the identified fluorescent puncta with amacrine and bipolar cell synapses, a maximum intensity projection of the labeled RGC dendrite was scaled and aligned to the EM reconstruction using TrakEM2. Each identified synaptic contact was scored based on the presence or absence of a corresponding fluorescence marker, and vice versa, within the local dendritic segment reconstructed. Because the EM sections were ~80 nm, it is possible that we did not detect some postsynaptic densities parallel to the plane of section, and thus our estimation of correlation is likely a lower bound (Kubota et al. 2009).

Statistics

When data passed tests of normality (Lillifors, Jarque-Bera), we utilized student's t-test. Otherwise we carried out the non-parametric Wilcoxon rank-sum test to determine significance. All other statistics are noted within the text.

3.4 RESULTS

Expression of YFPγ2 in the retina of *Thy1-YFPγ2* mice.

YFPγ2 expression was present as early as postnatal day (P)7 in the retina of *Thy1-YFPγ2* mice, but the labeling was diffuse and the signal to noise too low to quantify synaptic sites (data not shown). By P12, punctate fluorescence was consistently observed throughout both the ON and OFF sublaminae of the

inner plexiform layer (IPL) although diffuse fluorescence was still visible in cell bodies of the ganglion cell layer (GCL) (Figure 3.1A). Although cell bodies remain labeled at P21, punctate labeling is more pronounced in the IPL. At both ages, the relative intensity and density of fluorescent puncta varies across layers in the IPL, with the highest density of expression localized to two substrata in the IPL (Figure 3.1A,B). Furthermore, expression was not observed in other layers of the retina at either age, except in a few cell bodies in the innermost layer of the inner nuclear layer (INL). The scarcity of cell bodies labeled in the INL compared to the GCL (Figure 3.1A,B), suggests that the majority of cells labeled in the *Thy1-YFPγ2* transgenic retina are RGCs. However, only ~20% of cells in the GCL layer express YFPγ2 (Figure 3.2A-C), while 40% of the cells are likely RGCs (Jeon et al. 1998), thus not all RGCs express YFPγ2 in the *Thy1-YFPγ2*. Likewise, not all puncta immunostained for the $GABA_AR$ γ2 subunit within the IPL also have YFPγ2 labeling, but all YFPγ2 puncta are labeled by anti-$GABA_AR$ γ2 (Figure 3.2D).

We quantified the level of expression of YFPγ2 in *Thy1-YFPγ2* mice by obtaining western blots of whole brain lysates (Figure 3.1C). We found that the overall expression level of the transgenic YFPγ2 was 31.5 % ± 1.3, relative to endogenous $GABA_AR$ γ2 protein level (n = 4). The YFPγ2 mice appeared undistinguishable from wild-type with respect to viability, fertility, and home cage behavior. Previous transgenic lines expressing untagged γ2 showed that even with expression at higher level, roughly 100% relative to endogenous, mice exhibited only a difference in acute functional tolerance to ethanol but no other differences in multiple behavioral and biochemical tests (Wick et al. 2000).

Cross-correlation analysis can detect overlapping spatial distributions between two fluorescent labels. We wished to determine how well fluorescence expression in *Thy1-YFPγ2* transgenic retina represents $GABA_AR$ distributions. To confirm correct localization of the punctate fluorescence in the *Thy1-YFPγ2* transgenic retina to sites of GABAergic synapses, we assessed the colocalization of YFPγ2 signal with immunostaining of proteins found at inhibitory postsynaptic sites. Because of variability in

immunostaining and fluorescence expression, it is often difficult to systematize methods of colocalization across samples. Here we used correlation analysis because it is strongly insensitive to differences in intensity between two fluorescent channels, and can be used to detect spatial correlations between two image volumes (Figure 3.3) (Wu et al. 2010; Soto et al. 2011).

We determined how well cross-correlation analysis can identify the spatial relationship between two separate fluorescence labels in retinal sections by obtaining the correlation profiles of a single protein visualized by distinct fluorescence signals found at inhibitory GABAergic synapses. To label a single protein with two fluorophores (568 and 649), we used primary antibodies against $GABA_AR$ α1 subunit that were raised in different hosts, guinea pig (~gp) and rabbit (~rb) (Figure 3.4A,C). We obtained two types of cross-correlation plots for both ages studied (P12 and P21): one that plots the observed correlation coefficient at various planes of IPL depth, and the other provides a 2D cross-correlogram of the two signals indicating how the correlation between the two channels is altered by changes in their relative spatial alignment. We found a strong correlation throughout the IPL for the two distributions of $GABA_AR$ α1 labeling, and the correlation coefficients at each sublamina are of similar magnitude (Figure 3.4B). The high degree of spatial similarity was also evident in single optical sections where the two signals overlap extensively (Figure 3.4A,C). To determine whether this observed correlation was due to random distributions of both fluorescence signals, we obtained a 2D cross-correlogram of the observed signals by shifting one channel (in x and y) with respect to the other. We found that for the entire IPL, the 2D cross-correlogram peaks at the observed spatial orientation (0,0), suggesting that the spatial correlation of the immuno-fluorescence from the two antibodies is not random (see Materials and Methods). This non-random correlation is also evident in the flat 2D correlogram obtained when one channel was rotated 180 degrees (in x and y) relative to the other (Figure 3.4B,D). Overall, the cross-correlation approach we use here is a reasonable quantitative method for assessing whether two signals are non-randomly associated with each other, and provides a metric

for assessing the relative strength of spatial correlation between two channels across multiple types of fluorescence labeling.

YFPγ2 expression correlates with immunolabeling of proteins at inhibitory but not excitatory postsynaptic sites.

The endogenous γ2 subunit incorporates into $GABA_AR$ localized to synaptic sites (Jacob et al. 2008) and is necessary for the clustering of $GABA_AR$ at synapses (Essrich et al. 1998). To determine whether exogenous expression of YFPγ2 in the *Thy1-YFPγ2* transgenic retina correctly localizes to GABAergic postsynaptic sites, we performed cross-correlation analysis of YFPγ2 fluorescence within the retina IPL immunostained for proteins known to be at inhibitory or excitatory synapses.

We first examined the distributions of YFPγ2 together with immunolabeling for gephyrin, a postsynaptic scaffolding molecule at GABAergic and glycinergic synapses (Sassoè-Pognetto and Wässle 1997)or PSD95, a postsynaptic scaffolding protein at glutamatergic synapses (Okabe et al. 1999) (Figure 3.4E-L). At both ages, we found a strong correlation between gephyrin staining and YFPγ2 expression throughout the IPL (Figure 3.4F,H). This correlation is also evident in the degree of overlap of fluorescence puncta signals observed in single optical sections taken from image stacks (Figure 3.4E,G). However, the strength of correlation in each sublamina is not merely a result of the intensity of fluorescence, because the normalized intensities of each channel do not follow the same pattern across IPL layers (Figure 3.4F,H). Note that for gephyrin the observed correlation for the entire IPL (peak at 0,0 in 2D correlogram) is not as strong as the peaks in some individual sublamina because it reflects an average of all layers. In contrast, the pattern of correlation within the IPL for PSD95 shows weak correlation across all layers, despite the high density of PSD95 labeling (Figure 3.4I-L), and no overlap in fluorescence signal is apparent in single optical sections (Figure 3.4I,K). The strong correlation of YFPγ2 fluorescence with gephyrin and weak correlation with PSD95 immunostaining at both ages suggests that

the *Thy1-YFPγ2* is reliably marking inhibitory and not excitatory postsynaptic sites within the IPL in the postnatal mouse retina.

***YFPγ2* is present at GABAergic synaptic sites.**

Although it is clear that YFPγ2 fluorescence is associated with inhibitory synapses, gephyrin immunostaining alone does not distinguish between GABAergic and glycinergic synapses in the retina (Sassoè-Pognetto et al. 1995; Zucker 1998). To determine whether YFPγ2 is found within $GABA_AR$ clusters, we asked how well YFPγ2 fluorescence correlates with immunolabeled $GABA_ARs$. Because the γ2 antibody would label both endogenous γ2 and YFPγ2, immunostaining for this receptor subunit will not help determine whether YFPγ2 correctly localizes to GABAergic postsynaptic sites. We thus immunolabeled endogenous α1, 2, and 3 subunits (Figure 3.5) because these subunits are found in the majority of synaptic $GABA_ARs$ (Vithlani et al. 2011).

In the retina, each $GABA_AR$ cluster bears only one type of α subunit (Greferath et al. 1995). We found that YFPγ2 colocalizes with $GABA_AR$ α1 (Figure 3.5A-D), $GABA_AR$ α2 (Figure 3.5E-H) and $GABA_AR$ α3 (Figure 3.5I-L). Peaks in the correlation with YFPγ2 occurred at different sublaminae in the IPL for each of the α-subunits. YFPγ2 expression appears to be most dense in two strata where $GABA_AR$ α2 receptors are concentrated, and the correlation coefficient is high between these two $GABA_AR$ labels. In contrast, there is less YFPγ2 expression in IPL strata that contain high densities of $GABA_AR$ α1 or $GABA_AR$ α3 labeling, most likely because fewer cells that predominantly express these α-subunits also express the transgene. It is therefore not unexpected that compared to α2, the correlation coefficient of YFPγ2 and the α1 or α3 signal is less pronounced (flatter correlogram), although still above chance. It is important to emphasize why not all immunolabeled $GABA_ARs$ colocalize with YFPγ2 signal. YFPγ2 is primarily expressed by RGCs, but not by all RGCs (Figure 3.1 and 3.2). Also, $GABA_ARs$ are expressed by RGCs, amacrine cells and bipolar cells whose processes all contribute to the inner plexiform layer. But, in the

transgenic line, YFPγ2 is expressed in very few amacrine cells and not in any bipolar cells. The antibody labeling for α subunits of the $GABA_AR$ will label all endogenous receptors in the retina including receptors in cells not expressing YFPγ2. We therefore determined how well YFPγ2 expression represents the total population of endogenous $GABA_ARs$ on an individual RGC.

We mapped YFPγ2 and $GABA_AR$ α3 puncta on the dendritic arbors of one type of RGC that stratifies its dendrites within the ON layer of the IPL. We chose the ON-S A-type RGC for this analysis because the probability of obtaining a cell-fill by biolistic transfection in the *Thy1-YFPγ2* retina, in which not all RGCs express the transgene, is reasonably high. To co-map YFPγ2 and $GABA_AR$ α3 puncta, we biolistically transfected retinas in the *Thy1-YFPγ2* retina with CMV-tdTomato at P21 (Figure 3.5M). We generated skeletons of the dendritic arbors that were subsequently used to isolate fluorescent puncta within the dendrites (Figure 3.5N), and then identified postsynaptic puncta using custom-written software (Morgan et al. 2008) (see Materials and Methods). We found that for individual dendritic segments (n = 4 cells), the fraction of identified YFPγ2 puncta that also contained $GABA_AR$ α3 was 73.3% ± 0.03, and the fraction of identified $GABA_AR$ α3 puncta associated with YFPγ2 was 74.9% ± 0.03 (Figure 3.5O). Thus, for individual RGCs, YFPγ2 is a reliable marker of $GABA_ARs$, and represents the majority of $GABA_ARs$ on an individual RGC dendritic arbor. Furthermore, our observations suggest that the ON-S A-type RGC expresses primarily $GABA_AR$ α3.

Distributions of PSD95CFP and YFPγ2 within individual dendritic arbors of distinct RGC types.

To map GABAergic and glutamatergic postsynaptic sites on individual RGCs, we biolistically transfected three functionally distinct RGC types (Figure 3.6) in the *Thy1-YFPγ2* retina with CMV-tdTomato and CMV-PSD95CFP (Figure 3.7A,C). We generated skeletonized dendritic arbors (Figure 3.7B,D) and used these to identify postsynaptic puncta (Morgan et al. 2008) (see Materials and Methods; examples in Figure 3.7B,D). We quantified the total densities and ratios of YFPγ2 and PSD95CFP puncta on the dendritic

arbors of each RGC at P12 and P21 by calculating the total numbers of puncta per dendritic length (Figure 3.8). We found that for ON-S A-type RGCs, the densities of both YFPγ2 and PSD95CFP increased from P12 to P21 (Figure 3.8A). However, their mature I/E ratio was already apparent at P12. Similarly, the mature OFF-S A-type RGC I/E ratio was attained by P12 (Figure 3.8B). However, at P21, OFF-S A-type RGCs I/E ratios are greater than that of ON-S A-type RGCs ($p = 0.01$ student's t-test). For bistratified DS cells, both inhibitory and excitatory synaptic densities showed greater variability at P12 (Coefficient of variation (CV), PSD95CFP = 34.2, YFPγ2 = 23.9) than at P21 (CV, PSD95CFP = 9.7, YFPγ2 = 5.0; Figure 3.8C). Although there was a clear increase in the density of inhibitory sites across ages, we did not detect a statistical change in the densities of excitatory synapses. It is evident that the ratio of I/E for each bistratified DS cell, and across all cells, increased between P12 and P21 (Figure 3.8C). This observation was true for both ON and OFF arbors of bistratified DS RGCs (Table 3.1). Although the I/E ratio at P21 for bistratified DS was greater than that of ON-S A-type RGCs ($p = 0.01$ student's t-test), there was no difference between the I/E ratios for OFF-S A-type and bistratified DS RGCs at this age. Taken together, mature I/E synapse density ratios, and rates at which these ratios are obtained during development, are different across RGC types.

It is known for cortical pyramidal neurons that the relative ratio of inhibitory to excitatory synapses is not evenly distributed across the dendritic arbor (Megias et al. 2001). It is possible that the patterns of postsynaptic sites on RGCs similarly show differential distributions across their arbors (Morgan et al. 2008; Xu et al. 2008; Koizumi et al. 2011). We therefore mapped the densities of YFPγ2 and PSD95CFP and their ratios across the dendritic arbors of each of three RGC types (Figure 3.9). For all RGC types examined, the gradients for both YFPγ2 and PSD95CFP across the arbors were shallow. The I/E ratios of ON A-type RGCs appear evenly distributed across the dendritic arbor at both P12 and P21 (see example, Figure 3.9A). Similarly, OFF-S A-type RGCs showed an even I/E distribution across their arbors, also at both ages (Figure 3.9C,D). The density distributions for bistratified DS RGCs showed more

variability for both ON and OFF arbors. While this variability appeared greater at the periphery of the dendritic arbor for some cells, we did not observe a systematic increase or decrease in the ratio of I/E in the periphery (Figure 3.9G,H).

Local spatial relationships between inhibitory and excitatory synapses on RGCs are established early in development.

Our experiments, thus far, considered how the densities of glutamatergic and GABAergic postsynaptic sites on RGCs alter with maturation. It has previously been suggested that dendritic remodeling and an increase in total synaptic number with maturation contribute to defining the adult densities of excitatory (Morgan et al. 2008) and inhibitory (Soto et al. 2011) synapses on RGCs. To gain a sense of how developmental increases in glutamatergic and GABAergic synapse densities are reflected locally at neighboring synapses, we assessed the nearest neighbor distances between PSD95CFP puncta, between YFPγ2 puncta, and between PSD95CFP and YFPγ2 puncta, at P12 and P21.

For ON-S A-type RGCs, the median distance between PSD95CFP puncta that are nearest neighbors decreased from P12 to P21 (Figure 3.10A). We found a similar decrease in the median distance between YFPγ2 puncta. However, the median distance between each PSD95CFP and YFPγ2 puncta was already established at P12. In order to determine if these local relationships could be due to a random arrangement of synaptic sites onto the RGC dendrites, we calculated the nearest neighbor distributions of simulated ON-S A-type RGCs by randomly placing puncta (same densities as measured for each cell) across the dendritic arbor (Figure 3.10B,D,F, see Materials and Methods). The simulated distributions also showed a decrease in the nearest neighbor distances for PSD95CFP and for YFPγ2 across ages. However, the median distance between neighboring PSD95CFP and YFPγ2 puncta in the simulated distribution was greater than the imaged populations (Figure 3.10B,D,F). For OFF-S A-type and bistratified DS RGCs, the relative spatial distribution of excitatory and inhibitory postsynaptic puncta was

also already present at P12. However, the median distances between nearest neighbor PSD95CFP and nearest neighbor YFPγ2 puncta were unchanged between P12 to P21 for both these cell types (Figure 3.10C,E).

It is possible that the decrease in nearest neighbor distances between PSD95CFP puncta and between YFPγ2 puncta in ON-S A-type RGCs with maturation, but not in the other RGC types, is, in part, due to the relatively greater increase in total synapse density in the ON A-type RGCs. For all RGC types studied, however, the median distance between neighboring PSD95CFP and YFPγ2 puncta is already established at P12, which cannot be accounted for by random distributions of GABAergic and glutamatergic synapse densities onto RGC arbors.

YFPγ2 and PSD95CFP puncta correspond respectively to amacrine and bipolar cell synapses on an individual RGC.

We wished to gain a better understanding of the local synaptic connectivity associated with GABAergic and glutamatergic postsynaptic sites identified using fluorescent markers, and to determine how well these sites correlated with amacrine and bipolar cell input onto the RGC. To this end, we performed serial electron microscopy (EM) on the dendritic arbors of an ON-S A-type RGC labeled with tdTomato and PSD95CFP in a *Thy1-YFPγ2* transgenic retina (Figure 3.11).

To identify the labeled RGC (Figure 3.11A, left) under EM, we used the near infrared branding (NIRB) method (Bishop et al. 2011), whereby fiduciary marks are burned into the fixed tissue using a multiphoton pulsed infrared laser (Figure 3.11A, middle, NIRB). These burn marks could then be identified in semi-thin resin sections of the tissue prepared for EM (Figure 3.11A, right). After identification of the labeled RGC, we followed the dendritic arbors through serial sections, and identified bipolar and amacrine cell synaptic profiles making contact with the RGC dendrite (Figure 3.11B). Synapses from bipolar cells were characterized by the presence of a presynaptic ribbon apposed to a

postsynaptic density (PSD) (Figure 3.11C; see Movie 3.1). Amacrine cell synapses were identified by the presence of PSDs with no ribbons (Dowling and Boycott 1966). Often amacrine cell presynaptic terminals also contained dense core vesicles (data not shown). An example of the correspondence between bipolar cell synapses and PSD95CFP puncta, and between amacrine cell synapses and YFPγ2 puncta obtained by comparing the fluorescence images with the serial EM sections is provided in Figure 3.11B.

To determine how reliable is our identification of GABAergic and glutamatergic postsynaptic sites on the RGC dendritic arbors by the fluorescence labeling, we quantified the proportion of synapses on primary, secondary, and tertiary dendrites of the RGC that was identified in both confocal and serial EM reconstructions (Figure 3.12A-C). The high correspondence of bipolar cell ribbon synapses and amacrine cell synapses found in EM serial sections that were apposed to sites of PSD95CFP (>70% apposed to ribbons) or YFPγ2 puncta (>80% apposed to amacrine contact), respectively, strongly suggests that the fluorescently tagged postsynaptic proteins reliably mark their respective postsynaptic sites on the RGCs (Figure 3.12C). We believe that these numbers represent lower limits because we counted all of the fluorescent puncta within the total length of dendrite visualized from our serial reconstructions, but in the EM reconstructions we were not always able to capture the full volume of the dendrite of interest and its presynaptic contacts. Furthermore, we often found ribbon synapses only visualized in single serial sections or with irregular profiles, which could contribute to an under estimate of actual numbers (Kubota et al. 2009). The high correspondence between the position of ribbon synapses observed under EM and sites of PSD95CFP (93%) suggests that of the ribbon synapses we were able to detect, most were also labeled by a PSD95CFP puncta in confocal reconstructions. The number of conventional synapses we detected in EM that corresponded to YFPγ2 puncta was lower (65%). This may not be surprising because amacrine profiles under EM can represent GABAergic or glycinergic synapses, both of which are present on ON-S A-type RGCs (Majumdar et al. 2007).

Our partial EM reconstruction also allowed us to obtain a small sample of the local connectivity of excitatory and inhibitory synapses on the RGC. We found examples where single bipolar cell varicosities made multiple ribbon contacts onto the dendrite (Figure 3.11B), characteristic of the predominant type of bipolar cell (Type 6) that can form more than one ribbon release site onto the ON-S A-type RGC (Morgan et al. 2011; Schwartz et al. 2012). We were also able to observe characteristic bipolar cell ribbon synapses in the retina, which often occur at a dyad junction (Dowling and Boycott 1966) (Figure 3.11C). Indeed, we found that 75% (40 of 53) of the ribbon synapses could accurately be identified as dyad synapses. When it was possible to determine the identity of the partners (33 of 40), we found that the composition of these dyad synapses were most often onto an amacrine cell and the RGC (79%, 26 of 33), with fewer dyads comprising two RGCs (24%, 8 of 33).

As in many CNS circuits, one form of interaction between inhibitory and excitatory synapses onto a postsynaptic target in the retina is feedforward inhibition (Chen et al. 2010). Retinal bipolar cells synapse onto amacrine cells, which in-turn can make close connections onto ganglion cells, and provide local feedforward inhibition (Calkins and Sterling 1996). We were able to find instances of such inhibition in our EM reconstructions. Of the dyad synapses making connections onto an amacrine cell and a ganglion cell, we found that 42% (11 of 26) made feedforward connections within the local reconstructed regions. Of the feedforward synapses, the median distance between the bipolar cell ribbon synapse and amacrine cell synapse (~675 nm) was similar to the median distance detected using fluorescence markers (Figure 3.10A). Furthermore, the median nearest neighbor distances between bipolar cell ribbon synapses (~936 nm) and between amacrine cell synapses (~970 nm) were also similar to those quantified from fluorescence images (Figure 3.10A). Together, these observations suggest that our use of fluorescence markers is predictive of the connective patterns of bipolar and amacrine cell contacts on RGCs, and furthermore that many of the excitatory puncta in close proximity to inhibitory puncta found on RGC dendrites could reflect local feedforward circuits.

3.5 DISCUSSION

Development of glutamatergic and GABAergic synapses on individual RGCs.

Like other CNS circuits, inhibitory synaptogenesis precedes excitatory synaptogenesis in the retina (Johnson et al. 2003). Conventional synapses from amacrine cells are present shortly after birth in mouse, and increase in number at a constant rate until P21. However, ribbon synapses, characteristic of bipolar cells, are not present until P11, after which they also increase at an equivalent rate (Fisher 1979). Indeed, functional drive from amacrine cells develops prior to glutamatergic transmission from bipolar cells (Unsoeld et al. 2008). Our previous studies separately mapping excitatory and inhibitory postsynaptic sites on individual RGCs also suggested that inhibitory and excitatory synaptogenesis may be coordinated during development to balance inhibition and excitation after glutamatergic synaptogenesis begins, at least for one RGC type (Morgan et al. 2008; Soto et al. 2011). Indeed, such balance occurs for cultured hippocampal neurons despite increases in both inhibitory and excitatory synapse densities over time (Benson and Cohen 1996; Zhao et al. 2005).

We compared I/E ratios for ON-S and OFF-S A-type RGCs (Majumdar et al. 2007; van Wyk et al. 2009) because of their similar morphologies but opposite stratification and function, and bistratified DS RGCs because of the well-defined functional role of GABAergic inhibition in bistratified DS RGCs (Fried et al. 2002; Euler et al. 2002; Weng et al. 2005; Taylor and Smith 2012). We found that the I/E ratio is set early in development for ON-S and OFF-S A-type RGCs, before eye-opening. This is consistent with previous results in mouse where the densities of excitatory and inhibitory synaptic sites were mapped separately onto ON monostratified RGCs (Morgan et al. 2008; Soto et al. 2011). However, bistratified DS RGC types only attained their mature I/E ratio after eye opening. The differential maturation rates across RGC types may seem in contrast to the parallel increase in amacrine and bipolar cell synaptogenesis suggested from past EM studies. However, amacrine cells also make connections with

each other and with bipolar cells (Wässle and Boycott 1991). Thus, differential synapse maturation rates may be obscured when pooling all amacrine synapses within the IPL.

How the mature I/E ratios contribute to the functional output of RGCs has yet to be determined. It is known that the mature frequencies of spontaneous inhibitory and excitatory postsynaptic currents in individual developing RGCs are not attained until several weeks after birth, but at each developmental age they appear balanced (Tian and Copenhagen 2001). Furthermore for ON and OFF RGCs both their spatial and temporal responses (Koehler et al. 2011)and inhibitory and excitatory postsynaptic currents (He et al. 2011) in response to light stimuli are not mature until the third of four postnatal week. Our results suggest that the density of inhibitory and excitatory synapses on individual RGCs is not mature until after eye opening. It is intriguing to note that for the DS RGC, the strength of inhibitory input underlying the null direction increases after eye opening as direction selectivity becomes well established (Wei et al. 2011). We observed that the density of GABAergic synapses on both the ON and OFF arbors of the bistratified DS RGC also matures after eye opening, paralleling the time course of increasing inhibition strength (Wei et al. 2011).

Global spatial relationships of inhibitory and excitatory synapses.

Few studies have measured the distributions of inhibitory and excitatory inputs onto the same neuron, particularly in tissue. Serial EM studies previously demonstrated that: (i) both apical and basal dendrites of a CA1 pyramidal neuron exhibit a pronounced proximal to distal I/E gradient of >30 fold (Megias et al. 2001), and (ii) the I/E ratios of three distinct types of hippocampal interneurons changed several fold across their arbors (Gulyás et al. 1999). In contrast, we found that the I/E ratios of three RGC types do not vary greatly across ≥80% of their dendritic field. This may be because unlike pyramidal neurons that receive distinct types of excitatory input onto their apical and basal dendrites (Klausberger and Somogyi 2008; Petreanu et al. 2009), inputs from a given bipolar cell type are distributed across the entire arbor

of a RGC (Schwartz et al. 2012). While inhibitory synapses vary greatly in density across the pyramidal neuron's arbor, reflecting contacts from diverse populations of inhibitory interneurons (Klausberger and Somogyi 2008), we found, instead, that GABAergic synapse density is relatively unchanged across the RGC arbor. It remains possible that synapses of a specific amacrine cell type are differentially localized across the RGC arbor, but it is not yet known which inhibitory amacrine cell types provide GABAergic input onto all RGC types. For DS RGCs where the primary presynaptic amacrine cell types are known, there is uniform distribution of amacrine contacts across the DS dendritic arbors (Jeon et al. 2002; Briggman et al. 2011). The relatively even distributions of GABAergic and glutamatatergic synapses onto RGCs may be a common result of bipolar and amacrine cells forming mosaics across the retina (Vaney 1990; Wässle et al. 2009).

Although previous fluorescence imaging studies reported little difference in the distributions of excitatory postsynaptic sites across different RGC types (Jakobs et al. 2008; Xu et al. 2008), this may not be true for all types (Morgan et al. 2008). Immunohistochemical markers for synaptic proteins also show that I/E ratios are more evenly matched across RGC types in marmoset (Percival et al. 2009; Percival et al. 2010), but EM reconstructions revealed considerable variation in the I/E ratio across RGC types of multiple species (Freed and Sterling 1988; Cohen and Sterling 1992; Kolb and Nelson 1993; Owczarzak and Pourcho 1999). We found that mature I/E ratios can vary across mouse RGC types with respect to GABAergic and glutamatergic synapses.

How does the overall distribution of synaptic inputs onto individual neurons inform us of cell function? At least for some RGCs, their functional properties can be predicted by the distribution of their inputs (Freed et al. 1992; Morgan et al. 2008), but this is not true for other RGCs. The 'preferred direction' of direction-selective RGCs is a consequence of the circuit properties of their presynaptic inhibitory input (Fried et al. 2002; Euler et al. 2002; Briggman et al. 2011; Taylor and Smith 2012) rather than the spatial distribution of their inhibitory inputs (Jeon et al. 2002). Together with the excitatory and

inhibitory synapse maps we provide here, future identification of the presynaptic partners, their functional properties and their connectivity should lead to a more complete understanding how the output of distinct RGC types are shaped.

Local spatial relationships between GABAergic and glutamatergic synapses onto RGCs

Functional studies that directly examined the spread of integration between synaptic inputs suggest that synaptic integration may be localized to dendritic segments spanning as little as 10 µm (Tao et al. 2001; Harvey and Svoboda 2007; Polsky et al. 2004), and for spiny neurons, to spines (Yuste 2011). However, much of this work focused primarily on the interaction of neighboring excitatory inputs. Modeling studies suggested that inhibitory inputs further the computational abilities of individual dendrites (Sjöström et al. 2008; Spolidoro et al. 2009). Moreover, cell culture studies demonstrated the capacity for inhibitory inputs to affect excitatory inputs with spatial constraints similar to those seen between excitatory inputs (Liu 2004), perhaps representing subcircuit arrangements. The axonal territories of most bipolar cell types are relatively small (10-25 µm diameter) and tile across a RGC dendritic arbor (Wässle et al. 2009) such that bipolar cell inputs likely represent repeated subcircuits. Inhibitory input onto RGCs may locally regulate excitation within these subcircuits across the RGC receptive field. Indeed, a key synaptic arrangement within the retina is the ribbon dyad synapse of bipolar cells, whereby a single bipolar cell release site is apposed to two processes (Dowling and Boycott 1966). Amacrine cells have been found to directly synapse onto the RGC at these dyad synapses, thus providing local feedforward inhibition. In primate, local feedforward inhibition is found at more than half of the amacrine cell contacts onto one RGC type (Calkins and Sterling 1996) and is important for cell function (Cafaro and Rieke 2010). But, these feedforward circuits may not dominate in all RGC types (Percival et al. 2010). Our EM observations suggest that for the ON-S A-type RGC in the mouse retina, ~42% of the dyad contacts sampled have local feedforward inhibition. We also found that the median distances

between fluorescently labeled excitatory and inhibitory postsynaptic sites resemble the distance between the bipolar cell contact and the amacrine cell feedforward synapse onto the RGC dendrite. This was true for all RGC types examined. Although we cannot conclude that these synapse arrangements visualized under light microscopy always reflect subcircuits comprising feedforward inhibition, we showed that the local spatial arrangements cannot occur merely by random organization of synaptic sites onto the RGC. Thus, there may exist local constraints on the spatial relationship between sites of glutamatergic excitation and GABAergic inhibition onto RGC dendritic arbors that favor local feedforward circuits.

In the primate retina, dyad synapses have been suggested to form from an initial monad contact between a bipolar cell and an RGC or amacrine cell followed by addition of a contact with one of these cell types (Nishimura and Rakic 1985; Nishimura and Rakic 1987). Our observation that the local spatial relationship between inhibitory and excitatory postsynaptic sites are set by P12 for all three RGC types, suggest that dyads form rapidly after bipolar cells make synapses. What remains unresolved is whether the dyad arrangement sets the median distances between neighboring amacrine and bipolar inputs, or whether some cue that initially imposes a spatial constraint on this distance facilitates dyad formation. In hippocampal cell culture, disruption to inhibitory transmission results in compensatory alterations in excitatory transmission only when these inputs are present on the same dendritic branch (Liu 2004). In addition, two recent studies have shown that alterations in excitatory activity during development result in decreases in a specific subset of inhibitory synapses next to excitatory inputs on dendritic spines (Chen et al. 2012; van Versendaal et al. 2012). The stereotypic synaptic dyad arrangement of inputs onto RGC dendrites clearly presents an accessible model for future work aimed at elucidating the mechanisms responsible for setting up local circuit architecture necessary for balancing inhibitory and excitatory input.

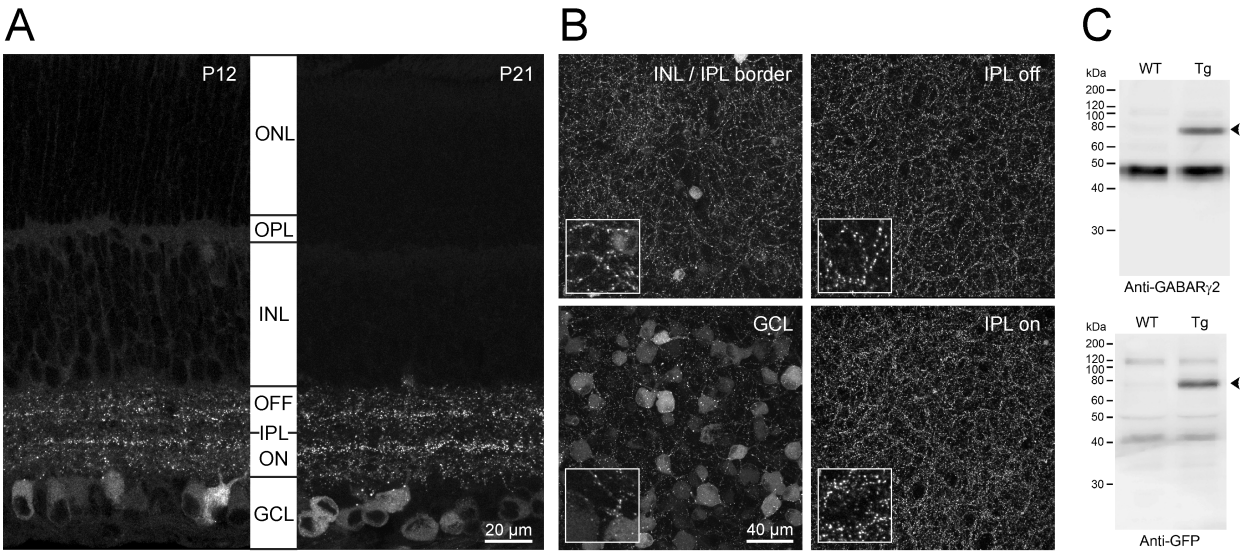

Figure 3.1 Pattern of YFPγ2 expression in retinas of Thy1-YFPγ2 transgenic mice.
(A) Maximum intensity projections (MIP) of confocal image stacks (2 µm total thickness) of vertical slices of *Thy1-YFPγ2* retinas at postnatal day (P)12 and P21. Diffuse fluorescence expression in cell bodies within the ganglion cell layer (GCL) at both ages, and punctate expression throughout both OFF and ON layers of the inner plexiform layer (IPL) are apparent. There was no expression in the outer plexiform layer (OPL) or the outer nuclear layer (ONL) at either age. **(B)** Images of MIPs (~20µm thick) at various depths of a P21 flat mount *Thy1-YFPγ2* retina. Inserts are 3x magnification of the images. **(C)** Western blot of whole brain lysates from *Thy1-YFPγ2* (Tg) and wildtype (WT) mice. YFPγ2 (arrowhead) was detected with anti-$GABA_A$Rγ2 (upper) and anti-GFP (lower).

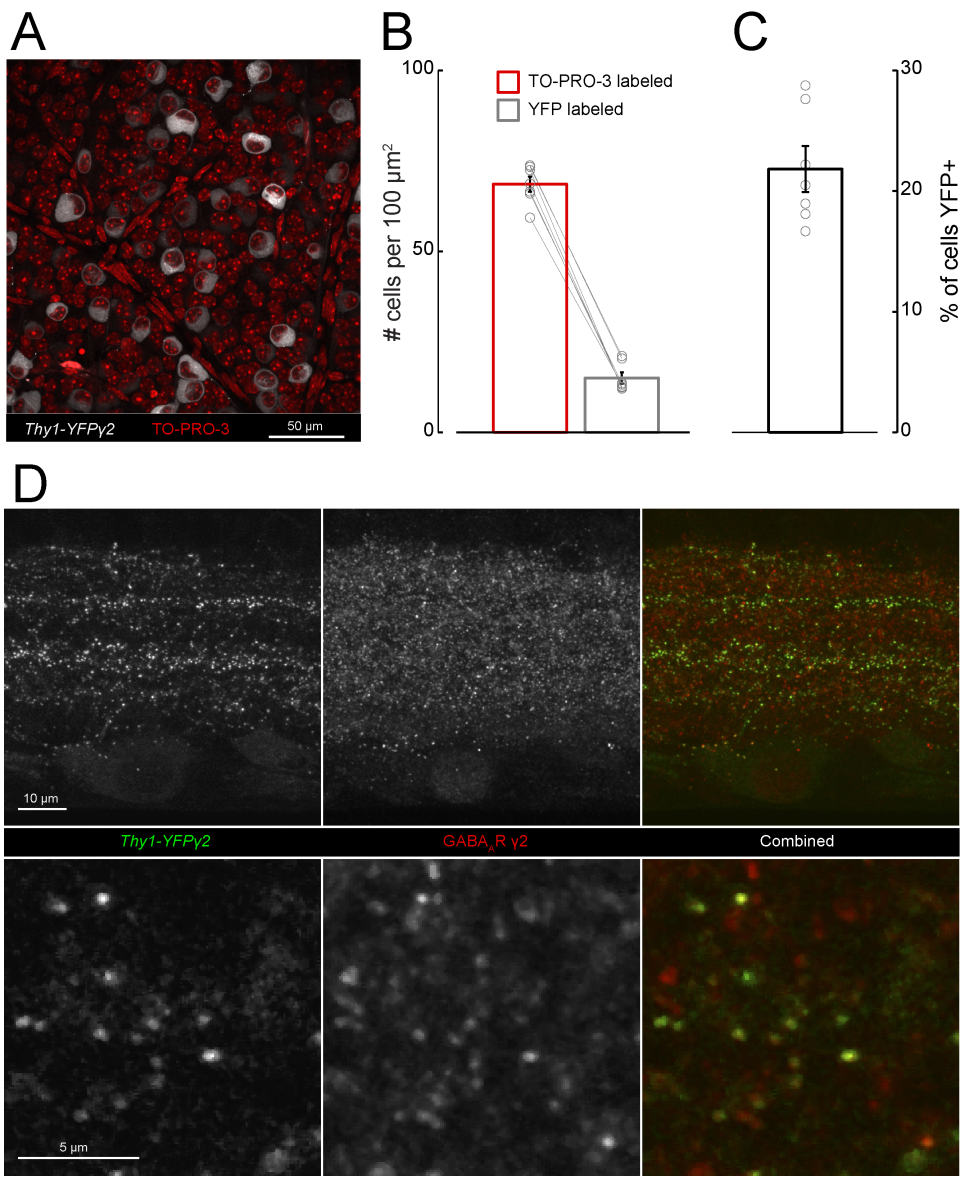

Figure 3.2 Only a fraction of the cells in the ganglion cell layer express YFPγ2.
(A) MIP of an image stack encompassing the ganglion cell layer from a P21 mouse. TO-PRO-3 staining reveals the nuclei of all cells in the ganglion cell layer (red), and cell bodies expressing YFPγ2 can be easily identified (gray). **(B)** Quantification of the density of TO-PRO-3 labeled cells, and YFPγ2 expressing cells within a 235 µm^2 sampled region (n = 4 retinas, 7 regions). **(C)** Cells expressing YFPγ2 represent 21.8% of the cells in the ganglion cell layer. **(D)** Vertical sections from a P21 retina immunostained with anti-GABA$_A$R γ2. Upper panels are MIPs of image stacks of 12 µm total thickness. Lower panels show single optical sections (0.3 µm) within the stack at higher magnification. Note that whereas all YFPγ2 puncta are also labeled by anti-GABA$_A$R γ2, not all anti-GABA$_A$R γ2 have YFPγ2.

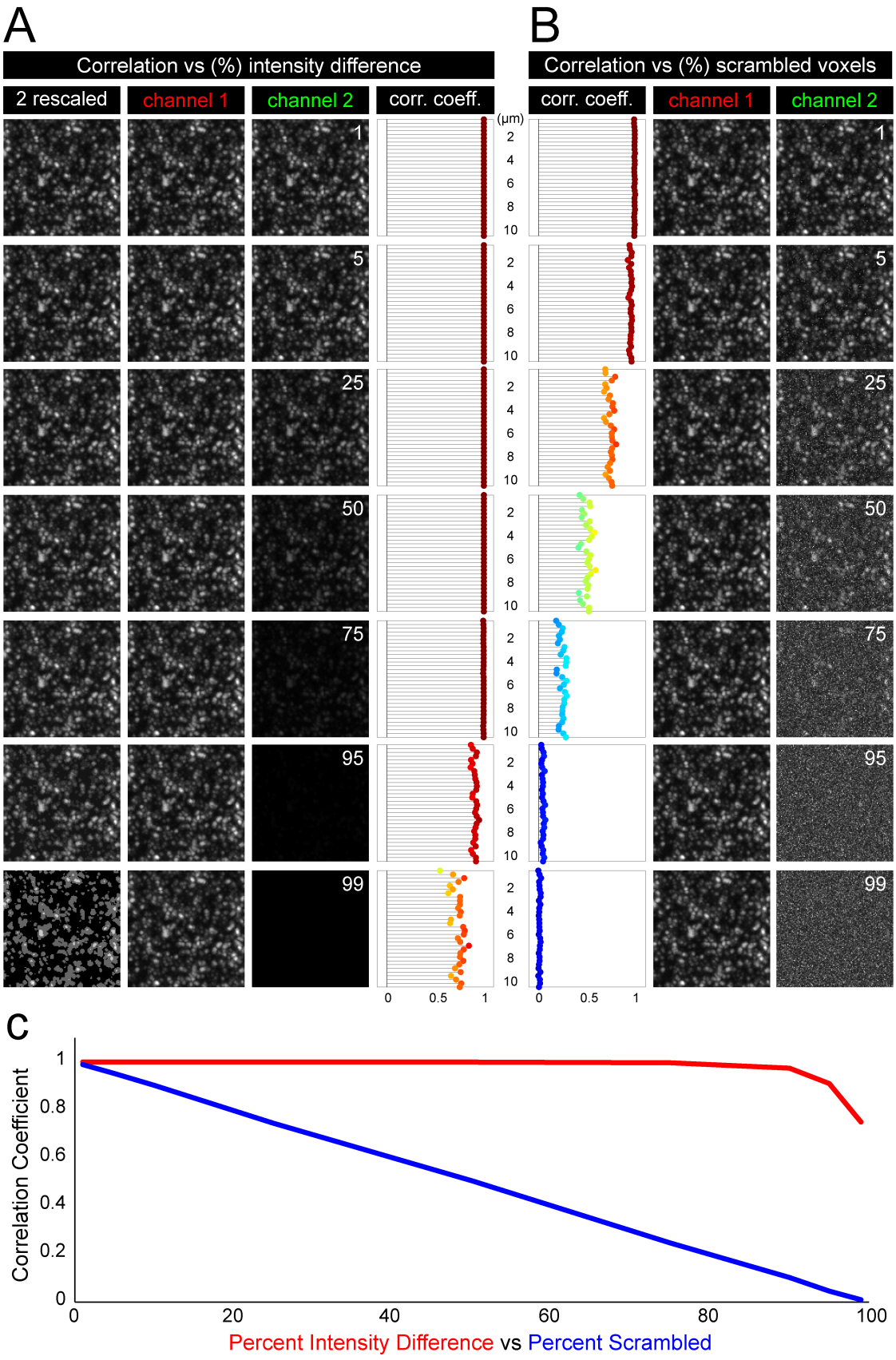
A
Correlation vs (%) intensity difference
2 rescaled
channel 1
channel 2
corr. coeff.
(μm)
1
5
25
50
75
95
99
2
4
6
8
10
0
0.5
1
B
Correlation vs (%) scrambled voxels
corr. coeff.
channel 1
channel 2
C
Correlation Coefficient
0
0.2
0.4
0.6
0.8
1
0
20
40
60
80
100
Percent Intensity Difference vs Percent Scrambled

Figure 3.3 Dependence of cross-correlation analysis on differences in intensity and signal to noise. **(A)** Demonstration of how differences in intensity between two channels affects the correlation coefficient. A 10x15x10µm (xyz) volume from P21 vertical retinal slices immunostained with gephyrin (channel 1 column), an inhibitory postsynaptic scaffolding protein (Vannier and Triller 1997; Tretter et al. 2012), is correlated with a duplicated volume (channel 2). In the duplicated channel, the percent intensity difference between the channels was varied from 1-99 by linearly scaling the intensity of the duplicate channel (channel 2 column). The correlation coefficient at each z-depth (µm) is relatively unchanged until the intensity difference between the channels is > 90% (corr. coeff column). This persistence in the correlation coefficient can best be demonstrated by observing that much of the signal-to-noise apparently lost by differences in intensity, can be recovered by rescaling the 'dimmer' image to the full bit depth (2 rescaled column). Only at intensity differences of >90% does the rescaled channel begin to be degraded. However, even at these extremes, much of the spatial patterns between the two channels are preserved. **(B)** To determine how changes in signal-to-noise between two fluorescence channels affect the correlation coefficient, the same immunostained volume (channel 1 column) was correlated with its duplicate when the percentage of voxels is systematically scrambled from 1-99 (channel 2 column). The strength of the correlation coefficient at each depth follows inversely the percent of scrambled voxels (corr. coeff column). **(C)** Plot of the average correlation coefficient vs changes in intensity (red) or scrambled voxels (green) at each interval.

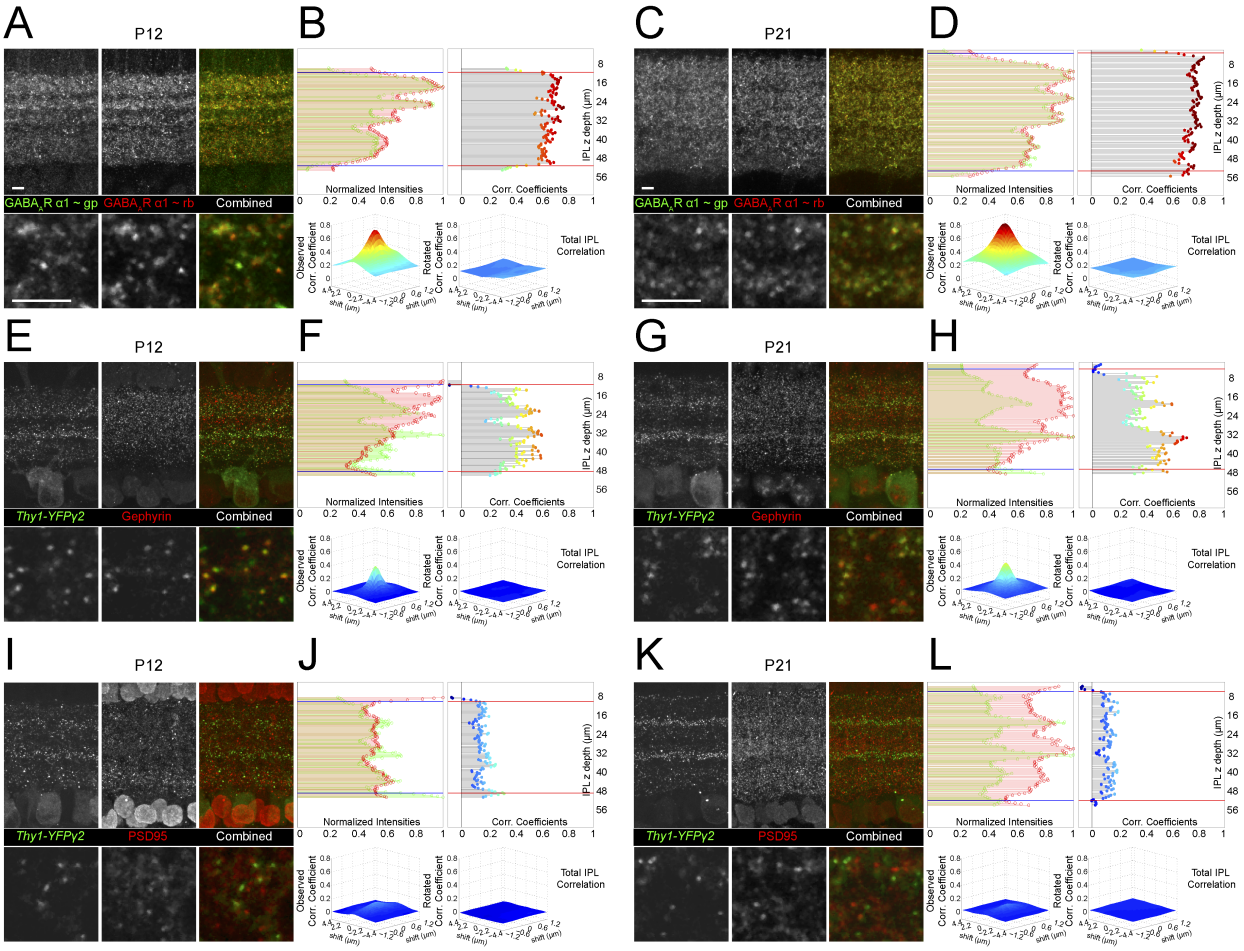

Figure 3.4 YFPγ2 fluorescence correlates with immunostaining of inhibitory postsynaptic, but not excitatory postsynaptic sites.

(A,C) Vertical sections from P12 and P21 retinas immunostained with anti-GABA$_A$R α1 raised in different hosts. Upper panels are MIPs of image stacks of 15 µm total thickness. Lower panels show single optical sections (0.3 µm) within the stack at higher magnification. **(B,D)** (Upper-Left) Normalized fluorescence intensities for GABA$_A$R α1 ~gp (green) and GABA$_A$R α1 ~rb (red) are plotted against the vertical (z) depth of the IPL. (Upper-right) The correlation coefficient obtained from the cross-correlation of the two fluorescent channels plotted against depth of the IPL. (Lower panels) 2D cross-correlation plots for the entire depth of the IPL (region between red lines in upper-right). Correlation between the two channels decreases when one channel is shifted in 'x and y' (left plot) away from 0,0 or if one channel is rotated 180° (right plot) with respect to the other. **(E-H)** Cross-correlation analysis was also performed for vertical sections from P12 and P21 *Thy1-YFPγ2* retinas immunostained with anti-gephyrin, a protein found at inhibitory postsynaptic sites. **(I-L)** Similar plots for the excitatory postsynaptic marker, PSD95 at P12 and P21. Strong correlation between *Thy1-YFPγ2* fluorescence and inhibitory, but not excitatory, postsynaptic markers is present early in postnatal development. Scale bars 5 µm.

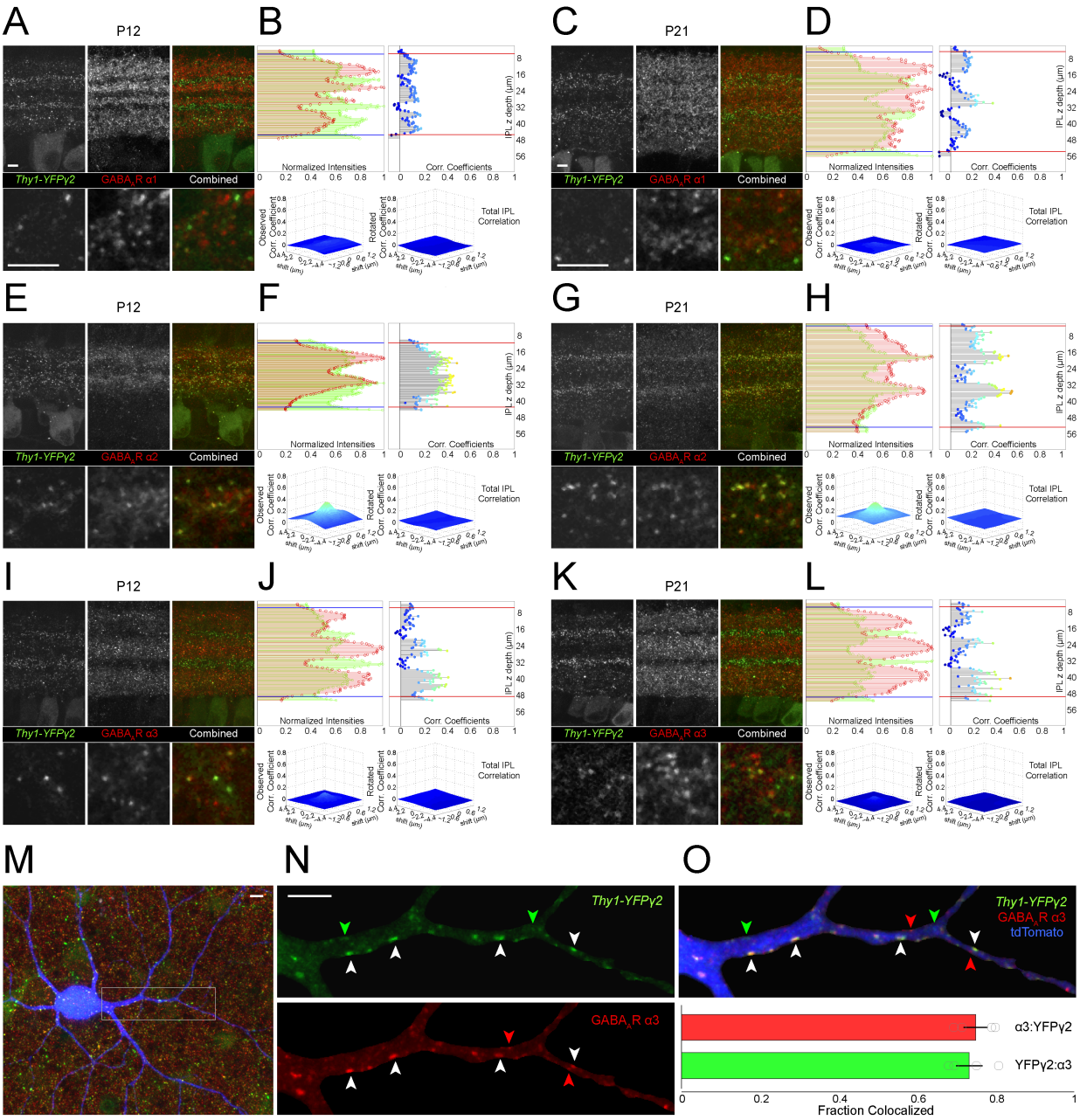

Figure 3.5 YFPγ2 fluorescence correlates with immunostaining for GABAAR α subunits.
Cross-correlation analysis of vertical sections from P12 and P21 *Thy1-YFPγ2* retinas stained with anti-GABA$_A$R α1 **(A-D)**, GABA$_A$R α2 **(E-H)**, or GABA$_A$R α3 **(I-L)**. **(M)** Image stack of a single ON RGC labeled by transfection of CMV:tdTomato in a *Thy1-YFPγ2* retina, immunostained for GABA$_A$R α3. **(N)** The dendritic label was used to mask out the YFPγ2 and GABA$_A$R α3 fluorescence. **(O)** (Upper) YFPγ2 and GABA$_A$R α3 puncta within sections of dendritic arbors identified by custom-written software. (Lower) Fraction of the population of YFPγ2 puncta that colocalized with GABA$_A$R α3, and vice-versa (average and SEM of 4 cells). White arrowheads are examples of colocalized puncta, green and red arrowheads, non-colocalized puncta. Scale bars 5 µm.

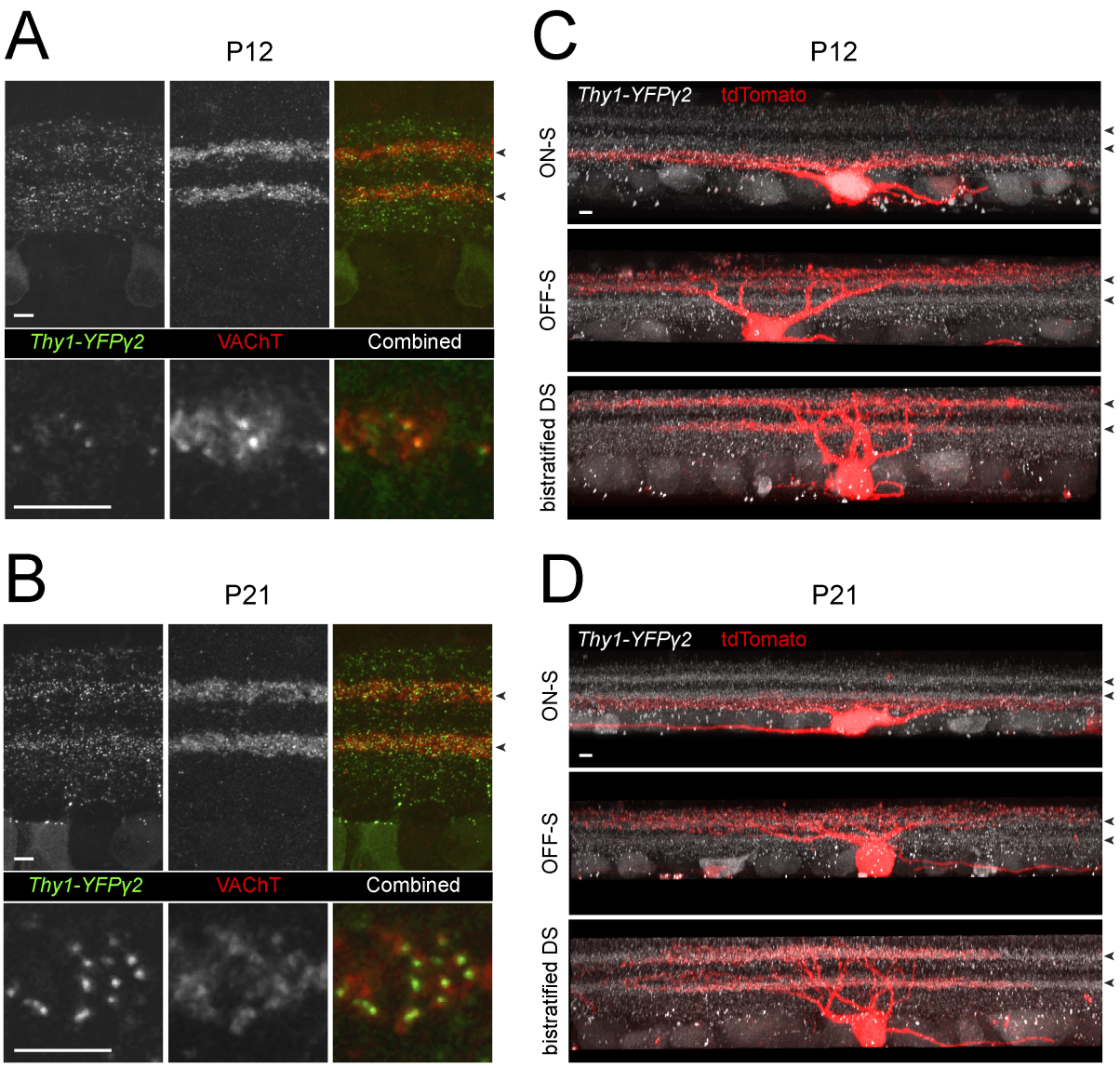

Figure 3.6 Stratification of ON-S A-type, OFF-S A-type and bistratified DS RGCs can be readily identified in Thy1-YFPγ2 retinas.

(A,B) Vertical sections from P12 and P21 retinas immunostained with anti-VAChT to label the presynaptic terminals of starburst amacrine cells (Koulen 1997; Dong et al. 2004). These characteristic cholinergic bands (arrow heads in A-C) can be utilized to identify stratification in the retina. Upper panels are maximum intensity projections (MIPs) of image stacks of 15 µm total thickness where two bands of relatively dense YFPγ2 fluorescence correspond to the VAChT positive sublaminae. The high degree of spatial apposition between VAChT staining and YFPγ2 fluorescence is apparent in single optical sections (0.3 µm) within the stack (lower panels). **(C,D)** Examples of vertical MIPs of ON-S, OFF-S A-type and bistratified DS RGCs labeled with tdTomato at P12 and P21. At both ages, the dendritic arbors of ON-S A-type RGCs consistently stratified below the lower VAChT band, whereas the arbors of

OFF-S A-type RGCs stratified above the upper VAChT band. The arbors of bistratified DS RGCs costratify with the VAChT bands. Scale bars are 5 µm.

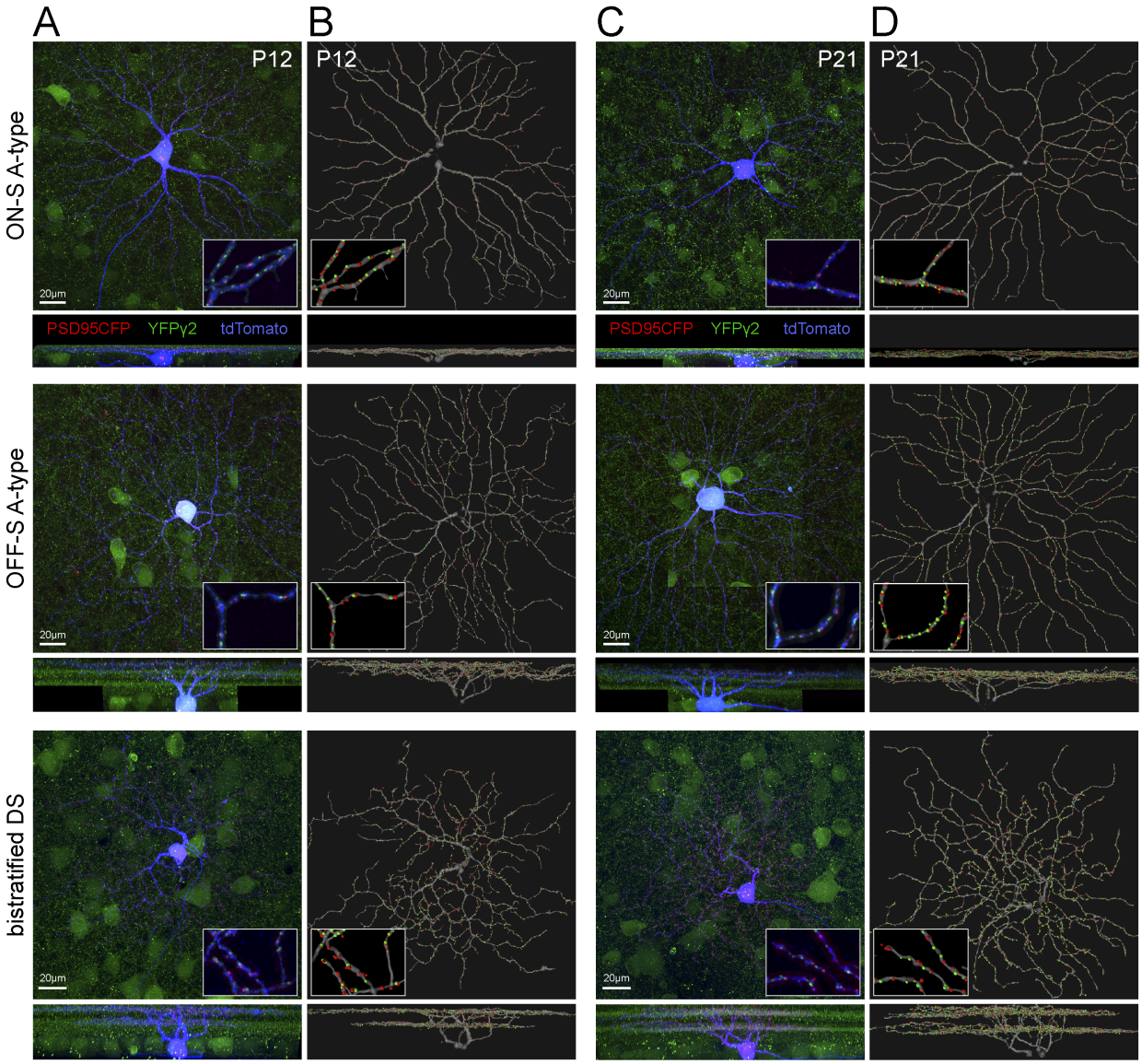

Figure 3.7 Distributions of GABAergic and glutamatergic postsynaptic sites on dendritic arbors of distinct types of RGCs.

Biolistic transfection of individual ganglion cells in *Thy1-YFPγ2* retinas with a cell label (tdTomato) and excitatory postsynaptic protein (PSD95CFP). **(A)** Representative flat mount (upper) and vertical (lower) MIPs of three distinct RGC types in P12 *Thy1-YFPγ2* retina; ON-S A-type, OFF-S A-type, and bistratified DS RGCs. Inserts are 4x magnifications of a region of the arbor showing PSD95CFP and YFPγ2 found only within the dendrites. **(B)** MIPs of the reconstructed dendritic skeletons and identified postsynaptic sites from the cells in (A). Inserts represent the same regions as inserts in (A). **(C,D)** Example MIPs of the raw images of P21 cells (C), their skeletonized dendrites and identified postsynaptic sites (D).

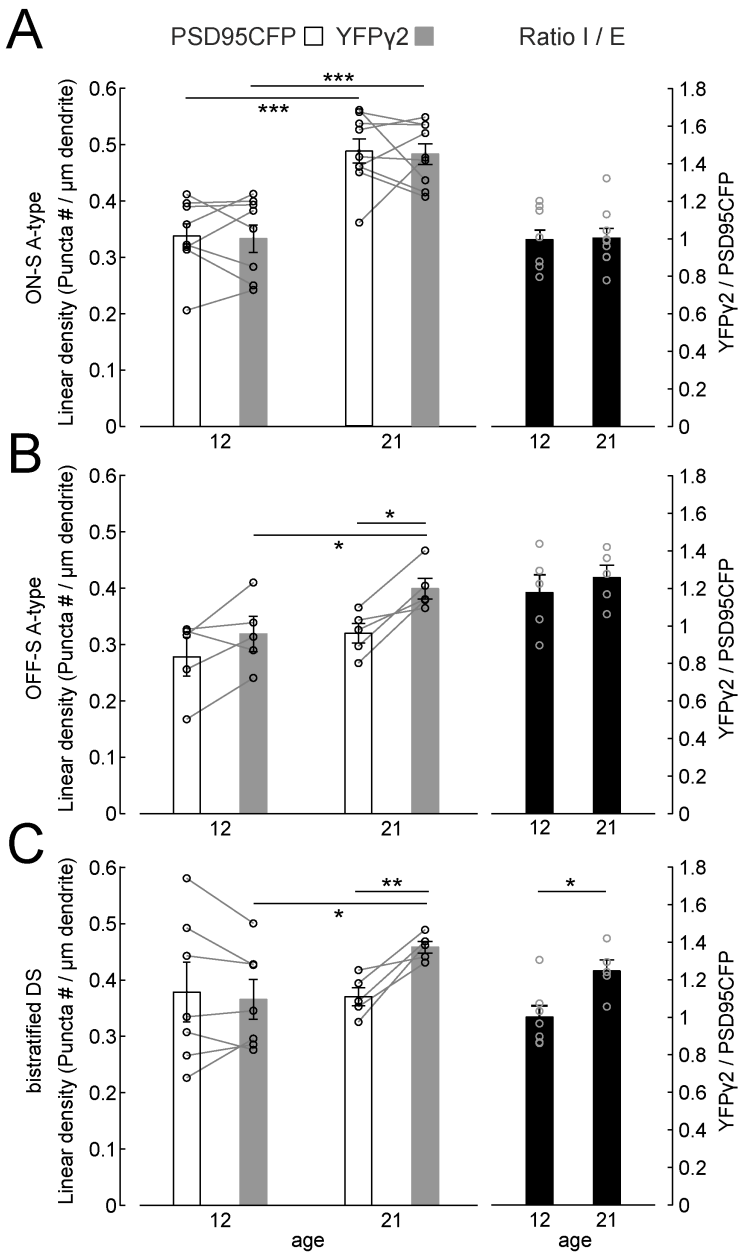

Figure 3.8 Densities and ratios of GABAergic to glutamatergic postsynaptic sites of three types of RGCs across development.

Linear densities (left axis) and ratio (right axis) of PSD95CFP (white bars) and YFPγ2 puncta (gray bars) on P12 and P21 ON-S A-type cells **(A)**, OFF-S A-type **(B)** and bistratified DS **(C)** RGCs. Lines link data points from the same cell. Statistical tests between ages were two sample student's t-test unequal variance, and within ages were two sample paired student's t-test. *** = P<0.001, **= P<0.01, * = P<0.05.

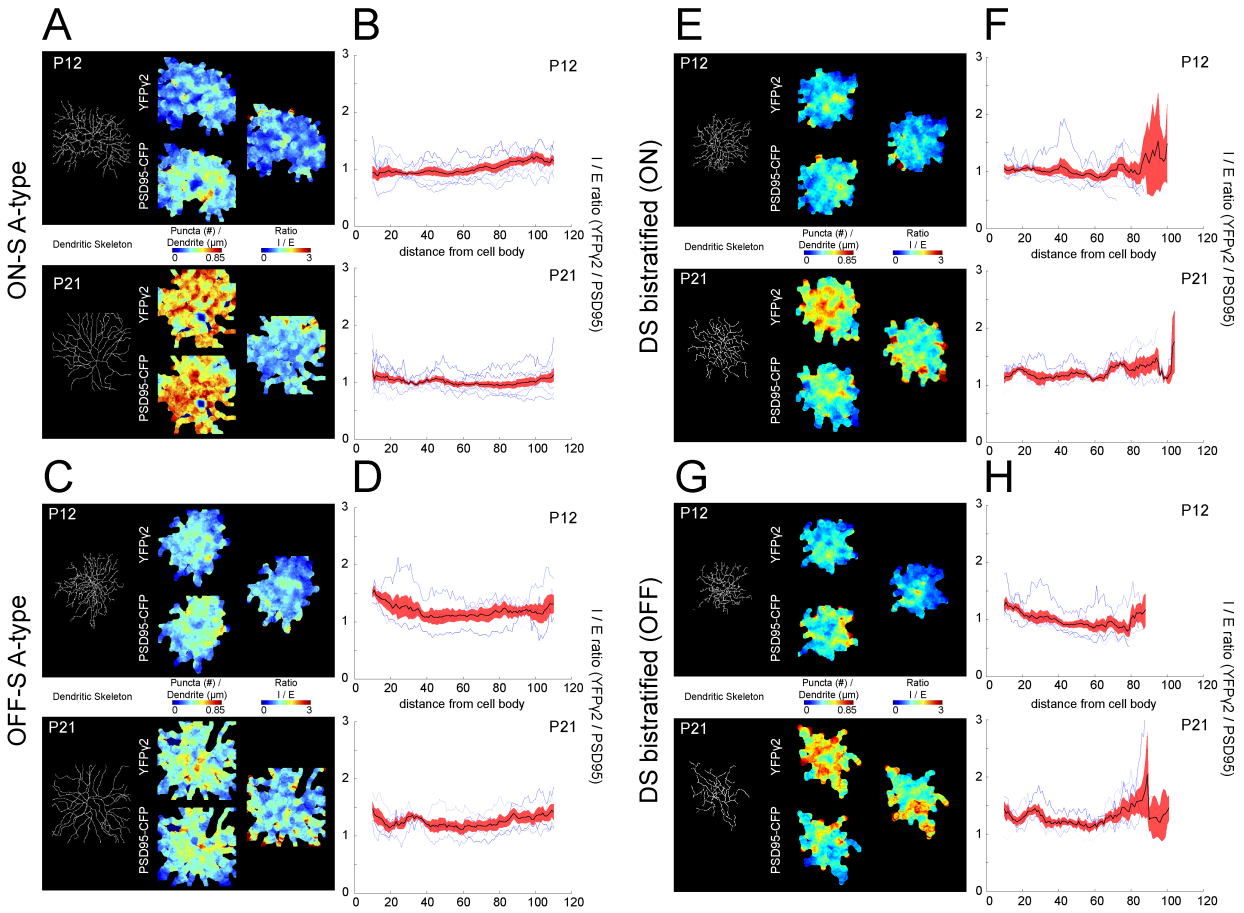

Figure 3.9 Spatial density heat maps of GABAergic and glutamatergic postsynaptic sites on RGC dendritic arbors.

(A) (Left) Dendritic skeletons of ON-S A-type RGCs at P12 and P21. (Middle) Synaptic density maps were created by convolving a 10μm disk centered on each pixel of the MIP of the dendritic skeleton puncta linear density [puncta (#) / dendrite (μm)] for YFPγ2 (upper) and PSD95CFP (lower). (Right) Ratio of YFPγ2/ PSD95CFP puncta across ages. **(B)** YFPγ2/ PSD95CFP ratio plotted against eccentricity (distance from cell body). Each blue line represents a cell, black line is mean and red shading SEM. Analysis of OFF-S A-type RGC is shown in **(C,D)** and of ON and OFF arbors of bistratified DS RGCs in **(E-H)**.

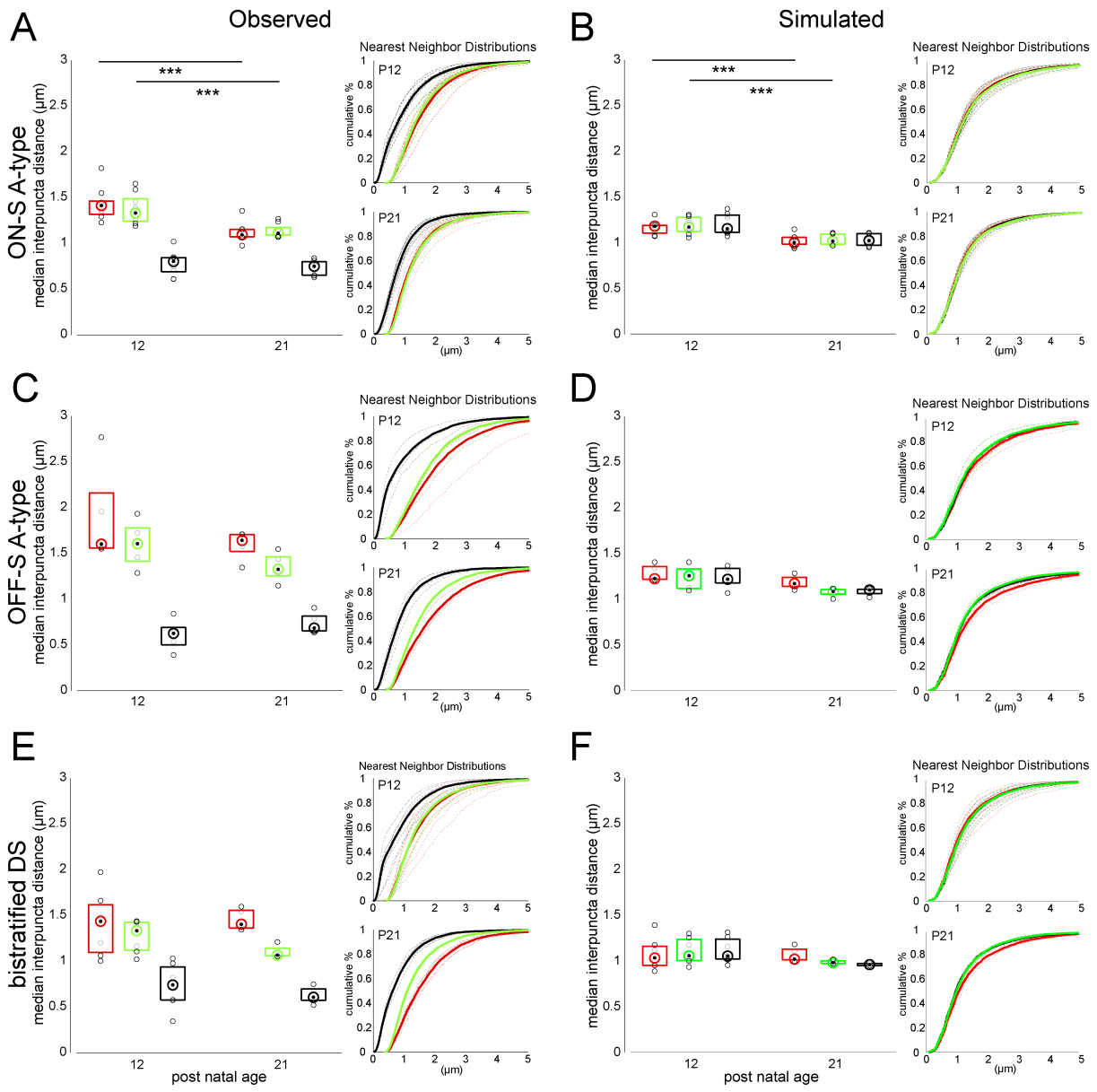

Figure 3.10 The nearest neighbor distance between PSD95CFP puncta and their nearest YFPγ2 punctum is established early in development.

(A) Plotted are the median nearest neighbor distances for each PSD95CFP punctum and its nearest neighbor (red box plot), each YFPγ2 punctum and its nearest neighbor (green box plot) and each PSD95CFP punctum and the nearest YFPγ2 punctum (black box plot) for ON-S A-type RGCs at P12 and P21. **(B)** The nearest neighbor distances calculated from simulating the same densities of PSD95CFP and YFPγ2 puncta from ON-S A-type RGCs randomly distributed over their dendritic arbors. Nearest neighbor analysis was also performed for OFF-S A-type **(C-D)**, and bistratified DS RGCs **(E-F)**. Box plots represent 25 and 75 percentiles. Inserts show cumulative nearest neighbor distributions for P12 (upper) and P21(lower). Dashed lines are individual cells, solid lines represent all cells. (Wilcoxon rank-sum test *** = P<0.001).

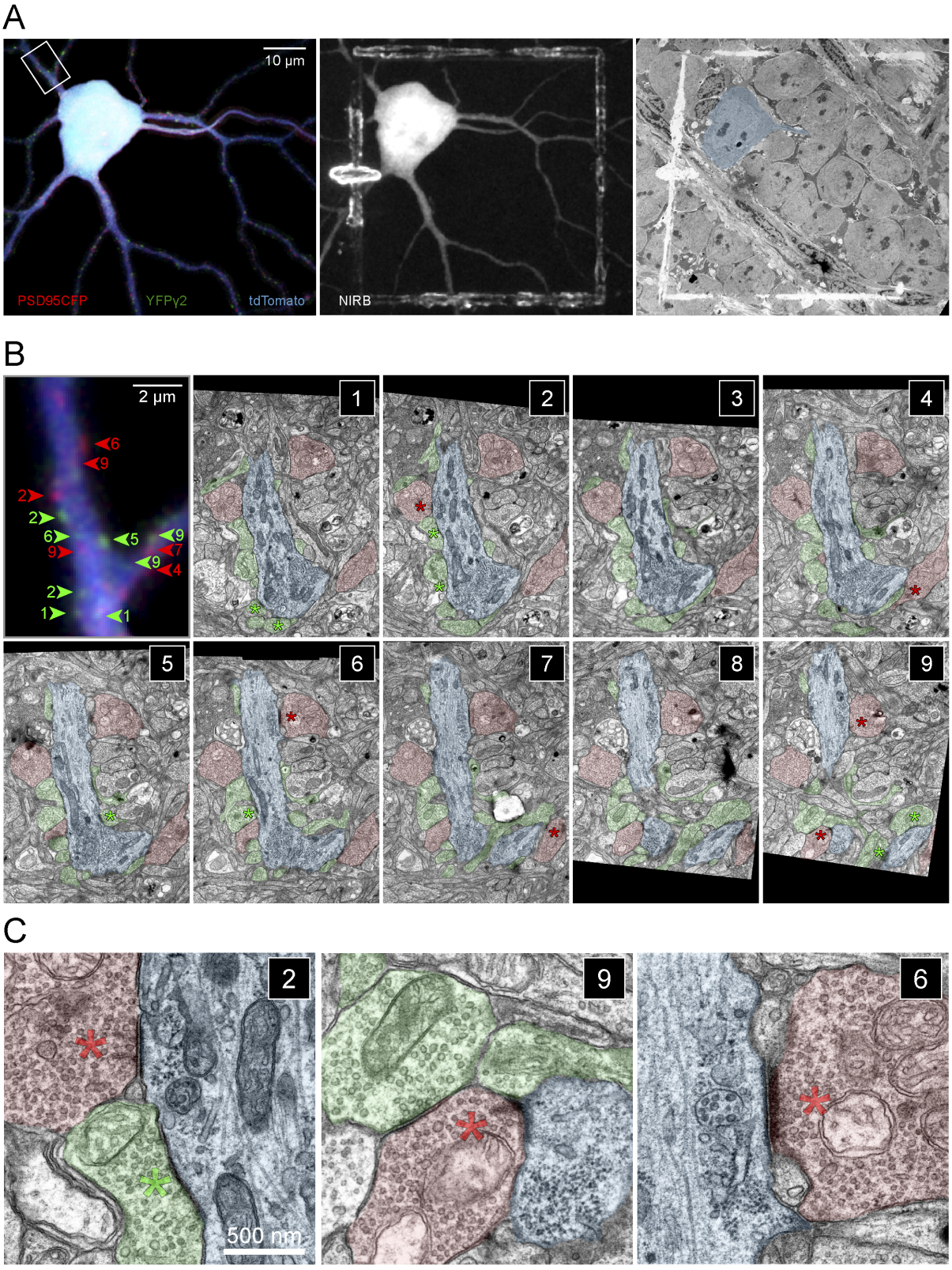
A
10 µm
PSD95CFP
YFPγ2
tdTomato
NIRB
B
2 µm
1
2
3
4
5
6
7
8
9
C
2
9
6
500 nm

Figure 3.11 Correlation of fluorescent labeled GABAergic and glutamatergic postsynaptic sites with ultrastructure.

(A) (Left) MIP of an ON-S A-type RGC labeled by biolistic transfection of tdTomato and PSD95CFP in a *Thy1-YFPγ2* retina. Shown here are PSD95CFP and YFPγ2 signal within the dendrites. (Middle) Image showing fiduciary marks burned at the level of the axon and cell body of the labeled RGC using the NIRBing technique (Bishop et al. 2011). (Right) EM micrograph showing the NIRBed window, allowing identification of the cell (colored blue). **(B)** MIP of a small section of a primary dendrite from the box in (A, left) showing YFPγ2 (green arrowheads) and PSD95CFP (red arrowheads) signal, and serial EM sections 1-9 of this region. Colored numbers in MIP indicate the serial section in which the corresponding synapse was identified (see green and red asterisks). EM sections are 80 nm thick. **(C)** Magnified views of bipolar (red) and amacrine (green) cell synapses on the RGC dendrite (blue) in sections (2,9,6). (Left) A cone bipolar cell terminal (red) makes a non-dyad ribbon synapse with the RGC dendrite, where two ribbons appear at the same synaptic site (red asterisk). An inhibitory amacrine cell synaptic profile can also be observed in close proximity (green asterisk). (Middle) A characteristic dyad ribbon synapse (red asterisk) between a cone bipolar cell and the RGC dendrite and an amacrine cell process (green). (Right) A contact between the ganglion cell and a bipolar cell at a plane where the postsynaptic density is evident but the ribbon is not orthogonally aligned. The synapse can be identified by examining the serial profiles in which a partial ribbon is visible (sections 4-7 in B; Movie 3.1).

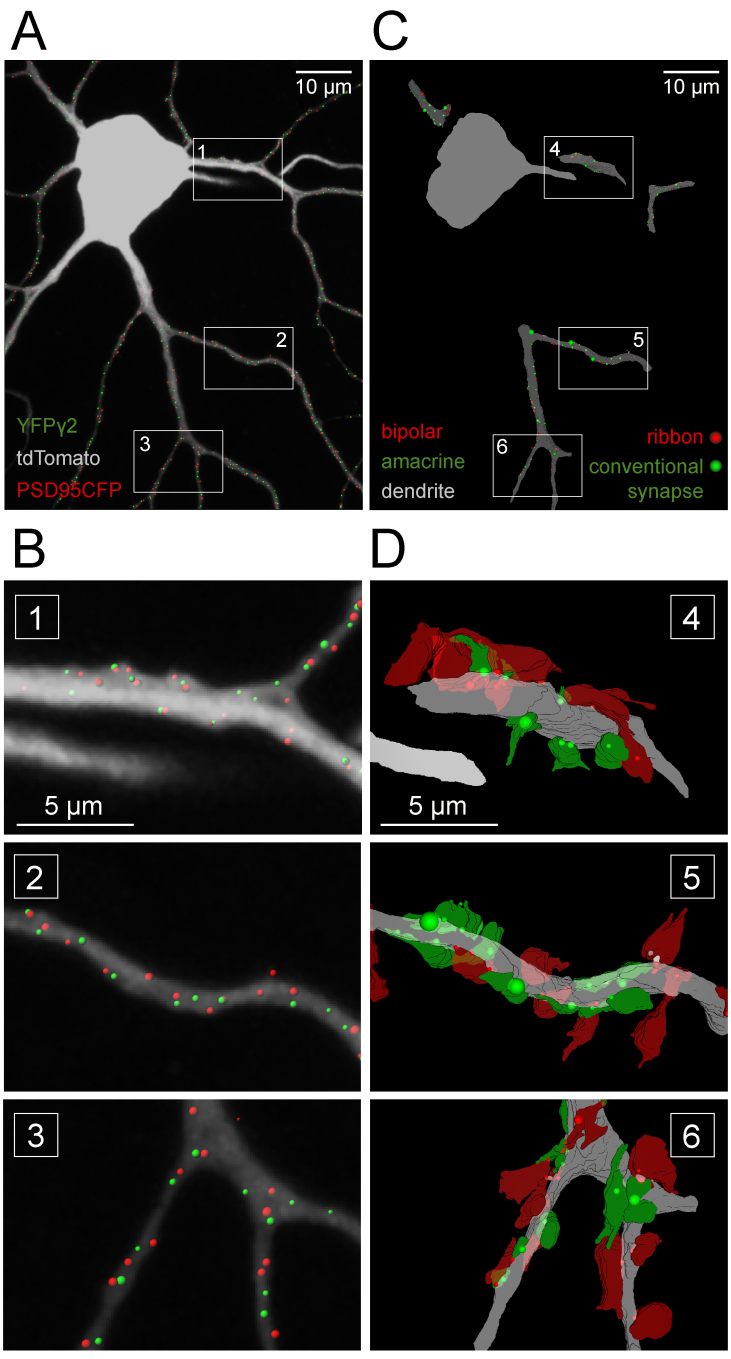

E

ribbons	PSD95CFP	ribbons w/ PSD95CFP	% ribbons apposed to PSD95CFP	% PSD95CFP apposed to ribbons
53	67	49	93%	73%

conventional synapses	YFPγ2	conv. synapses w/ YFPγ2	% conv. synapses apposed to YFPγ2	% YFPγ2 apposed to conv. synapses
65	52	42	65%	81%

Figure 3.12 PSD95CFP and YFPγ2 puncta on RGC dendrites correspond to sites of bipolar cell and amacrine cell synapses.

(A) ON A-type RGC (gray) with identified PSD95 (red dots) and YFPγ2 (green dots). **(B)** Higher magnification of the boxed regions 1-3 in (A). **(C)** Three dimensional reconstructions of serial EM sections showing the locations of amacrine (conventional) and bipolar cell (ribbon) synapses on the reconstructed dendrites (gray). **(D)** Higher magnification of the boxed regions in **(C)** showing amacrine (red) and bipolar (green) cell processes apposed to the dendrite. Locations of synapses are marked by the colored dots (red, ribbon; green, conventional). The size of the dot is proportional to the length of the postsynaptic density at the synapse. **(E)** Table representing the number and correlation of fluorescence and anatomical profiles from the reconstructions.

RGC type	Age	Dendritic Length (µm)	PSD95CFP number	YFPγ2 number	PSD95CFP linear density	YFPγ2 linear density	I / E ratio	n
ON-S A-type	12	3583.9 ± 247.6	1185.2 ± 71.4	1171.1 ± 79.8	0.34 ± 0.02	0.33 ± 0.02	0.99 ± 0.05	9
	21	3102.3 ± 119.2	1534.6 ±102.3	1511.3 ± 91.9	0.49 ± 0.02	0.49 ± 0.02	1.00 ± 0.05	9
OFF-S A-type	12	4235.8 ± 336.1	1163.8 ± 172.0	1340.0 ± 169.7	0.28 ± 0.03	0.32 ± 0.03	1.18 ± 0.15	5
	21	4337.0 ± 223.4	1382.4 ± 96.0	1738.4 ± 151.6	0.32 ± 0.02	0.40 ± 0.02	1.26 ± 0.07	5
Bistratified DS	12	4028.0 ± 246.8	1508.4 ± 192.4	1454.0 ± 118.9	0.38 ± 0.05	0.37 ± 0.04	1.00 ± 0.06	7
ON arbor	12	2247.1 ± 154.7	839.6 ± 144.0	799.9 ± 99.3	0.37 ± 0.05	0.36 ± 0.03	0.99 ± 0.06	
OFF arbor	12	1780.9 ± 179.8	668.9 ± 80.6	654.1 ± 57.4	0.39 ± 0.05	0.38 ± 0.04	1.01 ± 0.07	
Bistratified DS	21	3766.4 ± 165.6	1401.4 ± 94.1	1729.8 ± 60.3	0.37 ± 0.02	0.46 ± 0.01	1.25 ± 0.06	5
ON arbor	21	2036.4 ± 56.4	768.0 ± 17.3	907.8 ± 39.9	0.38 ± 0.02	0.45 ± 0.01	1.19 ± 0.07	
OFF arbor	21	1730.0 ± 170.0	633.4 ± 83.7	822.0 ± 84.2	0.36 ± 0.02	0.47 ± 0.02	1.32 ± 0.06	

Table 3.1 Summary data for total dendritic length, puncta linear densities, and total inhibitory to excitatory ratios for all RGCs sampled.

Numbers are averages and SEM for all cells, for each parameter. Total dendritic length was calculated as the sum of all dendritic segment lengths within the (~.045 mm^2) region sampled.

Movie 3.1 is available at the following location: http://dx.doi.org/10.1371/journal.pone.0069612

Movie 3.1 Serial walk-through of bipolar cell ribbon contacts with a RGC dendrite.
Serial sections through the synaptic contact between the bipolar cell axon terminal (red) and the RGC dendrite (blue) highlighted in Figure 3.11B,C panel 6. Two ribbon synapses can be seen (arrowheads): 1) A ribbon synapse parallel to the plane of sectioning and 2) a ribbon synapse orthogonal to the plane of sectioning. Both forming dyad synapses with the RGC and a dendritic process from a different cell.

CHAPTER IV

INHIBITORY NEUROTRANSMISSION SELECTIVELY REGULATES SYNAPTIC CONNECTIVITY ONTO DISTINCT COMPARTMENTS OF INDIVIDUAL RETINAL GANGLION CELLS

4.1 INTRODUCTION

The fundamental role for neurotransmission in mature circuits is the communication between neurons underlying normal circuit activity. However communication is also critical during development when the mature wiring patterns and synaptic connections between individual neurons are becoming established. In particular, excitatory neurotransmission has been implicated in regulating multiple components of circuit development across diverse circuits (Hua and Smith 2004; Hong and Chen 2011; Bleckert and Wong 2011). In addition to their effects on early developmental processes such as cell proliferation, migration, and differentiation (Owens and Kriegstein 2002), in recent work, classical inhibitory neurotransmitters GABA and glycine have also been shown capable of regulating pre- and postsynaptic components of circuit assembly (Huang 2009).

The role of inhibitory neurotransmission in the establishment of mature neuronal circuits has been examined by disrupting inhibitory neurotransmission through various methods. Selective disruption of the receptors or scaffolding molecules located on postsynaptic cells, reveal that inhibitory neurotransmission is not essential for the clustering of inhibitory receptors, but has been implicated in the correct targeting of and organization of receptors and scaffolding proteins at inhibitory synaptic sites (Rao et al. 2000; Kneussel et al. 2001; Lévi et al. 2002; Brünig et al. 2002; Schweizer et al. 2003; Lévi et al. 2004; Takeuchi et al. 2005; Christie et al. 2006; Patrizi et al. 2008; Poulopoulos et al. 2009). In addition, disruption of inhibitory neurotransmission by blocking release of GABA and glycine, either by knockout of the genes encoding the synthesizing enzymes for GABA (*GAD1/GAD2*) or the vesicular inhibitory amino acid transporter (*VIAAT/VGAT*) have implicated inhibitory transmission in the correct

maturation of the pre- and postsynaptic components of GABAergic synapses (Chattopadhyaya et al. 2007a; Huang 2009; Wu et al. 2012; Schubert et al. 2013).

Part of the challeng in elucidating the roles of neurotransmission in circuit assembly is the difficulties in disrupting neuronal activity and diversity of effects that have been observed across various methods (Bleckert and Wong 2011). Furthermore, the complexity of many neuronal circuits has often limited the examination of the affects of inhibitory transmission onto isolated components of individual cells such as axon terminals or somata (Chattopadhyaya et al. 2007a; Wu et al. 2012; Schubert et al. 2013). To selectively disrupt inhibitory neurotransmission, we utilized the conditional KO of the sole vesicular transporter of GABA and glycine (VIAAT/VGAT (McIntire et al. 1997; Wojcik et al. 2006)). To gain a more complete understanding of the effects of inhibitory neurotransmission on establishing the patterns of synaptic input onto individual cells, we take advantage of the compact circuitry of the mouse retina and its well defined cell types (Coombs et al. 2006; Völgyi et al. 2009; Wei and Feller 2011; Farrow et al. 2013; Dhande et al. 2013; Bleckert et al. 2014), to map inhibitory and excitatory synaptic distributions across the somata and dendritic arbors of individual retinal ganglion cells.

4.2 METHODS

Mice

All procedures were conducted with the approval of the University of Washington Institutional Animal Care and Use Committee. Mice were euthanized by isoflurane overdose followed by decapitation, or by cervical dislocation. Mice in which the second exon of *Slc32a1* encoding the vesicular inhibitory amino acid transporter (VIAAT/VGAT) is flanked by lox sites (*Slc32a1*$^{flox/flox}$ *(Tong et al. 2008)*) were obtained from Jackson Labs. *Thy1-YFPγ2* mice were generated as previously described (Bleckert et al. 2013; Feng et al. 2000). Mice of postnatal day (P)24 were used for anatomical experiments, and P24-30 for physiological experiments.

Fixed Tissue Preparation

Mice were euthanized, enucleated and the eyes were immersed in oxygenated mouse artificial cerebral spinal fluid (mACSF) containing the following in (mM): 119 NaCl, 2.5 KCl, 2.5 $CaCl_2$, 1.3 $MgCl_2$, 1 NaH_2PO_4, 11 glucose, and 20 HEPES, brought to pH 7.42 with NaOH. Retinas were mounted flat, ganglion cell side up, onto filter paper (Millipore), and the tissue was subsequently fixed in 4% PFA for 20 min at room temperature. Retinal orientation was preserved using a anatomical landmarks previously described (Wei et al. 2010)

Biolistic transfection

Plasmids for which a cytomegalovirus promoter drives expression of tandem dimer Tomato (tdTomato) or postsynaptic density protein 95 fused to cyan fluorescent protein (PSD95CFP) were coprecipitated onto gold particles (Bio-Rad) (Morgan and Kerschensteiner 2012). Gold particles were propelled into whole mount retinas using a Helios Gene Gun (Bio-Rad), and the tissue then incubated at ~34°C in oxygenated mACSF in a humidified chamber for 24 hr. Afterwards, retinas were fixed in 4% paraformaldehyde in mACSF for 20-30 min, rinsed in PBS, and flat mounted in vectashield (Vector Laboratories) for confocal imaging.

Immunohistochemistry

Retinas were washed in PBS and blocked overnight at 4°C in normal donkey serum. Retinas were then incubated in primary antibodies for 4 nights at 4°C. Primary antibodies used were: anti-VIAAT/VGAT (~rabbit [1:500], 131 003, Synaptic Systems), anti-gephyrin (mAb7a ~mouse [1:500], 147 011, Synaptic Systems), anti-GAD67 (~mouse [1:1000], MAB5406, Millipore), anti-$GABA_AR$ α2 (~guinea pig [1:2000],

gift of JM Fritschy). Retinas were then washed and incubated with secondary antibodies, Alexa (Invitrogen, 1:1000), or DyLight (Jackson Laboratory, 1:1000) conjugated fluorophores overnight at 4°C.

Fluorescence Image Acquisition

Image stacks were acquired using an Olympus FV-1000 laser scanning confocal microscope with an oil-immersion 60x objective (Olympus, UPLSAPO 1.35 NA). Voxel dimensions were minimum (x-y-z in µm) 0.103-0.103-0.3 for reconstructions ooDS RGCs. Images were median filtered to remove noise, corrected for xy drift (Thévenaz et al. 1998), and compressed to 8-bits after normalization of the entire stack histogram using Fiji (Schindelin et al. 2012).

Image Analysis

Quantification of RGC dendrites:

Branching patterns of ooDS RGC dendrites were skeletonized and volume rendered using the filament function of Imaris (Bitplane). Total dendritic length was calculated from the skeletonized filament. Sholl numbers of dendritic crossing every 5 µm from the soma (SHOLL 1953) were calculated from the filament in Imaris (Bitplane). To exclude the cell body the initial 10 µm were omitted Bistratified RGCs were assumed to be ON OFF direction selective (DS) RGCs based upon their dendritic morphology and by their stratification within the densely labeled sublaminae of *Thy1-YFPγ2* expression that strongly correlated with VAChT and $GABA_AR$ α2 labeling (Bleckert et al. 2013).

Identification and quantification of postsynaptic puncta:

The dendritic volume was expanded (xy 1.0 µm, z 0.5 µm) and used as a mask for segmenting YFPγ2 or PSD95-CFP fluorescence within and juxtaposed to the dendrites. PSD95CFP or YFPγ2 puncta within this masked volume were identified using custom MATLAB scripts previously described (Morgan et al. 2008).

Briefly, fluorescence within the synaptic marker channel was iteratively thresholded, filtered by size and contrast, and their ratio of fluorescence to cytosolic fluorescence intensity. In addition, puncta contacting the edge of the expanded mask were removed, and a final user-guided error minimization step was conducted by manual identification of the found puncta in 3D using the spots function of Imaris (Bitplane).

Correlative Fluorescence and Electron Microscopy:

Preparation of tissue for correlative fluorescence and electron microscopy was performed as described previously (Bleckert et al. 2013), with some modification. Briefly, *Thy1-YFPγ2* mouse retinas were biolistically transfected as described above. After incubation for 24 hrs, the retina was fixed in 1.5% glutaraldehyde / 2.5% paraformaldehyde for 40 min. The tissue was washed and mounted under coverglass in 0.1M sodium cacodylate buffer for confocal imaging. An image stack of the YFPγ2 somatic puncta was obtained, and an image stack of the 'shadow' of surrounding cell bodies and blood vessels was imaged by adding Alexa 594 to the buffer (Kitamura et al. 2008). The retina was unmounted and fixed in 4% glutaraldehyde overnight. The retina was again washed and remounted in 0.1M sodium cacodylate buffer. Using a custom-built two-photon microscope with a Ti:sapphire laser (Spectra-Physics) the original imaged cell was identified by the surrounding cell somata and blood vessel patterns and fiduciary marks were burned around the cell of interest into the tissue using the near-infrared branding (NIRB) method (Bishop et al. 2011). These marks were clearly evident as autofluorescence under multiphoton imaging and by the absence of tissue under electron microscopy. The retina was unmounted and a small section of retina encompassing the imaged cell somata was isolated (~1 mm^2). This tissue block was then prepared for TEM or SBFEM

Correlative fluorescence and TEM

The block of tissue prepared as described above washed in 0.1M sodium cacodylate buffer and post-fixed for 45 min in cacodylate buffered 1% osmium tetroxide. The tissue was washed in dH_2O, en bloc-stained in 1% aqueous uranyl acetate, and washed again in dH_2O before being dehydrated through a series of ethanol and propylene oxide and embedded in Epon Araldite resin. Semi-thin resin sections were cut until the burn marks could be identified in Richardsons stain (Methyl Blue Azure II) tissue sections. Serial thin sections (80 nm) were cut, placed on Formvar-coated slot grids and stained with Reynolds lead citrate. Micrographs were taken at 8000x (7.25 nm / pixel) for image registration, and 40000x (1.45 nm / pixel) for identification of synaptic contacts. The EM micrographs were manually aligned and serially registered using TrakEM2 (Cardona et al. 2012). Amacrine cell synaptic connections onto the RGC dendrites were identified using established criteria (Dowling and Boycott 1966). Amacrine cell contacts were identified by the presence of a PSD and presynaptic vesicles. To correlate the identified fluorescent puncta with amacrine and bipolar cell synapses, a maximum intensity projection of the labeled YFPγ2 puncta image stack was scaled and aligned to the EM reconstruction using TrakEM2.

Correlative fluorescence and SBFEM

Tissue blocks for scanning block face microscopy were prepared as described in (Deerinck et al. 2010). Image stacks were acquired using a GATAN 3View and Ziess SIGMA scanning electron microspcope. Voxel demensions of micrograph stacks were (x-y-z): 5-5-50 nm. The EM micrographs were aligned and serially registered using TrakEM2 (Cardona et al. 2012). RGC and amacrine cell process were manually traced and segmented using the AreaTree function of TrakEM2. Volume reconstructions were visualized using the 3D Viewer plugin for Fiji (Schmid et al. 2010).

Physiological recordings

Cell recordings were performed as described previously (Murphy and Rieke 2006) Briefly, wedges of dark-adapted retina were removed from the sclera and retinal pigment epithelium and mounted, photoreceptor-side down, on a D-polylysine coated coverslip. ooDS RGCs were targeted for whole-cell recording according to their soma size and dendritic morphology and ON and OFF spike responses to light stimuli during loose-patch recording. Loose patch-recording pipettes contained Ames' solution and whole-cell voltage clamp recordings were made using a cesium-based internal solution containing the following in (mM): 105 $CsCH_3SO_3$, 10 TEA-Cl, 20 HEPES, 10 EGTA, 5 Mg-ATP, 0.5 Tris-GTP, 2 QX- 314 and 0.2 Alexa Fluor 594). Excitatory (inhibitory) currents were isolated by holding the cell at the reversal potential for inhibitory (excitatory) currents, with E_{inh} ~ -60 mV, and E_{exc} ~0 mV. Small deviations from these holding potentials (<10 mV) were sometimes used to improve isolation. For subsequent imaging and immunohistochemistry, retinas were transferred onto filter paper (Millipore), ganglion cell side up, and the tissue was subsequently fixed in 4% PFA for 20 min at room temperature.

Visual stimulation

Visual stimuli were designed using custom MATLAB software and the Psychophysics Toolbox package. Stimuli were presented using an OLED monitor (eMagin, Bellevue, WA) were focused onto the photoreceptor outer segments from below. All experiments were carried out in darkness, using positive contrast steps or moving bars generating approximately 100 Rhodopsin isomerizations/rod/sec. In both wildtype and VIAAT CKO retina, retina was recorded from only if judged healthy by visual inspection. In wildtype retina, tissue was further inspected by recording from ON-S A-type RGCs (Bleckert et al. 2014). Only tissue whose ON-S A-type RGCs reliably produced robust spike responses to 10% positive contrast steps over the receptive field center, from a mean of 50 Rhodopsin isomerizations/rod/sec, was used for recordings. The contrast sensitivity in VIAAT CKO tissue was too weak and variable for application of this standard.

Mapping of direction selectivity

To measure direction selective responses, moving positive contrast bars were presented over the center of the cell's receptive field. Eight directions of motion were used, spaced 45 degrees apart.

Statistical Analysis

All data are shown as median box plots with edges demarcating 25th and 75th percentiles, unless otherwise stated. Statistical analysis was performed using the two-sided Wilcoxon ranksum test.

4.3 RESULTS

Selective disruption of inhibitory neurotransmission in the retina by conditional VIAAT knockout (KO)

To determine how a loss of inhibitory neurotransmission during development alters the mature patterns of synaptic connectivity onto individual neurons, we generated a retina specific conditional knock out of the vesicular inhibitory amino acid transporter (VIAAT, also known as VGAT (McIntire et al. 1997; Wojcik et al. 2006; Saito et al. 2010)). To do so, we bred floxed VIAAT mice (*Slc32a1*$^{flox/flox}$ *(Tong et al. 2008)*) with mice expressing Cre under the control of the retinal specific promoter *αPax6Cre-IRES-GFP (Marquardt et al. 2001)*, henceforth referred to as VIAAT^{KO}. The unique pattern of *αPax6Cre* expression in the retina results in the loss of VIAAT +ve cells, observed as an absence of immunostaining by anti - VIAAT, in nasal and temporal retina, whereas VIAAT +ve cells remain in a medial strip of retina running dorsal - to - ventral (Figure 4.1). However, within the nasal and temporal regions, which can also be identified by their higher densities of GFP labeled cells (Figure 4.1B,C), sparse VIAAT +ve long-range processes can be observed emanating from cells within the medial strip. Because VIAAT is the sole known vesicular transporter for the inhibitory amino acids GABA and glycine, and is necessary for inhibitory neurotransmission (McIntire et al. 1997; Wojcik et al. 2006; Saito et al. 2010), the nasal and

temporal regions of the VIAAT^{KO} retina should have a pronounced loss of inhibitory neurotransmission. Thus, to examine how disruption of inhibitory neurotransmission affects the mature patterns of synaptic connectivity, we examined synaptic distributions within the nasal and temporal retinal regions of VIAAT^{KO} mice.

Alterations to inhibitory synaptic patterns within the inner retina of VIAAT^{KO} mice

To characterize the patterns of inhibitory synaptic distributions in the inner retina of the VIAAT^{KO}, we crossed VIAAT^{KO} mice with *Thy1-YFPγ2* mice, in which the γ2 subunit of $GABA_A$ receptors are tagged with YFP. In the *Thy1-YFPγ2* transgenic line, GABAergic synapses on approximately 50% of RGCs are visualized (Bleckert et al. 2013). We confirmed that YFPγ2 puncta in the inner retina of wild type (WT) mice are apposed to VIAAT +ve axon terminals by immunostaining with antibodies against VIAAT. YFPγ2 puncta within the inner plexiform layer and on RGC somata appeared apposed to VIAAT +ve processes (Figure 4.2A). Whereas the density of YFPγ2 puncta appears decreased within the ON and OFF plexiform layers of *Thy1-YFPγ2*/VIAAT^{KO} mice, puncta onto some RGC somata appear more numerous and enlarged (Figure 4.2B,C). Even though we observed sparse VIAAT +ve terminals in the nasal and temporal KO regions of VIAAT^{KO} mice (Figure 4.1C,D) and that appeared to be long range projections from cells in the medial retina (Figure 2C), we observed few VIAAT +ve terminal apposed to YFPγ2 puncta throughout the inner retina, and none onto the YFPγ2 puncta found on RGC somata, or in the more intense bands within the ON and OFF plexuses of the KO regions. The selective increase in size and number of YFPγ2 puncta onto some RGCs, led us to ask whether a specific type of RGC was preferentially affected by the loss of inhibitory neurotransmission in the VIAAT^{KO} mouse. We thus examined YFPγ2 puncta distributions on RGC types identified by their dendritic morphology.

Disrupted somatic inhibitory synapses are restricted to specific RGC types in the VIAAT^{KO}

We biolistically transfected individual RGCs with CMV-tdTomato to label their somata and dendritic arbors in retinas from *Thy1-YFPγ2*/VIAAT^{KO} mice. We then utilized the distinct dendritic morphologies of known RGC types (Coombs et al. 2006; Völgyi et al. 2009; Wei and Feller 2011; Farrow et al. 2013; Dhande et al. 2013; Bleckert et al. 2014) to ascertain if a particular RGC type displayed the enlarged inhibitory somatic contacts observed in VIAAT^{KO} mouse retina. We examined ON-Sustained, OFF-Transient, and OFF-Sustained A-type RGCs (Pang et al. 2003; Völgyi et al. 2005; Murphy and Rieke 2006; Huberman et al. 2008b; van Wyk et al. 2009; Bleckert et al. 2014) ON direction selective RGCs (Dhande et al. 2013), and bistratified ON OFF direction selective (ooDS) RGCs (Huberman et al. 2009; Kay et al. 2011; Wei and Feller 2011). The inhibitory somatic contacts onto all A-type and ON direction selective RGCs appeared grossly normal (data not shown), whereas, every ooDS RGC displayed enlarged YFPγ2 somatic puncta (n = 10 of 10 cells) compared to WT (Figure 4.3). Because inhibitory neurotransmission has been shown to affect neurite development (Sernagor et al. 2010), we skeletonized the labeled dendritic arbors from individual ooDS RGCs from WT and VIAAT^{KO} retinas (Figure 4.3A,C) and characterized their dendritic morphology. We find that ooDS RGCs maintained bistratified dendritic arbors ramifying in both ON and OFF plexuses (Figure 4.3A,C). Furthermore, neither the total dendritic length nor the total number of dendritic segments of ooDS RGC arbors changed as a result of the loss of inhibitory neurotransmission (Figure 4.4A,B). The branching patterns of ooDS RGCs, determined by Sholl analysis (SHOLL 1953), were also similar (Figure 4.4C).

To characterize the patterns of inhibitory synaptic distributions onto each ooDS RGC we utilized the tdTomato cell fill and skeletonization to map the somatic and dendritic synaptic sites labeled by YFPγ2 punctate expression (see Methods). We find that the median number of inhibitory somatic synaptic sites onto ooDS RGCs almost doubles (WT = 8, VIAAT^{KO} = 14 puncta/soma, Figure 4.4D). In addition, the median volume of the inhibitory somatic contacts almost triples (WT = 0.60, VIAAT^{KO} = 1.55 um^3, Figure 4.4E), resulting from a skew in the distribution towards larger volume YFPγ2 clusters (Figure

4.4F). Intriguingly, the median linear density of inhibitory sites onto the ooDS RGC dendrites decreased, though modestly (WT = 0.46, VIAAT^{KO} = 0.40 puncta/µm, Figure 4.4G). We did not observe any change to the volume of dendritic synaptic sites (Figure 4.4H,I). It is possible that the enlarged somatic clusters could represent aberrant aggregates of receptors rather than synaptic sites (Poulopoulos et al. 2009; Saiepour et al. 2010).To distinguish between these two possibilities, we first determined if the somatic YFPγ2 puncta are colocalized with other known inhibitory synaptic proteins.

Enlarged somatic clusters of YFPγ2 puncta onto ooDS RGCs colocalize with postsynaptic, but not presynaptic proteins associated with inhibitory synapses

The endogenous γ2 subunit of GABA$_A$ receptors is localized to postsynaptic sites (Jacob et al. 2008), and is necessary for the function and clustering of GABA$_A$ receptors (Essrich et al. 1998). We have previously shown that YFPγ2 clusters in the *Thy1-YFPγ2* mouse retina colocalize with postsynaptic proteins found at inhibitory, but not excitatory synapses (Bleckert et al. 2013). Here we determined whether or not the enlarged somatic YFPγ2 clusters observed in the VIAAT^{KO} were also colocalized with inhibitory synaptic proteins. We find that the enlarged somatic YFPγ2 puncta characteristic of ooDS RGCs in the VIAAT^{KO} retinas, were colocalized with clusters labeled by gephyrin, a postsynaptic scaffolding protein found at GABAergic and glycinergic synapses in the retina (Sassoè-Pognetto and Wässle 1997) (Figure 4.5A). In addition, enlarged somatic YFPγ2 puncta also colocalized with clusters immunostained by antibodies against the α2 subunit of the GABA$_A$ receptor, which is known to be the essential α subunit on ooDS RGCs (Auferkorte et al. 2012) (Figure 4.5B). Furthermore, we find that in the VIAAT^{KO} alone, immunostaining for gephyrin (Figure 4.5C) or the GABA$_A$ receptor α2 subunit (Figure 4.5D) revealed enlarged somatic puncta. In contrast, we did not observe presynaptic inhibitory axon terminals labeled by GAD67, the primary synthesizing enzyme for GABA apposed to the somatic YFPγ2 puncta (Figure 4.5E), nor did we observe any remaining VIAAT labeling adjacent to somatic YFPγ2 puncta (Figure 4.2C).

The existence of gephyrin and the $GABA_A$ α2 subunit colocalized with YFPγ2 somatic puncta suggests that the somatic YFPγ2 puncta are not aberrant aggregates, but the confirmed presence of a presynaptic terminal would fully validate their position at synaptic sites. Thus, we performed correlative light and electron microscopy (LM-EM) to determine if presynaptic structures are apposed to the enlarged somatic YFPγ2 puncta.

Presynaptic axonal terminals observed under EM are apposed to YFPγ2 puncta onto ooDS RGCs

The acid test of synaptic connectivity lies in recognition of synaptic contacts observed via electron microscopy. Here we used the near infrared branding technique (NIRB, (Bishop et al. 2011; Bleckert et al. 2013)) to correlate the somatic YFPγ2 fluorescence with potential presynaptic axonal contacts observed in micrographs from serial section transmission electron microscopy (ssTEM) (Figure 4.6A,B). For one RGC somata, we found that all enlarged YFPγ2 puncta were apposed to presynaptic terminals (Figure 4.6B). The postsynaptic densities observed under EM associated with the corresponding sites of contact identified by YFPγ2 fluorescence between the presynaptic axons and ooDS RGC soma were often crenated and enlarged (Figure 4.6C). Furthermore, the synaptic vesicles within the presynaptic terminals appeared more diffuse, and constricted. We quantified the median diameter of the synaptic vesicles within the presumed inhibitory amacrine cell presynaptic terminals (AC = 27.17 µm, n = 5 sections, 30 vesicles/section) and compared them with the diameter of synaptic vesicles within nearby rod bipolar cell terminals (RBC = 32.14 µm, n = 5 sections, 30 vesicles/section). The amacrine cell vesicles were indeed smaller (Figure 4.6E). This decrease in vesicle size is indicative of unfilled or depleted neurotransmitter vesicles { (Van der Kloot et al. 2002; Daniels et al. 2006; Budzinski et al. 2009; Rodrigues et al. 2013). Intriguingly, we noted that amacrine cell boutons apposed to two of the YFPγ2 clusters originated from the same presynaptic process (see asterisks in Figure 4.6B), however, the difficulties of recapturing enough serial sections using ssTEM only allowed us the ability to partially

reconstruct the connectivity between the ooDS RGC and its presynaptic cell types. To overcome this limitation, we performed an additional LM/EM reconstruction of an ooDS RGC using scanning block face electron microscopy (SBFEM).

We imaged the YFPγ2 puncta on an individual ooDS RGCs somata and marked the soma location with a NIRB fiduciary mark (Figure 4.7A). After registration of the fluorescent image with the EM micrographs we subsequently segmented and reconstructed the ooDS RGC and its associated inhibitory presynaptic contacts (Figure 4.7B). For this cell, we did not observe multiple contacts from the same presynaptic process, however, the reconstructed axon terminals associated with the three largest YFPγ2 puncta (Figure 4.7A white arrowheads) on the ooDS RGC soma all displayed a similar pattern of connectivity (Figure 4.7B,C). Each presynaptic terminal initially made contact with a primary dendritic arbor of the ooDS RGC above the soma (see Figure 4.7C, white arrowheads). These presynaptic processes then fasciculated down the primary dendrite and made a terminal varicosity, which was apposed to the enlarged somatic YFPγ2 puncta (Figure 4.7C black arrowheads). This unique pattern of connectivity across presynaptic terminals may be indicative of a distinct type of amacrine cell that provides the primary somatic inhibition to ooDS RGCs. The remaining somatic connections associated with the smaller YFPγ2 puncta do not contact the ooDS RGCs dendrites, and make contacts from processes that stratify at the level of the soma. It is known that alterations to inhibitory transmission can alter circuit activity and result in homeostatic changes to excitatory transmission (Turrigiano and Nelson 2004). The diversity of effects resulting from disrupted inhibitory neurotransmission on the structural arrangements of inhibitory synapses observed onto ooDS RGCs begs the question of whether or not the patterns of excitatory synaptic connections are additionally disrupted.

Excitatory synapse densities on the dendritic arbors of ooDS RGCs are increased following loss of inhibitory neurotransmission

To map the densities of excitatory synaptic sites onto individual ooDS RGCs, we biolistically co-transfected RGCs in the VIAAT^{KO} with CMV-tdTomato and PSD95-CFP (Figure 4.8A). We find that the PSD95 puncta densities in VIAAT^{KO} are modestly increased compared to those from WT retina (WT = 0.36, KO = 0.42 puncta/µm, Figure 4.8B). When observed in conjunction with the changes in the density of YFPγ2 puncta, we find that the combined decrease in inhibitory synaptic density, and increase in excitatory synaptic density results in a more balanced inhibitory-to-excitatory (I/E) ratio across the dendritic arbors of ooDS RGCs (WT = 1.24, KO = 0.99, Figure 4.9C).

The inhibitory input onto ooDS RGCs has been shown to be essential for conferring their direction selectivity. This input derives from connections with a specific population of inhibitory interneurons, called starburst amacrine cells (SACs), whose processes co-stratify with the ooDS RGC dendritic arbors (Euler et al. 2002; Fried et al. 2002; Wei and Feller 2011; Taylor and Smith 2012; Vaney et al. 2012a). However, for some ooDS RGCs direction selectivity can also be partially mediated by excitatory inputs (Trenholm et al. 2011). The loss of VIAAT in SACs should result in a loss of direction selectivity in ooDS RGCs, however, it is unclear how the absence of inhibitory input to ooDS RGCs during development would affect their responses to light stimuli (Elstrott et al. 2008). To address these questions, we target ooDS RGCs for electrophysiology in the VIAAT^{KO} retina and recorded their current responses to stationary and moving light stimuli.

Direction selectivity in ooDS RGC persists in the VIAAT^{KO} retina

Individual ooDS RGCs within *Thy1-YFPγ2*/VIAAT^{KO} retinas were targeted by their soma size and identified by their characteristic dendritic branching patterns and stratification, and presence of enlarged YFPγ2 somatic puncta (Figure 9A,B). In response to brief flashes of light, ooDS RGCs displayed both ON and OFF spike responses (data not shown). To determine what inputs underlie these responses, we performed whole-cell recordings of the current inputs to the ooDS RGCs during brief flashes of light (Figure 9B,C).

Our preliminary results suggest that the excitatory inputs to ooRGCs appeared relatively normal (Figure 9B). Surprisingly, in the VIAAT^{KO} retinas we still observed inhibitory inputs to ooRGCs (Figure 9C). Furthermore, these inhibitory currents were blocked by application of SR95531 (gabazine) suggesting that they arise from GABAergic transmission and activation of $GABA_A$ receptors (Figure 9D). Thus it may be that a particular amacrine cell is still capable of transmitting GABA even in the absence of VIAAT. We first asked if the inhibitory inputs could be coming from their primary presynaptic partners the SACs. Becuase SACs provide direction selective inhibitory input to ooDS RGCs, we recorded inhibitory currents from ooDS RGCs in response to moving bars of light across different directions of motion. Intriguingly, the inhibitory current responses recorded from the ooDS RGCs in VIAATKO retinas still showed a preferred direction, strongly suggesting that the persistent inhibitory input to ooDS RGCs comes from SACs (Figure 9E).

4.4 Discussion

Regulation of somatic inhibitory connectivity by inhibitory neurotransmission

The pronounced increase in the number of somatic inhibitory contacts onto ooDS RGCs is similar to previous results from visual cortex where conditional KO of VIAAT resulted in an increase in the number of contacts inhibitory basket cell axons make onto pyramidal neuron somata (Wu et al. 2012). However, basket cell terminals show a decrease in synaptic size following blockade of either GABAergic transmission by KO of VIAAT or KO of GAD1/GAD2, the synthesizing enzymes for GABA (Chattopadhyaya et al. 2007a; Wu et al. 2012). The authors posit that the increased number and decreased size of somatic contacts results from a persistence of nascent immature synapses, which under normal conditions would be eliminated during development. In contrast here we observe a pronounced increase in somatic inhibitory synaptic size, and number that is not a result of normal loss of inhibitory somatic synapses during development, as we did not observe a decrease in somatic contacts onto ooDS RGCs

during development under wildtype conditions (data not shown). This discrepancy could in part result from the different methods of KO utilized between the cortex and retina (Bleckert and Wong 2011). In the studies in cortex, GABAergic transmission was blocked in single neurons, whereas their neighbors remained wildtype. In the $VIAAT^{KO}$ retina presumably all amacrine contacts onto the soma no longer transmit GABA. It may be that competition between the different amacrine cell contacts is necessary for establishing the mature patterns of inhibitory connections, as has been observed for excitatory connections onto the somata and dendrites of Purkinje cells in the cerebellum (Kano and Hashimoto 2009; Frola et al. 2013), and is a dominant feature of synaptic development within many excitatory circuits (Personius and Balice-Gordon 2002; Hua and Smith 2004; Rodríguez-Contreras et al. 2008; Hong and Chen 2011).

Aberrant increases in proteins associated at perisomatic densities have also been observed after disruption to inhibitory postsynaptic scaffolding proteins such as neuroligin2 (NL2) (Poulopoulos et al. 2009), though these clusters are likely representative of intracellular or submembraneous aggregates (Saiepour et al. 2010), and not synaptic sites. Our results from electron microscopy reconstructions confirm that indeed, the enlarged somatic GABAergic receptor clusters are bonafide synapses. It is surprising that we were not able to visualize presynaptic terminals apposed to the enlarged somatic YFPγ2 clusters using immuno markers for GAD67 (see Figure 4.5). However, decreased GAD expression and localization to terminals has previously been observed after germline KO of VIAAT in spinal cord and brain (Wojcik et al. 2006).

Disrupting inhibitory neurotransmission produces contrasting alterations to dendritic and somatic synaptic connectivity

Disparate effects on dendritic and somatic inhibitory synapses resulting from disruptions to inhibitory neurotransmission have been observed onto pyramidal neurons of the hippocampus (Panzanelli et al.

2011). These studies demonstrated that the KO of the α2 subunit of the $GABA_A$ receptors results in a selective disruption of GABAergic synapses onto the somata of pyramidal neurons, whereas synapses onto the dendrites are unaffected. However, this differential affect may result from the selective organization of GABA receptors with unique combinations of α subunits segregated to distinct cellular compartments (Nyíri et al. 2001; Prenosil et al. 2006; Kasugai et al. 2010; Panzanelli et al. 2011). These disctinct cellular compartments are also often innervated by diverse populations of inhibitory interneurons (Somogyi et al. 1998; Huang et al. 2007; Klausberger and Somogyi 2008; Burkhalter 2008). Similarly, disruption to inhibitory or excitatory transmission onto Purkinje cells in the cerebellum by knockout of specific subunits of GABA receptor (Fritschy et al. 2006; Frola et al. 2013) or glutamate receptor (Hashimoto et al. 2001b; Watanabe 2008) can also result in distinct effects to synaptic connectivity onto distinct cellular compartments (e.g either dendrite, soma, or axon initial segment).

In the retina, different α subunits of $GABA_A$ receptors are also found in distinct stratification patterns within the inner retina (Haverkamp and Wässle 2000), however, it is unknown if individual neurons within the retina localize different combinations of $GABA_A$ receptors at different cellular compartments. Furthermore, unlike in cortex where $GABA_A$ receptor clusters can contain heterologous combinations of α subunits, in the retina, GABA receptor clusters are composed of a single type of α subunit (Greferath et al. 1995; Koulen et al. 1996). Here we observe that the GABAergic synaptic sites onto the somata of ooDS RGCs identified by YFPγ2 puncta, and gephyrin immunostaining, colocalize with the $GABA_A$ receptor α2 subunit. It has been previously shown that the $GABA_A$ receptor α2 subunit is also the dominant subunit localized to inhibitory synapses on the dendrites of ooDS RGCs, and is essential for conferring direction selective inhibitory input from starburst amacrine cells (Auferkorte et al. 2012). Thus it appears that ooDS RGCs do not utilize different $GABA_A$ receptor subunit combinations to segregate and encode inputs from distinct populations of their presynaptic amacrine cells. Thus, it is unlikely that the differential result we observed between inhibitory synaptic connections onto somata

and dendrites of ooDS RGCs was a result of differential distributions of $GABA_A$ subunit composition. We suggest that contrasting affects are, instead, a result of diverse affects of KO of VIAAT on the different populations of amacrine cells making contacts onto distinct compartments of ooDS RGCs.

The decreased size of synaptic vesicles in amacrine presynaptic terminals observed by EM contacting the soma suggest that these vesicles are devoid of inhibitory neurotransmitters and do not provide inhibitory input to the somata of ooDS RGCs. In contrast, the persistence of direction selective GABAergic input to ooDS RGCs suggests that even in the $VIAAT^{KO}$, SACs are able to maintain transmission to ooDS RGCs, although the efficacy of this transmission is likely reduced. The observed reduction in dendritic GABAergic synapses onto the ooDS RGCs in the presence of reduced GABAergic transmission is consistent with a reduction in GABAergic synapses observed in visual cortex after KO of GAD67 (Chattopadhyaya et al. 2007b) and disruption to visual activity (Chattopadhyaya et al. 2004). This moderate decrease in inhibitory synaptic density may reflect an inability of ooDS RGCs to increase synaptic density after contacts initially form, as the density of dendritic YFPγ2 puncta observed in ooDS RGCs $VIAAT^{KO}$ is closer to the median density observed in immature ooDS RGCs (P12 ooDS RGCs = 0.35 puncta/µm (Bleckert et al. 2013)). Similar deficits in establishing mature patterns of inhibitory connections after KO of GAD67 have also been observed at the axon terminals of rod bipolar cells in the retina (Schubert et al. 2013) and the somata of pyramidal cells in cortex (Chattopadhyaya et al. 2007a; Wu et al. 2012).

Regulation of excitatory synaptic connectivity by inhibitory neurotransmission

Considerable work has shown that excitatory neurotransmission can alter the development of neuronal circuits and patterns of excitatory synaptic connectivity (Personius and Balice-Gordon 2002; Hua and Smith 2004; Rodríguez-Contreras et al. 2008; Hong and Chen 2011; Bleckert and Wong 2011). In the retina in particular, alterations to excitatory glutamatergic neurotransmission have been shown to

bidirectionally regulate synaptogenesis onto individual retinal ganglion cells; decreases in glutamatergic transmission decrease synaptogenesis (Kerschensteiner et al. 2009), whereas increased transmission results in greater excitatory synaptic density (Soto et al. 2012). Similar bidirectional regulation of inhibitory synaptogenesis by inhibitory neurotransmission has also been observed onto cortical pyramidal neurons (Chattopadhyaya et al. 2007a), however few studies have examined the affects of disrupting one transmitter system on the development of the other. During development, spontaneous patterns of circuit activity are regulated by different neurotransmitter systems (Blankenship and Feller 2010; Kerschensteiner 2013). In addition, within mature neuronal circuits it is clear that alterations to either excitatory or inhibitory neurotransmission can result in perturbations to circuit function, however, circuit function often is able to recover through homeostatic regulation and compensatory changes to excitatory and inhibitory connectivity and activity (Turrigiano 2008). Alterations to neurotransmitters during development may also result in homeostatic mechanisms to maintain normal patterns of activity (Turrigiano and Nelson 2004). It has been shown that inhibitory and excitatory inputs onto tectal neurons in Xenopus tadpoles become balanced during development (Tao and Poo 2005), and that alterations to excitatory activity can regulate GABAergic synapse development (Liu et al. 2007; Akerman and Cline 2007). Similar regulation of inhibitory synaptic connectivity by excitatory activity has also been observed in hippocampal cultures (Liu 2004) and in visual cortex (van Versendaal et al. 2012; Chen et al. 2012).

Our observation that a disruption of inhibitory input to ooDS RGCs from KO of VIAAT results in an increased excitatory synaptic density is unexpected in relation to homeostatic mechanisms. In mature neurons (Turrigiano et al. 1998), and developing neurons in culture (Liu 2004) disruption of inhibitory neurotransmission often results in a reduction of excitatory input to individual cells. We speculate that the increase in excitatory synaptic density on ooDS RGCs may in part be a result of decreased inhibitory neurotransmission in the $VIAAT^{KO}$ retina onto the bipolar cells axon terminals.

Previous work has shown that disruption to GABAergic transmission can result in an increase in glutamatergic transmission from bipolar cells early in development (Schubert et al. 2013). Furthermore an increase in spontaneous glutamatergic activity in bipolar cells during development has been shown to increase excitatory synaptic densities onto individual RGCs (Soto et al. 2012). Thus it may be that alterations to bipolar cell circuits presynaptic to the ooDS RGCs contribute to the observed increase in excitatory synaptic density.

Roles of inhibitory neurotransmission onto ooDS RGCs

Throughout the retina, the most studied and well-defined role of inhibitory neurotransmission comes from the circuitry underlying direction selectivity onto ooDS RGCs (Barlow and Hill 1963; Famiglietti 1987; Weng et al. 2005; Euler et al. 2002; Fried et al. 2002; Wei and Feller 2011; Briggman et al. 2011; Yonehara et al. 2011; Wei et al. 2011; Taylor and Smith 2012; Vaney et al. 2012a; Kim et al. 2014). Within this circuit, motion is computed by presynaptic starburst amacrine cells (Euler et al. 2002; Lee and Zhou 2006), and direction selectivity primarily arises by stereotyped patterns of connectivity between SACs and ooDS RGCs (Briggman et al. 2011). Most surprising, was the fact that ooDS RGCs continued to receive direction selective GABAergic input in the $VIAAT^{KO}$, as VIAAT is believed to be the sole vesicular transporter of inhibitory neurotransmitters (McIntire et al. 1997; Wojcik et al. 2006; Saito et al. 2010). Whereas we do still observe sparse long range VIAAT +ve processes in the KO region of the $VIAAT^{KO}$ retina, there is a complete absence of VIAAT staining in the ON and OFF layers of the inner retina where SACs stratify (see Figure 4.1 and 4.2). Previous results from germline KO of VIAAT, have shown that inhibitory GABAergic and glycinergic inhibition is not completely lost in all inhibitory neurons (Wojcik et al. 2006). A proportion of inhibitory neurons examined from striatum and spinal cord continued to be able to transmit even after the loss of VIAAT, however at a much reduced rate and efficiency. The authors propose that a potential candidate transporter mechanism if still present should

have similar substrate specificity to VIAAT, however there is no current evidence of a transporter with high sequence homology to VIAAT (Wojcik et al. 2006). Thus, they suggest that the putative transporter may not actually utilize GABA/glycine as its primary substrate. Intriguingly, it has recently been shown in the striatum that the transporter for dopamine (VMAT2) is capable of transporting GABA into synaptic vesicles in the absence of VIAAT (Tritsch et al. 2012). In addition to GABA, SACs also co-release acetylcholine (ACh). It is known that the vesicular ACh transporter (VAChT) has high structural similarity to VMAT2 and both are within the same gene family (SLC18A2 and SLC18A3) (Blakely and Edwards 2012; Chaudhry et al. 2008; Eiden et al. 2004), we hypothesize that the VAChT transporter may also be capable of compensating for the loss of VIAAT in SACs.

Whereas the patterns and function of inhibitory input within the inner retina onto the dendrites of RGCs and the axon terminals of bipolar cells has received considerable attention (Wässle et al. 1998; Zhang and McCall 2012; Jadzinsky and Baccus 2013), little is known about the function or patterns of connectivity of inhibition onto RGC somata. Previous reports from EM microscopy of cat β-cells suggest that inhibitory somatic contacts may originate from a single type of GABAergic amacrine cell for the RGC type (Kolb and Nelson 1993). In the Thy1-YFPγ2 retinas, we observed somatic puncta onto almost all cell bodies within the ganglion cell layer. This suggests that for many RGC types, somatic inhibitory input may serve an important function. Our observation of stereotyped patterns of connectivity between amacrine cell terminals and the primary dendrites and somata of ooDS RGCs suggests that a single type of amacrine cell may provide a predominant input to ooDS RGCs. However, the function of somatic inputs onto ooDS RGCs and onto other RGCs remains to be determined. Whereas the inhibitory input from SACs to ooDS RGCs has been extensively studied, little is known about inhibition from other amacrine cells. ooDS RGCs receive inhibition onto their dendrites from amacrine cells other than SACs (Dacheux et al. 2003; Famiglietti 2005), and our current results further suggest they also receive input onto their somata from a yet to be identified type or types of amacrine cells. The unique pattern of

fasciculation we observed between some somatic amacrine contacts and the ooDS RGC is suggestive of a molecular gradient as has been observed at inhibitory neuron connections onto Purkinje cells in the cerebellum (Ango et al. 2004).

Our results raise the question of how different patterns and inputs from inhibitory amacrine cells shape the function of RGC output (Koch et al. 1983), and more specifically what function somatic input from such amacrine cells may provide to ooDS and other RGCs. Throughout the cortex and cerebellum, unique populations of inhibitory interneurons have been identified which selectively target the somatic or axon initial segment of principle neurons (Ango et al. 2004; Huang et al. 2007; Klausberger and Somogyi 2008), and their regulation of neuronal activity differs substantially from dendritic inhibitory input (Miles et al. 1996; Bar-Ilan et al. 2012), which ultimately may provide more global regulation of cell activity (Woodruff et al. 2010; Freund and Katona 2007; Ellender and Paulsen 2010). It has been hypothesized that the patterns of inhibitory input onto RGCs could have pronounced affects on RGC output (Koch et al. 1983). Together our results underscore a need to determine the combined role of somatic and dendritic inhibition to RGC output. Furthermore, our finding emphasize that the development of inhibitory inputs onto an individual neuron is selectively influenced by the distinct amacrine cells making contacts at each cellular compartment.

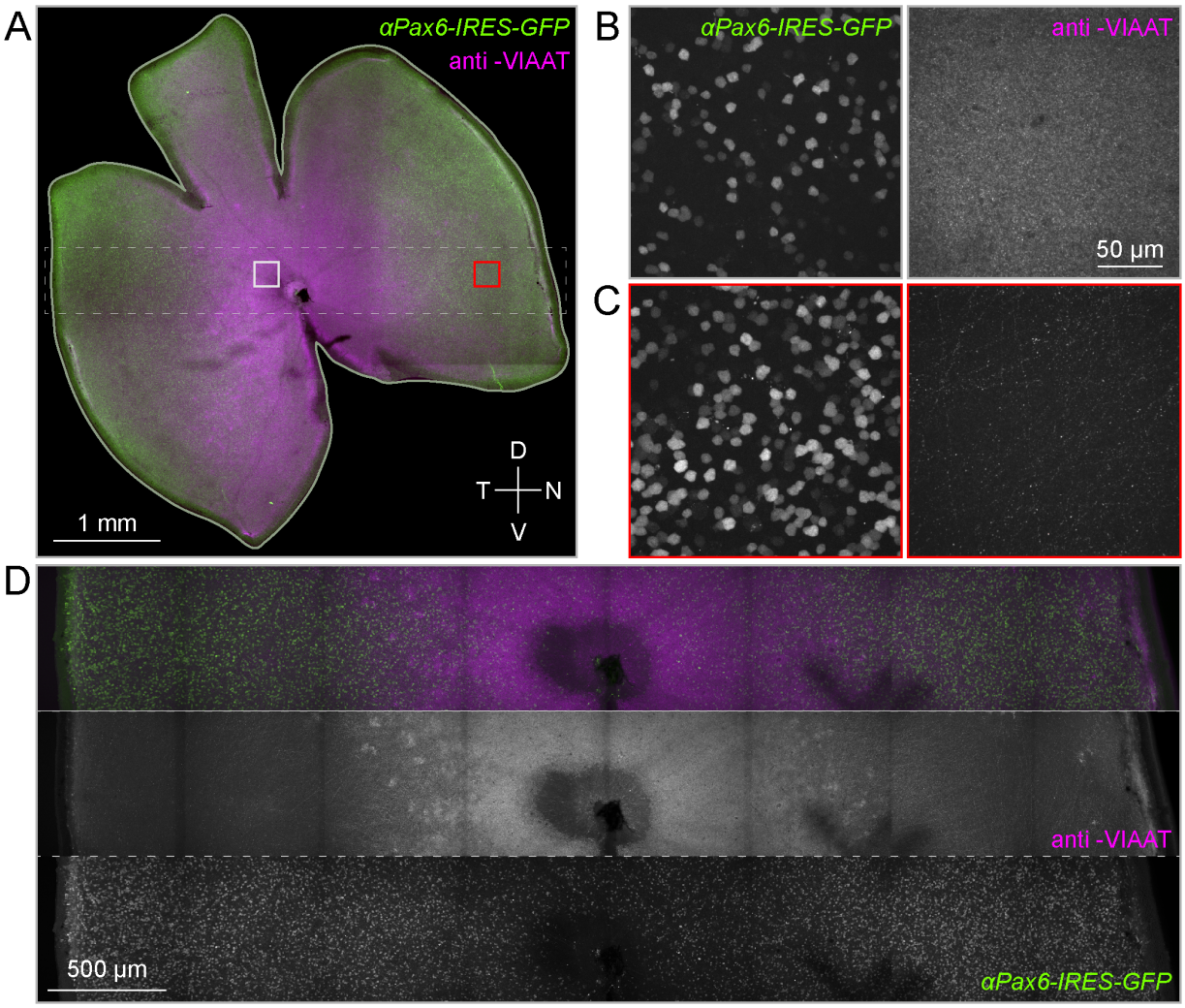

Figure 4.1 Conditional knock out of VIAAT in the mouse retina.
(A) VIAATKO retina stained with antibodies against VIAAT reveals a loss of protein expression in amacrine cell processes in nasal and temporal retina, where a greater proportion of amacrine cells are expressing αPax6-Cre-IRES-GFP. **(B)** Maximum intensity projection of the amacrine cell layer (left) and the inner plexiform layer (right) showing the density of αPax6-Cre-IRES-GFP labeled amacrine cells in a medial (dorsal-to-ventral) strip where VIAAT +ve processes in the inner plexiform layer are more abundant (white box in A). **(C)** The density of αPax6-Cre-IRES-GFP labeled amacrine cells somata in nasal retina is increased and little VIAAT +ve processes remain (red box in A). **(D)** Maximum intensity projection of the inner nuclear layer of the retina in (A, dashed box) reveal the gradual decrease in VIAAT +ve processes from central to peripheral retina. The remaining VIAAT +ve processes present in (C) emanate from amacrine cells in the dorsal ventral strip whose long range processes extend into nasal and temporal retina.

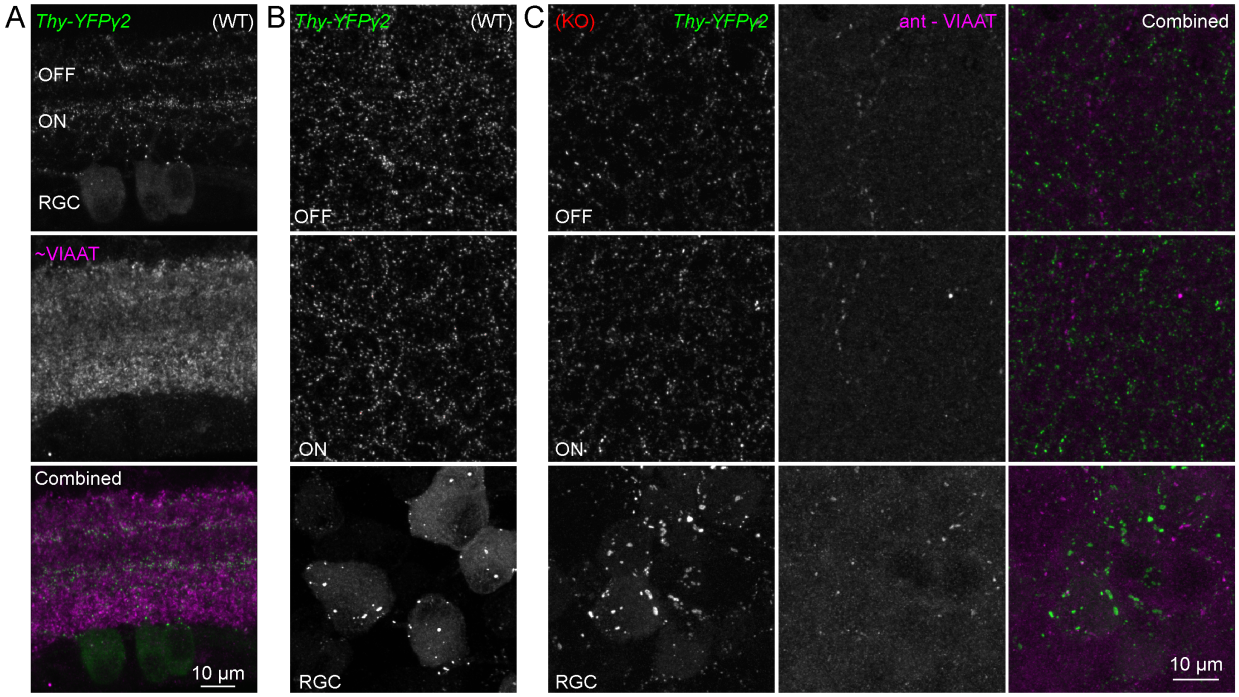

Figure 4.2 Patterns of YFPγ2 labeled GABAergic synapses in the inner retina of VIAATKO mouse. **(A)** Maximum intensity projection (MIPs) from vertical sections of the inner retina of Thy1-YFPγ2 mice immunostained for VIAAT. YFPγ2 puncta in this transgenic line readily identify synaptic GABAA receptors on RGCs (Bleckert et al. 2013). **(B)** MIPs from whole mount image stacks encompassing OFF, ON, and RGC layer depicted in (A). **(C)** (Left column) MIPs from the same inner retinal layers from the Thy1-YFPγ2 - VIAATKO mouse show less dense puncta fluorescence within OFF and ON layers, but fluorescent puncta on some retinal ganglion cell (RGC) somas appear larger and more numerous within the RGC layer. Immunostaining with antibodies against VIAAT (center column) reveal sparse long range processes, but no contacts with YFPγ2 puncta are observed in the combined images (right column).

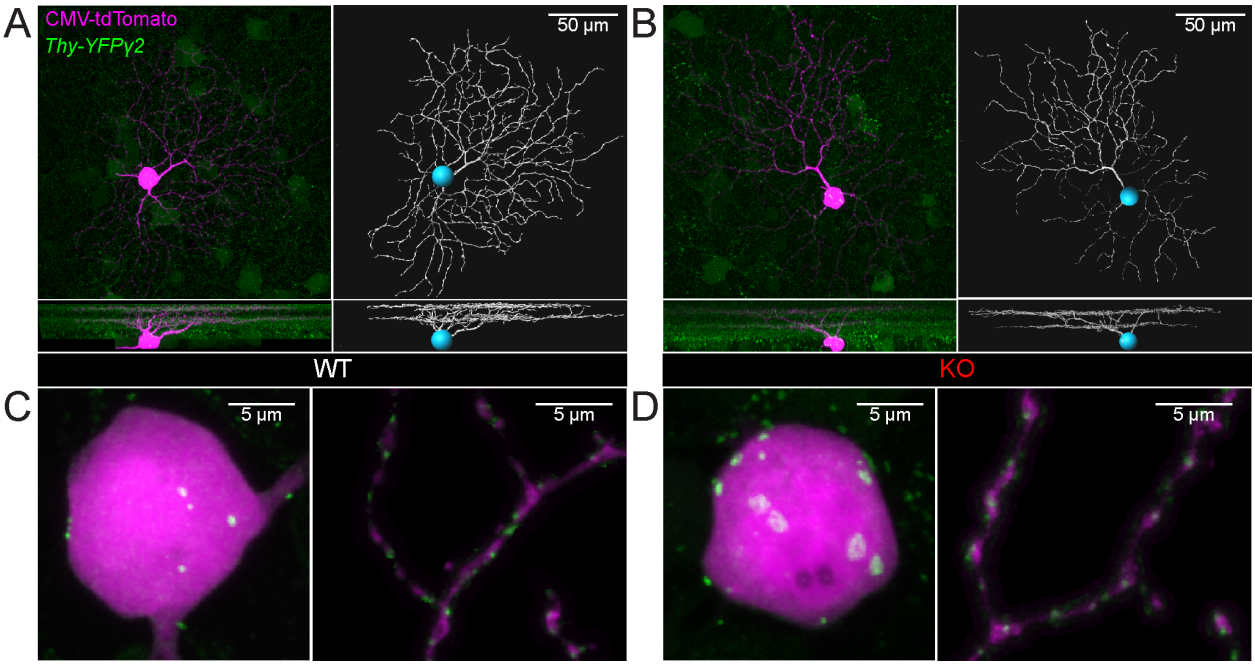

Figure 4.3 Large YFPγ2 somatic puncta are found on bistratified direction selective RGCs.
(A) (Left) MIP of an example bistratified direction selective (ooDS) RGC biolistically labeled with CMV-tdTomato in a *Thy1-YFPγ2* mouse retina (WT - wildtype), and (right) the skeletonized filament of its dendritic arbor. (Below) vertical projections of the image stacks. **(B)** Magnified view of YFPγ2 fluorescence on ooDS RGC somata and dendritic segments from (A) reveal punctate distributions. **(C)** MIP of an example ooDS RGC and skeletonized arbor from the *Thy1-YFPγ2* - VIAAT^{KO} mouse retina. **(D)** Magnified view of the YFPγ2 fluorescence on ooDS RGC somata are more numerous and enlarged, whereas the puncta on dendritic segments appear similar to WT.

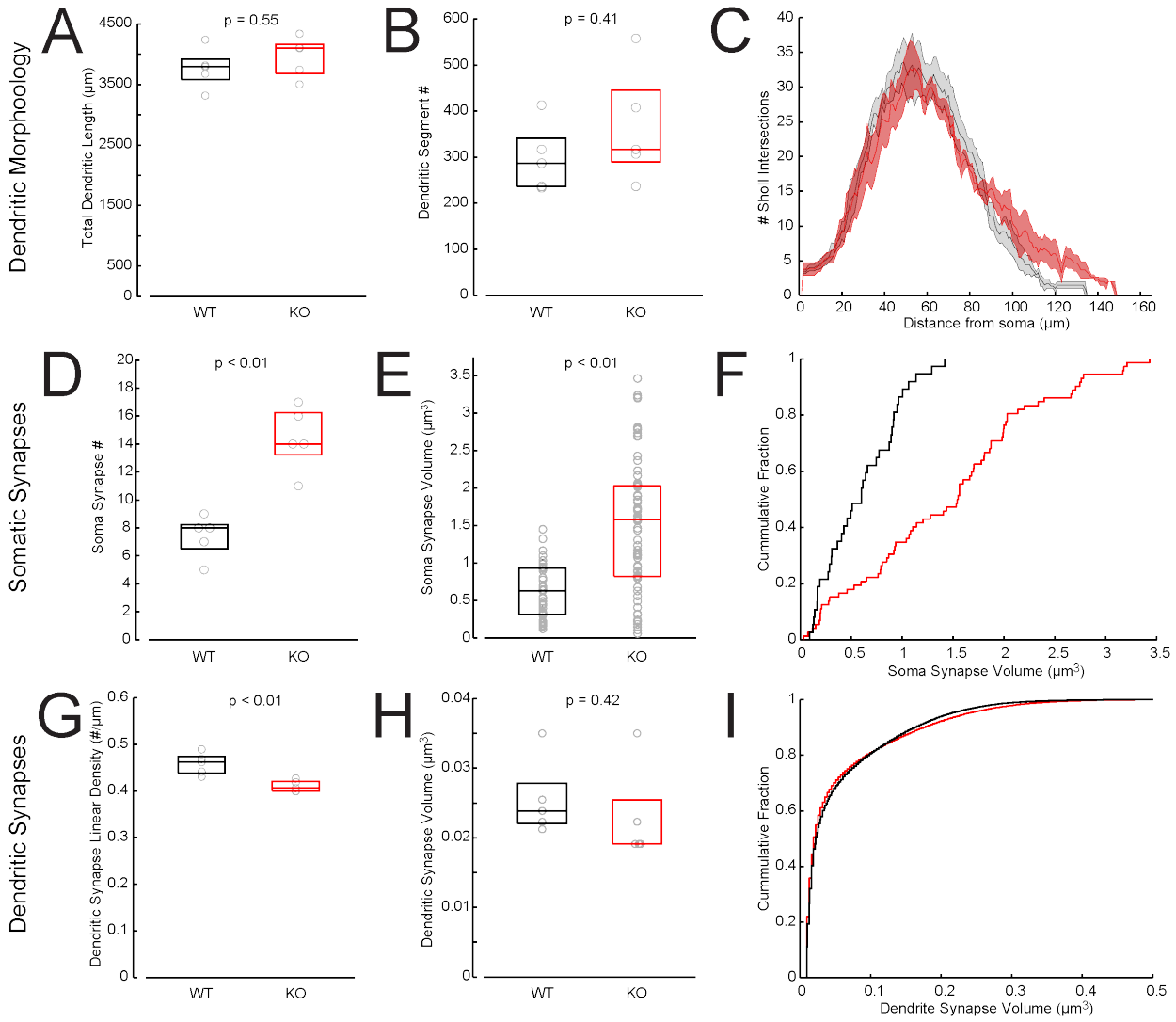

Figure 4.4 Quantification of ooDS RGC dendritic arbors and YFPγ2 puncta distributions.
(A) Plotted are the total dendritic length, **(B)** total dendritic segment number, and **(C)** and number of Sholl branch crossings vs distance from the soma for ooDS RGCs from wildtype (WT) and VIAAT^{KO} (KO) retinas. **(D)** Plotted are the median numbers of somatic synaptic puncta, **(E)** median somatic synapse volume, and **(F)** somatic synapse volume cumulative distribution. **(G)** Plotted are the dendritic synapse linear density, **(H)** median dendritic synapse volume, and **(I)** dendritic synapse volume cumulative distribution. WT values in (A) and (D) are re-plotted from (Bleckert et al. 2014).

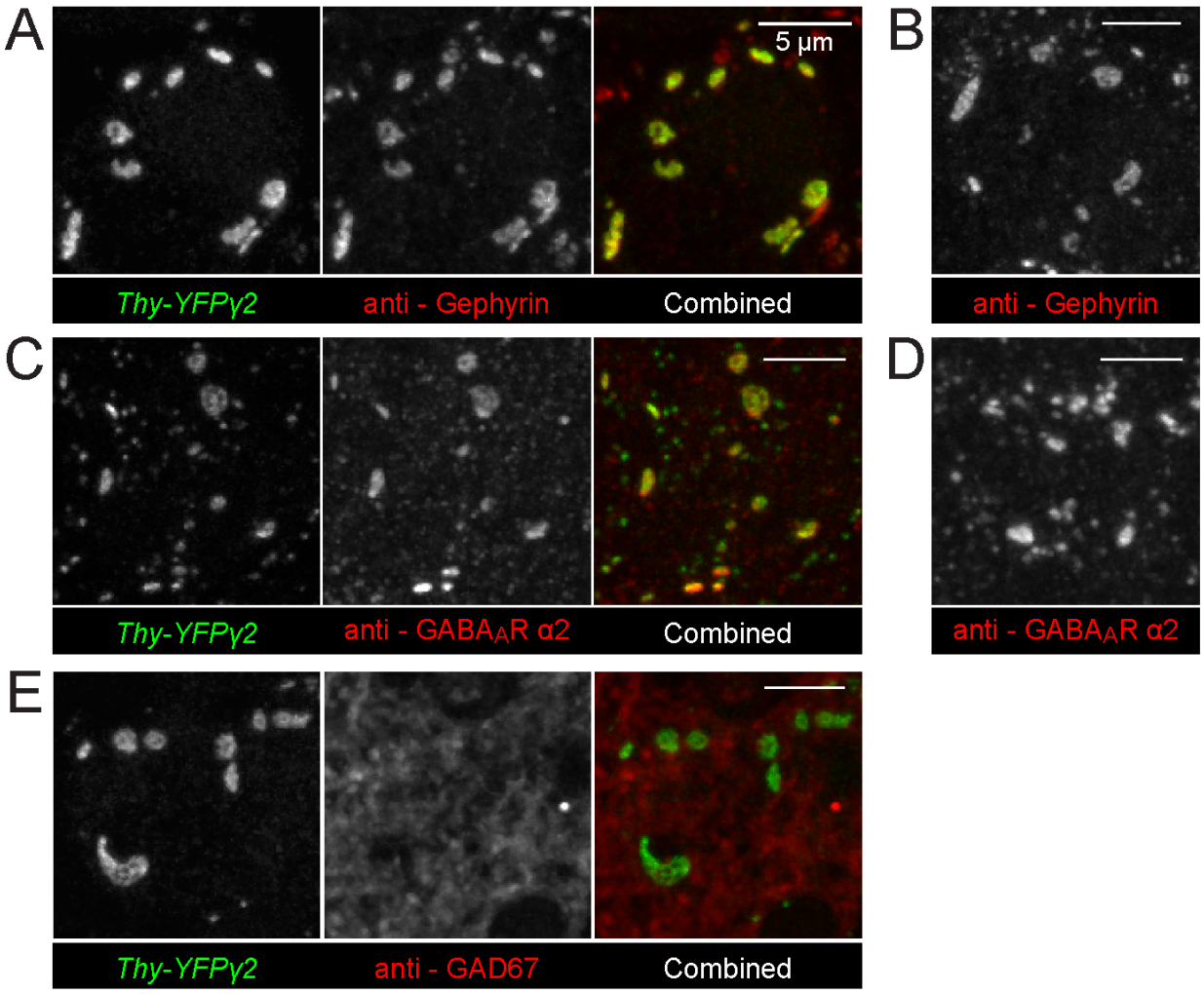

Figure 4.5 Somatic YFPγ2 puncta colocalize with postsynaptic, but not presynaptic proteins found at GABAergic synapses.

(A) MIP of fluorescent somatic puncta from a *Thy1-YFPγ2* - VIAAT^{KO} mouse retina immunostained for the postsynaptic scaffolding protein Gephyrin. **(B)** Somatic puncta from *Thy1-YFPγ2* - VIAAT^{KO} mouse retina colabel with the $GABA_A$ receptor α2 subunit. **(C)** Gephyrin immunostaining or **(D)** $GABA_A$ receptor α2 subunit immunostaining alone in the VIAAT^{KO} also labels enlarged somatic puncta. **(E)** *Thy1-YFPγ2* - VIAAT^{KO} mouse retina immunostained with GAD67 does not show somatic YFPγ2 puncta apposed to presynaptic GAD67 +ve terminals, GAD67 staining appears diffuse with no clustering adjacent to YFPγ2 puncta.

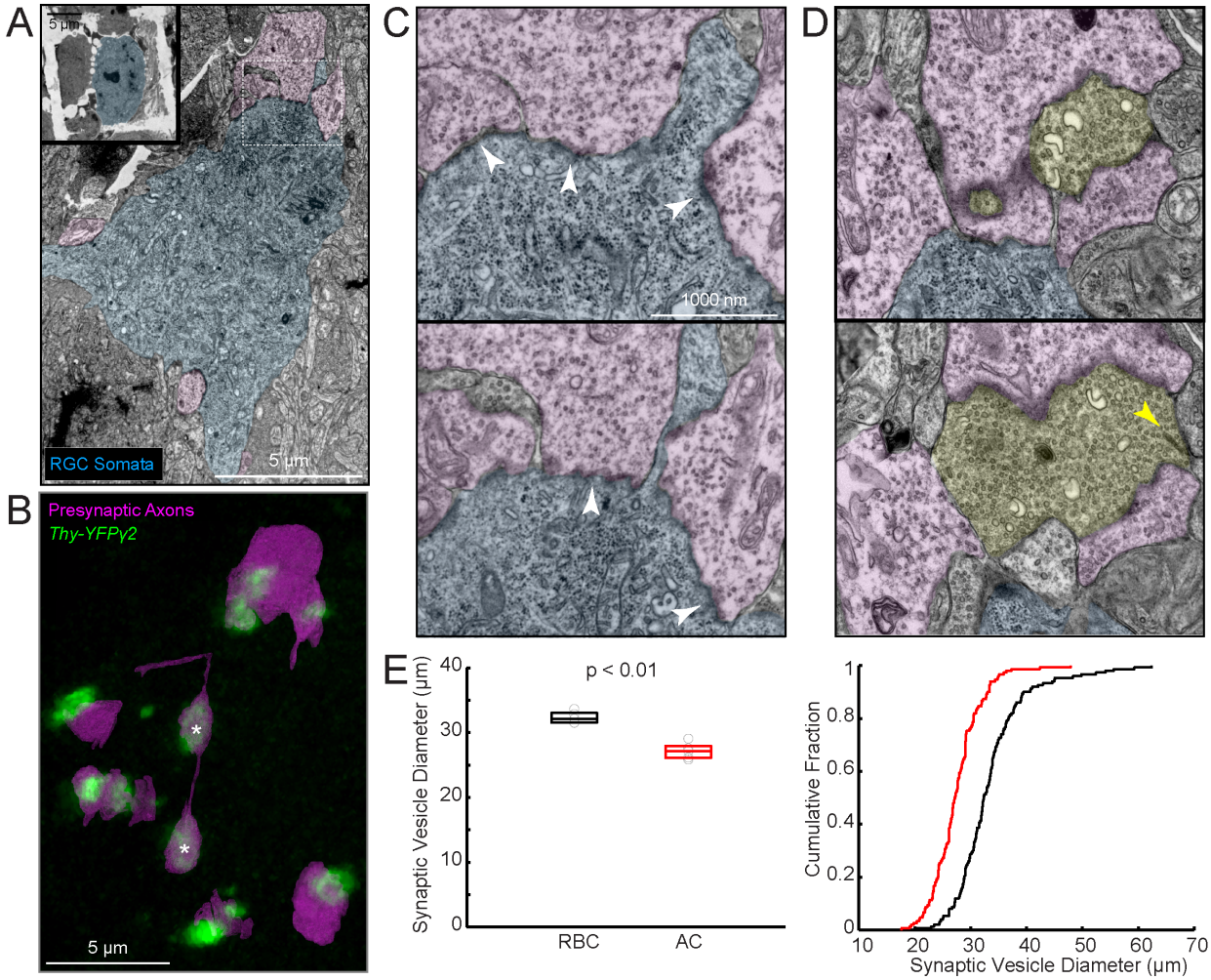

Figure 4.6 Correlative light and ssTEM microscopy reveal YFPγ2 puncta on ooDS RGC somata are apposed to presynaptic axon terminals.

(A) Electron micrograph of a single section depicting an ooDS RGC soma (blue) and its presynaptic contacts (magenta). Inset shows a lower magnification image of the soma at the level of the NIRB mark utilized to identify the confocal imaged soma. **(B)** MIP of the YFPγ2 puncta (green) aligned to the reconstructed axon terminals (magenta) identified in partial serial sections. Note that two YFPγ2 puncta are contacted by the same presynaptic cell (white asterisks). **(C)** High magnification serial sections from the boxed region in (A) depicting sites of synaptic contact (white arrowheads). **(D)** Sequential serial sections containing the presynaptic terminals in (C) at the stratification level of rod bipolar terminals (yellow) identified by their synaptic ribbon (yellow arrowhead) to compare vesicle sizes. **(E)** Quantification of the diameter of synaptic vesicles in somatic amacrine cell terminals (AC) and rod bipolar cell terminals (RBC).

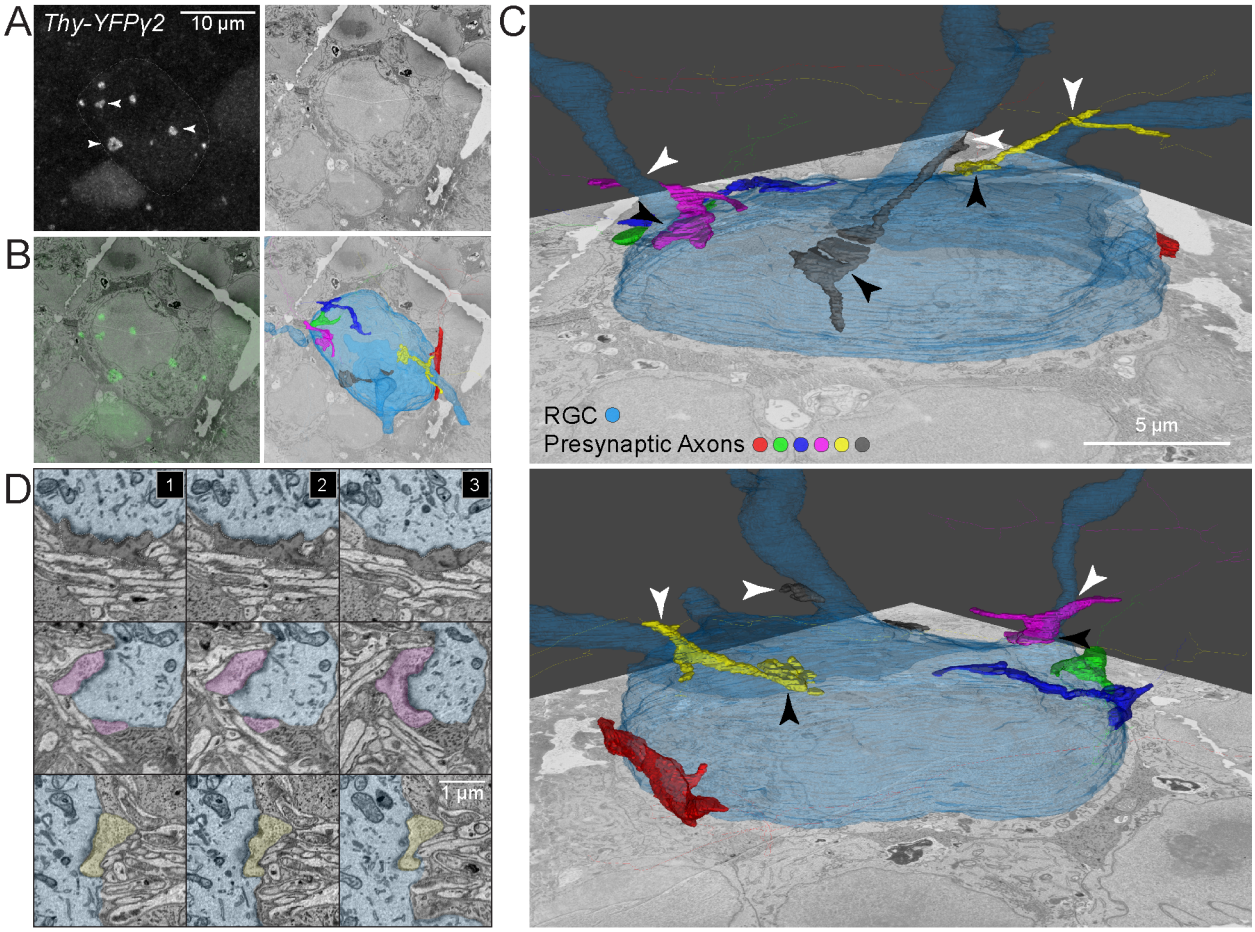

Figure 4.7 Reconstruction of the inhibitory somatic contacts on ooDS RGC somata.
(A) (Left) MIP of the YFPγ2 puncta onto an ooDS RGC, (dashed line represents soma boundary, white arrowheads point to three largest somatic puncta). (Right) Single EM micrograph at the level of the soma and NIRB mark (white absence of tissue) used for identification of the ooDS RGC. **(B)** (Left)Overlay of YFPγ2 fluorescence from (A, green) and EM micrograph from (A). (Right) Reconstructed ooDS RGC soma (blue) and axon terminals from its presynaptic inhibitory cells from SBFEM. **(C)** (Upper) Front and (Lower) Rear view of rotated reconstructed volume from (D) reveals that three of the inhibitory connections (gray - yellow - magenta) make initial contact with the primary dendritic arbors of the ooDS RGC (white arrowheads) and fasciculate down to make the final somatic contact (black arrowheads). These represent the largest somatic YFPγ2 puncta in (A). The other three presynaptic terminals (red - blue - green) do not make contact with the ooDS RGCs dendrites. **(D)** High resolution serial section micrographs of the three largest somatic contacts (gray - yellow - magenta).

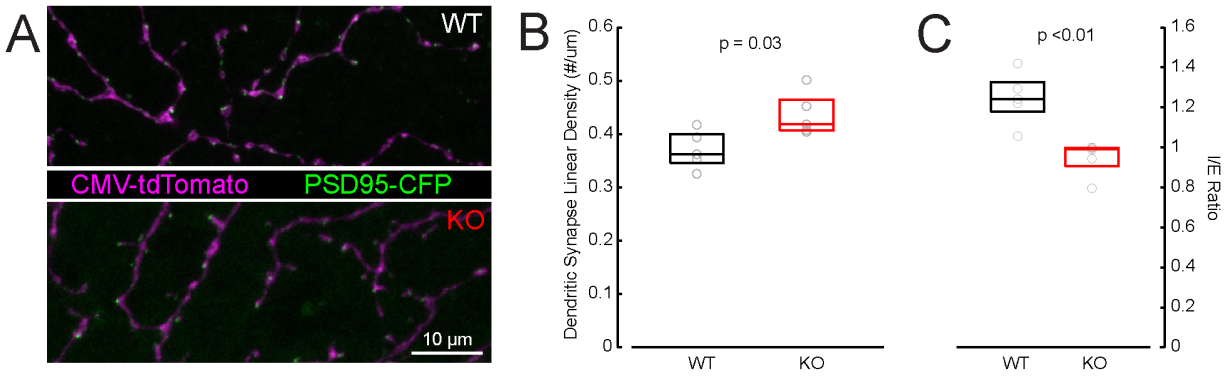

Figure 4.8 Excitatory synaptic distributions onto ooDS RGCs in the VIAATKO retina.
(A) (Upper) Example MIP of the dendritic arbor from an ooDS RGC biolistiacally co-transfected with CMV-tdTomato and PSD95-CFP in wildtype WT, and (Lower) VIAAT^{KO} retinas. **(B)** Plotted are the linear dendritic densities for PSD95-CFP in the WT and KO ooDS RGC, and **(C)** the median inhibitory/excitatory (I/E) ratios for WT and KO ooDSRGCs. WT values in (B) and (C) are re-plotted from (Bleckert et al. 2014).

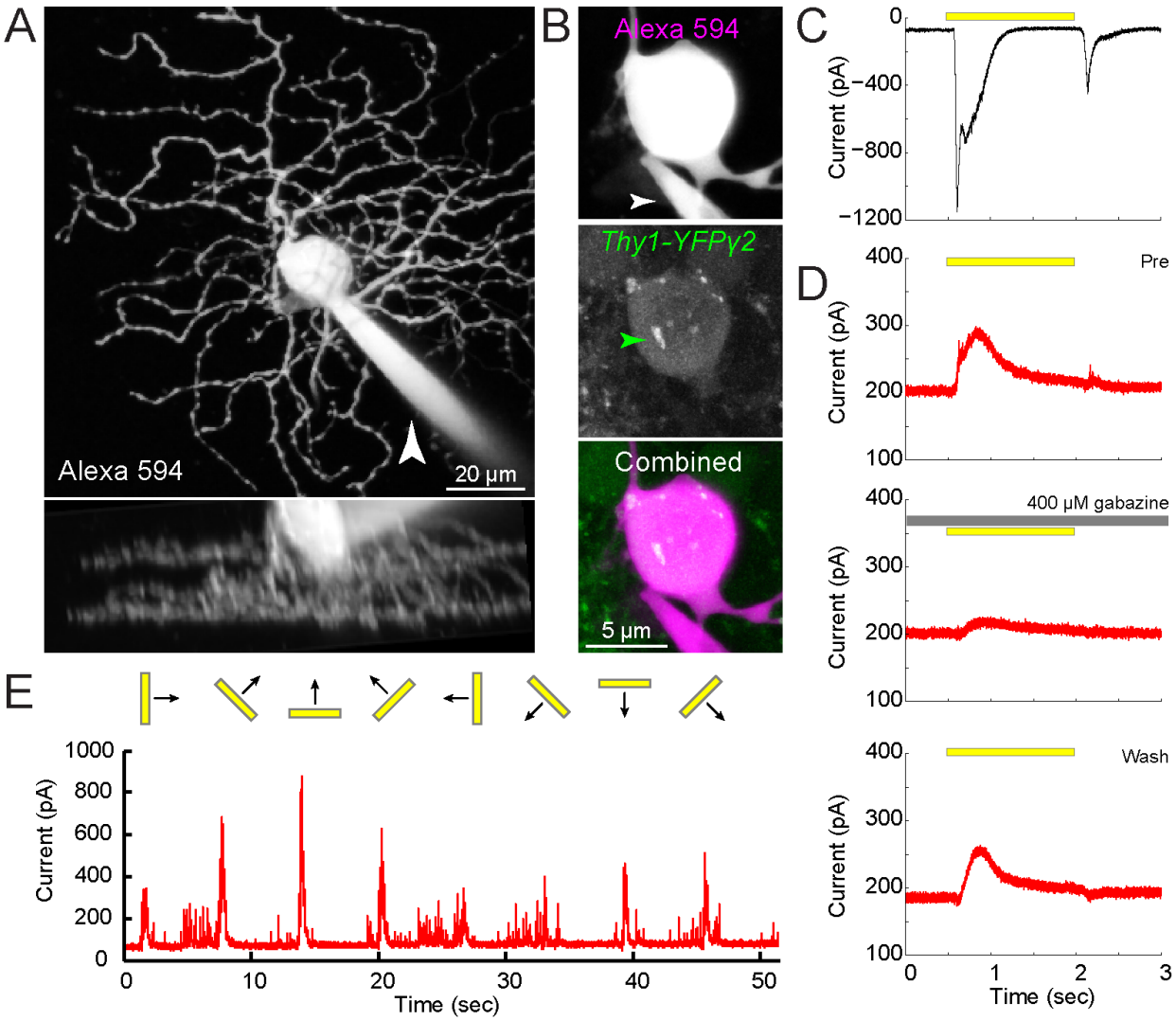

Figure 4.9 Direction selective inhibitory inputs to ooDS RGC persists in the VIAATKO retina.
(A) Example images of ooDS RGC dendritic arbors (upper) and stratification (lower) recorded from the VIAAT^{KO} retina (white arrowhead - recording pipette). **(B)** Higher resolution MIP of ooDS RGC somata, which displays enlarged YFPγ2 puncta (green arrowhead). **(C)** Example excitatory current traces (black) recorded from the cell in (A) in response to a brief flash of light (yellow bar). **(D)** Example inhibitory currents (red) recorded from cell in (A) show sensitivity to SR95531 (400 µM gabazine - gray bar). **(E)** Example inhibitory (red) current traces from an ooDR RGC in response to moving bars of light displayed successively over time (yellow bars - 8 orientations). Note the increased current response to bars moving upward vs. bars moving downward.

CHAPTER V

SUMMARY AND FUTURE DIRECTIONS

5.1 SUMMARY

From the pioneering work of Golgi and Cajal (Bullock et al. 2005; Glickstein 2006), a central goal has emerged within the field of neuroscience to identify the unique populations of neurons across circuits and to map their patterns of connectivity. This goal stems from an underlying tenet in neuroscience that 'form begets function', thus from the characterization of the structure of individual cellular elements and their connections, the potential functional properties of the circuit will emerge. The central theme of this thesis parallels this principle and asserts that an understanding of the patterns of cellular and synaptic distributions, particularly within sensory circuits, will provide insight to the salient features or regions within external environment to which an organism is attuned, and the potential computations performed by individual neurons to detect and encode these features. However, neuronal circuits are dynamic and their patterns of connectivity must be sculpted during development. Thus we also attempt to gain additional insight into how 'function may beget form' by examining how communication between neurons within a circuit during development can alter the patterns of connectivity onto individual neurons.

5.2 NONUNIFORM TOPOGRAPHIES OF MOUSE RETINAL GANGLION CELLS

In chapter 2, we mapped the distributions of unique populations of retinal ganglion cells (the A-type RGCs) across the mouse retina. We find that the ON-(S)ustained A-type RGC displays a nasal-to-temporal gradient in size (decreased) and density (increased) across the mouse retina. Whereas the OFF-S A-type RGCs likely parallel the ON-S RGCs in size and density, the OFF-(T)ransient A-type RGCs are more

uniformly distributed across the retina. This pronounced gradient in ON-S and OFF-S RGCs contrast sharply with the distribution of all RGCs, and the distributions of other known RGC types in mouse. We further showed that the anatomical and functional sampling of visual space by the ON-S A-type RGCs is enhanced within temporal retina, and corresponds to a biased representation of frontal and binocular visual space by ON-S and likely OFF-S A-type RGCs. Our work, together with the characterizations of other known RGC types, suggests that visual space in the mouse is not sampled uniformly by parallel processing circuits across the retina, but instead distinct populations of RGCs may be organized in separate topographies to encode specific visual regions or features.

5.3 SPATIAL DISTRIBUTIONS OF SYNAPTIC INPUTS ONTO INDIVIDUAL MOUSE RETINAL GANGLION CELLS

In chapter 3, we mapped the distributions of inhibitory and excitatory synaptic inputs onto individual RGCs during development. We examined how the ratios and densities of inhibitory and excitatory synaptic sites are set up during development and distributed across the dendritic arbors for 3 types of RGCs, the ON-S and OFF-S A-type RGCs, and the bistratified direction selective (DS) RGC. We find that the mature ratio of inhibitory to excitatory synaptic sites can vary across RGC types, and that these mature ratios are established at different times during development for the different RGC types. For all RGC types, the ratio of inhibitory to excitatory synaptic sites was evenly distributed across their dendritic arbors. In addition, we observed that inhibitory and excitatory sites are more closely apposed than would be predicted by random distribution. We found that these close spatial associations between excitatory and inhibitory synaptic sites appear to represent local feed-forward synaptic circuits revealed by correlative light and EM reconstruction of a single RGC's dendrites.

5.4 REGULATION OF SYNAPITIC DISTRIBUTIONS BY INHBITORY NEUROTRANSMITTERS

In chapter 4, we examined how the loss of inhibitory neurotransmission during development affects the establishment of inhibitory and excitatory patterns of connectivity onto individual RGCs. We selectively blocked inhibitory neurotransmission in the retina using conditional knock out of the vesicular inhibitory amino acid transporter (VIAAT). We find that the loss if inhibitory neurotransmission does not affect all RGC types equally. In particular the patterns of inhibitory synaptic distributions onto bistratified directions selective (ooDS) RGCs are disrupted, whereas inhibitory synaptic distributions onto other RGC types appear grossly normal. Furthermore, by using a combination of light and electron microscopy, we reveal that the inhibitory connections onto the somata of ooDS RGCs are preferentially affected, as compared to the inhibitory inputs onto the dendrites. We further show that excitatory synaptic distributions onto ooDS RGCs are also disrupted, though modestly. By recording inhibitory and excitatory currents from ooDS RGCs we find that the differential affects on somatic and dendritic synaptic distributions may result from the persistence of inhibitory input onto the dendrites of ooDS RGCs even in the absence of VIAAT. We speculate that this continued inhibitory input is likely coming from starburst amacrine cells, the predominant inhibitory presynaptic partners of the ooDS RGCs.

5.5 Future directions

Within the preceding chapters the results presented in this thesis have been discussed within the context of what has already been discovered. In the proceeding sections, we will provide some speculation as to the impact of these results, and some potential future directions for intriguing questions emerging from this work.

5.6 Retinal ganglion cell topographies in mouse vision

The distributions of RGCs in the mouse have previously been believed to be rather uniformly distributed across the retina (Jeon et al. 1998; Sun et al. 2002). This has led to the persistent notion that the mouse

visual system is less specialized that that of primates or carnivores. However, an ever-increasing accumulation of evidence shows that the mouse retina is more complex than previously believed (Gollisch and Meister 2010) and that mice can utilize their visual systems for quite complex behavioral tasks (Huberman and Niell 2011; Niell 2011; Niell 2013). The diversity of RGC topographies within the mouse retina that our work on A-type RGCs reveals raises the question: *Are distinct types of RGCs in mice utilized for detecting and responding to specific features within the visual environment?* The best evidence for the specialized usage of RGCs in mice actually comes from the characterization of RGCs that do not provide image-forming input to higher cortical areas. These are the intrinsically photosensitive RGCs, which project to the suprachiasmatic nucleus and regulate circadian rhythms (Schmidt et al. 2011b; Schmidt et al. 2011a). Intriguingly, it has recently been shown that these RGC types display a nonuniform distribution across the mouse retina that may be organized to encode spatial differences in spectral properties within the environment (Hughes et al. 2013). A second population of RGCs that provides non-image forming input to higher cortical regions that has also been implicated in regulating mouse behavior, are the ON direction selective RGCs (Dhande et al. 2013). There are believed to be 3 populations of ON DS RGCs that are sensitive to forward, downward, and upward motion, conjugate to the motions encoded by the vestibular system (Simpson 1984). These ON DS RGCs project to the accessory optic system and help to stabilize images on the retina by encoding the slip in motion of the visual world across the retina as the mouse moves its head (Simpson 1984). Two additional types of direction selective RGCs have been identified in the mouse that likely provide visual input to higher visual cortical regions. The most well studied direction selective RGCs are the bistratified ON OFF (ooDS) RGCs (Wei and Feller 2011; Dhande and Huberman 2014). There are believed to be 4 populations of ooDS RGCs, which are specialized in detecting motion in the 4 cardinal directions across the retina. It has recently been shown that these RGC types provide direct input into higher visual cortical areas, and could influence visual discrimination of direction and orientation (Cruz-Martín et al. 2014). The second

population of direction selective RGCs that project, and likely provide direct visual information, to higher visual cortical areas are OFF DS RGCs, which respond to upward motion (Kim et al. 2008). However little is known about the function of OFF DS RGCs. Intriguingly, the topographies of all types of direction selective RGC are similar, in that they are all relatively uniformly distributed across the mouse retina, which together may be indicative of a role in detecting global motion across the retina as apposed to specific regions of the visual field. The only RGC type that has been implicated in mediating a direct behavioral response to perceived visual input is the object motion detecting RGC (Zhang et al. 2012). These RGCs are specialized at detecting small moving objects against a static background, and have been suggested to be capable of mediating an aversive response (either escape or freezing) to overhead motion (Yilmaz and Meister 2013). It may be apt then that these RGCs show enhanced density within ventral retina, which captures upper visual space (Zhang et al. 2012). Taken together, it appears that some RGCs in mice are specialized for sampling particular regions of visual space, while others are organized for a more even sampling of the environment. However, there are still a number of RGC types, which have not yet been fully characterized.

Our description of A-type RGCs has also helped to clarify the characterization of RGCs types within the mouse retina, which has often been marred by lack of unique identifiers for distinct RGC types (see Chapter 2, Table 1). There are a likely 21 RGC types, which have been identified (Sun et al. 2002; Badea and Nathans 2004; Kong et al. 2005; Völgyi et al. 2005; Coombs et al. 2006; Völgyi et al. 2009; Hong et al. 2011; Ecker et al. 2010; Farrow et al. 2013), but for most we do not currently have means for their systematic identification. Together, our characterization of the A-type RGCs with the other known RGC types begins to provide a picture of how visual space is sampled by the mouse retina. However, in total the A-type RGCs and all other characterized RGC types described above only account for approximately 60% of the total RGC population (Jeon et al. 1998). Thus, one outstanding and critical question remains: *Do the remaining RGCs types have similar or distinct topographies across the mouse*

retina? It is only a matter of time before genetic markers for these RGC types become available and our question will be answered (Dhande and Huberman 2014).

5.7 POTENTIAL FUNCTIONS OF A-TYPE RGCS IN MOUSE

The A-type RGCs characterized in chapter 4 are likely the equivalent of alpha (α) RGCs identified in almost every mammalian species (Peichl 1991), and are the equivalent of brisk transient, or Y-type RGCs characterized by physiology (Cleland and Levick 1974a; Peichl and Wässle 1981; Saito 1983). However, we chose the nomenclature of A-type RGCs as apposed to α RGCs for the following reasons: (1) The physiological classification of ON α RGCs in cat show a brisk transient response, whereas ON A-type RGCs in mouse display a sustained response (Boycott and Wässle 1974b; Cleland et al. 1975; Pang et al. 2003; Murphy and Rieke 2006; van Wyk et al. 2009) (2) In all mammalian species α RGCs are found as ON and OFF pairs, except for possibly the rat (Peichl 1989), whereas 1 ON and 2 OFF populations of A-type RGCs are found in mouse (Peichl 1991; Pang et al. 2003; Murphy and Rieke 2006; van Wyk et al. 2009) and (3) The A-type nomenclature has already been presented as a valid naming paradigm for α RGCs in mouse (Majumdar et al. 2007).

In cats, and other mammals α RGCs show non-uniform topographies wherein they scale in size and density towards central visual regions of the retina (Peichl et al. 1987). However most other RGCs in cat also share a similar topography. Thus the sharp contrast between the topographies of known RGCs in mouse, and the ON-S and OFF-S A-type RGCs raises the question: *What is the potential function of the distribution of A-type RGCs?* Recently it has been shown that dominant physiological profile of cells in the dorsal lateral geniculate nucleas (dLGN) of the thalamus, the relay center from retina to higher cortical visual regions in mouse, are ON-S, OFF-S and OFF-T responses (Piscopo et al. 2013). In addition, the majority of inputs into to the primary input layer (4) of visual cortex in mouse can be traced back

through the dLGN to A-type RGCs (Cruz-Martín et al. 2014). Together, this suggests that A-type RGCs may provide a majority of direct input to primary visual cortex.

In addition to their connections within the thalamus, A-type RGCs have also been shown to have considerable input to superior colliculus (SC). The SC is a laminated midbrain structure involved in directing the head and eyes to particular locations in visual space. Retinal input to SC is primarily restricted to superficial layers, whereas auditory and somatosensory input occurs in deeper layers (May 2006). A-type RGCs project to deeper portion of the retino-recipient layers of the SC (Huberman et al. 2008b; Hong et al. 2011). Intriguingly, within deeper layers of the SC, cells can be multimodal and receive a combination of retinal, auditory and somatosensory input. Furthermore, it has been shown that within the mouse SC there is a strong correlation between the topographies of the receptive fields of visual and somatosensory input, particularly from the vibrissae. Thus the projection fields of the retina that overlay a given whisker have matched topographies in the SC (Drager and Hubel 1975a; Drager and Hubel 1975b; Drager and Hubel 1976). Because the A-type RGCs are biased towards enhanced sampling of the frontal visual fields, which projects through visual space occupied by the vibrissae, we speculate that a prominent role for A-type RGCs may be in correlating somatosensory and visual input to orient the mouse to particular targets in the environment. Studies from a variety of species have shown that α RGCs have high contrast sensitivity, and non-linear receptive fields (Enroth-Cugell and Robson 1966; Demb et al. 1999; Brown et al. 2000), which may aid their detection of fine scale spatial stimuli, much smaller than their receptive field (Schwartz et al. 2012). Thus A-type RGCs could be well adept at detecting textures in the visual environment with spatial frequencies similar to those encoded by the vibrissae (Kleinfeld et al. 2006; Diamond et al. 2008). It would be intriguing to determine what influence activation of A-type RGCs has on visual and somatosensory behaviors. Ideally the identification of specific genetic markers for A-type RGCs would greatly advance our ability to

selectivity manipulate the activity of these RGC types, and to determine their roles in visually guided behaviors.

5.8 Role of synaptic distributions across RGCs

A considerable amount of work has shown that the distributions of excitatory inputs to RGCs strongly predict their functional responses to light stimuli (Freed and Sterling 1988; Freed et al. 1992; Brown et al. 2000; Morgan et al. 2008; Schwartz et al. 2012). However the roles of direct inhibitory input onto individual retinal ganglion cells are less well known. Inhibition in the retina is responsible in creating the classic polarized center-surround response of RGCs (Kuffler 1953). However, the majority of inhibitory input regulating this mechanism comes from presynaptic inhibition in the outer retina between horizontal cells and photoreceptors, or in the inner retina from amacrine cells to bipolar cell axon terminals (Roska et al. 2000; Jadzinsky and Baccus 2013). A defined role for direct inhibition onto RGCs is best exemplified by the input from starburst amacrine cells (SACs) to direction selective RGCs. Through the patterns of connectivity and physiological input from SACs and DS RGCs, a defined role for direct inhibitory neurotransmission onto a RGC has been determined (Euler et al. 2002; Fried et al. 2002; Wei and Feller 2011; Briggman et al. 2011; Taylor and Smith 2012; Vaney et al. 2012b). Our results examining the spatial patterns of inhibitory and excitatory inputs onto individual RGCs suggest that the close apposition of excitatory and inhibitory inputs may underlie local feedforward circuits onto the RGC dendritic arbors. *What then may be the function of these close appositions and local feed forward circuits?* A number of modeling studies have shown that the spatial distributions of inhibitory and excitatory inputs onto the arbors of RGCs could mediate functions such as direction selectivity (Grzywacz and Koch 1987; Torre and Poggio 1978; Poggio and Koch 1987; Koch et al. 1983). Furthermore, results from *in vitro* and *in vivo* studies of cortical neurons suggest that inhibitory and excitatory inputs can only influence each other if they are confined to the same local regions of dendritic

segments (Liu 2004; van Versendaal et al. 2012; Chen et al. 2012). Local feed forward circuits have also been found to be a prominent circuit element onto midget ganglion cells in primate (Calkins and Sterling 1996). Our observation that both A-type and ooDS RGCs showed similar local constraints on the distributions of excitatory and inhibitory inputs raises the question: *Are local feedforward inputs a dominant feature of all mouse RGCs?* Further analysis of additional RGC types in the mouse retina will ultimately shed light on this question. Our hypothesis is that these close appositions are designed to allow for compartmentalized computations across the dendritic arbors of RGCs (Koch et al. 1982; Oesch et al. 2011). One way to test this hypothesis would be to utilize the random and observed distributions from our study to model the output of an A-type RGC to physiological patterns of excitatory and inhibitory input. There are many parameters that could affect the computation of inhibitory and excitatory inputs (e.g. distribution of synaptic weights, correlation of input at individual dendritic arbors). One could test how varying the spatial distributions between random and observed would affect the output of the model A-type RGC across different parameters. This could reveal how much the close spatial appositions between inhibitory and excitatory inputs can potentially influence the computation of excitatory and inhibitory inputs.

5.9 Regulation of synaptic development by inhibitory neurotransmission

From initial studies in the neuromuscular junction and the visual system, there has been an increasing interest in how activity dependent processes facilitate the correct wiring patterns and development of neuronal circuits (Sanes and Lichtman 1999; Waites et al. 2005). There are many ways in which activity can be regulated and disrupted, and diverse mechanisms appear to have disparate affects across many neuronal circuits (Bleckert and Wong 2011). We have focused on the role of neurotransmission, because it has been shown capable of regulating synaptic development in the retina (Morgan et al. 2011; Soto et al. 2012). However, much of the work examining the roles of neurotransmitters in circuit development

has focused on excitatory neurotransmission. Somewhat surprising to us was the differential effects caused by disrupting inhibitory neurotransmission across specific cell types (e.g. the somatic contacts onto ooDS RGCs). In contrast, disruption to excitatory neurotransmission has previously been shown to affect the distributions of excitatory synaptic contacts across multiple types of RGCs (Morgan et al. 2011; Soto et al. 2012). We thus ask the question: *Why does loss of inhibitory neurotransmission produce different results across RGC types?* We have previously presented evidence that the mature patterns of inhibitory and excitatory synaptic inputs onto ooDS RGCs are established at a later developmental time than for ON-S and OFF-S A-type RGCs (Bleckert et al. 2013). It may be that the prolonged synaptic development on ooDS RGCs is more susceptible to disruption by loss of inhibitory neurotransmission. In addition, whereas a critical role for mature inhibitory neurotransmission mediating direction selectivity onto ooDS RGCs has been established, there is far less understanding of the role of inhibitory input onto ON-S and OFF-S A-type RGCs. A more detailed characterization of the loss of inhibitory neurotransmission across multiple RGC types may help to determine which cells are particularly dependent upon inhibitory neurotransmission.

Our results showing a preferential disruption of inhibitory synaptic sites onto distinct cellular compartments of ooDS RGCs (eg. somata and dendrites) suggest that like excitatory neurotransmission (Morgan et al. 2011; Soto et al. 2012), inhibitory neurotransmission acts locally at the synapses which have been disrupted. We suggest that this may result from the continued release of inhibitory neurotransmitters from the starburst amacrine cells, which are the primary inhibitory contacts onto ooDS RGCs. The pronounced effects onto the somata of ooDS RGCs in the VIAAT^{KO} retinas, and the presence of somatic contacts onto most of the RGCs observed in the Thy1-YFPγ2 transgenic begs the question: *What is the role of inhibitory input onto RGC somata?* There is almost no information as to the types of amacrine cells that provide inhibition onto the somata of RGCs, and little examination of their potential affects on RGC function. Throughout other cortical circuits, diverse populations of inhibitory

interneurons are found which directly target the output of principle excitatory neurons (i.e somata or axon initial segment) (Ango et al. 2004; Huang et al. 2007; Klausberger and Somogyi 2008). The activity of these interneurons has been suggested to modulate more global patterns of cell activity (Miles et al. 1996; Bar-Ilan et al. 2012; Woodruff et al. 2010; Freund and Katona 2007; Ellender and Paulsen 2010). The extreme diversity and number of amacrine cells within the retina far exceeds that found in any of the other retinal neuron types (MacNeil and Masland 1998; Masland 2012; Strettoi and Masland 1996; Lin and Masland 2006; Wässle et al. 2009; Menger et al. 1998; Jeon et al. 1998), and they are likely they least well studied. This lack of information highlights that will still have much to learn about retinal circuitry and patterns of connectivity. We suggest that a foray into the characterization of amacrine cells and their contribution to retinal circuitry will provide a substantial re-evaluation of the complexity and intrigue of the mouse retina. The identification of transgenic markers for specific amacrine cell types will be pivotal for this endeavor.

BIBLIOGRAPHY

Adams AD, Forrester JM. The projection of the rat's visual field on the cerebral cortex. *Experimental Physiology* 53: 327-336, 1968.

Akerman CJ, Cline HT. Depolarizing GABAergic conductances regulate the balance of excitation to inhibition in the developing retinotectal circuit in vivo. *J Neurosci* 26: 5117-5130, 2006.

Akerman CJ, Cline HT. Refining the roles of GABAergic signaling during neural circuit formation. *Trends Neurosci* 30: 382-389, 2007.

Amthor FR, Takahashi ES, Oyster CW. Morphologies of rabbit retinal ganglion cells with complex receptive fields. *J Comp Neurol* 280: 97-121, 1989.

Andermann ML, Kerlin AM, Roumis DK, Glickfeld LL, Reid RC. Functional specialization of mouse higher visual cortical areas. *Neuron* 72: 1025-1039, 2011.

Anderson TR, Shah PA, Benson DL. Maturation of glutamatergic and GABAergic synapse composition in hippocampal neurons. *Neuropharmacology* 47: 694-705, 2004.

Ango F, di Cristo G, Higashiyama H, Bennett V, Wu P, Huang ZJ. Ankyrin-based subcellular gradient of neurofascin, an immunoglobulin family protein, directs GABAergic innervation at purkinje axon initial segment. *Cell* 119: 257-272, 2004.

Archer SN, Djamgoz MBA, Loew ER, Partridge JC, Vallerga S, and Collin SP. Behavioural ecology and retinal cell topography, In: *Adaptive Mechanisms in the Ecology of Vision*. Springer Netherlands, 1999.

Asada H, Kawamura Y, Maruyama K, Kume H, Ding R-G, Ji FY, Kanbara N, Kuzume H, Sanbo M, Yagi T, Obata K. Mice Lacking the 65 kDa Isoform of Glutamic Acid Decarboxylase (GAD65) Maintain Normal Levels of GAD67 and GABA in Their Brains but Are Susceptible to Seizures. *Biochemical and Biophysical Research Communications* 229: 891-895, 1996.

Asada H, Kawamura Y, Maruyama K, Kume H, Ding RG, Kanbara N, Kuzume H, Sanbo M, Yagi T, Obata K. Cleft palate and decreased brain gamma-aminobutyric acid in mice lacking the 67-kDa isoform of glutamic acid decarboxylase. *Proc Natl Acad Sci U S A* 94: 6496-6499, 1997.

Auferkorte ON, Baden T, Kaushalya SK, Zabouri N, Rudolph U, Haverkamp S, Euler T. GABA(A) receptors containing the α2 subunit are critical for direction-selective inhibition in the retina. *PLoS One* 7: e35109, 2012.

Azeredo da Silveira R, Roska B. Cell Types, Circuits, Computation. *Curr Opin Neurobiol* , 2011.

Badea TC, Nathans J. Quantitative analysis of neuronal morphologies in the mouse retina visualized by using a genetically directed reporter. *J Comp Neurol* 480: 331-351, 2004.

Bar-Ilan L, Gidon A, Segev I. The role of dendritic inhibition in shaping the plasticity of excitatory synapses. *Front Neural Circuits* 6: 118, 2012.

Barlow HB, Hill RM. Selective sensitivity to direction of movement in ganglion cells of the rabbit retina. *Science* , 1963.

Barlow HB, Levick WR. The mechanism of directionally selective units in rabbit's retina. *J Physiol* 178: 477-504, 1965.

Baumhardt PE, Moore BA, Doppler M, Fernández-Juricic E. Do American Goldfinches See Their World Like Passive Prey Foragers? A Study on Visual Fields, Retinal Topography, and Sensitivity of Photoreceptors. *Brain Behav Evol* , 2014.

Ben-Ari Y. Excitatory actions of gaba during development: the nature of the nurture. *Nat Rev Neurosci* 3: 728-739, 2002.

Ben-Ari Y, Khazipov R, Leinekugel X, Caillard O, Gaiarsa J-L. GABAA, NMDA and AMPA receptors: a developmentally regulated [`]ménage à trois'. *Trends in Neurosciences* 20: 523-529, 1997.

Benson DL, Cohen PA. Activity-independent segregation of excitatory and inhibitory synaptic terminals in cultured hippocampal neurons. *J Neurosci* 16: 6424-6432, 1996.

Berson DM, Castrucci AM, Provencio I. Morphology and mosaics of melanopsin-expressing retinal ganglion cell types in mice. *J Comp Neurol* 518: 2405-2422, 2010.

Berson DM, Dunn FA, Takao M. Phototransduction by retinal ganglion cells that set the circadian clock. *Science* 295: 1070-1073, 2002.

Berson DM, Masland RH, Albright TD, Dallos P, Oertel D, Firestein S, Beauchamp GK, Bushnell MC, Basbaum AI, Kaas JH, and Gardner EP. 1.25 - Retinal Ganglion Cell Types and Their Central Projections, In: *The Senses: A Comprehensive Reference*. New York: Academic Press, 2008.

Berson DM, Pu M, Famiglietti EV. The zeta cell: a new ganglion cell type in cat retina. *Journal of Comparative Neurology* 399: 269, 1998.

Bi G, Poo M. Synaptic modification by correlated activity: Hebb's postulate revisited. *Annu Rev Neurosci* 24: 139-166, 2001.

Bishop D, Nikić I, Brinkoetter M, Knecht S, Potz S, Kerschensteiner M, Misgeld T. Near-infrared branding efficiently correlates light and electron microscopy. *Nat Methods* 8: 568-570, 2011.

Blakely RD, Edwards RH. Vesicular and plasma membrane transporters for neurotransmitters. *Cold Spring Harb Perspect Biol* 4: , 2012.

Blankenship AG, Feller MB. Mechanisms underlying spontaneous patterned activity in developing neural circuits. *Nat Rev Neurosci* 11: 18-29, 2010.

Bleckert A, Gaiarsa J-L, Parker ED, Kang Y, Pancaroglu R, Soto F, Lewis R, Craig AM, Wong ROL. Spatial Relationships between GABAergic and Glutamatergic Synapses on the Dendrites of Distinct Types of Mouse Retinal Ganglion Cells across Development. *PLoS One* 8: e69612, 2013.

Bleckert A, Schwartz GW, Turner MH, Rieke F, Wong RO. Visual Space Is Represented by Nonmatching Topographies of Distinct Mouse Retinal Ganglion Cell Types. *Curr Biol* , 2014.

Bleckert A, Wong RO. Identifying roles for neurotransmission in circuit assembly: insights gained from multiple model systems and experimental approaches. *Bioessays* 33: 61-72, 2011.

Bodnarenko SR, Chalupa LM. Stratification of ON and OFF ganglion cell dendrites depends on glutamate-mediated afferent activity in the developing retina. *Nature* 364: 144-146, 1993.

Bollmann JH, Engert F. Subcellular topography of visually driven dendritic activity in the vertebrate visual system. *Neuron* 61: 895-905, 2009.

Bormann J. The [`]ABC' of GABA receptors. *Trends in Pharmacological Sciences* 21: 16-19, 2000.

Borst A, Euler T. Seeing things in motion: models, circuits, and mechanisms. *Neuron* 71: 974-994, 2011.

Bosman LW, Takechi H, Hartmann J, Eilers J, Konnerth A. Homosynaptic long-term synaptic potentiation of the "winner" climbing fiber synapse in developing Purkinje cells. *J Neurosci* 28: 798-807, 2008.

Boycott BB, Wässle H. The morphological types of ganglion cells of the domestic cat's retina. *J Physiol* 240: 397-419, 1974a.

Boycott BB, Wässle H. The morphological types of ganglion cells of the domestic cat's retina. *J Physiol* 240: 397-419, 1974b.

Branco T, Häusser M. The single dendritic branch as a fundamental functional unit in the nervous system. *Curr Opin Neurobiol* 20: 494-502, 2010.

Brandstätter JH, Greferath U, Euler T, Wässle H. Co-stratification of GABAA receptors with the directionally selective circuitry of the rat retina. *Vis Neurosci* 12: 345-358, 1995.

Briggman KL, Helmstaedter M, Denk W. Wiring specificity in the direction-selectivity circuit of the retina. *Nature* 471: 183-188, 2011.

Brown SP, He S, Masland RH. Receptive field microstructure and dendritic geometry of retinal ganglion cells. *Neuron* 27: 371-383, 2000.

Brünig I, Suter A, Knuesel I, Lüscher B, Fritschy JM. GABAergic terminals are required for postsynaptic clustering of dystrophin but not of GABA(A) receptors and gephyrin. *J Neurosci* 22: 4805-4813, 2002.

Budzinski KL, Allen RW, Fujimoto BS, Kensel-Hammes P, Belnap DM, Bajjalieh SM, Chiu DT. Large structural change in isolated synaptic vesicles upon loading with neurotransmitter. *Biophys J* 97: 2577-2584, 2009.

Buffelli M, Burgess RW, Feng G, Lobe CG, Lichtman JW, Sanes JR. Genetic evidence that relative synaptic efficacy biases the outcome of synaptic competition. *Nature* 424: 430-434, 2003.

Bullock TH, Bennett MV, Johnston D, Josephson R, Marder E, Fields RD. Neuroscience. The neuron doctrine, redux. *Science* 310: 791-793, 2005.

Burkhalter A. Many specialists for suppressing cortical excitation. *Front Neurosci* 2: 155-167, 2008.

Cafaro J, Rieke F. Noise correlations improve response fidelity and stimulus encoding. *Nature* 468: 964-967, 2010.

Calkins DJ, Sterling P. Absence of spectrally specific lateral inputs to midget ganglion cells in primate retina. *Nature* 381: 613-615, 1996.

Calkins DJ, Tsukamoto Y, Sterling P. Microcircuitry and mosaic of a blue-yellow ganglion cell in the primate retina. *J Neurosci* 18: 3373-3385, 1998.

Cardona A, Saalfeld S, Schindelin J, Arganda-Carreras I, Preibisch S, Longair M, Tomancak P, Hartenstein V, Douglas RJ. TrakEM2 software for neural circuit reconstruction. *PLoS One* 7: e38011, 2012.

Carrasco M, McElree B, Denisova K, Giordano AM. Speed of visual processing increases with eccentricity. *Nature neuroscience* 6: 699-700, 2003.

Chalupa LM, Williams RW, Henderson Z. Binocular interaction in the fetal cat regulates the size of the ganglion cell population. *Neuroscience* 12: 1139-1146, 1984.

Chang L, Breuninger T, Euler T. Chromatic coding from cone-type unselective circuits in the mouse retina. *Neuron* 77: 559-571, 2013.

Chan TL, Martin PR, Clunas N, Grünert U. Bipolar cell diversity in the primate retina: morphologic and immunocytochemical analysis of a new world monkey, the marmoset Callithrix jacchus. *Journal of Comparative Neurology* 437: 219-239, 2001.

Chattopadhyaya B, Di Cristo G, Higashiyama H, Knott GW, Kuhlman SJ, Welker E, Huang ZJ. Experience and activity-dependent maturation of perisomatic GABAergic innervation in primary visual cortex during a postnatal critical period. *J Neurosci* 24: 9598-9611, 2004.

Chattopadhyaya B, Di Cristo G, Wu CZ, Knott G, Kuhlman S, Fu Y, Palmiter RD, Huang ZJ. GAD67-mediated GABA synthesis and signaling regulate inhibitory synaptic innervation in the visual cortex. *Neuron* 54: 889-903, 2007a.

Chattopadhyaya B, Di Cristo G, Wu CZ, Knott G, Kuhlman S, Fu Y, Palmiter RD, Huang ZJ. GAD67-mediated GABA synthesis and signaling regulate inhibitory synaptic innervation in the visual cortex. *Neuron* 54: 889-903, 2007b.

Chaudhry FA, Edwards RH, Fonnum F. Vesicular neurotransmitter transporters as targets for endogenous and exogenous toxic substances. *Annu Rev Pharmacol Toxicol* 48: 277-301, 2008.

Chelazzi L, Rossi F, Tempia F, Ghirardi M, Strata P. Saccadic Eye Movements and Gaze Holding in the Head-Restrained Pigmented Rat. *European Journal of Neuroscience* 1: 639-646, 1989.

Chen C, Regehr WG. Developmental remodeling of the retinogeniculate synapse. *Neuron* 28: 955-966, 2000.

Chen J, Villa K, Cha J, So P, Kubota Y, Nedivi E. Clustered Dynamics of Inhibitory Synapses and Dendritic Spines in the Adult Neocortex. *Neuron* 74: 361-373, 2012.

Chen X, Hsueh HA, Greenberg K, Werblin FS. Three forms of spatial temporal feedforward inhibition are common to different ganglion cell types in rabbit retina. *J Neurophysiol* 103: 2618-2632, 2010.

Chen X, Leischner U, Rochefort NL, Nelken I, Konnerth A. Functional mapping of single spines in cortical neurons in vivo. *Nature* , 2011.

Chklovskii DB, Koulakov AA. Maps in the brain: what can we learn from them? *Annu Rev Neurosci* 27: 369-392, 2004.

Christie SB, Li RW, Miralles CP, Yang BY, De Blas AL. Clustered and non-clustered GABAA receptors in cultured hippocampal neurons. *Mol Cell Neurosci* 31: 1-14, 2006.

Christie SB, Miralles CP, De Blas AL. GABAergic innervation organizes synaptic and extrasynaptic GABAA receptor clustering in cultured hippocampal neurons. *J Neurosci* 22: 684-697, 2002.

Cleland BG, Levick WR. Brisk and sluggish concentrically organized ganglion cells in the cat's retina. *J Physiol* 240: 421-456, 1974a.

Cleland BG, Levick WR. Properties of rarely encountered types of ganglion cells in the cat's retina and an overall classification. *J Physiol* 240: 457-492, 1974b.

Cleland BG, Levick WR, Wässle H. Physiological identification of a morphological class of cat retinal ganglion cells. *J Physiol* 248: 151-171, 1975.

Cohen-Cory S. BDNF modulates, but does not mediate, activity-dependent branching and remodeling of optic axon arbors in vivo. *J Neurosci* 19: 9996-10003, 1999.

Cohen E, Sterling P. Convergence and divergence of cones onto bipolar cells in the central area of cat retina. *Philos Trans R Soc Lond B Biol Sci* 330: 323-328, 1990.

Cohen E, Sterling P. Microcircuitry related to the receptive field center of the on-beta ganglion cell. *J Neurophysiol* 65: 352-359, 1991.

Cohen E, Sterling P. Parallel Circuits from Cones to the On-Beta Ganglion Cell. *Eur J Neurosci* 4: 506-520, 1992.

Coimbra JP, Hart NS, Collin SP, Manger PR. Scene from above: retinal ganglion cell topography and spatial resolving power in the giraffe (Giraffa camelopardalis). *J Comp Neurol* 521: 2042-2057, 2013.

Collin SP. A web-based archive for topographic maps of retinal cell distribution in vertebrates. *Clin Exp Optom* 91: 85-95, 2008.

Coombs J, van der List D, Wang GY, Chalupa LM. Morphological properties of mouse retinal ganglion cells. *Neuroscience* 140: 123-136, 2006.

Coombs JL, Van Der List D, Chalupa LM. Morphological properties of mouse retinal ganglion cells during postnatal development. *J Comp Neurol* 503: 803-814, 2007.

Craig AM, Blackstone CD, Huganir RL, Banker G. Selective clustering of glutamate and gamma-aminobutyric acid receptors opposite terminals releasing the corresponding neurotransmitters. *Proc Natl Acad Sci U S A* 91: 12373-12377, 1994.

Cramer KS, Bermingham-McDonogh O, Krull CE, Rubel EW. EphA4 signaling promotes axon segregation in the developing auditory system. *Dev Biol* 269: 26-35, 2004.

Cramer KS, Karam SD, Bothwell M, Cerretti DP, Pasquale EB, Rubel EW. Expression of EphB receptors and EphrinB ligands in the developing chick auditory brainstem. *J Comp Neurol* 452: 51-64, 2002.

Crescitelli F, and Meyer D. The Avian Eye and its Adaptations, In: *The Visual System in Vertebrates*. Springer Berlin Heidelberg, 1977.

Crick F, Jones E. Backwardness of human neuroanatomy. *Nature* 361: 109-110, 1993.

Cruz-Martín A, El-Danaf RN, Osakada F, Sriram B, Dhande OS, Nguyen PL, Callaway EM, Ghosh A, Huberman AD. A dedicated circuit links direction-selective retinal ganglion cells to the primary visual cortex. *Nature* , 2014.

Curcio CA, Allen KA. Topography of ganglion cells in human retina. *Journal of Comparative Neurology* 300: 5-25, 1990.

DACEY D. 20 Origins of Perception: Retinal Ganglion Cell Diversity and the Creation of Parallel Visual Pathways. *The cognitive neurosciences* 281, 2004.

Dacey DM, Lee BB. The 'blue-on' opponent pathway in primate retina originates from a distinct bistratified ganglion cell type. *Nature* 367: 731-735, 1994.

Dacey DM, Packer OS. Colour coding in the primate retina: diverse cell types and cone-specific circuitry. *Curr Opin Neurobiol* 13: 421-427, 2003.

Dacey DM, Petersen MR. Dendritic field size and morphology of midget and parasol ganglion cells of the human retina. *Proc Natl Acad Sci U S A* 89: 9666-9670, 1992.

Dacheux RF, Chimento MF, Amthor FR. Synaptic input to the on-off directionally selective ganglion cell in the rabbit retina. *J Comp Neurol* 456: 267-278, 2003.

da Costa NM, Martin KA. Sparse reconstruction of brain circuits: or, how to survive without a microscopic connectome. *Neuroimage* 80: 27-36, 2013.

Daniels RW, Collins CA, Chen K, Gelfand MV, Featherstone DE, DiAntonio A. A single vesicular glutamate transporter is sufficient to fill a synaptic vesicle. *Neuron* 49: 11-16, 2006.

Deerinck TJ, Bushong EA, Thor A, Ellisman MH. NCMIR methods for 3D EM: A new protocol for preparation of biological specimens for serial block face scanning electron microscopy. *Microscopy* 6-8, 2010.

DeFelipe J. From the connectome to the synaptome: an epic love story. *Science* 330: 1198-1201, 2010.

Deitch JS, Rubel EW. Afferent influences on brain stem auditory nuclei of the chicken: time course and specificity of dendritic atrophy following deafferentation. *J Comp Neurol* 229: 66-79, 1984.

Del Viva MM, Punzi G, Benedetti D. Information and Perception of Meaningful Patterns. *PLoS One* 8: e69154, 2013.

Demb JB, Haarsma L, Freed MA, Sterling P. Functional circuitry of the retinal ganglion cell's nonlinear receptive field. *J Neurosci* 19: 9756-9767, 1999.

Devries SH, Baylor DA. Mosaic arrangement of ganglion cell receptive fields in rabbit retina. *J Neurophysiol* 78: 2048-2060, 1997.

Dhande OS, Estevez ME, Quattrochi LE, El-Danaf RN, Nguyen PL, Berson DM, Huberman AD. Genetic dissection of retinal inputs to brainstem nuclei controlling image stabilization. *J Neurosci* 33: 17797-17813, 2013.

Dhande OS, Huberman AD. Retinal ganglion cell maps in the brain: implications for visual processing. *Curr Opin Neurobiol* 24: 133-142, 2014.

Diamond ME, von Heimendahl M, Arabzadeh E. Whisker-Mediated Texture Discrimination. *PLoS Biol* 6: e220, 2008.

Diao L, Sun W, Deng Q, He S. Development of the mouse retina: emerging morphological diversity of the ganglion cells. *J Neurobiol* 61: 236-249, 2004.

Dobie FA, Craig AM. Inhibitory Synapse Dynamics: Coordinated Presynaptic and Postsynaptic Mobility and the Major Contribution of Recycled Vesicles to New Synapse Formation. *J Neurosci* 31: 10481-10493, 2011.

Do-Nascimento JL, Do-Nascimento RS, Damasceno BA, Silveira LC. The neurons of the retinal ganglion cell layer of the guinea pig: quantitative analysis of their distribution and size. *Brazilian journal of medical and biological research= Revista brasileira de pesquisas medicas e biologicas/Sociedade Brasileira de Biofisica...[et al.]* 24: 199-214, 1990.

Dong W, Sun W, Zhang Y, Chen X, He S. Dendritic relationship between starburst amacrine cells and direction-selective ganglion cells in the rabbit retina. *J Physiol* 556: 11-17, 2004.

Douglas RJ, Martin KA. Mapping the matrix: the ways of neocortex. *Neuron* 56: 226-238, 2007.

Dowling JE, Boycott BB. Organization of the primate retina: electron microscopy. *Proc R Soc Lond B Biol Sci* 166: 80-111, 1966.

Drager UC, Hubel DH. Physiology of visual cells in mouse superior colliculus and correlation with somatosensory and auditory input. , 1975a.

Drager UC, Hubel DH. Responses to visual stimulation and relationship between visual, auditory, and somatosensory inputs in mouse superior colliculus. *J Neurophysiol* 38: 690-713, 1975b.

Drager UC, Hubel DH. Topography of visual and somatosensory projections to mouse superior colliculus. *J Neurophysiol* 39: 91-101, 1976.

Dräger UC, Olsen JF. Origins of crossed and uncrossed retinal projections in pigmented and albino mice. *Journal of Comparative Neurology* 191: 383-412, 1980.

Dräger UC, Olsen JF. Ganglion cell distribution in the retina of the mouse. *Invest Ophthalmol Vis Sci* 20: 285-293, 1981.

Dreher B, Sefton AJ, Ni SYK, Nisbett G. The Morphology, Number, Distribution and Central Projections of Class I Retinal Ganglion Cells in Albino and Hooded Rats (Part 1 of 3). *Brain, behavior and evolution* 26: 10-22, 1985.

Ecker JL, Dumitrescu ON, Wong KY, Alam NM, Chen SK, LeGates T, Renna JM, Prusky GT, Berson DM, Hattar S. Melanopsin-expressing retinal ganglion-cell photoreceptors: cellular diversity and role in pattern vision. *Neuron* 67: 49-60, 2010.

Eiden LE, Schäfer MK, Weihe E, Schütz B. The vesicular amine transporter family (SLC18): amine/proton antiporters required for vesicular accumulation and regulated exocytotic secretion of monoamines and acetylcholine. *Pflugers Arch* 447: 636-640, 2004.

Ellender TJ, Paulsen O. The many tunes of perisomatic targeting interneurons in the hippocampal network. *Front Cell Neurosci* 4: , 2010.

Elstrott J, Anishchenko A, Greschner M, Sher A, Litke AM, Chichilnisky EJ, Feller MB. Direction selectivity in the retina is established independent of visual experience and cholinergic retinal waves. *Neuron* 58: 499-506, 2008.

Enroth-Cugell C, Robson JG. The contrast sensitivity of retinal ganglion cells of the cat. *J Physiol* 187: 517-552, 1966.

Essrich C, Lorez M, Benson JA, Fritschy J-M, Luscher B. Postsynaptic clustering of major GABAA receptor subtypes requires the [gamma]2 subunit and gephyrin. *Nat Neurosci* 1: 563-571, 1998.

Estevez ME, Fogerson PM, Ilardi MC, Borghuis BG, Chan E, Weng S, Auferkorte ON, Demb JB, Berson DM. Form and function of the M4 cell, an intrinsically photosensitive retinal ganglion cell type contributing to geniculocortical vision. *J Neurosci* 32: 13608-13620, 2012.

Euler T, Detwiler PB, Denk W. Directionally selective calcium signals in dendrites of starburst amacrine cells. *Nature* 418: 845-852, 2002.

Famiglietti EV. Starburst amacrine cells in cat retina are associated with bistratified, presumed directionally selective, ganglion cells. *Brain Res* 413: 404-408, 1987.

Famiglietti EV. Synaptic organization of complex ganglion cells in rabbit retina: type and arrangement of inputs to directionally selective and local-edge-detector cells. *J Comp Neurol* 484: 357-391, 2005.

Farrant M, Nusser Z. Variations on an inhibitory theme: phasic and tonic activation of GABAA receptors. *Nat Rev Neurosci* 6: 215-229, 2005.

Farrow K, Teixeira M, Szikra T, Viney TJ, Balint K, Yonehara K, Roska B. Ambient illumination toggles a neuronal circuit switch in the retina and visual perception at cone threshold. *Neuron* 78: 325-338, 2013.

Felleman DJ, Van Essen DC. Distributed hierarchical processing in the primate cerebral cortex. *Cerebral cortex* 1: 1-47, 1991.

Feng G, Mellor RH, Bernstein M, Keller-Peck C, Nguyen QT, Wallace M, Nerbonne JM, Lichtman JW, Sanes JR. Imaging neuronal subsets in transgenic mice expressing multiple spectral variants of GFP. *Neuron* 28: 41-51, 2000.

Fernández-Juricic E, Moore BA, Doppler M, Freeman J, Blackwell BF, Lima SL, DeVault TL. Testing the terrain hypothesis: Canada geese see their world laterally and obliquely. *Brain, behavior and evolution* 77: 147-158, 2011.

Field GD, Chichilnisky EJ. Information processing in the primate retina: circuitry and coding. *Annu Rev Neurosci* 30: 1-30, 2007.

Field GD, Gauthier JL, Sher A, Greschner M, Machado TA, Jepson LH, Shlens J, Gunning DE, Mathieson K, Dabrowski W, Paninski L, Litke AM, Chichilnisky EJ. Functional connectivity in the retina at the resolution of photoreceptors. *Nature* 467: 673-677, 2010.

Fisher LJ. Development of synaptic arrays in the inner plexiform layer of neonatal mouse retina. *J Comp Neurol* 187: 359-372, 1979.

Freed MA, Smith RG, Sterling P. Computational model of the on-alpha ganglion cell receptive field based on bipolar cell circuitry. *Proc Natl Acad Sci U S A* 89: 236-240, 1992.

Freed MA, Sterling P. The ON-alpha ganglion cell of the cat retina and its presynaptic cell types. *J Neurosci* 8: 2303-2320, 1988.

Freund TF, Katona I. Perisomatic inhibition. *Neuron* 56: 33-42, 2007.

Fried SI, Münch TA, Werblin FS. Mechanisms and circuitry underlying directional selectivity in the retina. *Nature* 420: 411-414, 2002.

Fritschy JM, Harvey RJ, Schwarz G. Gephyrin: where do we stand, where do we go? *Trends Neurosci* 31: 257-264, 2008.

Fritschy JM, Panzanelli P, Kralic JE, Vogt KE, Sassoè-Pognetto M. Differential dependence of axo-dendritic and axo-somatic GABAergic synapses on GABAA receptors containing the alpha1 subunit in Purkinje cells. *J Neurosci* 26: 3245-3255, 2006.

Frola E, Patrizi A, Goetz T, Medrihan L, Petrini EM, Barberis A, Wulff P, Wisden W, Sassoè-Pognetto M. Synaptic competition sculpts the development of GABAergic axo-dendritic but not perisomatic synapses. *PLoS One* 8: e56311, 2013.

Fukuda Y, Hsiao CF, Watanabe M. Morphological correlates of Y, X and W type ganglion cells in the cat's retina. *Vision Res* 25: 319-327, 1985.

Fukuda Y, Hsiao CF, Watanabe M, Ito H. Morphological correlates of physiologically identified Y-, X-, and W-cells in cat retina. *J Neurophysiol* 52: 999-1013, 1984.

Ghosh KK, Grünert U. Synaptic input to small bistratified (blue-ON) ganglion cells in the retina of a new world monkey, the marmoset Callithrix jacchus. *J Comp Neurol* 413: 417-428, 1999.

Gibson JR, Bartley AF, Hays SA, Huber KM. Imbalance of neocortical excitation and inhibition and altered UP states reflect network hyperexcitability in the mouse model of fragile X syndrome. *J Neurophysiol* 100: 2615-2626, 2008.

Glickstein M. Golgi and Cajal: The neuron doctrine and the 100th anniversary of the 1906 Nobel Prize. *Curr Biol* 16: R147-R151, 2006.

Gollisch T, Meister M. Eye smarter than scientists believed: neural computations in circuits of the retina. *Neuron* 65: 150-164, 2010.

Greferath U, Grünert U, Fritschy JM, Stephenson A, Möhler H, Wässle H. GABAA receptor subunits have differential distributions in the rat retina: in situ hybridization and immunohistochemistry. *J Comp Neurol* 353: 553-571, 1995.

Grzywacz NM, Koch C. Functional properties of models for direction selectivity in the retina. *Synapse* 1: 417-434, 1987.

Gulyás AI, Megías M, Emri Z, Freund TF. Total number and ratio of excitatory and inhibitory synapses converging onto single interneurons of different types in the CA1 area of the rat hippocampus. *J Neurosci* 19: 10082-10097, 1999.

Güntürkün O, and Whittow GC. Chapter 1 - Sensory Physiology: Vision, In: *Sturkie's Avian Physiology (Fifth Edition)*. San Diego: Academic Press, 2000.

Gütig R, Gollisch T, Sompolinsky H, Meister M. Computing complex visual features with retinal spike times. *PLoS One* 8: e53063, 2013.

Harman A, Abrahams B, Moore S, Hoskins R. Neuronal density in the human retinal ganglion cell layer from 16-77 years. *Anat Rec* 260: 124-131, 2000.

Harvey CD, Svoboda K. Locally dynamic synaptic learning rules in pyramidal neuron dendrites. *Nature* 450: 1195-1200, 2007.

Hashimoto K, Ichikawa R, Kitamura K, Watanabe M, Kano M. Translocation of a "winner" climbing fiber to the Purkinje cell dendrite and subsequent elimination of "losers" from the soma in developing cerebellum. *Neuron* 63: 106-118, 2009.

Hashimoto K, Ichikawa R, Takechi H, Inoue Y, Aiba A, Sakimura K, Mishina M, Hashikawa T, Konnerth A, Watanabe M, Kano M. Roles of glutamate receptor delta 2 subunit (GluRdelta 2) and metabotropic glutamate receptor subtype 1 (mGluR1) in climbing fiber synapse elimination during postnatal cerebellar development. *J Neurosci* 21: 9701-9712, 2001a.

Hashimoto K, Ichikawa R, Takechi H, Inoue Y, Aiba A, Sakimura K, Mishina M, Hashikawa T, Konnerth A, Watanabe M, Kano M. Roles of glutamate receptor delta 2 subunit (GluRdelta 2) and metabotropic glutamate receptor subtype 1 (mGluR1) in climbing fiber synapse elimination during postnatal cerebellar development. *J Neurosci* 21: 9701-9712, 2001b.

Hashimoto K, Kano M. Functional differentiation of multiple climbing fiber inputs during synapse elimination in the developing cerebellum. *Neuron* 38: 785-796, 2003.

Hashimoto K, Yoshida T, Sakimura K, Mishina M, Watanabe M, Kano M. Influence of parallel fiber-Purkinje cell synapse formation on postnatal development of climbing fiber-Purkinje cell synapses in the cerebellum. *Neuroscience* 162: 601-611, 2009.

Hata Y, Stryker MP. Control of Thalamocortical Afferent Rearrangement by Postsynaptic Activity in Developing Visual Cortex. *Science* 265: 1732-1735, 1994.

Hattar S, Liao HW, Takao M, Berson DM, Yau KW. Melanopsin-containing retinal ganglion cells: architecture, projections, and intrinsic photosensitivity. *Science* 295: 1065-1070, 2002.

Haverkamp S, Wässle H. Immunocytochemical analysis of the mouse retina. *J Comp Neurol* 424: 1-23, 2000.

Heine WF, Passaglia CL. Spatial receptive field properties of rat retinal ganglion cells. *Vis Neurosci* 28: 403-417, 2011.

Helmstaedter M, Briggman KL, Denk W. 3D structural imaging of the brain with photons and electrons. *Curr Opin Neurobiol* 18: 633-641, 2008.

Hennou S, Khalilov I, Diabira D, Ben-Ari Y, Gozlan H. Early sequential formation of functional GABA(A) and glutamatergic synapses on CA1 interneurons of the rat foetal hippocampus. *Eur J Neurosci* 16: 197-208, 2002.

He Q, Wang P, Tian N. Light-evoked synaptic activity of retinal ganglion and amacrine cells is regulated in developing mouse retina. *Eur J Neurosci* 33: 36-48, 2011.

He S, Masland RH. ON direction-selective ganglion cells in the rabbit retina: dendritic morphology and pattern of fasciculation. *Vis Neurosci* 15: 369-375, 1998.

Homanics GE, DeLorey TM, Firestone LL, Quinlan JJ, Handforth A, Harrison NL, Krasowski MD, Rick CE, Korpi ER, Mäkelä R, Brilliant MH, Hagiwara N, Ferguson C, Snyder K, Olsen RW. Mice devoid of gamma-aminobutyrate type A receptor beta3 subunit have epilepsy, cleft palate, and hypersensitive behavior. *Proc Natl Acad Sci U S A* 94: 4143-4148, 1997a.

Homanics GE, Ferguson C, Quinlan JJ, Daggett J, Snyder K, Lagenaur C, Mi ZP, Wang XH, Grayson DR, Firestone LL. Gene knockout of the alpha6 subunit of the gamma-aminobutyric acid type A receptor: lack of effect on responses to ethanol, pentobarbital, and general anesthetics. *Mol Pharmacol* 51: 588-596, 1997b.

Hong YK, Chen C. Wiring and rewiring of the retinogeniculate synapse. *Curr Opin Neurobiol* 21: 228-237, 2011.

Hong YK, Kim IJ, Sanes JR. Stereotyped axonal arbors of retinal ganglion cell subsets in the mouse superior colliculus. *J Comp Neurol* 519: 1691-1711, 2011.

Hooks BM, Chen C. Distinct roles for spontaneous and visual activity in remodeling of the retinogeniculate synapse. *Neuron* 52: 281-291, 2006.

Hooks BM, Chen C. Vision triggers an experience-dependent sensitive period at the retinogeniculate synapse. *J Neurosci* 28: 4807-4817, 2008.

Hoon M, Bauer G, Fritschy JM, Moser T, Falkenburger BH, Varoqueaux F. Neuroligin 2 controls the maturation of GABAergic synapses and information processing in the retina. *J Neurosci* 29: 8039-8050, 2009.

Horton JC, Adams DL. The cortical column: a structure without a function. *Philosophical Transactions of the Royal Society B: Biological Sciences* 360: 837-862, 2005.

Hua JY, Smith SJ. Neural activity and the dynamics of central nervous system development. *Nat Neurosci* 7: 327-332, 2004.

Huang ZJ. Activity-dependent development of inhibitory synapses and innervation pattern: role of GABA signalling and beyond. *J Physiol* 587: 1881-1888, 2009.

Huang ZJ, Di Cristo G, Ango F. Development of GABA innervation in the cerebral and cerebellar cortices. *Nat Rev Neurosci* 8: 673-686, 2007.

Hubel DH, Wiesel TN. Receptive fields, binocular interaction and functional architecture in the cat's visual cortex. *J Physiol* 160: 106, 1962.

Hubel DH, Wiesel TN, LeVay S. Plasticity of ocular dominance columns in monkey striate cortex. *Philos Trans R Soc Lond B Biol Sci* 278: 377-409, 1977.

Huberman AD, Feller MB, Chapman B. Mechanisms underlying development of visual maps and receptive fields. *Annu Rev Neurosci* 31: 479-509, 2008a.

Huberman AD, Manu M, Koch SM, Susman MW, Lutz AB, Ullian EM, Baccus SA, Barres BA. Architecture and activity-mediated refinement of axonal projections from a mosaic of genetically identified retinal ganglion cells. *Neuron* 59: 425-438, 2008b.

Huberman AD, Niell CM. What can mice tell us about how vision works? *Trends Neurosci* 34: 464-473, 2011.

Huberman AD, Wei W, Elstrott J, Stafford BK, Feller MB, Barres BA. Genetic identification of an On-Off direction-selective retinal ganglion cell subtype reveals a layer-specific subcortical map of posterior motion. *Neuron* 62: 327-334, 2009.

Huckfeldt RM, Schubert T, Morgan JL, Godinho L, Di Cristo G, Huang ZJ, Wong RO. Transient neurites of retinal horizontal cells exhibit columnar tiling via homotypic interactions. *Nat Neurosci* 12: 35-43, 2009.

Hughes A. Topographical relationships between the anatomy and physiology of the rabbit visual system. *Doc Ophthalmol* 30: 33-159, 1971.

Hughes A. A quantitative analysis of the cat retinal ganglion cell topography. *Journal of Comparative Neurology* 163: 107-128, 1975.

Hughes A. *The topography of vision in mammals of contrasting life style: comparative optics and retinal organisation*. Springer, 1977.

Hughes S, Watson TS, Foster RG, Peirson SN, Hankins MW. Nonuniform distribution and spectral tuning of photosensitive retinal ganglion cells of the mouse retina. *Curr Biol* 23: 1696-1701, 2013.

Hume RI, Role LW, Fischbach GD. Acetylcholine release from growth cones detected with patches of acetylcholine receptor-rich membranes. *Nature* 305: 632-634, 1983.

Jacob TC, Moss SJ, Jurd R. GABA(A) receptor trafficking and its role in the dynamic modulation of neuronal inhibition. *Nat Rev Neurosci* 9: 331-343, 2008.

Jadzinsky PD, Baccus SA. Transformation of visual signals by inhibitory interneurons in retinal circuits. *Annu Rev Neurosci* 36: 403-428, 2013.

Jakobs TC, Koizumi A, Masland RH. The spatial distribution of glutamatergic inputs to dendrites of retinal ganglion cells. *J Comp Neurol* 510: 221-236, 2008.

Jennings C. Developmental neurobiology. Death of a synapse. *Nature* 372: 498, 1994.

Jeon CJ, Kong JH, Strettoi E, Rockhill R, Stasheff SF, Masland RH. Pattern of synaptic excitation and inhibition upon direction-selective retinal ganglion cells. *J Comp Neurol* 449: 195-205, 2002.

Jeon CJ, Strettoi E, Masland RH. The major cell populations of the mouse retina. *J Neurosci* 18: 8936-8946, 1998.

Jia H, Rochefort NL, Chen X, Konnerth A. Dendritic organization of sensory input to cortical neurons in vivo. *Nature* 464: 1307-1312, 2010.

Johnson J, Tian N, Caywood MS, Reimer RJ, Edwards RH, Copenhagen DR. Vesicular neurotransmitter transporter expression in developing postnatal rodent retina: GABA and glycine precede glutamate. *J Neurosci* 23: 518-529, 2003.

Kaas JH. What, if anything, is SI? Organization of first somatosensory area of cortex. *Physiological Reviews* 63: 206-231, 1983.

Kaas JH. Topographic maps are fundamental to sensory processing. *Brain research bulletin* 44: 107-112, 1997.

Kano M, Hashimoto K. Synapse elimination in the central nervous system. *Curr Opin Neurobiol* 19: 154-161, 2009.

Kasthuri N, Lichtman JW. The role of neuronal identity in synaptic competition. *Nature* 424: 426-430, 2003.

Kasugai Y, Swinny JD, Roberts JD, Dalezios Y, Fukazawa Y, Sieghart W, Shigemoto R, Somogyi P. Quantitative localisation of synaptic and extrasynaptic GABA(A) receptor subunits on hippocampal pyramidal cells by freeze-fracture replica immunolabelling. *Eur J Neurosci* , 2010.

Katz LC, Shatz CJ. Synaptic activity and the construction of cortical circuits. *Science* 274: 1133-1138, 1996.

Kay JN, Chu MW, Sanes JR. MEGF10 and MEGF11 mediate homotypic interactions required for mosaic spacing of retinal neurons. *Nature* 483: 465-469, 2012.

Kay JN, De la Huerta I, Kim IJ, Zhang Y, Yamagata M, Chu MW, Meister M, Sanes JR. Retinal ganglion cells with distinct directional preferences differ in molecular identity, structure, and central projections. *J Neurosci* 31: 7753-7762, 2011.

Kerschensteiner D. Spontaneous Network Activity and Synaptic Development. *Neuroscientist* , 2013.

Kerschensteiner D, Morgan JL, Parker ED, Lewis RM, Wong RO. Neurotransmission selectively regulates synapse formation in parallel circuits in vivo. *Nature* 460: 1016-1020, 2009.

Kier CK, Buchsbaum G, Sterling P. How retinal microcircuits scale for ganglion cells of different size. *J Neurosci* 15: 7673-7683, 1995.

Kim IJ, Zhang Y, Meister M, Sanes JR. Laminar restriction of retinal ganglion cell dendrites and axons: subtype-specific developmental patterns revealed with transgenic markers. *J Neurosci* 30: 1452-1462, 2010.

Kim IJ, Zhang Y, Yamagata M, Meister M, Sanes JR. Molecular identification of a retinal cell type that responds to upward motion. *Nature* 452: 478-482, 2008.

Kim JS, Greene MJ, Zlateski A, Lee K, Richardson M, Turaga SC, Purcaro M, Balkam M, Robinson A, Behabadi BF, Campos M, Denk W, Seung HS, the EyeWirers. Space-time wiring specificity supports direction selectivity in the retina. *Nature* , 2014.

Kirby MA, Chalupa LM. Retinal crowding alters the morphology of alpha ganglion cells. *J Comp Neurol* 251: 532-541, 1986.

Kitamura K, Judkewitz B, Kano M, Denk W, Häusser M. Targeted patch-clamp recordings and single-cell electroporation of unlabeled neurons in vivo. *Nat Methods* 5: 61-67, 2008.

Klausberger T, Somogyi P. Neuronal diversity and temporal dynamics: the unity of hippocampal circuit operations. *Science* 321: 53-57, 2008.

Kleinfeld D, Ahissar E, Diamond ME. Active sensation: insights from the rodent vibrissa sensorimotor system. *Curr Opin Neurobiol* 16: 435-444, 2006.

Kleinfeld D, Bharioke A, Blinder P, Bock DD, Briggman KL, Chklovskii DB, Denk W, Helmstaedter M, Kaufhold JP, Lee WC, Meyer HS, Micheva KD, Oberlaender M, Prohaska S, Reid RC, Smith SJ, Takemura S, Tsai PS, Sakmann B. Large-scale automated histology in the pursuit of connectomes. *J Neurosci* 31: 16125-16138, 2011.

Kneussel M, Brandstätter JH, Gasnier B, Feng G, Sanes JR, Betz H. Gephyrin-independent clustering of postsynaptic GABA(A) receptor subtypes. *Mol Cell Neurosci* 17: 973-982, 2001.

Knudsen EI, du Lac S, Esterly SD. Computational maps in the brain. *Annu Rev Neurosci* 10: 41-65, 1987.

Koch C, Poggio T, Torres V. Retinal ganglion cells: a functional interpretation of dendritic morphology. *Philosophical Transactions of the Royal Society of London. B, Biological Sciences* 298: 227-263, 1982.

Koch C, Poggio T, Torre V. Nonlinear interactions in a dendritic tree: localization, timing, and role in information processing. *Proc Natl Acad Sci U S A* 80: 2799-2802, 1983.

Koch K, McLean J, Berry M, Sterling P, Balasubramanian V, Freed MA. Efficiency of information transmission by retinal ganglion cells. *Current Biology* 14: 1523-1530, 2004.

Koehler CL, Akimov NP, Rentería RC. Receptive field center size decreases and firing properties mature in ON and OFF retinal ganglion cells after eye opening in the mouse. *J Neurophysiol* 106: 895-904, 2011.

Koizumi A, Jakobs TC, Masland RH. Regular mosaic of synaptic contacts among three retinal neurons. *J Comp Neurol* 519: 341-357, 2011.

Kolb H. The architecture of functional neural circuits in the vertebrate retina. The Proctor Lecture. *Invest Ophthalmol Vis Sci* 35: 2385-2404, 1994.

Kolb H, Dekorver L. Midget ganglion cells of the parafovea of the human retina: a study by electron microscopy and serial section reconstructions. *J Comp Neurol* 303: 617-636, 1991.

Kolb H, Nelson R. OFF-alpha and OFF-beta ganglion cells in cat retina: II. Neural circuitry as revealed by electron microscopy of HRP stains. *J Comp Neurol* 329: 85-110, 1993.

Kong JH, Fish DR, Rockhill RL, Masland RH. Diversity of ganglion cells in the mouse retina: unsupervised morphological classification and its limits. *J Comp Neurol* 489: 293-310, 2005.

Koulen P. Vesicular acetylcholine transporter (VAChT): a cellular marker in rat retinal development. *Neuroreport* 8: 2845-2848, 1997.

Koulen P, Fletcher EL, Craven SE, Bredt DS, Wässle H. Immunocytochemical localization of the postsynaptic density protein PSD-95 in the mammalian retina. *J Neurosci* 18: 10136-10149, 1998.

Koulen P, Sassoè-Pognetto M, Grünert U, Wässle H. Selective clustering of GABA(A) and glycine receptors in the mammalian retina. *J Neurosci* 16: 2127-2140, 1996.

Kowler E. Eye movements: the past 25 years. *Vision Res* 51: 1457-1483, 2011.

Kubota Y, Hatada S, Kondo S, Karube F, Kawaguchi Y. Neocortical inhibitory terminals innervate dendritic spines targeted by thalamocortical afferents. *J Neurosci* 27: 1139-1150, 2007.

Kubota Y, Hatada SN, Kawaguchi Y. Important factors for the three-dimensional reconstruction of neuronal structures from serial ultrathin sections. *Front Neural Circuits* 3: 4, 2009.

Kuffler SW. Discharge patterns and functional organization of mammalian retina. *J Neurophysiol* 16: 37-68, 1953.

Leamey CA, Van Wart A, Sur M. Intrinsic patterning and experience-dependent mechanisms that generate eye-specific projections and binocular circuits in the visual pathway. *Curr Opin Neurobiol* 19: 181-187, 2009.

Lee CC, Winer JA. Principles Governing Auditory Cortex Connections. *Cerebral Cortex* 15: 1804-1814, 2005.

Lee S, Zhou ZJ. The synaptic mechanism of direction selectivity in distal processes of starburst amacrine cells. *Neuron* 51: 787-799, 2006.

Lee SC, Cowgill EJ, Al-Nabulsi A, Quinn EJ, Evans SM, Reese BE. Homotypic regulation of neuronal morphology and connectivity in the mouse retina. *J Neurosci* 31: 14126-14133, 2011.

Legg CR, Lambert S. Distance estimation in the hooded rat: experimental evidence for the role of motion cues. *Behavioural brain research* 41: 11-20, 1990.

Lettvin JY, Maturana HR, McCulloch WS, Pitts WH. What the frog's eye tells the frog's brain. *Proceedings of the IRE* 47: 1940-1951, 1959.

LeVay S, Wiesel TN, Hubel DH. The development of ocular dominance columns in normal and visually deprived monkeys. *J Comp Neurol* 191: 1-51, 1980.

Levick WR. Receptive fields and trigger features of ganglion cells in the visual streak of the rabbits retina. *J Physiol* 188: 285-307, 1967.

Lévi S, Grady RM, Henry MD, Campbell KP, Sanes JR, Craig AM. Dystroglycan is selectively associated with inhibitory GABAergic synapses but is dispensable for their differentiation. *J Neurosci* 22: 4274-4285, 2002.

Lévi S, Logan SM, Tovar KR, Craig AM. Gephyrin is critical for glycine receptor clustering but not for the formation of functional GABAergic synapses in hippocampal neurons. *The Journal of neuroscience* 24: 207-217, 2004.

Liang F, Jones EG. Peripheral nerve stimulation increases Fos immunoreactivity without affecting type II Ca2+/calmodulin-dependent protein kinase, glutamic acid decarboxylase, or GABAA receptor gene expression in cat spinal cord. *Exp Brain Res* 111: 326-336, 1996.

Lichtman JW, Denk W. The big and the small: challenges of imaging the brains circuits. *Science* 334: 618-623, 2011.

Liman ER, Zhang YV, Montell C. Peripheral Coding of Taste. *Neuron* 81: 984-1000, 2014.

Lin B, Masland RH. Populations of wide-field amacrine cells in the mouse retina. *J Comp Neurol* 499: 797-809, 2006.

Lin B, Wang SW, Masland RH. Retinal ganglion cell type, size, and spacing can be specified independent of homotypic dendritic contacts. *Neuron* 43: 475-485, 2004.

Lisney TJ, Stecyk K, Kolominsky J, Schmidt BK, Corfield JR, Iwaniuk AN, Wylie DR. Ecomorphology of eye shape and retinal topography in waterfowl (Aves: Anseriformes: Anatidae) with different foraging modes. *J Comp Physiol A Neuroethol Sens Neural Behav Physiol* 199: 385-402, 2013.

Liu G. Local structural balance and functional interaction of excitatory and inhibitory synapses in hippocampal dendrites. *Nat Neurosci* 7: 373-379, 2004.

Liu Y, Zhang LI, Tao HW. Heterosynaptic scaling of developing GABAergic synapses: dependence on glutamatergic input and developmental stage. *J Neurosci* 27: 5301-5312, 2007.

Lohmann C, Bonhoeffer T. A role for local calcium signaling in rapid synaptic partner selection by dendritic filopodia. *Neuron* 59: 253-260, 2008.

Long KO, Fisher SK. The distributions of photoreceptors and ganglion cells in the California ground squirrel, Spermophilus beecheyi. *Journal of Comparative Neurology* 221: 329-340, 1983.

Luo L, Flanagan JG. Development of continuous and discrete neural maps. *Neuron* 56: 284-300, 2007.

Lüscher B, Keller CA. Regulation of GABAA receptor trafficking, channel activity, and functional plasticity of inhibitory synapses. *Pharmacology & Therapeutics* 102: 195-221, 2004.

MacNeil MA, Masland RH. Extreme diversity among amacrine cells: implications for function. *Neuron* 20: 971-982, 1998.

Majumdar S, Heinze L, Haverkamp S, Ivanova E, Wässle H. Glycine receptors of A-type ganglion cells of the mouse retina. *Vis Neurosci* 24: 471-487, 2007.

Mariani J, Changeux JP. Ontogenesis of olivocerebellar relationships. I. Studies by intracellular recordings of the multiple innervation of Purkinje cells by climbing fibers in the developing rat cerebellum. *J Neurosci* 1: 696-702, 1981.

Markram H, Toledo-Rodriguez M, Wang Y, Gupta A, Silberberg G, Wu C. Interneurons of the neocortical inhibitory system. *Nat Rev Neurosci* 5: 793-807, 2004.

Marquardt T, Ashery-Padan R, Andrejewski N, Scardigli R, Guillemot F, Gruss P. Pax6 is required for the multipotent state of retinal progenitor cells. *Cell* 105: 43-55, 2001.

Masland, Richard H. *Invest Ophthalmol Vis Sci.* United States: 2011. [UNKNOWN REFERENCE TYPE]

Masland RH. Neuronal diversity in the retina. *Curr Opin Neurobiol* 11: 431-436, 2001.

Masland RH. The neuronal organization of the retina. *Neuron* 76: 266-280, 2012.

Matsuoka RL, Chivatakarn O, Badea TC, Samuels IS, Cahill H, Katayama K, Kumar SR, Suto F, Chédotal A, Peachey NS, Nathans J, Yoshida Y, Giger RJ, Kolodkin AL. Class 5 transmembrane semaphorins control selective Mammalian retinal lamination and function. *Neuron* 71: 460-473, 2011a.

Matsuoka RL, Nguyen-Ba-Charvet KT, Parray A, Badea TC, Chédotal A, Kolodkin AL. Transmembrane semaphorin signalling controls laminar stratification in the mammalian retina. *Nature* , 2011b.

May PJ. The mammalian superior colliculus: laminar structure and connections. *Progress in brain research* 151: 321-378, 2006.

McGuire BA, Stevens JK, Sterling P. Microcircuitry of beta ganglion cells in cat retina. *J Neurosci* 6: 907-918, 1986.

McIntire SL, Reimer RJ, Schuske K, Edwards RH, Jorgensen EM. Identification and characterization of the vesicular GABA transporter. *Nature* 389: 870-876, 1997.

McKee SP, Nakayama K. The detection of motion in the peripheral visual field. *Vision research* 24: 25-32, 1984.

Megias M, Emri ZS, Freund TF, Gulyas AI. Total number and distribution of inhibitory and excitatory synapses on hippocampal CA1 pyramidal cells. *Neuroscience* 102: 527-540, 2001.

Meier J. The enigma of transmitter-selective receptor accumulation at developing inhibitory synapses. *Cell Tissue Res* 311: 271-276, 2003.

Meier J, Akyeli J, Kirischuk S, Grantyn R. GABAA receptor activity and PKC control inhibitory synaptogenesis in CNS tissue slices. *Molecular and Cellular Neuroscience* 23: 600-613, 2003.

Meister M. Multineuronal codes in retinal signaling. *Proceedings of the National Academy of Sciences* 93: 609-614, 1996.

Menger N, Pow DV, Wässle H. Glycinergic amacrine cells of the rat retina. *J Comp Neurol* 401: 34-46, 1998.

Merigan WH. Chromatic and achromatic vision of macaques: role of the P pathway. *The Journal of Neuroscience* 9: 776-783, 1989.

Miles R, Tóth K, Gulyás AI, Hájos N, Freund TF. Differences between somatic and dendritic inhibition in the hippocampus. *Neuron* 16: 815-823, 1996.

Misgeld T, Burgess RW, Lewis RM, Cunningham JM, Lichtman JW, Sanes JR. Roles of neurotransmitter in synapse formation: development of neuromuscular junctions lacking choline acetyltransferase. *Neuron* 36: 635-648, 2002.

Miyazaki T, Hashimoto K, Shin HS, Kano M, Watanabe M. P/Q-type Ca2+ channel alpha1A regulates synaptic competition on developing cerebellar Purkinje cells. *J Neurosci* 24: 1734-1743, 2004.

Mombaerts P. Axonal wiring in the mouse olfactory system. *Annu Rev Cell Dev Biol* 22: 713-737, 2006.

Montero VM, Rojas A, Torrealba F. Retinotopic organization of striate and peristriate visual cortex in the albino rat. *Brain Res* 53: 197-201, 1973.

Morgan JL, Kerschensteiner D. Coating gold particles with DNA (biolistics). *Cold Spring Harb Protoc* 2012: 114-117, 2012.

Morgan JL, Schubert T, Wong RO. Developmental patterning of glutamatergic synapses onto retinal ganglion cells. *Neural Dev* 3: 8, 2008.

Morgan JL, Soto F, Wong RO, Kerschensteiner D. Development of cell type-specific connectivity patterns of converging excitatory axons in the retina. *Neuron* 71: 1014-1021, 2011.

Mumm JS, Williams PR, Godinho L, Koerber A, Pittman AJ, Roeser T, Chien CB, Baier H, Wong RO. In vivo imaging reveals dendritic targeting of laminated afferents by zebrafish retinal ganglion cells. *Neuron* 52: 609-621, 2006.

Murphy GJ, Rieke F. Network variability limits stimulus-evoked spike timing precision in retinal ganglion cells. *Neuron* 52: 511-524, 2006.

Münch TA, da Silveira RA, Siegert S, Viney TJ, Awatramani GB, Roska B. Approach sensitivity in the retina processed by a multifunctional neural circuit. *Nat Neurosci* 12: 1308-1316, 2009.

Nadal-Nicolás FM, Jiménez-López M, Salinas-Navarro M, Sobrado-Calvo P, Alburquerque-Béjar JJ, Vidal-Sanz M, Agudo-Barriuso M. Whole number, distribution and co-expression of brn3 transcription factors in retinal ganglion cells of adult albino and pigmented rats. *PLoS One* 7: e49830, 2012.

Nassi JJ, Callaway EM. Parallel processing strategies of the primate visual system. *Nat Rev Neurosci* 10: 360-372, 2009.

Niell CM. Exploring the next frontier of mouse vision. *Neuron* 72: 889-892, 2011.

Niell CM. Vision: more than expected in the early visual system. *Curr Biol* 23: R681-R684, 2013.

Nishimura Y, Rakic P. Development of the rhesus monkey retina. I. Emergence of the inner plexiform layer and its synapses. *J Comp Neurol* 241: 420-434, 1985.

Nishimura Y, Rakic P. Development of the rhesus monkey retina: II. A three-dimensional analysis of the sequences of synaptic combinations in the inner plexiform layer. *J Comp Neurol* 262: 290-313, 1987.

Nummenmaa L, Glerean E, Hari R, Hietanen JK. Bodily maps of emotions. *Proc Natl Acad Sci U S A* 111: 646-651, 2014.

Nyíri G, Freund TF, Somogyi P. Input-dependent synaptic targeting of α2-subunit-containing GABAA receptors in synapses of hippocampal pyramidal cells of the rat. *European Journal of Neuroscience* 13: 428-442, 2001.

Oesch NW, Wade Kothmann W, Diamond JS. Illuminating synapses and circuitry in the retina. *Curr Opin Neurobiol* , 2011.

Okabe S, Kim HD, Miwa A, Kuriu T, Okado H. Continual remodeling of postsynaptic density and its regulation by synaptic activity. *Nat Neurosci* 2: 804-811, 1999.

Okabe S, Miwa A, Okado H. Spine formation and correlated assembly of presynaptic and postsynaptic molecules. *J Neurosci* 21: 6105-6114, 2001.

Okawa H, Della Santina L, Schwartz GW, Rieke F, Wong RO. Interplay of Cell-Autonomous and Nonautonomous Mechanisms Tailors Synaptic Connectivity of Converging Axons In Vivo. *Neuron* 82: 125-137, 2014.

Ortinski PI, Turner JR, Barberis A, Motamedi G, Yasuda RP, Wolfe BB, Kellar KJ, Vicini S. Deletion of the GABAA Receptor {alpha}1 Subunit Increases Tonic GABAA Receptor Current: A Role for GABA Uptake Transporters. *J Neurosci* 26: 9323-9331, 2006.

Owczarzak MT, Pourcho RG. Transmitter-specific input to OFF-alpha ganglion cells in the cat retina. *Anat Rec* 255: 363-373, 1999.

Owens DF, Kriegstein AR. Is there more to GABA than synaptic inhibition? *Nat Rev Neurosci* 3: 715-727, 2002.

Palmer SM, Rosa MGP. A distinct anatomical network of cortical areas for analysis of motion in far peripheral vision. *European Journal of Neuroscience* 24: 2389-2405, 2006.

Pang JJ, Gao F, Wu SM. Light-evoked excitatory and inhibitory synaptic inputs to ON and OFF alpha ganglion cells in the mouse retina. *J Neurosci* 23: 6063-6073, 2003.

Panzanelli P, Gunn BG, Schlatter MC, Benke D, Tyagarajan SK, Scheiffele P, Belelli D, Lambert JJ, Rudolph U, Fritschy JM. Distinct mechanisms regulate GABAA receptor and gephyrin clustering at perisomatic and axo-axonic synapses on CA1 pyramidal cells. *J Physiol* 589: 4959-4980, 2011.

Pasternak T, Merigan WH, Flood DG, Zehl D. The role of area centralis in the spatial vision of the cat. *Vision Res* 23: 1409-1416, 1983.

Patrizi A, Scelfo B, Viltono L, Briatore F, Fukaya M, Watanabe M, Strata P, Varoqueaux F, Brose N, Fritschy JM, others. Synapse formation and clustering of neuroligin-2 in the absence of GABAA receptors. *Proceedings of the National Academy of Sciences* 105: 13151, 2008.

Patz S, Wirth MJ, Gorba T, Klostermann O, Wahle P. Neuronal activity and neurotrophic factors regulate GAD-65/67 mRNA and protein expression in organotypic cultures of rat visual cortex. *Eur J Neurosci* 18: 1-12, 2003.

Peichlcu L. Topography of ganglion cells in the dog and wolf retina. *Journal of Comparative Neurology* 324: 603-620, 1992.

Peichl L. Alpha and delta ganglion cells in the rat retina. *J Comp Neurol* 286: 120-139, 1989.

Peichl L. Alpha ganglion cells in mammalian retinae: common properties, species differences, and some comments on other ganglion cells. *Visual Neuroscience* 7: 155-169, 1991.

Peichl L, Ott H, Boycott BB. Alpha ganglion cells in mammalian retinae. *Proc R Soc Lond B Biol Sci* 231: 169-197, 1987.

Peichl L, Wässle H. Morphological identification of on- and off-centre brisk transient (Y) cells in the cat retina. *Proc R Soc Lond B Biol Sci* 212: 139-153, 1981.

Peichl L, Wässle H. The structural correlate of the receptive field centre of alpha ganglion cells in the cat retina. *J Physiol* 341: 309-324, 1983.

Percival KA, Jusuf PR, Martin PR, Grünert U. Synaptic inputs onto small bistratified (blue-ON/yellow-OFF) ganglion cells in marmoset retina. *J Comp Neurol* 517: 655-669, 2009.

Percival KA, Martin PR, Grünert U. Synaptic inputs to two types of koniocellular pathway ganglion cells in marmoset retina. *J Comp Neurol* 519: 2135-2153, 2010.

Perry H. The Ganglion Cell Layer of the Retina of the Rat: A Golgi Study. *Proceedings of the Royal Society B: Biological Sciences* 204: 363-375, 1979.

Perry VH, Cowey A. The ganglion cell and cone distributions in the monkey's retina: implications for central magnification factors. *Vision Res* 25: 1795-1810, 1985.

Personius KE, Balice-Gordon RJ. Activity-dependent synaptic plasticity: insights from neuromuscular junctions. *Neuroscientist* 8: 414-422, 2002.

Petersen CC. The functional organization of the barrel cortex. *Neuron* 56: 339-355, 2007.

Petreanu L, Mao T, Sternson SM, Svoboda K. The subcellular organization of neocortical excitatory connections. *Nature* 457: 1142-1145, 2009.

Piscopo DM, El-Danaf RN, Huberman AD, Niell CM. Diverse visual features encoded in mouse lateral geniculate nucleus. *J Neurosci* 33: 4642-4656, 2013.

Poché RA, Raven MA, Kwan KM, Furuta Y, Behringer RR, Reese BE. Somal positioning and dendritic growth of horizontal cells are regulated by interactions with homotypic neighbors. *Eur J Neurosci* 27: 1607-1614, 2008.

Poggio T, Koch C. Synapses that compute motion. , 1987.

Poggio T, Reichardt W. Considerations on models of movement detection. *Kybernetik* 13: 223-227, 1973.

Polsky A, Mel BW, Schiller J. Computational subunits in thin dendrites of pyramidal cells. *Nat Neurosci* 7: 621-627, 2004.

Poulopoulos A, Aramuni G, Meyer G, Soykan T, Hoon M, Papadopoulos T, Zhang M, Paarmann I, Fuchs C, Harvey K, Jedlicka P, Schwarzacher SW, Betz H, Harvey RJ, Brose N, Zhang W, Varoqueaux F. Neuroligin 2 drives postsynaptic assembly at perisomatic inhibitory synapses through gephyrin and collybistin. *Neuron* 63: 628-642, 2009.

Preibisch S, Saalfeld S, Tomancak P. Globally optimal stitching of tiled 3D microscopic image acquisitions. *Bioinformatics* 25: 1463-1465, 2009.

Prenosil GA, Gasser EMS, Rudolph U, Keist R, Fritschy J-M, Vogt KE. Specific subtypes of GABAA receptors mediate phasic and tonic forms of inhibition in hippocampal pyramidal neurons. *J Neurophysiol* 96: 846-857, 2006.

Provis JM. The distribution and size of ganglion cells in the retina of the pigmented rabbit: a quantitative analysis. *Journal of Comparative Neurology* 185: 121-137, 1979.

Provis JM, Dubis AM, Maddess T, Carroll J. Adaptation of the central retina for high acuity vision: cones, the fovea and the avascular zone. *Prog Retin Eye Res* 35: 63-81, 2013.

Prusky GT, West PW, Douglas RM. Behavioral assessment of visual acuity in mice and rats. *Vision Res* 40: 2201-2209, 2000.

Rao A, Cha EM, Craig AM. Mismatched appositions of presynaptic and postsynaptic components in isolated hippocampal neurons. *J Neurosci* 20: 8344-8353, 2000.

Rao A, Craig AM. Activity regulates the synaptic localization of the NMDA receptor in hippocampal neurons. *Neuron* 19: 801-812, 1997.

Smith SJ, Jahr CE. Rapid induction of filopodial sprouting by application of glutamate to hippocampal neurons. *The Nerve Growth C* 19-26, 1992.

Redfern PA. Neuromuscular transmission in new-born rats. *J Physiol* 209: 701-709, 1970.

Reese BE. Development of the Retina and Optic Pathway. *Vision Res* , 2010.

Reese BE, Cowey A. Large retinal ganglion cells in the rat: their distribution and laterality of projection. *Exp Brain Res* 61: 375-385, 1986.

Reese BE, Raven MA, Stagg SB. Afferents and homotypic neighbors regulate horizontal cell morphology, connectivity, and retinal coverage. *J Neurosci* 25: 2167-2175, 2005.

Reichardt W. Evaluation of optical motion information by movement detectors. *J Comp Physiol A* 161: 533-547, 1987.

Rockhill RL, Daly FJ, MacNeil MA, Brown SP, Masland RH. The diversity of ganglion cells in a mammalian retina. *J Neurosci* 22: 3831-3843, 2002.

Rodieck RW. The density recovery profile: a method for the analysis of points in the plane applicable to retinal studies. *Vis Neurosci* 6: 95-111, 1991.

Rodieck RW, Watanabe M. Survey of the morphology of macaque retinal ganglion cells that project to the pretectum, superior colliculus, and parvicellular laminae of the lateral geniculate nucleus. *J Comp Neurol* 338: 289-303, 1993.

Rodrigues HA, Fonseca Mde C, Camargo WL, Lima PM, Martinelli PM, Naves LA, Prado VF, Prado MA, Guatimosim C. Reduced expression of the vesicular acetylcholine transporter and neurotransmitter content affects synaptic vesicle distribution and shape in mouse neuromuscular junction. *PLoS One* 8: e78342, 2013.

Rodríguez-Contreras A, van Hoeve JS, Habets RL, Locher H, Borst JG. Dynamic development of the calyx of Held synapse. *Proc Natl Acad Sci U S A* 105: 5603-5608, 2008.

Roska B, Nemeth E, Orzo L, Werblin FS. Three levels of lateral inhibition: A space-time study of the retina of the tiger salamander. *J Neurosci* 20: 1941-1951, 2000.

Saiepour L, Fuchs C, Patrizi A, Sassoè-Pognetto M, Harvey RJ, Harvey K. Complex role of collybistin and gephyrin in GABAA receptor clustering. *J Biol Chem* 285: 29623-29631, 2010.

Saito H-A. Morphology of physiologically identified X-, Y-, and W-type retinal ganglion cells of the cat. *Journal of Comparative Neurology* 221: 279-288, 1983.

Saito K, Kakizaki T, Hayashi R, Nishimaru H, Furukawa T, Nakazato Y, Takamori S, Ebihara S, Uematsu M, Mishina M, Miyazaki J, Yokoyama M, Konishi S, Inoue K, Fukuda A, Fukumoto M, Nakamura K,

Obata K, Yanagawa Y. The physiological roles of vesicular GABA transporter during embryonic development: a study using knockout mice. *Mol Brain* 3: 40, 2010.

Salinas-Navarro M, Jiménez-López M, Valiente-Soriano FJ, Alarcón-Martínez L, Avilés-Trigueros M, Mayor S, Holmes T, Lund RD, Villegas-Pérez MP, Vidal-Sanz M. Retinal ganglion cell population in adult albino and pigmented mice: a computerized analysis of the entire population and its spatial distribution. *Vision Res* 49: 637-647, 2009.

Sanes JR, Lichtman JW. Development of the vertebrate neuromuscular junction. *Annu Rev Neurosci* 22: 389-442, 1999.

Sanes JR, Yamagata M. Many paths to synaptic specificity. *Annu Rev Cell Dev Biol* 25: 161-195, 2009.

Sanes JR, Zipursky SL. Design principles of insect and vertebrate visual systems. *Neuron* 66: 15-36, 2010.

Sassoè-Pognetto M, Kirsch J, Grünert U, Greferath U, Fritschy JM, Möhler H, Betz H, Wässle H. Colocalization of gephyrin and GABAA-receptor subunits in the rat retina. *J Comp Neurol* 357: 1-14, 1995.

Sassoè-Pognetto M, Wässle H. Synaptogenesis in the rat retina: subcellular localization of glycine receptors, GABA(A) receptors, and the anchoring protein gephyrin. *J Comp Neurol* 381: 158-174, 1997.

Schiller PH. Parallel information processing channels created in the retina. *Proceedings of the National Academy of Sciences* 107: 17087-17094, 2010.

Schindelin J, Arganda-Carreras I, Frise E, Kaynig V, Longair M, Pietzsch T, Preibisch S, Rueden C, Saalfeld S, Schmid B, Tinevez JY, White DJ, Hartenstein V, Eliceiri K, Tomancak P, Cardona A. Fiji: an open-source platform for biological-image analysis. *Nat Methods* 9: 676-682, 2012.

Schmid B, Schindelin J, Cardona A, Longair M, Heisenberg M. A high-level 3D visualization API for Java and ImageJ. *BMC Bioinformatics* 11: 274, 2010.

Schmidt TM, Chen SK, Hattar S. Intrinsically photosensitive retinal ganglion cells: many subtypes, diverse functions. *Trends Neurosci* 34: 572-580, 2011a.

Schmidt TM, Do MT, Dacey D, Lucas R, Hattar S, Matynia A. Melanopsin-positive intrinsically photosensitive retinal ganglion cells: from form to function. *J Neurosci* 31: 16094-16101, 2011b.

Schnitzer MJ, Meister M. Multineuronal firing patterns in the signal from eye to brain. *Neuron* 37: 499-511, 2003.

Schreiner CE. Order and disorder in auditory cortical maps. *Curr Opin Neurobiol* 5: 489-496, 1995.

Schreiner CE, Winer JA. Auditory cortex mapmaking: principles, projections, and plasticity. *Neuron* 56: 356-365, 2007.

Schubert T, Degen J, Willecke K, Hormuzdi SG, Monyer H, Weiler R. Connexin36 mediates gap junctional coupling of alpha-ganglion cells in mouse retina. *J Comp Neurol* 485: 191-201, 2005.

Schubert T, Hoon M, Euler T, Lukasiewicz PD, Wong RO. Developmental Regulation and Activity-Dependent Maintenance of GABAergic Presynaptic Inhibition onto Rod Bipolar Cell Axonal Terminals. *Neuron* 78: 124-137, 2013.

Schwartz GW, Okawa H, Dunn FA, Morgan JL, Kerschensteiner D, Wong RO, Rieke F. The spatial structure of a nonlinear receptive field. *Nature Neuroscience* , 2012.

Schweizer C, Balsiger S, Bluethmann H, Mansuy IM, Fritschy JM, Mohler H, Lüscher B. The gamma 2 subunit of GABA(A) receptors is required for maintenance of receptors at mature synapses. *Mol Cell Neurosci* 24: 442-450, 2003.

Sefton AJ, Dreher B, Harvey A. Visual system. *The rat nervous system* 1: 169-221, 1995.

Sernagor E, Chabrol F, Bony G, Cancedda L. GABAergic control of neurite outgrowth and remodeling during development and adult neurogenesis: general rules and differences in diverse systems. *Front Cell Neurosci* 4: 11, 2010.

Sernagor E, Eglen SJ, Wong ROL. Development of retinal ganglion cell structure and function. *Progress in Retinal and Eye Research* 20: 139-174, 2001.

SHOLL DA. Dendritic organization in the neurons of the visual and motor cortices of the cat. *J Anat* 87: 387-406, 1953.

Sieghart W, Fuchs K, Tretter V, Ebert V, Jechlinger M, Höger H, Adamiker D. Structure and subunit composition of GABAA receptors. *Neurochemistry International* 34: 379-385, 1999.

Silver MA, Stryker MP. Synaptic density in geniculocortical afferents remains constant after monocular deprivation in the cat. *J Neurosci* 19: 10829-10842, 1999.

Simpson JI. The accessory optic system. *Annu Rev Neurosci* 7: 13-41, 1984.

Sjöström PJ, Rancz EA, Roth A, Häusser M. Dendritic excitability and synaptic plasticity. *Physiol Rev* 88: 769-840, 2008.

Somogyi P, Tamas G, Lujan R, Buhl EH. Salient features of synaptic organisation in the cerebral cortex. *Brain Research Reviews* 26: 113-135, 1998.

Soto F, Bleckert A, Lewis R, Kang Y, Kerschensteiner D, Craig AM, Wong RO. Coordinated increase in inhibitory and excitatory synapses onto retinal ganglion cells during development. *Neural Dev* 6: 31, 2011.

Soto F, Ma X, Cecil JL, Vo BQ, Culican SM, Kerschensteiner D. Spontaneous activity promotes synapse formation in a cell-type-dependent manner in the developing retina. *J Neurosci* 32: 5426-5439, 2012.

Spolidoro M, Sale A, Berardi N, Maffei L. Plasticity in the adult brain: lessons from the visual system. *Exp Brain Res* 192: 335-341, 2009.

Stanford LR. X-cells in the cat retina: relationships between the morphology and physiology of a class of cat retinal ganglion cells. *J Neurophysiol* 58: 940-964, 1987.

Sterratt DC, Lyngholm D, Willshaw DJ, Thompson ID. Standard anatomical and visual space for the mouse retina: computational reconstruction and transformation of flattened retinae with the Retistruct package. *PLoS Comput Biol* 9: e1002921, 2013.

Stone J. A quantitative analysis of the distribution of ganglion cells in the cat's retina. *Journal of Comparative Neurology* 124: 337-352, 1965.

Stone J. The number and distribution of ganglion cells in the cat's retina. *Journal of Comparative Neurology* 180: 753-771, 1978.

Strettoi E, Masland RH. The number of unidentified amacrine cells in the mammalian retina. *Proc Natl Acad Sci U S A* 93: 14906-14911, 1996.

Studler B, Fritschy J-, Brünig I. GABAergic and glutamatergic terminals differentially influence the organization of GABAergic synapses in rat cerebellar granule cells in vitro. *Neuroscience* 114: 123-133, 2002.

Sugihara I. Organization and remodeling of the olivocerebellar climbing fiber projection. *Cerebellum* 5: 15-22, 2006.

Sugihara I, Wu HS, Shinoda Y. The entire trajectories of single olivocerebellar axons in the cerebellar cortex and their contribution to Cerebellar compartmentalization. *J Neurosci* 21: 7715-7723, 2001.

Sun W, Deng Q, Levick WR, He S. ON direction-selective ganglion cells in the mouse retina. *J Physiol* 576: 197-202, 2006.

Sun W, Li N, He S. Large-scale morphological survey of mouse retinal ganglion cells. *J Comp Neurol* 451: 115-126, 2002.

Swindale NV. Cortical organization: modules, polymaps and mosaics. *Curr Biol* 8: R270-R273, 1998.

Swindale NV. How many maps are there in visual cortex? *Cerebral cortex* 10: 633-643, 2000.

Takeuchi T, Miyazaki T, Watanabe M, Mori H, Sakimura K, Mishina M. Control of synaptic connection by glutamate receptor delta2 in the adult cerebellum. *J Neurosci* 25: 2146-2156, 2005.

Tao HW, Poo MM. Activity-dependent matching of excitatory and inhibitory inputs during refinement of visual receptive fields. *Neuron* 45: 829-836, 2005.

Tao HW, Zhang LI, Engert F, Poo M. Emergence of input specificity of ltp during development of retinotectal connections in vivo. *Neuron* 31: 569-580, 2001.

Taylor J, Docherty M, Gordon-Weeks PR. GABAergic growth cones: release of endogenous gamma-aminobutyric acid precedes the expression of synaptic vesicle antigens. *J Neurochem* 54: 1689-1699, 1990.

Taylor WR, Smith RG. The role of starburst amacrine cells in visual signal processing. *Vis Neurosci* 29: 73-81, 2012.

Telkes I, Lee SC, Jusuf PR, Grünert U. The midget-parvocellular pathway of marmoset retina: a quantitative light microscopic study. *J Comp Neurol* 510: 539-549, 2008.

Thévenaz P, Ruttimann UE, Unser M. A pyramid approach to subpixel registration based on intensity. *IEEE Trans Image Process* 7: 27-41, 1998.

Threadgill R, Bobb K, Ghosh A. Regulation of dendritic growth and remodeling by Rho, Rac, and Cdc42. *Neuron* 19: 625-634, 1997.

Tian N, Copenhagen DR. Visual deprivation alters development of synaptic function in inner retina after eye opening. *Neuron* 32: 439-449, 2001.

Tong Q, Ye CP, Jones JE, Elmquist JK, Lowell BB. Synaptic release of GABA by AgRP neurons is required for normal regulation of energy balance. *Nat Neurosci* 11: 998-1000, 2008.

Torre V, Poggio T. A Synaptic Mechanism Possibly Underlying Directional Selectivity to Motion. *Proceedings of the Royal Society B: Biological Sciences* 202: 409-416, 1978.

Trenholm S, Johnson K, Li X, Smith RG, Awatramani GB. Parallel mechanisms encode direction in the retina. *Neuron* 71: 683-694, 2011.

Tretter V, Mukherjee J, Maric HM, Schindelin H, Sieghart W, Moss SJ. Gephyrin, the enigmatic organizer at GABAergic synapses. *Front Cell Neurosci* 6: 23, 2012.

Tritsch NX, Ding JB, Sabatini BL. Dopaminergic neurons inhibit striatal output through non-canonical release of GABA. *Nature* 490: 262-266, 2012.

Tu DC, Zhang D, Demas J, Slutsky EB, Provencio I, Holy TE, Van Gelder RN. Physiologic diversity and development of intrinsically photosensitive retinal ganglion cells. *Neuron* 48: 987-999, 2005.

Turrigiano GG. The self-tuning neuron: synaptic scaling of excitatory synapses. *Cell* 135: 422-435, 2008.

Turrigiano GG, Leslie KR, Desai NS, Rutherford LC, Nelson SB. Activity-dependent scaling of quantal amplitude in neocortical neurons. *Nature* 391: 892-896, 1998.

Turrigiano GG, Nelson SB. Homeostatic plasticity in the developing nervous system. *Nat Rev Neurosci* 5: 97-107, 2004.

Tusa RJ, Palmer LA, Rosenquist AC. The retinotopic organization of area 17 (striate cortex) in the cat. *Journal of Comparative Neurology* 177: 213-235, 1978.

Tyrrell LP, Moore BA, Loftis C, Fernández-Juricic E. Looking above the prairie: localized and upward acute vision in a native grassland bird. *Sci Rep* 3: 3231, 2013.

Tyzio R, Represa A, Jorquera I, Ben-Ari Y, Gozlan H, Aniksztejn L. The establishment of GABAergic and glutamatergic synapses on CA1 pyramidal neurons is sequential and correlates with the development of the apical dendrite. *J Neurosci* 19: 10372-10382, 1999.

Unsoeld T, Stradomska AM, Wang R, Rathjen FG, Jüttner R. Early maturation of GABAergic synapses in mouse retinal ganglion cells. *Int J Dev Neurosci* 26: 233-238, 2008.

Van der Kloot W, Molgó J, Cameron R, Colasante C. Vesicle size and transmitter release at the frog neuromuscular junction when quantal acetylcholine content is increased or decreased. *J Physiol* 541: 385-393, 2002.

Van Essen DC, Anderson CH, Felleman DJ. Information processing in the primate visual system: an integrated systems perspective. *Science* 255: 419-423, 1992.

Vaney DI. The mosaic of amacrine cells in the mammalian retina. *Progress in retinal research* 9: 49-100, 1990.

Vaney DI, Sivyer B, Taylor WR. Direction selectivity in the retina: symmetry and asymmetry in structure and function. *Nat Rev Neurosci* 13: 194-208, 2012a.

Vaney DI, Sivyer B, Taylor WR. Direction selectivity in the retina: symmetry and asymmetry in structure and function. *Nat Rev Neurosci* 13: 194-208, 2012b.

Vannier C, Triller A. Biology of the postsynaptic glycine receptor. *International review of cytology* 176: 201-244, 1997.

Van Rullen R, Thorpe SJ. Rate coding versus temporal order coding: what the retinal ganglion cells tell the visual cortex. *Neural computation* 13: 1255-1283, 2001.

van Versendaal D, Rajendran R, Saiepour MH, Klooster J, Smit-Rigter L, Sommeijer JP, De Zeeuw CI, Hofer SB, Heimel JA, Levelt CN. Elimination of inhibitory synapses is a major component of adult ocular dominance plasticity. *Neuron* 74: 374-383, 2012.

van Wyk M, Taylor WR, Vaney DI. Local edge detectors: a substrate for fine spatial vision at low temporal frequencies in rabbit retina. *J Neurosci* 26: 13250-13263, 2006.

van Wyk M, Wässle H, Taylor WR. Receptive field properties of ON- and OFF-ganglion cells in the mouse retina. *Vis Neurosci* 26: 297-308, 2009.

Varoqueaux F, Jamain S, Brose N. Neuroligin 2 is exclusively localized to inhibitory synapses. *Eur J Cell Biol* 83: 449-456, 2004.

Varoqueaux F, Sigler A, Rhee JS, Brose N, Enk C, Reim K, Rosenmund C. Total arrest of spontaneous and evoked synaptic transmission but normal synaptogenesis in the absence of Munc13-mediated vesicle priming. *Proc Natl Acad Sci U S A* 99: 9037-9042, 2002.

Verhage M, Maia AS, Plomp JJ, Brussaard AB, Heeroma JH, Vermeer H, Toonen RF, Hammer RE, van den Berg TK, Missler M, others. Synaptic assembly of the brain in the absence of neurotransmitter secretion. *Science* 287: 864, 2000.

Vithlani M, Terunuma M, Moss SJ. The dynamic modulation of GABA(A) receptor trafficking and its role in regulating the plasticity of inhibitory synapses. *Physiol Rev* 91: 1009-1022, 2011.

Völgyi B, Abrams J, Paul DL, Bloomfield SA. Morphology and tracer coupling pattern of alpha ganglion cells in the mouse retina. *J Comp Neurol* 492: 66-77, 2005.

Völgyi B, Chheda S, Bloomfield SA. Tracer coupling patterns of the ganglion cell subtypes in the mouse retina. *J Comp Neurol* 512: 664-687, 2009.

Wagor E, Mangini NJ, Pearlman AL. Retinotopic organization of striate and extrastriate visual cortex in the mouse. *J Comp Neurol* 193: 187-202, 1980.

Waites CL, Craig AM, Garner CC. Mechanisms of vertebrate synaptogenesis. *Annu Rev Neurosci* 28: 251-274, 2005.

Wallace DJ, Greenberg DS, Sawinski J, Rulla S, Notaro G, Kerr JN. Rats maintain an overhead binocular field at the expense of constant fusion. *Nature* 498: 65-69, 2013.

Walsh MK, Lichtman JW. In vivo time-lapse imaging of synaptic takeover associated with naturally occurring synapse elimination. *Neuron* 37: 67-73, 2003.

Wandell BA. *Foundations of vision*. Sunderland, MA, US: Sinauer Associates, 1995, p. xvi, 476-xvi, 476.

Wang DD, Kriegstein AR. GABA regulates excitatory synapse formation in the neocortex via NMDA receptor activation. *J Neurosci* 28: 5547-5558, 2008.

Warland DK, Reinagel P, Meister M. Decoding visual information from a population of retinal ganglion cells. *J Neurophysiol* 78: 2336-2350, 1997.

Warrant E. Vision in the dimmest habitats on earth. *J Comp Physiol A Neuroethol Sens Neural Behav Physiol* 190: 765-789, 2004.

Wassle H, Peichl L, Boycott BB. Morphology and Topography of on- and off-Alpha Cells in the Cat Retina. *Proceedings of the Royal Society of London. Series B, Biological Sciences* 212: 157-175, 1981.

Watanabe M. Molecular mechanisms governing competitive synaptic wiring in cerebellar Purkinje cells. *Tohoku J Exp Med* 214: 175-190, 2008.

Watanabe M, Rodieck RW. Parasol and midget ganglion cells of the primate retina. *J Comp Neurol* 289: 434-454, 1989.

Wässle H, Boycott BB. Functional architecture of the mammalian retina. *Physiol Rev* 71: 447-480, 1991.

Wässle H, Grünert U, Röhrenbeck J, Boycott BB. Cortical magnification factor and the ganglion cell density of the primate retina. *Nature* 341: 643-646, 1989.

Wässle H, Grünert U, Röhrenbeck J, Boycott BB. Retinal ganglion cell density and cortical magnification factor in the primate. *Vision Res* 30: 1897-1911, 1990.

Wässle H, Heinze L, Ivanova E, Majumdar S, Weiss J, Harvey RJ, Haverkamp S. Glycinergic transmission in the Mammalian retina. *Front Mol Neurosci* 2: 6, 2009.

Wässle H, Koulen P, Brandstätter JH, Fletcher EL, Becker CM. Glycine and GABA receptors in the mammalian retina. *Vision Res* 38: 1411-1430, 1998.

Wässle H, Peichl L, Boycott BB. Dendritic territories of cat retinal ganglion cells. *Nature* 292: 344-345, 1981.

Wässle H, Puller C, Müller F, Haverkamp S. Cone contacts, mosaics, and territories of bipolar cells in the mouse retina. *J Neurosci* 29: 106-117, 2009.

Wei W, Elstrott J, Feller MB. Two-photon targeted recording of GFP-expressing neurons for light responses and live-cell imaging in the mouse retina. *Nat Protoc* 5: 1347-1352, 2010.

Wei W, Feller MB. Organization and development of direction-selective circuits in the retina. *Trends Neurosci* , 2011.

Wei W, Hamby AM, Zhou K, Feller MB. Development of asymmetric inhibition underlying direction selectivity in the retina. *Nature* 469: 402-406, 2011.

Weng S, Sun W, He S. Identification of ON-OFF direction-selective ganglion cells in the mouse retina. *J Physiol* 562: 915-923, 2005.

Wick MJ, Radcliffe RA, Bowers BJ, Mascia MP, Lüscher B, Harris RA, Wehner JM. Behavioural changes produced by transgenic overexpression of gamma2L and gamma2S subunits of the GABAA receptor. *Eur J Neurosci* 12: 2634-2638, 2000.

Wojcik SM, Katsurabayashi S, Guillemin I, Friauf E, Rosenmund C, Brose N, Rhee JS. A shared vesicular carrier allows synaptic corelease of GABA and glycine. *Neuron* 50: 575-587, 2006.

Wong WT, Wong RO. Changing specificity of neurotransmitter regulation of rapid dendritic remodeling during synaptogenesis. *Nat Neurosci* 4: 351-352, 2001.

Woodruff AR, Anderson SA, Yuste R. The enigmatic function of chandelier cells. *Front Neurosci* 4: 201, 2010.

Woolsey CN. *Cortical Sensory Organization: Volume 2: Multiple Visual Areas*. Humana Press, 1982.

Wu G, Malinow R, Cline HT. Maturation of a central glutamatergic synapse. *Science* 274: 972-976, 1996.

Wu X, Fu Y, Knott G, Lu J, Di Cristo G, Huang ZJ. GABA Signaling Promotes Synapse Elimination and Axon Pruning in Developing Cortical Inhibitory Interneurons. *J Neurosci* 32: 331-343, 2012.

Wu Y, Eghbali M, Ou J, Lu R, Toro L, Stefani E. Quantitative determination of spatial protein-protein correlations in fluorescence confocal microscopy. *Biophys J* 98: 493-504, 2010.

Xu Y, Vasudeva V, Vardi N, Sterling P, Freed MA. Different types of ganglion cell share a synaptic pattern. *J Comp Neurol* 507: 1871-1878, 2008.

Yang G, Masland RH. Receptive fields and dendritic structure of directionally selective retinal ganglion cells. *J Neurosci* 14: 5267-5280, 1994.

Yilmaz M, Meister M. Rapid innate defensive responses of mice to looming visual stimuli. *Current Biology* 23: 2011-2015, 2013.

Yizhar O, Fenno LE, Prigge M, Schneider F, Davidson TJ, O'Shea DJ, Sohal VS, Goshen I, Finkelstein J, Paz JT, Stehfest K, Fudim R, Ramakrishnan C, Huguenard JR, Hegemann P, Deisseroth K. Neocortical excitation/inhibition balance in information processing and social dysfunction. *Nature* , 2011.

Yonehara K, Balint K, Noda M, Nagel G, Bamberg E, Roska B. Spatially asymmetric reorganization of inhibition establishes a motion-sensitive circuit. *Nature* 469: 407-410, 2011.

Yonehara K, Ishikane H, Sakuta H, Shintani T, Nakamura-Yonehara K, Kamiji NL, Usui S, Noda M. Identification of retinal ganglion cells and their projections involved in central transmission of information about upward and downward image motion. *PLoS One* 4: e4320, 2009.

Yoshida Y. Semaphorin signaling in vertebrate neural circuit assembly. *Front Mol Neurosci* 5: 71, 2012.

Yuste R. Dendritic spines and distributed circuits. *Neuron* 71: 772-781, 2011.

Zhang C, McCall MA. Receptor targets of amacrine cells. *Vis Neurosci* 29: 11-29, 2012.

Zhang Y, Kim IJ, Sanes JR, Meister M. The most numerous ganglion cell type of the mouse retina is a selective feature detector. *Proc Natl Acad Sci U S A* 109: E2391-E2398, 2012.

Zhao X, Shoji S, Lau P. Balanced GABAergic and glutamatergic synapse development in hippocampal neurons. *Biochem Biophys Res Commun* 330: 1110-1115, 2005.

Ziv NE, Smith SJ. Evidence for a role of dendritic filopodia in synaptogenesis and spine formation. *Neuron* 17: 91-102, 1996.

Zoccolan D, Oertelt N, DiCarlo JJ, Cox DD. A rodent model for the study of invariant visual object recognition. *Proceedings of the National Academy of Sciences* 106: 8748-8753, 2009.

Zou DJ, Cline HT. Postsynaptic calcium/calmodulin-dependent protein kinase II is required to limit elaboration of presynaptic and postsynaptic neuronal arbors. *J Neurosci* 19: 8909-8918, 1999.

Zucker CL. Localization of gephyrin and glycine receptor subunit immunoreactivity in the rabbit retina. *Vis Neurosci* 15: 389-395, 1998.

ADAM BLECKERT

University of Washington
Department of Biological Structure
1959 NE Pacific Street Box 357420
Seattle, Washington 98195

bleckert@uw.edu
(w) 206-616-2883
(c) 206 422-5085

EDUCATION

University of Washington, Seattle WA — 2007-present
PhD candidate in Neurobiology and Behavior

The Colorado College, Colorado Springs, CO — 2000-2004
BA in Neuroscience, *cum laude*

RESEARCH EXPERIENCE

Doctoral Research — 2008-2014
University of Washington – Biological Structure
Advisor: Dr. Rachel O Wong
Thesis Project: Structural and Functional Connectivity of the Inner Retina

- Performed combined fluorescence microscopy and serial electron microscopy to map the distributions of inhibitory and excitatory synapses onto individual retinal ganglion cells (RGCs) across development *(completed)*
- Mapped the nonuniform topographies of RGCs across the mouse retina by characterizing the spatial distributions and function of distinct RGC types *(completed)*
- Identified a differential role for inhibitory transmission in setting up synaptic connectivity onto distinct cellular compartments of identified RGCs *(in progress)*

Graduate Research — 2008 winter
University of Washington – Pharmacology
Advisor: Dr. Sandra M Bajjalieh
Project: Leveteracetam Reverses Synaptic Deficits Produced by Synaptic Vesicle Protein 2 (SV2) Overexpression

- Quantified the effects of Leveteracetam on synaptic transmission using whole cell voltage clamp recordings of hippocampal pyramidal neurons in autaptic cultures

Graduate Research — 2007 fall
University of Washington – Biology
Advisor: Dr. William Moody
Project: A Pacemaker for Spontaneous, Synchronized Activity in the Neonatal Mouse Cortex

- Recorded spontaneous activity in individual developing cortical neurons in culture to characterize their responses and participation in synchronous bouts of correlated activity

Laboratory Research — 2005-2007
University of Illinois, Chicago – Laboratory of Integrative Neuroscience
Advisor: Dr. Simon Alford
Project(1): Dual Pools of Functionally Distinct Actin at Presynaptic Sites

- Identified two functionally distinct pools of actin at presynaptic terminals
- Performed paired cell sharp electrode and patch clamp recordings to monitor the effects

of disrupting actin on synaptic transmission

- Visualized and disrupted actin filaments and utilized live imaging of FM1-43 vital dyes to monitor synaptic vesicle recycling

Project(2): 5HT G-protein-coupled Receptors Regulate Synaptic Fusion and Cleft Glutamate Concentration

- Characterized a shift in vesicle fusion modes during different stimulus paradigms based on motor unit activity during fictive locomotion
- Measured alterations in vesicle fusion rates by imaging FM1-43 vital dye release from labeled pools of synaptic vesicles

Undergraduate Research 2005 spring
Sea Education Association (SEA) – Woods Hole, MA – Caribbean
Advisor: Dr. Lisa Graziano

Project: Diel Variation in Cyanobacteria Abundance in Surface Waters of the Sargasso Sea.

- Quantified the daily cyclical abundance and distribution of cyanobacteria sampled from the waters of the Sargasso Sea using fluorescence microscopy counts of cell densities

Undergraduate Behavioral Health Internship 2003-2004
Penrose St Francis Community Hospital – Colorado Springs, CO
Advisor: Dr. Kristi Erdal

Honors Thesis: Mass Effect: A Case Study on the Effects of Traumatic Brain Injury on the Family

- Shadowed a clinical neuropsychologist and helped performed cognitive skills tests on patients who suffered traumatic brain injuries (TBI)
- Interviewed one patient and his family to conduct a case study of the short and long term effects TBI causes to a family

National Science Foundation Undergraduate Research Fellowship 2003 summer
University of Illinois-Chicago – Laboratory of Integrative Neuroscience
Advisor: Dr. Simon T. Alford

Project: The Role of Actin in Presynaptic Vesicle Cycling and Ca^{2+} Channel Location

- Mapped the distribution of presynaptic actin filaments associated with sites of Ca^{2+} influx

PUBICATIONS

Bleckert, A., Schwartz, G. W., Turner, M. H., Rieke, F. & Wong, R. O. Visual Space Is Represented by Nonmatching Topographies of Distinct Mouse Retinal Ganglion Cell Types. *Curr Biol* (2014).
*****article recommended in F1000prime (DOI: 10.3410/f.718243182.793491684)

Suzuki, S. C., **Bleckert, A.**, Williams, P. R., Takechi, M., *et al.* Cone photoreceptor types in zebrafish are generated by symmetric terminal divisions of dedicated precursors. *Proc Natl Acad Sci U S A* 110, 15109-15114 (2013).

Bleckert, A., Gaiarsa, J. -L., Parker, E. D., Kang, Y., *et al.* Spatial Relationships between GABAergic and Glutamatergic Synapses on the Dendrites of Distinct Types of Mouse Retinal Ganglion Cells across Development. *PLoS ONE* 8, e69612 (2013).

Bleckert, A., Photowala, H. & Alford, S. Dual pools of actin at presynaptic terminals. *J Neurophysiol* 107, 3479-3492 (2012).
*****article recommended in F1000prime (DOI: 10.3410/f.715498051.791003055)

Nowack, A., Malarkey, E. B., Yao, J., **Bleckert, A.**, *et al.* Levetiracetam Reverses Synaptic Deficits Produced by Overexpression of SV2A. *PLoS One* 6, e29560 (2011).

Soto, F., **Bleckert, A.**, Lewis, R., Kang, Y., *et al.* Coordinated increase in inhibitory and excitatory synapses onto retinal ganglion cells during development. *Neural Dev* 6, 31 (2011).

Bleckert, A. & Wong, R. O. Identifying roles for neurotransmission in circuit assembly: insights gained from multiple model systems and experimental approaches. *Bioessays* 33, 61-72 (2011).

Gerachshenko, T., Schwartz, E., **Bleckert, A.**, Photowala, H., *et al.* Presynaptic G-protein-coupled receptors dynamically modify vesicle fusion, synaptic cleft glutamate concentrations, and motor behavior. *J Neurosci* 29, 10221-10233 (2009).

TECHNICAL EXPERIENCE

Imaging

- Confocal Microscopy
- Electron Microscopy (TEM, SEM)
- Correlative Light – Electron Microscopy
- 2 Photon Microscopy
- In Vitro Time Lapse Imaging

Electrophysiology

- Whole Cell Patch Clamp Recording
- Paired Cell Recording
- Multi Electrode Recording

Additional

- Immunohistochemistry
- Biolistic Transfection
- Transgenic Mouse Care
- Programming – MATLAB
- Imaging Software – Fiji (ImageJ), Imaris, Vaa3D, Amira

MEETINGS AND PRESENTATIONS

European Retina Meeting Sept. 2011
Amsterdam, Netherlands
Development of inhibitory and excitatory connections onto individual retinal ganglion cells
A. Bleckert, Y. Kang, R. Lewis, A.M. Craig, RO Wong

Gordon Research Conference and Seminar: Dendrites March 2011
Ventura CA, USA
GABAergic transmission and the maturation of synaptic connections onto retinal ganglion cells
A. Bleckert, F. Soto, R. Lewis, Y. Kang, A.M. Craig, RO Wong

Society for Neuroscience Conference Oct. 2009
Chicago IL, USA
Inhibitory synaptogenesis on retinal ganglion cell dendrites
F. Soto, D. Kerschensteiner, **A. Bleckert**, R. Lewis, Y. Kang, A.M. Craig, ROL Wong

Society for Neuroscience Conference Oct. 2008
Washington DC, USA
Presynaptic G-proteins regulate synaptic vesicle fusion and motor behavior
S. T. Alford, T. Gerachshenko, E. Schwartz, **A. Bleckert**, A. Seymour, H. Photowala

A pacemaker for spontaneous, synchronized activity in the neonatal mouse cortex
W.J. Moody, J. Lischalk, A. Latimer, J. Weber, L. Hanson, **A. Bleckert**

FASEB Retinal Neurobiology and Visual Processing July 2008
Snowmass Village CO, USA
Attended

Society for Neuroscience Conference Oct. 2006
Atlanta GA, USA
FM1-43 labeled vesicle clouds associate with active actin rings at the presynaptic terminal
S.T. Alford, **A. Bleckert**, S. Ramachandran, H. Photowala

AWARDS AND GRANTS

Neurobiology and Behavior Training Grant, University of Washington	2012-2013
Development Biology Training Grant, University of Washington	2009-2012
National Science Foundation Research Experience for Undergraduates Fellowship	2003 summer

REFERENCES

Dr. Rachel O Wong
University of Washington
Department of Biological Structure
1959 NE Pacific Street H-519 HSB
Box 357420
Seattle, WA 98195
(206) 616-3275
wongr2@uw.edu

Dr. Fred Rieke
University of Washington
Department of Physiology and Biophysics
1959 NE Pacific Street H-405 HSB
Box 357290
Seattle, WA 98195
(206) 616-6956
rieke@uw.edu

Dr. Andres Barria
University of Washington
Department of Physiology and Biophysics
1959 NE Pacific Street H-405 HSB
Box 357290
Seattle, WA 98195
(206) 221-6446
barria@uw.edu

Dr. Simon T Alford
University of Illinois Chicago
Department of Biological Sciences
840 West Taylor Street SEL 4263 M/C 067
Chicago, IL 60607
(312) 355-0328
sta@uic.edu